Experimental Retinal Projections to The Ferret Auditory Thalamus: Morphology, Development and Effects on Auditory Cortical Organization

by

Alessandra Angelucci

M.D.
University of Rome "La Sapienza", 1990

SUBMITTED TO THE DEPARTMENT OF BRAIN AND COGNITIVE SCIENCES IN PARTIAL FULFILLMENT OF THE REQUIREMENTS FOR THE DEGREE OF

DOCTOR OF PHILOSOPHY
AT THE
MASSACHUSETTS INSTITUTE OF TECHNOLOGY

SEPTEMBER 1996
[February 1997]

Signature of Author:_____
Department of Brain and Cognitive Sciences
23 September, 1996

Certified by:_____
Mriganka Sur
Professor of Neuroscience
Thesis Supervisor

Accepted by:_____
Gerald E. Schneider
Chairman, Department Graduate Committee

Experimental Retinal Projections to The Ferret Auditory Thalamus: Morphology, Development and Effects on Auditory Cortical Organization

by

Alessandra Angelucci

Submitted to the Department of Brain and Cognitive Sciences
on September 18, 1996 in Partial Fulfillment of the
Requirements for the Degree of Doctor of Philosophy in
Brain and Cognitive Sciences

ABSTRACT

We have used a novel preparation to examine the relative roles of afferents and targets, as well as of patterned input activity, in the development of specific patterns of thalamic and cortical connections.

1) We have first shown that in ferrets, retinal axons can be induced to innervate the auditory thalamus following extensive neonatal deafferentation of the medial geniculate nucleus (MGN). The extent of MGN deafferentation correlates well with the extent of the novel projection.

2) Similar to the normal retinogeniculate projection, inputs from the two eyes are spatially segregated in the MGN. However, while retinal projections to the lateral geniculate nucleus (LGN) form eye-specific terminal layers, retinal projections to the MGN are arranged in terminal clusters whose shape, size and orientation closely match those of relay cell dendrites in the MGN. In addition, the retinal termination zones are aligned within the normal cellular organization of the MGN, resembling the normal pattern of inputs from the inferior colliculus to the MGN. Both clustering and eye-specific segregation in MGN arise as a refinement of initially diffuse and overlapped projections, over a time period that parallels pattern formation by retinal afferents in the LGN. We conclude that afferent-driven mechanisms are implicated in the development of clustering and eye-specific segregation, whereas target-driven mechanisms specify shape, size and distribution of terminal clusters.

3) The normal ferret MGN, like that of other mammalian species, is organized into four main subdivisions distinguishable on the basis of their specific cyto- and chemoarchitecture. The projections from the MGN to the auditory cortex are highly divergent. Single focal injections of anterograde tracers in the MGN produce terminal labeling in at least two different auditory cortical fields. Within each of the tonotopically organized cortical fields terminal labeling appears as multiple "patches" aligned along one main axis, thus forming "slabs" whose longer axis is oriented parallel to the presumed isofrequency contours. A possible functional correlate of the "patches" is that of the binaural interaction bands. Preliminary data on thalamocortical projections in "rewired" ferrets indicate that these projections are also highly divergent and resemble the projections in normal animals, thus suggesting that visual activity does not alter the normal pattern of auditory thalamocortical projections.

4) The pattern of intrinsic long-range horizontal connections within primary auditory cortex (A1) of "rewired" ferrets was examined by injections of a retrograde tracer into visual A1 domains, identified using optical imaging of intrinsic signals. Visually-responsive cells in "rewired" A1 are organized into large clustered domains. Horizontal connections occur between visual cells within the same domain and do not extend to surrounding visually-unresponsive

regions of A1. While intrinsic connections in normal A1 are highly anisotropic and elongated along the presumed isofrequency axis, these connections in "rewired" A1 are more symmetric, and their longer axis does not bear any consistent relation to the orientation of isofrequency contours. We conclude that visual activity shapes the intrinsic horizontal connections in A1 into more symmetric and unoriented patterns.

Thesis Supervisor: Mriganka Sur
Title: Professor of Neuroscience

To my parents
for teaching me that I could do anything,
and that whatever I did I should do well

A mamma e papa'
per avermi dato la possibilita' di scegliere,
e per avermi insegnato che qualsiasi cosa
avessi scelto avrei dovuto farla al meglio

Table of Contents

Acknowledgments

During my Ph.D. years I have received support and help from many people. This is my first opportunity to thank them all:

Mriganka Sur: my supervisor, for his constant support and encouragement as well as for his great enthusiasm for science, which have given me the motivation and confidence to do all this and to continue doing research in the future.

Francisco Clascá: my teacher, colleague and friend, for sharing with me the best and worst times in the lab. I have great memories of our painful, long successful and unsuccessful experiments, as well as of our intense and enthusiastic discussions on science and life in the US. I owe him much of what I presently know about neuroanatomy.

Peter Dayan: my thesis committee member, for his patience, his time and most of all his constructive criticism of my data.

Gerry Schneider: my thesis committee member and a pioneer in the field of developmental neuroscience, for his constant interest in my work. His research has greatly inspired mine.

Jitendra Sharma: a great colleague, for all those long nights spent together recording, injecting, talking about science, life and bs trying to keep awake.

I would also like to thank my best friends in the lab who have made my working life enjoyable, and who have greatly improved the quality of my work with useful intellectual contributions: Karina Cramer, Louis Toth, Dae-Shik Kim.

I wish to thank Peter Kind and Emanuela Bricolo for their friendship, support and help, especially in the last and most difficult days of my thesis preparation. I am indebted to Emanuela also for writing computer programs and for help in the quantification of data.

I would like to express my gratitude to people who have provided me with great technical assistance: Suzanne Kuffler, for helping with histology, photography and animal care and for being a friend; Bob Marini, for his expert assistance with surgery and amazing veterinarian

skills, but most of all for his great sense of humor which made those long surgery days much more enjoyable!!

Lastly, I would like to thank the people I have met in Boston, whose friendship and company have contributed greatly to my mental sanity and made my life in the US. worth it as well as unforgettable: Emanuela, Domenico, Luca, Peter, Eleonora, Caterina, Ruben, Lamberto, Elena, Sarah, Henry.

My last and most important gratitude is for the the one person in my life who, more than anyone else and myself, besides my parents, has believed in me, and demonstrated it in all possible ways: Mark.

Introduction

The issue of what determines the functional and structural specificity of a brain area is fundamental in the study of brain development and plasticity. Is development of specific functions and connections in a target structure dependent on specific properties of afferent inputs, or is it dependent on intrinsic features of the target? One way of addressing this issue is to alter the input to a target early in development, and subsequently examine the resulting pattern of connectivity along with the target's functional properties. This can be achieved by transplanting one part of the brain into a different brain area (O'Leary and Stanfield, 1989; Schlaggar and O'Leary, 1991), or alternatively by redirecting specific inputs to targets that they would not normally innervate. We have chosen the latter approach, and used a preparation in which, by surgical manipulations performed in neonatal ferrets, retinal fibers are induced to innervate a non-visual thalamic target, the auditory thalamus or medial geniculate nucleus (MGN). Since the MGN retains its projections to the auditory cortex, both the auditory thalamus and cortex are forced to develop under the influence of visual, rather than auditory, inputs. This experimental paradigm is thus particularly suited to address issues of afferent versus target control of thalamic and cortical specificity. Indeed, one can ask how functionally and structurally similar to normal visual thalamus and cortex are the auditory thalamus and cortex induced to develop under the influence of visual inputs.

Routing retinal projections to the auditory thalamus

Redirection of inputs to ectopic targets in the mammalian brain following surgical manipulations has been previously reported, mainly in rodents. In particular, it has been shown that when normal targets in the visual, somatosensory and olfactory systems are ablated, and alternative space is created by partially deafferenting a target of a different modality, ingrowing axons innervate these novel targets (Schneider, 1973; Devor, 1975; Graziadei et al., 1979; Frost, 1981,1982, 1986; Asanuma and Stanfield, 1990).

Our interest is to examine the structural and functional consequences of redirecting visual inputs to non-visual structures, and to consider the implications such consequences might have for normal development and developmental plasticity. Redirection of retinal inputs to thalamic targets of a different modality, such as the auditory and somatosensory thalami, has been previously shown to occur in hamsters following neonatal ablation of the superior colliculus (SC), a principal retinal target, and partial transections of the major ascending inputs to the MGN or the ventrobasal complex (VB) (Schneider, 1973; Kalil and Schneider, 1975; Frost, 1981). The ectopic retinal projections to VB and MGN in hamsters exhibited some crude retinotopic order (Frost, 1981) and, at the ultrastructural level, showed a synaptic organization similar to that of the normal inputs to the VB or MGN (Campbell and Frost, 1987, 1988). Moreover, the ectopic retino-VB projection conferred visual responsivity to cells in the primary and secondary somatosensory cortical areas (Frost and Metin, 1985; Metin and Frost, 1989), indicating that the ectopic projections are functional.

Sur et al. (1988) have successfully extended the "rewired" paradigm to the ferret, an animal with a well developed visual pathway, and thus better suited than rodents for studying the development and plasticity of visual functions. Ferrets are carnivores with a visual system quite similar to that of the cat (Zahs and Stryker, 1985; Law et al., 1988). However, compared to cats, they are born at a much earlier stage of development (gestation is 41±1 days in ferrets, compared to 63 days in cats) which makes them particularly well suited for early developmental manipulations.

Cross-modal plasticity in the ferret was induced by surgical reduction of the two principal retinal targets, the SC and lateral geniculate nucleus (LGN), and sectioning the main ascending inputs to the MGN, i.e. the brachium of the inferior colliculus (BIC), on the day of birth (Sur et al., 1988). As a result of these neonatal manipulations, some retinal axons innervated the MGN. Moreover, since normally the SC sends inputs to the lateral posterior thalamic nucleus (LP), SC ablation induced retinal fibers to send ectopic projections also to LP (Pallas et al., 1990; Rocha et al., 1993). Subsequent physiological studies demonstrated

that this novel visual pathway is functional, since some cells in MGN and primary auditory cortex (AI) could be driven by electrical stimulation of the optic chiasm, or by visual stimulation (Sur et al., 1988; Roe et al., 1990, 1992, 1993). The physiological properties of visually responsive cells in MGN and AI showed that the retino-MGN projection arises from retinal cells with slow axonal conduction velocities (Sur et al., 1988; Roe et al., 1992, 1993) similar to those of the W-class of retinal ganglion cells. Consistently, anatomical studies indicated that retino-MGN cells have small soma sizes (Roe et al., 1993), and their terminal axon arbors resemble morphologically the axon arbors of normal retinal W cells (Pallas et al., 1994). Remarkably, some receptive field properties of visual cells in AI, such as orientation and direction selectivity, as well as binocularity, resembled those of normal cells in primary visual cortex (VI) (Roe et al., 1992), and were not observed in visually driven MGN cells which, instead, had concentric, non-oriented, and strictly monocular receptive fields (Roe et al., 1993). Moreover, it was reported that the retina maps topographically to AI (Roe et al., 1990), an intriguing finding if one considers the highly convergent and divergent nature of the normal auditory thalamocortical projection (discussed in Sur et al., 1990). Together, the above observations suggest that visual input might induce structural changes in auditory thalamic and/or cortical connectivity. With the present study we aim to uncover if, and to what extent, visual inputs influence the development of connections in the auditory pathway of experimentally manipulated ferrets.

The first part of the dissertation focuses on issues of thalamic specificity. The occurrence of anomalous connections between retinal axons and ectopic thalamic sites following neonatal manipulations demonstrates that an intrinsic preference of retinal axons to terminate in their normal targets, if present, is at best relative rather than absolute. However, the small extent of retinal projections to ectopic targets following surgical manipulations (Schneider, 1973; Frost, 1981; Rocha et al., 1993), seems to suggest that only a small set of retinal ganglion cells is developmentally susceptible to environmental influences with respect

to targeting choices. In chapter 1, in order to assess whether retinal axons can be induced to innervate the MGN in a significant number, we examine the precise conditions under which these axons can be induced to form connections with non-retinal targets. Possible factors that might influence the axons' choice of a target are discussed.

Experimentally induced retinal projections to the auditory thalamus: relative roles of afferents and targets in the development of connections.

A central question in the development of connectivity concerns the relative roles of afferents and targets. At present, evidence exists in support of both afferent and target control of connectivity. For example, there is evidence that synaptic morphology can be regulated by afferents (Graziadei and Monti Graziadei, 1985; Cantore and Scalia, 1987; Scalia, 1987; Graziadei et al., 1979). However, other studies suggest that synaptic morphology is controlled by intrinsic features of the target (Palay and Chan-Palay, 1974; Campbell and Frost, 1987,1988). The finding that, in cats, individual Y retinal ganglion cell axons form different types of terminals in the SC (Behan, 1981) than they do in the LGN (Wilson et al., 1984), supports the target control hypothesis. Previous studies from our laboratory (Pallas et al., 1994; Pallas and Sur, 1994) demonstrated that, in "rewired" ferrets, optic tract arbors to the MGN more closely resemble in size and morphology W cell axon arbors in their normal targets (the C laminae of the LGN and the superficial SC), than arbors of axons from the inferior colliculus to the normal MGN. These data argue for afferent determination of axon arbor size and morphology. Afferent specification of connectivity is also supported by the finding that maps and modules can form in novel targets (Frost, 1981; Roe et al., 1991). Thus, retinotopic maps of the visual field have been described in the ventrobasal thalamic (VB) complex and MGN of "rewired" hamsters (Frost, 1981) and in the MGN of "rewired" ferrets (Roe et al., 1991). These findings argue strongly for a self-organizing capacity of afferent inputs, and are consistent with previous evidence for activity-dependent sorting of retinal afferents to the LGN (Shatz and Stryker, 1988; Hahm et al., 1991). However, these

same studies (Frost, 1982; Roe et la., 1991) showed that the orientation and the specific pattern of the visual map in the novel target was quite different from that in the LGN, suggesting that these aspects of the projection might be regulated by the target.

It is likely that the roles of targets and afferents are not mutually exclusive, and that some aspects of the development of connectivity are regulated by afferents while others are regulated by the target. The "rewired" paradigm is particularly well suited to directly address the issue of what aspects of connectivity are afferent or target dependent. In this preparation, retinal afferents are induced to project to novel targets, such as the MGN and LP, whose cytological organization differs significantly from that of normal retinal targets. Major differences in the organization of retinothalamic projections between normal and "rewired" ferrets would argue for target control, while similarities would indicate that afferents play a crucial role in specifying connectivity.

In chapter 2 we address these issues by examining the detailed anatomical organization of retino-MGN and retino -LP projections with respect to their extent, location, binocular organization and pattern of termination within the ectopic targets. We also examine how the adult pattern of retino-MGN projections is established over development. In order to examine the precise anatomical organization and morphology of retino-MGN projections, it is necessary to employ a highly sensitive anterograde tracer that labels axons and terminals in detail, and that can be combined with WGA-HRP for the binocular organization study. For this reason, we have adapted the use of cholera toxin B as an anterograde tracer to label retinofugal projections in adult and developing ferrets. We report on this tracing method in the first part of chapter 2 (chapter 2A).

Role of afferents and input activity patterns in the specification of thalamocortical and intracortical connections

The role of afferent activity on the development of thalamocortical connections and neuronal responses in primary visual cortex has been well documented (see Shatz, 1990, for a

review). If one eye is deprived of vision by suturing the eyelid during the "critical period" of development, most visual cortical cells can be driven only by the non-deprived eye (Hubel and Wiesel, 1970; Hubel et al., 1977; Shatz and Stryker, 1978). Monocular deprivation (MD) at the peak of the critical period, causes a large shift in ocular dominance within 2-3 days of deprivation (Van Sluyters, 1978; Malach et al., 1984). Anatomically, the organization of LGN axons within layer 4 of area 17 is profoundly altered by longer periods of MD: ocular dominance bands representing the non-deprived eye expand, while those representing the deprived eye shrink (Hubel et al., 1977; Shatz and Stryker, 1978). Single axon studies have shown that the anatomical effects of MD are due to altered thalamocortical axon arbors: 1) prolonged MD causes alterations in the morphology of geniculocortical synapses serving the deprived and non-deprived eyes (Friedlander et al., 1991); 2) the size and complexity of geniculocortical arbors are profoundly changed by MD, with the loss of arbors serving the closed eye taking place more rapidly than the expansion of the non-deprived arbors (Antonini and Stryker, 1993b). Blocking retinal activity during the critical period, by intraocular injections of TTX, prevents the segregation of LGN axons into ocular dominance columns (Stryker and Harris, 1986; Antonini and Stryker, 1993a). Physiologically, layer 4 neurons in primary visual cortex (VI), normally monocularly driven, are driven by both eyes.

Intrinsic long-range horizontal connections in primary visual cortex display a clustered pattern in the adult animals (Gilbert and Wiesel, 1979, 1983) , and link cells with similar orientation tuning (Ts'o et al., 1986; Ts'o and Gilbert, 1988; Sharma et al., 1995; but see also Matsubara et al., 1985). Similarly to visual thalamocortical connections, the adult clustered pattern develops from initially diffuse and randomly distributed connections (Callaway and Katz, 1990), and is significantly influenced by lid suture (Callaway and Katz, 1991).

All these studies have involved manipulations of the overall level of activity. To date, only a few studies have examined the effects on the cortex of manipulating the pattern of activity. Artificial strabismus, produced early in development, disrupts normal eye alignment such that corresponding points in the two retinae are never stimulated simultaneously, but the

total amount of vision received by each eye is the same. Neurons in VI become entirely monocular (Van Sluyters and Levitt, 1980) and ocular dominance bands appear sharper and larger than normal (Lowel and Singer, 1993), suggesting that the relative pattern of input activity in the two eyes is important in the sorting of geniculocortical axons into eye-specific patches. Stryker and Strickland (1984) further demonstrated a role for temporal patterning. They first blocked visual activity by intraocular injections of TTX, and then stimulated the optic nerves either synchronously or asynchronously. Synchronous stimulation of the two nerves prevented the formation of ocular dominance columns, which instead formed normally when the two nerves were stimulated asynchronously.

In "rewired" ferrets, the MGN receives visual rather than auditory inputs, and retains its projections to auditory cortex (Pallas et al., 1990). Thus, redirecting retinal fibers to the MGN causes AI to be stimulated early in development, with a very different temporal and spatial pattern of input activity compared to normal AI. For this reason, the "rewired" ferret provides a good model to determine the role of the pattern of input activity in the development of thalamocortical and intracortical projections. In chapter 3 we examine how the pattern of auditory thalamocortical connections in the experimental ferrets differs from that in normal animals. In chapter 4 we compare the patterns of long-range intracortical connections in the normal ferret VI and AI to that in "rewired" AI.

References

Antonini, A., and M.P. Stryker (1993a) Development of individual geniculocortical arbors in cat striate cortex and effects of binocular impulse blockade. J. Neurosci. 13:3549-3573.

Antonini, A., and M.P. Stryker (1993b) Rapid remodeling of axonal arbors in the visual cortex. Science 260:1819-1821.

Asanuma, C., and B.B. Stanfield (1990) Induction of somatosensory inputs to the lateral geniculate nucleus in congenitally blind mice and in phenotypically normal mice. Neurosci. 39:533-545.

Behan, M. (1981) Identification and distribution of retinocollicular terminals in the cat: an electron microscopic autoradiographic analysis. J. Comp. Neurol. 199:1-15.

Callaway, E.M., and L.C. Katz (1990) Emergence and refinement of clustered horizontal connections in the cat striate cortex. J. Neurosci. 10:1134-1153.

Callaway, E.M., and L.C. Katz (1991) Effects of binocular deprivation on the development of clustered horizontal connections in cat striate cortex. Proc. Natl. Acad. Sci. USA 88:745-749.

Campbell, G., and D.O. Frost (1987) Target-controlled differentiation of axon terminals and synaptic organization. Proc. Natl. Acad. Sci. USA 84:6929-6933.

Campbell, G., and D.O. Frost (1988) Synaptic organization of anomalous retinal projections to the somatosensory and auditory thalamus: target-controlled morphogenesis of axon terminals and synapti glomeruli. J. Comp. Neurol. 272:383-408.

Cantore, W.A., and F. Scalia (1987) Ultrastructural evidence of the formation of synapses by retinal ganglion cell axons in two nonstandard targets. J. Comp. Neurol. 261:137-147.

Devor, M. (1975) Neuroplasticity in the sparing or deterioration of function after early olfactory tract lesions. Science 190:998-1000.

Friedlander, M.J., K.A.C. Martin, and D. Wassenhove-McCarthy (1991) Effects of monocular visual deprivation of geniculocortical innervation of area 18 in cat. J. Neurosci. 11:3268-3288.

Frost, D.O. (1981) Orderly anomalous retinal projections to the medial geniculate, ventrobasal and lateral posterior nuclei. J. Comp. Neurol. 203:227-256.

Frost, D.O. (1982) Anomalous visual connections to somatosensory and auditory systems following brain lesions in early life. Dev. Brain Res. 3:627-635.

Frost, D.O. (1986) Development of anomalous retinal projections to non-visual thalamic nuclei in syrian hamsters: a quantitative study. J. Comp. Neurol. 252:95-105.

Frost, D.O., and C. Metin (1985) Induction of functional retinal projections to the somatosensory system. Nature 317:162-164.

Gilbert, C.D., and T.N. Wiesel (1979) Morphology and intracortical projections of functionally identified neurons in cat visual cortex. Nature 280:120-125.

Gilbert, C.D., and T.N. Wiesel (1983) Clustered intrinsic connections in cat visual cortex. J. Neurosci. 3:1116-1133.

Graziadei, P.P.C., R.R. Levine, and G.A. Monti-Graziadei (1979) Plasticity of connections of the olfactory sensory neuron: regeneration into the forebrain following bulbectomy in the neonatal mouse. Neurosci. 4:713-727.

Graziadei, P.P.C., and G.A. Monti-Graziadei (1985) Neuronal changes in the forebrain of mice following penetration by regenerating olfactory axons. J. Comp. Neurol. 247:344-356.

Hahm, J.-O., R.B. Langdon, and M. Sur (1991) Disruption of retinogeniculate afferent segregation by antagonists to NMDA receptors. Nature 351:568-570.

Hubel, D.H., and T.N. Wiesel (1970) The period of susceptibility to the physiological effects of unilateral eye closure in kittens. J. Physiol. 206:419-436.

Hubel, D.H., T.N. Wiesel, and S. LeVay (1977) Plasticity of ocular dominance columns in the monkey striate cortex. Phil. Trans. R. Soc. (Lond.) B 278:377-409.

Kalil, R.E., and E.R. Schneider (1975) Abnormal synaptic connections of the optic tract in the thalamus after midbrain lesions in newborn hamsters. Brain Res 100:690-698.

Law, M.I., K.R. Zahs, and M.P. Stryker (1988) Organization of primary visual cortex (area 17) in the ferret. J. Comp. Neurol. 278:157-180.

Lowell, S., and W. Singer (1993) Monocularly induced 2-deoxyglucose patterns in the visual cortex and lateral geniculate nucleus of the cat: II. Awake animal and strabismic animals. European J. Neurosci. 5:857-869.

Malach, R., R. Ebert, R.C. Van Sluyters (1984) Recovery from effects of brief monocular deprivation in the kitten. J. Neurophysiol. 51:538.

Matsubara, J.A., M. Cynader, N.V. Swindale, and M.P. Stryker (1985) Intrinsic projections with visual cortex: evidence for orientation specific local connections. Proc. Natl. Acad. Sci. USA 82:935-939.

Métin, C, and D.O. Frost (1989) Visual responses of neurons in somatosensory cortex of hamsters with experimentally induced retinal projections to somatosensory thalamus. Proc. Natl. Acad. Sci. USA 86:357-361.

O'Leary, D.D.M., and B.B. Stanfield (1989) Selective elimination of axons extended by developing cortical neurons is dependent on regional locale: experiments utilizing fetal cortical transplants. J. Neurosci. 9:2230-2246.

Palay, S.L., and V. Chan-Palay (1974) Cerebellar Cortex: Cytology and Organization. Berlin: Springer.

Pallas, S.L., A.W. Roe, and M. Sur (1990) Visual projections induced into the auditory pathway of ferrets. I. Novel inputs to primary auditory cortex (AI) from the LP/pulvinar complex and the topography of the MGN-AI projection. J. Comp. Neurol. 298:50-68.

Pallas, S.L., J. Hahm, and M. Sur (1994) Morphology of retinal axons induced to arborize in a novel target, the medial geniculate nucleus. I. Comparison with arbors in normal targets. J. Comp. Neurol. 349:343-362.

Pallas, S.L., and M. Sur (1994) Morphology of retinal axons induced to arborize in a novel target, the medial geniculate nucleus. II.Comparison with arbors from the inferior colliculus. J. Comp. Neurol. 349:363-376.

Rocha, M., F. Clascá, A. Angelucci, and M. Sur (1993) Experimentally induced retino-thalamic projections in ferrets: density and distribution of axon arbors. Soc. Neurosci. Abst. 19:45.

Roe, A.W., S.L. Pallas, J.-O. Hahm, and M. Sur (1990) A map of visual space induced into primary auditory cortex. Science 250:818-820.

Roe, A.W., J. Hahm, and M. Sur (1991) Experimentally induced establishment of visual topography in auditory thalamus. Soc. Neurosci. Abst. 17:898.

Roe, A.W., S.L. Pallas, Y.H. Kwon, and M. Sur (1992) Visual projections routed to the auditory pathway in ferrets: receptive fields of visual neurons in primary auditory cortex. J. Neurosci. 12:3651-3664.

Roe, A.W., P.E. Garraghty, M. Esguerra, and M. Sur (1993) Experimentally induced visual projections to the auditory thalamus: evidence for a W cell pathway. J. Comp. Neurol. 334:263-280.

Scalia, F. (1987) Synapse formation in the olfactory cortex by regenerating optic axons: Ultrastructural evidence for polyspecific chemoaffinity. J. Comp. Neurol. 263:497-513.

Schlaggar, B.L. and D.D.M., O'Leary (1991) Potential of visual cortex to develop an array of functional units unique to somatosensory cortex. Science 252:1556-1560.

Schneider, G.E. (1973) Early lesions of the superior colliculus: factors affecting the formation of abnormal retinal projections. Brain Behav. Evol. 8:73-109.

Sharma, J., A. Angelucci, S.C. Rao, B.R. Sheth, and M. Sur (1996) Auditory cortex with induced visual projections: horizontal connectivity and optical imaging of functional responses. Soc. Neurosci. Abst. 22: in press.

Shatz, C.J., and M.P. Stryker (1978) Ocular dominance in layer IV of the cat's visual cortex and the effects of monocular deprivation. J. Physiol. 281:267-283.

Shatz, C.J., and M.P. Stryker (1988) Prenatal tetrodotoxin infusion blocks segregation of retinogeniculate afferents. Science 242:87-89.

Shatz, C.J. (1990) Impulse activity and the patterning of connections during CNS development. Neuron 5:745-756.

Stryker, M.P., and S.L. Strickland (1984) Physiological segregation of ocular dominance columns depends on the pattern of afferent electrical activity. Invest. Ophthalmol. Vis. Sci. (suppl) 25:278.

Stryker, M.P., and W. Harris (1986) Binocular impulse blockade prevents the formation of ocular dominance columns in cat visual cortex. J. Neurosci. 6:2117-2133.

Sur, M., P.E. Garraghty, A.W. Roe (1988) Experimentally induced visual projections into auditory thalamus and cortex. Science 242:1437-1441.

Sur, M., S.L. Pallas, and A.W. Roe (1990) Cross-modal palsticity in cortical development: differentiation and specification of sensory neocortex. TINS 13:227-233.

Ts'o, D., C. Gilbert, and T.N. Wiesel (1986) Relationships between horizontal connections and functional architecture in cat striate cortex as revealed by cross-correlation analysis. J. Neurosci. 6:1160-1170.

Ts'o, D., and C. Gilbert (1988) The organization of chromatic and spatial interactions in the primate striate cortex. J. Neurosci. 8:1712-1727.

Van Sluyters, R.C. (1978) Reversal of the physiological effects of brief periods of monocular deprivation in the kitten. J. Physiol. (London) 284:1-17.

Van Sluyters, R.C., and F.B. Levitt (1980) Experimental strabismus in kitten. J. Neurophysiol. 43:686-699.

Wilson, J.R., M.J. Friedlander and S.M. Sherman (1984) Fine structural morphology of identified X- and Y-cells in the cat's lateral geniculate nucleus. Proc. R. Soc. Lond. B 221:411-436.

Zahs, K.R., and M.P. Stryker (1985) The projection of the visual field onto the lateral geniculate nucleus of the ferret. J.Comp. Neurol. 241:189-211.

Chapter 1

Experimentally Induced Retinal Projections to the Ferret Auditory Thalamus: Factors Affecting the Formation and Quantity of Anomalous Projections.

Introduction

In the adult brain, each thalamic nucleus receives specific sets of ascending inputs. Conversely, afferent systems establish a very precise pattern of connections with specific thalamic nuclei, and often with multiple targets. A central question in developmental neurobiology is how axons grow to specific regions of the brain and then select appropriate targets. One possibility is that axons are predetermined to make specific sets of connections. The occurrence of developmental "mistakes", such as the formation of transient or exuberant projections to inappropriate targets (reviewed by Innocenti, 1981a; Innocenti, 1981b; Stanfield and O'Leary, 1985; Schneider et al., 1987; Ramoa et al., 1989; Langdon and Frost, 1991), suggests that target choice is not completely prespecified, and that axons have a potential capacity for making connections with targets other than their "proper" ones. However, due to their stereotyped pattern of formation, transient or exuberant projections might be viewed not as erroneous connections but as reflecting a specific axonal program of development of a particular neuronal population. One way of understanding the mechanisms that regulate target choice is to investigate whether the process of target selection can be experimentally modified. Previous studies in rodents (Schneider, 1973; Devor, 1975; Graziadei et al., 1979; Frost, 1981, 1982, 1986; Asanuma and Stanfield, 1990) and ferrets (Sur et al., 1988) have shown that, following early or late brain lesions, axons can be induced to form stable terminal arbors in targets that they would not normally innervate. The occurrence of anomalous connections *in vivo* suggests that the process of target selection is not predetermined, and that if a "preference" of specific afferents for their targets does exist, then this "preference" is relative. Under which conditions can axons choose inappropriate targets? Uncovering the developmental rules that govern the establishment of anomalous connections might shed some light on how normal connections are formed, since these two processes might share similar developmental mechanisms.

Redirection of specific afferents to inappropriate loci has been shown to occur when normal targets are reduced in size early in development , and alternative space is created by partially deafferenting an ectopic target. Thus, for example, in rodents (Schneider, 1973; Frost, 1981, 1982) and ferrets (Sur et al., 1988; Roe et al., 1993), retinal axons have been redirected to the auditory thalamus by partial neonatal ablation of the lateral geniculate nucleus (LGN) and/or the superior colliculus (SC), along with partial deafferentation of the medial geniculate nucleus (MGN). Based on those studies, it was suggested that two important factors that regulate the formation of anomalous connections are the intrinsic tendency of axons to conserve their total amount of terminal arbor, and the competition among axons for terminal space (Schneider, 1973). It was argued that both factors are necessary to induce sprouting of retinal axons into an ectopic target (Roe et al., 1993). Thus, an axon will form connections with inappropriate targets if it is deprived of part of its normal site of termination, and at the same time, it is provided with vacated terminal space (Schneider, 1973). However, studies of cross-modal plasticity seem to indicate that the ability to form abnormal connections is limited. Only a small fraction of axons have been induced to innervate novel targets. Moreover, in ferrets, novel retinal projections to the MGN appear to be formed only by one subpopulation of retinal ganglion cells, namely the W-cells (Roe et al., 1993; Pallas et al., 1994). One possible explanation for the limited induction of fibers to anomalous targets is that only some populations of neurons are endowed with intrinsic plastic properties. Alternatively, since the susceptibility of cells to environmental changes is age dependent, the limited amount of retinal axons that can be induced to innervate the MGN might depend on the developmental age at which the experimental manipulations are performed. According to the latter hypothesis, a larger proportion of cells would undergo plastic changes if their environment were modified at earlier developmental ages (Roe et al., 1993). An alternative hypothesis, and the one that we have tested in the present study, is that what limits the extent of anomalous retinal projections to the MGN is the specific type of manipulations performed at birth. In previous lesion paradigms, both removal of normal

retinal targets and deafferentation of the MGN were incomplete (Frost, 1981,1982; Sur et al., 1988; Roe et al., 1993). If, as previously proposed (Schneider, 1973), these two factors play an essential role in regulating the induction and quantity of anomalous retino-MGN projections, then increasing either or both factors should increase the extent of this projection. In previous studies, ablation of the LGN was obtained indirectly by lesioning the visual cortex. With this type of lesion, although the LGN was reduced in size, a significant part was consistently spared (Sur et al., 1988; Roe et al., 1993). Moreover, deafferentation of the MGN was achieved by transection of the brachium of the inferior colliculus (BIC; Schneider, 1973; Frost, 1982; Sur et al., 1988; Roe et al., 1993), the main ascending pathway to the MGN. However, over the last decade, anatomical studies on the connectivity of the cat MGN have shown that, in addition to brachial afferents from the ipsilateral inferior colliculus (IC), the MGN receives many other ascending auditory and non-auditory inputs from other brainstem nuclei (reviewed by Winer, 1992). If the connectivity of the ferret MGN resembles that of the cat MGN, then ablating the BIC alone should leave many MGN inputs intact.

In the present study, we have tested a specific component of our hypothesis - that more extensive deafferentation of the MGN would cause more extensive retinal innervation - by using anatomical tracing methods to identify the inputs to the ferret MGN before and after moderate or extensive ablation of its normal afferents. We have subsequently examined the roles of extensive normal target removal and ectopic target deafferentation in determining the extent to which retinal ganglion cells could be induced to innervate the medial geniculate nucleus.

Materials and Methods

Animals

The animals used in the present study were pigmented ferrets (*Mustela putorius furo*, family Mustelidae, order Carnivora) bred in our colony or purchased from a vendor (Marshall Farms). A total of 23 adult ferrets were used. Most of these animals (n= 21) had received neonatal brain lesions (see below), while two normal animals were used as controls.

Identification of auditory thalamic afferents by injections of retrograde tracers in the medial geniculate nucleus

To identify sources of inputs to the medial geniculate nucleus (MGN) in normal ferrets and ferrets in which the MGN had been deafferented at birth (see below), retrograde tracers were injected in 2 normal and 4 lesioned adult animals. In adult ferrets that had been operated at birth, a slight but variable displacement of the various thalamic nuclei was usually observed. Thus, in these animals it was impossible to reach the MGN under stereotaxic guidance. For this reason, we developed a surgical protocol to perform intrathalamic tracer injections under direct visual guidance. The animals were pre-anesthetized with a mixture of ketamine (30 mg/kg) and xylazine (1.5 mg/kg). Atropine (0.04 mg/kg) and dexamethasone (0.7 mg/kg) were administered i.m. to prevent respiratory congestion and cerebral edema, respectively. Prophylactic doses of antibiotics were also given at this time (amoxicillin, 20 mg/kg, i.m.). Animals were intubated with an endotracheal tube and placed in a stereotaxic apparatus. Anesthesia was subsequently maintained with 1-2% isofluorane in a 1/1 mixture of nitrous oxide and oxygen. Heart and respiration rates were monitored closely throughout the surgery, body temperature was maintained at 38°C, and fluids (1-2 cc/kg/hr) were administered intravenously to replace blood losses. Surgery was performed under sterile conditions and microscopic observation. After incision of the skin and of the underlying head muscles, a large craniotomy and durotomy were performed. To protect the cortex, small

pieces of spongostan were inserted between the skull and the underlying cortical surface around the anterior and ventral border of the craniotomy. Throughout surgery the cortex was kept moist by repeated irrigations with normal saline. Using a curved and smooth brain retractor, the occipital cortex was gently pulled forward, exposing the posterior veins. These blood vessels were cauterized with an electric bipolar cautery and subsequently cut. The occipital cortex was then gently lifted until the midbrain became visible. To expose the caudal part of the thalamus it was usually necessary to remove part of the overlying cortical white matter and hippocampus by applying a gentle suction. As a result of this surgical procedure the dorsal surface of the LGN could be clearly visualized, and the caudal tip of the MGN appeared as a small structure located just lateral and slightly posterior to the LGN. A micropipette (20-30 μm inside tip diameter) sealed to a 1 μl Hamilton microsyringe was inserted into the caudal tip of the MGN with an anteroventral inclination of 20-30° from vertical, and advanced 0.5-1 mm within the nucleus. A mixture of 3% wheat germ agglutinin conjugated to horseradish peroxidase (WGA-HRP) and 20% HRP in saline (150-250 nl) was pressure injected. In two neonatally operated animals an additional injection of cholera toxin subunit B (CTB) was made in the MGN. CTB (2% in 0.1M phosphate buffer, pH 6.0) was iontophoresed through a glass micropipette (15 μm inside tip diameter) by applying 2 μA positive current in 7 s on/off cycles for 15 min. On completion of surgery, the cortex was allowed to return to its natural position, and the craniotomy was closed with parafilm sealed to the skull with dental acrylic. The muscle and then the skin were sutured with 3-0 Ethilon. Throughout the postoperative period dexamethasone (0.7 mg/kg) and amoxicillin (10-15 mg/kg) were administered every 8 hours. The animals were allowed to survive for 2-3 days, euthanized with sodium pentobarbital (80 mg/kg, i.p.) and transcardially perfused with saline for 3-5 min, followed in most cases by a fixation solution of 1% paraformaldehyde and 1.25% glutaraldehyde in 0.1M phosphate buffer pH 7.4 (PB) for 30 min. In the animals injected with both WGA-HRP/HRP and CTB, 2% paraformaldehyde was used as fixative. In all cases excess fixative was removed from the tissue by perfusing with 5-10% sucrose in PB for 30

min. The brains were then blocked stereotaxically, removed from the skull, cryoprotected and sectioned with a freezing microtome at 40-50 μm in the coronal plane. In two neonatally operated animals the cervical spinal cord was also removed and sectioned in the parasagittal plane. One series of sections was processed using tetramethylbenzidine (TMB) to reveal HRP according to the protocol of Mesulam (1978). In the brains injected with both WGA-HRP/HRP and CTB, another series of sections was post-fixed in 2-4% paraformaldehyde for at least one day after cutting, soaked for 20 min in 90% methanol and 0.3% H_2O_2, to bleach injected peroxidase activity, and then processed for CTB immunohistochemistry according to the protocol of Angelucci et al. (1996). For cytoarchitectonic identification of brain structures, an adjacent series of sections were stained for Nissl substance. Sections were mounted, air dried, dehydrated and coverslipped.

Neonatal surgery to induce retinal innervation of the medial geniculate nucleus

To test whether the extent of the novel retinal projection to the auditory thalamus correlated with the extent of MGN deafferentation and/or the extent of removal of normal retinal targets, we used a variety of combinations of lesions in different animals. The extent of each lesion was also varied. Lesions aimed at reducing or entirely ablating the principal retinal targets included partial or complete ablation of the following brain structures: 1) the visual cortex, to induce partial retrograde degeneration of the lateral geniculate nucleus (LGN); 2) the LGN and/or the pretectal nuclei (PT); 3) the superior colliculus (SC). Lesions aimed at reducing brainstem inputs to the MGN included: 1) transection of the brachium of the inferior colliculus (BIC); 2) transection of ipsilateral extrabrachial auditory inputs (inputs from the ipsilateral nuclei of the lateral lemniscus, the nucleus of the BIC, and the nuclei of the superior olivary complex); 3) ablation of contralateral auditory brainstem inputs; 4) removal of the deep layers of SC; and 5) ablation of both inferior colliculi (IC). In different animals (n=21), lesions were combined as follows: 1) small deafferentation of the MGN with

small or extensive removal of the principal retinal targets; or 2) extensive MGN deafferentation with small or extensive removal of retinal targets (see figure 5 for details).

Surgical procedures were similar to those described previously (Sur et al., 1988; Pallas et al., 1994). One day after birth, ferret kits were anesthetized by hypothermia. Under sterile conditions and microscopic observation, the scalp was incised along the sagittal midline, and a small craniotomy was made in the occipital bone to expose the mesencephalon and the occipital cortex. The visual cortex, SC and IC were directly cauterized. To ablate LGN and PT the caudal aspect of the diencephalon was exposed by gently pulling the occipital cortex forward, and the caudodorsal thalamus was lesioned by heat cauterization. To sever the ipsilateral auditory inputs to the MGN ascending in the BIC, the lateral third of the mesencephalon was coronally sectioned at the midcollicular level. To obtain a more extensive deafferentation of MGN, the lateral mesencephalic cut was extended medial and ventral to the BIC in order to transect ascending ipsilateral extrabrachial inputs. The contralateral auditory brainstem inputs to the MGN were severed by cauterizing the commissure of the SC (SCC) and the contralateral IC. All lesions were made unilaterally, except in five animals which received bilateral lesions. On completion of surgery, the skin was sutured with reabsorbable 5-0 suture. The kits were revived under a heat lamp and returned to the jill for rearing to adulthood. At adulthood, 4 animals received injections of retrograde tracers in the MGN (see above). All the remaining animals received intraocular injections of anterograde tracers (see below).

Labeling of retino-MGN projections by intraocular injections of anterograde tracers

To estimate the extent of retino-MGN projections obtained following different types of lesions, a first group of animals (n=15) received injections of WGA-HRP (4-5% in saline, 8-10 µl) in each eye. To measure axon diameters of the population of retinal cells projecting to the MGN, a separate group of animals (n=2) received injections of CTB (1% in distilled water, 10 µl) into the eye contralateral to the lesioned hemisphere. CTB was previously

shown to yield complete filling of retinofugal fibers (Angelucci et al., 1996), and thus, it is the tracer of choice for examining axon caliber.

Adult animals were anesthetized with ketamine and xylazine and a local anesthetic was applied to the conjunctiva. The tracers were injected into the vitreal chamber using a 10 µl Hamilton microsyringe. Survival times of 2 and 4 days were allowed for the WGA-HRP- and CTB-injected animals, respectively. Fixation, sectioning and processing of WGA-HRP material were performed as described above. Animals injected with CTB were perfused with saline followed by 4% paraformaldehyde, post-fixed in the same fixative overnight, and cut at 40 µm in the coronal plane. CTB was then revealed immunohistochemically (Angelucci et al., 1996). Adjacent series of brain sections were processed for Nissl and cytochrome oxidase.

Data Analysis

Microscopic analysis of CTB labeled sections was carried out under brightfield illumination, while sections reacted with TMB were analyzed under darkfield and polarized light.

Cell bodies and fiber pathways labeled by injections of retrograde tracers in the MGN were reconstructed using camera lucida and a 25x objective. Brainstem and thalamic nuclei, as well as cortical layers were identified on adjacent Nissl stained sections. For each experiment, retrogradely labeled cells were counted on an entire series (1:4) of brain sections.

For each case that had received neonatal brain lesions, verifications of the lesioned structures and of the extent of the lesions was performed on Nissl and cytochrome oxidase stained sections. Lesions were classified as moderate (involving approximately less than 50% of the structure), extensive (> 50%) and complete (100%) by comparison with the contralateral unlesioned side.

To allow for computerized calculations of the extent of retino-MGN projections, camera lucida drawings of coronal MGN sections and WGA-HRP labeling were digitized. One in two sections throughout the rostrocaudal extent of MGN were analyzed for each case.

The area of each MGN section was calculated as the sum of all the pixels in the section. The area of retino-MGN projections was estimated as the sum of all the pixels in the projection. Each pixel in the images corresponded to a square of side 4.2 μm. The extent of retino-MGN projections for each case was expressed as the percentage of the MGN area occupied by retinal projections.

Axon diameters of retinal ganglion cells projecting to the MGN were measured on two coronal and two horizontal CTB stained sections taken from two different adult cases which had received extensive neonatal MGN deafferentation and complete ablation of the SC. The diameter of all the axons entering MGN in these four representative sections (n=44) was measured directly from the camera lucida, using a 100x objective. Because of the large number of filled axons, it was impossible to measure axon diameters in the optic tract. Thus, measurements were taken every 50 μm along the axon trunk, from its point of entrance into the MGN to a distance of 150 μm within the nucleus. Measurements for each axon were then averaged.

Results

The present study was designed to test the hypotheses illustrated in figure 1A-D. Based on available anatomical data in the cat (reviewed in Winer, 1992), we first hypothesized that in addition to inputs from the ipsilateral inferior colliculus (IC), the MGN in ferrets receives afferents from other auditory and non-auditory brainstem nuclei (Fig. 1A). Thus, in order to extensively deafferent the auditory thalamus both collicular and non-collicular inputs would have to be severed. Our second hypothesis was that deafferentation of the MGN is at least one important factor that influences the quantity of anomalous retinal projections to this nucleus. Based on this hypothesis, we predicted that partial ablation of MGN afferents and normal retinal targets would induce only a small fraction of retinal axons to innervate the MGN (Fig. 1B), whereas complete removal of inputs to the MGN would result in a more extensive retinal innervation of this thalamic nucleus (Fig. 1C). No difference in the extent of the novel projection would be observed after partial or complete removal of MGN afferents, if deafferentation of this nucleus were not a crucial factor. Our third hypothesis was that ablation of normal retinal targets may also influence the extent of retinal projections to MGN. This hypothesis predicts that extensive or complete ablation of normal retinal targets, along with extensive MGN deafferentation would further increase the amount of retino-MGN projections, particularly when compared to those obtained after extensive MGN deafferentation and only partial SC and LGN ablation (Fig. 1D).

Identification of inputs to the MGN in normal and experimentally manipulated ferrets

Injections of WGA-HRP and free HRP in the MGN of two normal adult ferrets produced retrograde labeling of cell bodies in several brainstem auditory and non-auditory nuclei. Ascending fibers to the MGN were also retrogradely labeled. One such case is shown in figure 2. The tracer deposits in both cases were of comparable size and were confined to the MGN. The HRP injections sites consisted of a core of dense reaction product surrounded

by a lighter region. In both cases, the core of the injection site in the coronal plane was cigar-shaped, measuring about 0.8-1.0 mm in width (mediolaterally) and 1.3-2.0 mm in length (dorsoventrally). Both injections extended from the caudal tip of the nucleus up to 0.8-1.0 mm anteriorly and involved, at least in part, the ventral (MGv), the dorsal (MGd) and the medial (MGm) subdivisions of the MGN. However, in one case the injection extended more medially, thus including a larger portion of MGm and part of the suprageniculate nucleus (Sg). In the second case (Fig. 2) the injection spared most of Sg.

As expected, following injections of retrograde tracers in the MGN of normal adult ferrets, the majority of the label was found in the ipsilateral IC, and involved all the subdivision of IC, including the central and lateral nuclei, as well as the dorsal cortex (Fig. 2). However, many retrogradely labeled cells were also found in other brainstem nuclei in both hemispheres (Fig. 2). The auditory nuclei that contained the largest number of retrogradely labeled cells were: the contralateral IC, the ipsilateral dorsal nucleus of the lateral lemniscus (LLD), the contra- and ipsilateral ventral nuclei of the lateral lemniscus (LLV), the ipsilateral nucleus of the brachium of the IC (BIN), the ipsilateral nucleus of the trapezoid body (T), and the contra- and ipsilateral superior olivary complex (SO). Within the SO, labeled cells were found in the contra- and ipsilateral lateral and medial nuclei (LSO and MSO, respectively). Moderate projections to the MGN arose also from the contralateral LLD and the ipsi- and contralateral nucleus sagulum (SAG). The main non-auditory afferents to the MGN arose from the ipsilateral thalamic reticular nucleus (RN), the contra- and ipsilateral locus coeruleus (CAE), the dorsal (DR) and the linear central (LC) nuclei of the raphe, and the pontine and midbrain reticular formation (LT), including the magnocellular (FTG), the lateral (FTL), the paralemniscal (FTP) and the central (FTC) tegmental fields on both sides. Moderate non-auditory projections to MGN arose also from the marginal nucleus of the brachium conjunctivum (BCM), the dorsal tegmental nucleus of Gudden (TD), and the ipsilateral SC (mainly from the deep layers, but also from the superficial, retinorecipient layers of SC). Only a few labeled cells were observed in the periaqueductal gray (PAG), the cuneiform nucleus

(Cu), and the contralateral vestibular nuclei (VN). In the case in which the injection site spared most of Sg, and involved only the lateral part of MGm (Fig. 2), no cells were seen in the VN, while only a few neurons were labeled in the deep layers of SC.

Figure 2 shows the pathways followed by ascending brainstem afferents to the MGN. Most retrogradely labeled fibers coursed caudorostrally in the ipsilateral brachium of the inferior colliculus (BIC), and entered the MGN ventromedially. However, just caudal to MGN, at the level where the BIC forms a protrusion on the lateral aspect of the midbrain, many fibers also coursed medial to BIC among the cell bodies of the BIN. At more caudal levels, some labeled axons were located ventral to BIC, in the lateral part of the lateral lemniscus nuclei. Another group of axons entered the MGN dorsomedially, at more rostral levels. These fibers arose from the ipsilateral SC and the contralateral brainstem nuclei. Inputs ascending from the contralateral brainstem crossed the midline at the level of the commissure of the SC (SCC) (Fig. 2).

The above observations suggested that ablation of the BIC and/or ipsilateral IC would spare many afferents to the auditory thalamus. Thus, we examined the sources and pathways of inputs to the MGN in adult ferrets (n=2) that had received partial MGN deafferentation along with partial ablation of retinal targets, at birth. In one case (F88-87), the MGN was partially deafferented by lesioning the ipsilateral BIC and IC (Fig. 3). In the second case (F95-23; not shown), in addition to the ipsilateral BIC and IC, SCC was also ablated in order to sever inputs ascending from the contralateral brainstem. Partial removal of retinal targets was obtained in one case (F88-87) by moderate ablation of the SC and LGN, and in the other case (F95-23) by complete ablation of the SC alone. Large unilateral injections of retrograde tracers in the auditory thalami of these ferrets indicated that, following BIC and IC removal on one side of the brain, many afferents still innervate the MGN (Fig. 3). In case F88-87, the injections site extended anteroposteriorly for about 1.6 mm from the caudal pole of MGN, and involved all the nuclear subdivisions, including also Sg and Po (Fig. 3). In the other case, the tracer deposit was smaller (600 μm in anteroposterior diameter, measured from the caudal

pole of MGN), and involved most of the caudal two third of MGd and MGv and the lateral parts of MGm and Sg. In both cases, label was found in the same brainstem nuclei and, although regional variations in the number of labeled cells were present, the total number of ipsilateral inputs to the MGN was comparable. Generally, on the side ipsilateral to the injection, labeled cells were more numerous in the nuclei of the lateral lemniscus (LLD and LLV), the BIN and in the pontine and midbrain tegmentum (LT). Numerous labeled cells were also observed in the deep layers of the remaining parts of SC (Fig. 3). Moderate projections to the MGN also arose from the ipsilateral CAE, SO and SAG. The two cases differed significantly in the number of labeled cells found in the brainstem nuclei contralateral to the injected MGN. In the case that had received ablation of the ipsilateral BIC and IC alone (F88-87; Fig. 3), four times as many contralateral labeled neurons were observed than in the case in which SCC had also been ablated (F95-23). The contralateral brainstem nuclei that contained a large number of labeled cells in case F88-87 (Fig. 3) were: the nuclei of the lateral lemniscus (LLD and LLV), the IC, the pontine and mesencephalic tegmentum, and the SO. Fewer cells were located in the contralateral BIN, SC, CAE and SAG. By contrast, in case F95-23 many fewer cells were found in the contralateral LLD, LLV and SO, while only a few cells were present in CAE, SAG and IC. No cells were observed in the contralateral SC and BIN; however, numerous inputs still arose from the pontine and mesencephalic tegmentum.

Figure 3 shows the pathways followed by ascending fibers to the MGN after unilateral lesions of BIC and IC. In coronal sections of caudal midbrain, retrogradely labeled fibers were observed in the lateral aspect of the mesencephalon, where they occupied the entire dorsoventral and mediolateral extent of the lateral lemniscus nuclei (LLV and LLD). Some fibers were also observed in the lateral part of the midbrain tegmentum, and appeared to course caudorostrally. In more rostral parts of the midbrain, at SC levels just caudal to the thalamus, although the BIC was clearly absent, a bundle of intensely stained fibers was observed in a region just medial to the site of the lesion. These fibers invaded the BIN and the lateral parts of the spinothalamic tract (STT). Ascending fibers from the contralateral

brainstem crossed the midline in the SCC, as in normal controls, traversed the deep layers of the ipsilateral SC, and either joined the fiber bundle in the BIN, or entered the dorsomedial aspect of the MGN more rostrally. Since in case F88-87 the caudal SC had been ablated at birth, at this level SCC was reduced in size. Fibers were observed to cross the midline in the remaining SCC, but also at more ventral positions, in the PAG.

Thus, following unilateral removal of BIC and IC, many afferents still innervated the MGN. Some of these afferents were fibers that normally do not course in the BIC and, thus, were spared by the lesion. However, other afferents consisted of fibers that followed novel trajectories to reach the MGN.

Injections of retrograde tracers in a ferret (F96-8) that had received a large bilateral transection of the lateral mesencephalon (including BIC and regions ventral to BIC, most of BIN, and the rostral part of LLD and LLV) along with bilateral removal of IC and SC, resulted in a marked reduction in the number of retrogradely labeled cells in the ipsi- and contralateral auditory brainstem nuclei (Fig. 4). The injection site involved most of the anteroposterior extent of the MGN, was centered in MGv, but included also Po and the lateral aspect of MGd and MGm. However, rostrally the tracer deposit also involved small parts of RN, LP and LGN. A large number of retrogradely labeled cells was found in non-auditory brainstem nuclei, including the pontine and mesencephalic tegmentum, the raphe nuclei, CAE and BCM (Fig. 4) . The larger number of labeled cells observed in these nuclei, compared to other lesioned and normal cases, can be attributed to the spread of tracer to the RN and LP. However, the number of inputs from auditory brainstem nuclei was markedly reduced compared to normal controls and cases with less extensive deafferentation of the MGN (see above). Some retrogradely labeled cells were observed in the remaining parts of LLD, LLV and ipsilateral BIN, while only a few cells were labeled in SO (Fig. 4).

Factors affecting the quantity of anomalous retinal projections to the auditory thalamus

We then tested whether the extent of MGN deafferentation correlates with the amount of anomalous retinal projections to the MGN (Fig. 1B-C), and whether extensive removal of normal retinal targets further increases the quantity of this projection (Fig. 1D). In different newborn ferrets, varying degrees of MGN deafferentation were combined with varying degrees of lesion of normal retinal targets (including SC, LGN and PT). Bilateral intraocular injections of WGA-HRP were made in these animals at adulthood, and the percentage of MGN area innervated by retinal fibers was estimated (see Materials and Methods). The results are summarized in figure 5. The animals with the most severe early damage to the ascending auditory pathway showed the most extensive retinal projection to the MGN. By contrast, the extent of removal of normal retinal targets did not correlate with the amount of retino-MGN projections. An example of retinal afferents to the auditory thalamus, following extensive removal of BIC, partial ablation of the ipsilateral IC, and complete lesion of SCC is shown in figure 6. The percentage of MGN innervated by retinal fibers (2%) in this case (F93-67; Fig. 5) was comparable to that observed in another animal (F93-70; Fig. 5) that received a similar extent of MGN deafferentation, but a less extensive removal of retinal targets. Figure 7 shows an example of retino-MGN projections in an animal (F93-158; Fig. 5) that received extensive neonatal MGN deafferentation along with complete bilateral removal of SC and extensive ablation of PT, but no lesion of LGN. The amount of retino-MGN projections in this case (4%), was significantly enhanced compared to animals with less severe removal of MGN inputs but similar ablation of normal retinal targets (compare, for example, cases F93-158 and F93-50; Fig. 5). Similarly, case F95-75 (Fig. 5), that received extensive MGN deafferentation and complete bilateral removal of SC, but no lesion of LGN or PT, showed a significantly larger amount of retino-MGN projections (6%) than case F93-67 (Figs. 5,6) which received a less severe removal of MGN afferents, but a more extensive ablation of normal retinal targets. No significant difference in the percentage of MGN innervated by retinal projections was observed in case F95-75, compared to other cases (F93-11, F93-138 and F93-158; Fig. 5)

with similar extent of MGN deafferentation but more extensive removal of retinal targets. Thus, the amount of anomalous retinal projections correlated well with the extent of MGN deafferentation, but not with the extent of removal of normal retinal targets.

Deafferentation of the auditory thalamus not only affected the quantity of anomalous retinal projections, but also appeared to be necessary to induce sprouting of retinal axons in the MGN. Indeed, regardless of the extent of removal of retinal targets, no or little ectopic projections were found when the BIC was not lesioned or was only minimally damaged, respectively (see for example case F93-50; Fig. 5). The latter results also indicates that ablation of SC and/or LGN alone is not sufficient to generate novel retinal projections. It was more difficult to determine whether deafferentation of MGN is by itself sufficient to induce retinal projections to the MGN, or whether removal of retinal targets is also required. Our results clearly indicated that removal of the LGN was neither necessary to induce retinal axons to the MGN, nor affected the quantity of the anomalous projection (Fig. 5). However, since it was technically difficult to perform a large lateral transection of the midbrain without producing some damage to the overlying SC, we could not directly assess whether removal of the SC is necessary to induce sprouting of retinal axons into the MGN. However, comparisons between cases F93-70 and F93-67 (Fig. 5) suggested that the extent of SC removal does not correlate with the extent of retinal projections to the MGN.

In one extreme case (F93-69; Fig. 5), complete ablation of SC and LGN, along with extensive damage to PT resulted in marked retrograde atrophy of the optic tract and no retinal projections to the MGN (not shown), even though BIC and SCC had been completely ablated. Intense labeling of the remaining retinal targets (nuclei and fiber tracts of the accessory optic system and remnants of PT) on the side of the lesion, as well as on the contralateral, unlesioned side, indicated that WGA-HRP had been effectively transported by retinal cells.

Novel non-retinal inputs to the MGN following early extensive removal of normal auditory afferents

Even after extensive removal of ascending auditory inputs to the MGN, retinal projections innervated approximately 6% of the MGN area (Fig. 5). This percentage reached about 10% in the rostral half of MGN, where most of the retinal afferents terminated. A "preference" of retinal axons for the rostral MGN was consistently observed across cases. Despite extensive removal of auditory afferents and only partial innervation by retinal fibers, the MGN usually appeared normal in size and morphology. This observation suggested that in addition to retinal inputs and remnants of brainstem inputs spared by the neonatal lesion (see above), other input types also innervated the MGN. To test this hypothesis retrograde tracers were injected into the MGN of 2 rewired ferrets (cases F95-23 and F96-8 described above) that had received moderate and extensive MGN deafferentation, respectively, coupled to ablation of SC. The resulting retrograde labeling of cell bodies in both cases revealed that, in addition to retinal fibers, other afferent systems innervated the MGN. Remnants of normal auditory and non-auditory brainstem afferents to the MGN observed in these cases are described above (see also Fig. 4). Novel non-retinal inputs to the MGN (Fig. 9) arose from the contralateral dorsal column nuclei in the medulla, including both the gracile (GR) and cuneate (CUN) nuclei, the contralateral spinal nucleus of the trigeminal nerve (5SP), the contralateral medial and lateral nuclei of the solitary tract (ST), and the contralateral dorsal horn of the cervical spinal cord (the thoracic and lumbar spinal cord were not analyzed). In addition, many more retrogradely labeled cells were observed in the ipsi- and contralateral vestibular nuclei (VN) compared to normal controls (Fig. 4). As in normal ferrets, in the operated ferrets many inputs to the MGN also arose from the reticular thalamic nucleus (RN) and layer 5 and 6 cells of the ipsilateral auditory cortex (not shown). The ratio of retrogradely labeled layer 5 versus layer 6 cells did not appear to differ from normal controls. Thus, as in normal adult animals, many more layer 6 than layer 5 auditory cortical cells projected to the MGN of the neonatally operated ferrets.

Classes of retinal ganglion cells projecting to the medial geniculate nucleus

Previous studies from this laboratory suggested that the novel retino-MGN projection arises from the W-class of retinal ganglion cells (Roe et al., 1993; Pallas et al., 1994). However, in those studies the lesion paradigm to redirect retinal projections to the auditory thalamus included ablation of the visual cortex, to induce partial retrograde degeneration of the LGN. The observation made in the present study that retinal axons can be induced to innervate the MGN without lesioning visual cortex or LGN, led us to examine the retinal cell types that project to the MGN under a lesion paradigm that spared the LGN. Since the MGN is surrounded by normal retinal targets and fiber tracts, it was difficult to deliver a large deposit of retrograde tracers that was exclusively confined to the MGN and did not minimally involve surrounding normal retinal structures. For this reason we did not use retrograde transport to identify retinal ganglion cells, but instead examined the axon caliber of retinal cells projecting to the MGN. Intraocular injections of CTB were made in adult ferrets with early extensive deafferentation of the MGN and complete ablation of the SC, and the diameters of retino-MGN axons were measured (see Materials and Methods). For comparison, we have included previously published data on the caliber of retinal axons in the MGN of ferrets with visual cortical lesions (Pallas et al., 1994), and of X, Y and W axons in the normal ferret LGN (Roe et al., 1989; Pallas et al., 1994). In the present study, the diameters of retinal axons in the MGN were found to range between 0.2 and 3.6 μm (mean= 1.04 μm, s.e.m.= 0.135, n= 44). These values overlap only in part with those reported for retino-MGN axons in previous studies (mean= 0.74 μm, s.e.m.= 0.07, n= 31; Pallas et al., 1994). Figure 10A shows the distribution of the two populations of retino-MGN axons. Comparisons with axon diameters of X axons (mean= 1.96 μm, s.e.m.= 0.10, n= 21; Roe et al., 1989), Y axons (mean= 2.37 μm, s.e.m.= 0.25, n= 6; Roe et al., 1989) and W axons (mean= 0.78 μm, s.e.m.= 0.09, n= 15; Pallas et al., 1994) in the normal LGN (Fig. 10B) demonstrated a complete overlap between the retino-MGN and retino-LGN axon populations, suggesting that the novel retinal projection to the auditory thalamus might arise from all classes of retinal ganglion

cells. However, in the present study, the majority of retino-MGN axons (approximately 60%) were finer than the X and Y LGN axons (Fig. 10B), suggesting that most of the projection arises from retinal W cells.

Discussion

Influence of novel target deafferentation on the establishment of anomalous retinal projections to the medial geniculate nucleus

In the present study, we have shown that abnormal availability of terminal space in the medial geniculate nucleus (MGN) is the factor that most influences the formation and quantity of anomalous retinal projections to the auditory thalamus. The extent of MGN deafferentation correlated well with the extent of the novel projection, and, as previously demonstrated (Schneider, 1973; Roe et al., 1993), this projection did not form when the MGN was not deafferented, regardless of the extent of removal of normal retinal targets. By contrast, no correlation was observed between the extent of ablation of normal retinal targets (SC, LGN, PT) and the amount of anomalous connections. Previous studies reported that both factors, removal of normal retinal targets and MGN deafferentation affect the extent of the anomalous retino-MGN projection (Roe et al., 1993). The discrepancy between our results and those of previous studies may be attributed to differences in the evaluation of the extent of MGN deafferentation. In previous studies, removal of normal MGN afferents was achieved by ablation of the brachium of the inferior colliculus (BIC) and/or the ipsilateral inferior colliculus (IC) (Schneider, 1973; Frost, 1982; Sur et al., 1988; Roe et al., 1993). In the present study, we have shown that, similar to the cat MGN (reviewed in Winer, 1992), the normal ferret MGN receives inputs from several brainstem auditory and non-auditory nuclei, including brachial inputs, mainly from the ipsilateral IC, but also non-brachial inputs. Injections of retrograde tracers revealed that many inputs still innervated the MGN after unilateral ablation of BIC and IC. While some of the remaining inputs consisted of fibers spared by the BIC lesion, many were fibers that reached the MGN via newly created pathways. One possible explanation for this finding is that injured axons were able to regenerate and grow around the injury site by following the course of axons spared by the damage. Consistent with this hypothesis, regeneration of optic, olfactory and pyramidal tract

axons, following early injuries, has been shown to occur in the hamster and rat (Devor, 1975, 1976; Kalil and Reh, 1979; Bernstein and Stelzner, 1981; So et al., 1981; Grafe, 1983). An alternative explanation is that new routes to the MGN were established by axons that had not yet reached the MGN at the time of lesion. Thus, our findings clearly show that unilateral removal of BIC and IC is not sufficient to deafferent the auditory thalamus. By contrast, more severe early damage to the ascending auditory pathway, obtained by performing a large transection of the lateral mesencephalon, along with ablation of SCC and both inferior colliculi, resulted in a marked reduction of MGN inputs from auditory brainstem nuclei.

Extensive deafferentation of the MGN always resulted in more extensive retino-MGN projections. However, retinal fibers could only be induced to innervate approximately 10% of the rostral half of MGN. One possible factor limiting the extent of retinal innervation of the auditory thalamus may be competition between retinal and other afferent systems for vacated terminal space in the MGN. Consistent with this hypothesis, the "denervated" MGN was found to receive some normal inputs from auditory and non-auditory brainstem nuclei, spared by the neonatal lesions, as well as novel inputs from the retina and other sensory nuclei, including somatosensory and visceral nuclei. It is conceivable that all these axonal afferents compete with each other for terminal space in the MGN. Support for competition between afferent axons in the MGN is demonstrated in section B of chapter 2, where we report that axons from the two eyes segregate into eye-specific clusters in the MGN of experimentally manipulated ferrets.

Undamaged axons innervating the MGN at the time of lesion might have a competitive advantage over retinal and other more distantly placed inputs. Thus, remnants of normal inputs spared by the lesion might sprout, retain exuberant projections or fail to retract misplaced collaterals within the MGN in response to denervation. Reactive sprouting of normal undamaged afferents, as well as retention of exuberant or misplaced collaterals into a partially denervated target has been previously shown to occur in several brain regions (Kalil, 1972; Lund, 1972; Lund et al., 1973; Schneider, 1973; Land and Lund, 1979). After early

coagulation of the vibrissa follicles in mice, an increased number of GABA-positive axon terminals (likely arising from the reticular thalamic nucleus) was observed in the ventrobasal complex. Surprisingly, many of these GABA-positive terminals replaced the ablated specific vibrissa afferents (Hámori et al., 1990), indicating that even axons of different types, normally terminating on different parts of the dendritic tree, can compete for terminal space. However, our results suggest that innervation of a deafferented target by novel afferents is not a completely non-specific process. The inputs that innervated the MGN following extensive removal of its afferents were either novel lemniscal afferents of a different sensory modality, or lemniscal and non-lemniscal afferents that normally innervate this nucleus. By contrast, non-lemniscal axons from nuclei that normally do not project to the MGN but are located in its vicinity, such as the substantia nigra, the red nucleus, or other thalamic nuclei, such as the ventrobasal complex or the lateral posterior nucleus, did not invade the deafferented MGN.

Recent anatomical data on specific patterns of connections between the cortex and thalamus, led us to hypothesize that another group of axons that could compete with retinal and other lemniscal afferents in the MGN are the auditory corticothalamic axons from layer 5. In various thalamic nuclei in normal animals, including the auditory thalamus, cortical layer 5 cells make synaptic contacts onto the proximal dendrites of relay neurons (Hoogland et al., 1991; Rouiller and Welker, 1991; Schwartz et al., 1991; Ojima, 1994), where subcortical lemniscal afferents also terminate (Majorossy and Réthelyi, 1968; Jones and Powell, 1969; Jones, 1985). In addition, layer 5 auditory corticothalamic axons are just about to enter the MGN at the time we perform the surgical manipulation (Clascá et al., 1995). Thus, layer 5 axons could compete for terminal space in the MGN with retinal and other lemniscal afferents. Clascá et al. (1995) have shown that the corticothalamic projection from layer 5 is very conspicuous early in development, outnumbering the projection from layer 6 cells. However, by adulthood, projections from layer 6 have markedly increased in number, while those from layer 5 have become drastically reduced. We examined whether removal of the specific MGN lemniscal subcortical afferents might induce stabilization of the early exuberant

projection from cortical layer 5 to the MGN. Following injections of retrograde tracers in the MGN of operated animals, the ratio of layer 5 vs. layer 6 cells did not appear to differ from that in normal adult animals. While this result indicates that exuberant projections from layer 5 cells are not stabilized in the MGN in response to ablation of normal auditory lemniscal afferents, it is still possible that the axons of layer 5 cells, that normally maintain a thalamic projection in the adult animal, sprout within the MGN in response to denervation. Anatomical studies using anterograde tracing methods would be required to test this hypothesis.

Influence of normal retinal target removal on the establishment of anomalous retinal projections to the medial geniculate nucleus

While deafferentation of the medial geniculate nucleus affected both the induction and amount of novel retino-MGN projections, removal of normal retinal targets did not seem to affect the quantity of the anomalous projection. In the present study, animals that received a comparable extent of MGN deafferentation, but a different extent of normal retinal target ablation, showed a similar amount of retino-MGN projections. Moreover, our results clearly indicate that ablation of the LGN is not required for retinal axons to sprout into the MGN. Although it is unclear whether removal of the SC is necessary for the induction of anomalous retinal projections, our findings suggest that the extent of SC removal does not affect the quantity of these projections. In addition, innervation of the "deafferented" MGN by novel afferents, such as somatosensory and visceral sensory fibers, whose normal targets were not ablated, strongly suggests that abnormal availability of terminal space is by itself sufficient to induce novel projections to an ectopic, denervated nucleus. Consistent with this finding, somatosensory fibers have been redirected to the LGN in rats by simply removing the two eyes i.e. by exclusively deafferenting the LGN (Asanuma and Stanfield, 1990).

Paradoxically, our findings seem to suggest that the presence of normal retinal targets is somehow necessary for optic tract axons to sprout into the auditory thalamus. In one case, where complete ablation of the LGN and SC, along with extensive removal of the PT, was

achieved, we observed a marked retrograde degeneration of optic tract fibers and no retinal projections to the MGN. A possible interpretation of this result is that retinal fibers innervating the MGN arise as collaterals of axons directed to normal targets, and that removal of the primary axon prevents the formation of collateral branches. It was previously shown that axonal development occurs in two distinct stages (Schneider et al., 1987; Terashima and O'Leary, 1989; Bhide and Frost, 1991; for a review see Jhaveri et al., 1990): axon elongation, during which axons approach their targets, and branch/arbor formation, during which axons invade targets and form terminal arbors. Recent evidence on the targeting behavior of axons has revealed that the permanent projections of neurons are often formed by collateral branches of an initially elongated primary axon, whose distal segment may eventually be eliminated (Ramoa et al., 1989; for reviews see O'Leary et al., 1990, and O'Leary, 1992). Collateralization begins only after, and may be dependent upon, completion of the first stage, i.e. only after axons have reached their most distal target, having already grown past several of the targets to which they will eventually send collateral branches (Schreyer and Jones, 1982; Jhaveri et al., 1983; Schneider et al., 1985; O'Leary and Terashima, 1988; Bhide and Frost, 1991). Current evidence suggests that for some axonal systems, such as the corticopontine (Heffner et al., 1990) and trigeminal (Erzurumlu et al., 1993) axons, the two stages of axonal growth are influenced by different target-derived cues. At the time we perform the surgical manipulations, retinal axons have already invaded all of their targets. They have already passed the elongation phase and have just entered the collateralization/arborization phase, but their terminal arbors are still fairly immature and susceptible to extrinsic influences (Hahm et al., 1991). Deafferentation of the MGN might, in a manner similar to that described for other axonal systems, trigger the release of an as yet unidentified molecule that stimulates axonal collateralization from the primary axon. If, as proposed, the two stages of axon development are susceptible to different extrinsic influences, then elimination of the main axon trunk will prevent the formation of anomalous connections.

The data presented here are, at least in principle, compatible with the "principle of conservation of total axonal arbor" (Schneider, 1973). Axons that terminate in the MGN might comprise W as well as X and Y axons (see Results and below). In normal animals, W and Y axons innervate the SC, which is partially or completely ablated in lesioned animals. Their arbors in the retinally-innervated MGN might compensate for missing portions of arbors in the SC. X and Y axons, as well as a subset of W axons, innervate the LGN in normal animals. We find that reduction in LGN size has no effect on retinal innervation of the MGN. Thus, the MGN arbors of LGN-projecting retinal ganglion cells either constitute additional terminations by these axons, or are compensated for by reductions in their LGN arbors. Further studies will be needed to examine the issue. An interesting possibility is that LGN-projecting and SC-projecting retinal ganglion cells have different developmental programs that enable them to innervate novel targets: SC-projecting (W) cells might require at least partial removal of their normal targets, while LGN-projecting (X,Y,W) cells might require an existing elongation of the axonal process to normal targets prior to innervating new targets that lie along this path.

Classes of retinal ganglion cells projecting to the medial geniculate nucleus

Previous physiological and anatomical results have suggested that retino-MGN projections arise from the W-class of retinal ganglion cells (RGCs) (Roe et al., 1993; Pallas et al., 1994; Pallas and Sur, 1994). However, the axon diameters of retino-MGN cells reported in our study are compatible with innervation of MGN by all classes of RGCs. This discrepancy might be attributed to the different lesion paradigm used in the present study which, in contrast to previous studies, does not include ablation of visual cortex. It is well established that in normal cats and experimentally manipulated ferrets, neonatal visual cortical lesions result in marked retrograde degeneration of X-RGCs (Tong et al., 1982; Callahan et al., 1984; Payne et al., 1984; Roe et al., 1993) and medium-sized W-RGCs (Rowe, 1990a; Roe et al., 1993). Moreover, it has been reported that following neonatal visual cortical lesions, Y-RGCs

show reduced soma size (Rowe, 1990a) and conduction velocity (Rowe, 1990b) as well as altered axon arbor morphology (Weber et al., 1986). Thus, it is likely that only small W-cells and modified Y-cells survived in the retinae of ferrets that received neonatal ablation of the visual cortex (Sur et al., 1988; Roe et al., 1993; Pallas et al., 1994). Physiological and further anatomical studies would be required to characterize in detail which RGC types innervate the MGN under a lesion paradigm that does not include lesions of the visual cortex or LGN.

Conclusions

We have shown that the abnormal availability of terminal space in the MGN is the main factor affecting the formation and quantity of anomalous retino-MGN projections. However, we have also shown that the retina cannot entirely take over this novel target. Our findings suggest that the factor that appears necessary for the induction of anomalous retinal projections might paradoxically be the same factor that limits the quantity of these projections, namely the competition among different sets of afferent systems for terminal synaptic space.

References

Angelucci, A., F. Clascá, and M. Sur (1996) Anterograde axonal tracing with the subunit B of cholera toxin: a highly sensitive immunohistochemical protocol for revealing fine axonal morphology in adult and neonatal brains. J. Neurosci. Methods *65*:101-112.

Asanuma, C., and B.B. Stanfield (1990) Induction of somatosensory inputs to the lateral geniculate nucleus in congenitally blind mice and in phenotypically normal mice. Neuroscience *39*:533-545.

Bernstein, D., and D. Stelzner (1981) Corticospinal tract (CST) plasticity in the early postnatal rat. Soc. Neurosci. Abst. *7*:678.

Bhide, P.G., and D.O. Frost (1991) Stages of growth of hamster retinofugal axons: implications for developing axonal pathways with multiple targets. J. Neurosci. *11*:485-504.

Callahan, E.C., L. Tong, and P.D. Spear (1984) Critical period for the marked loss of retinal X-cells following visual cortex damage in cats. Brain Res. *323*:302-306.

Clascá, F., A. Angelucci, and M. Sur (1995) Layer-specific programs of development in neocortical projection neurons. Proc. Natl. Acad. Sci. USA *92*:11145-11149.

Devor, M. (1975) Neuroplasticity in the sparing or deterioration of function after early olfactory tract lesions. Science *190*:998-1000.

Devor, M. (1976) Neuroplasticity in the rearrangement of olfactory tract fibers after neonatal transection in hamsters. J. Comp. Neurol. *166*:31-48.

Erzurumlu, R.S., S. Jhaveri, H. Takahashi, and R.D.G. McKay (1993) Target-derived influences on axon growth modes in cultures of trigeminal neurons. Proc. Natl. Acad. Sci. USA *90*:7235-7239.

Frost, D.O. (1981) Orderly anomalous retinal projections to the medial geniculate, ventrobasal, and lateral posterior nuclei of the hamster. J. Comp. Neurol. *203*:227-256.

Frost, D.O. (1982) Anomalous visual connections to somatosensory and auditory systems following brain lesions in early life. Dev. Brain Res. *3*:627-635.

Frost, D.O. (1986) Development of anomalous retinal projections to non-visual thalamic nuclei in syrian hamsters: a quantitative study. J. Comp. Neurol. *252*:95-105.

Grafe, M. (1983) Developmental factors affecting regeneration in the central nervous system: early but not late formed mitral cells reinnervate olfactory cortex after neonatal tract section. J. Neurosci. *3*:617-630.

Graziadei, P.P.C., R.R. Levine, and G.A. Monti-Graziadei (1979) Plasticity of connections of the olfactory sensory neuron: regeneration into the forebrain following bulbectomy in the neonatal mouse. Neuroscience *4*:713-727.

Hahm, J.-O., R.B. Langdon, and M. Sur (1991) Disruption of retinogeniculate afferent segregation by antagonists to NMDA receptors. Nature *351*:568-570.

Hámori, J., J. Takács, R. Verley, P. Petrusz, and E. Farkas-Bargeton (1990) Plasticity of GABA- and glutamate-containing terminals in the mouse thalamic ventrobasal complex deprived of vibrissal afferents: An immunogold-electron microscopic study. J. Comp. Neurol. *302*:739-748.

Heffner, C.D., A.G.S. Lumsden, and D.D.M. O'Leary (1990) Target control of collateral extension and directional axon growth in the mammal brain. Science *247*:217-220.

Hoogland, P.V., F.G. Wouterlood, E. Welker, and H. Van der Loos (1991) Ultrastructure of giant and small thalamic terminals of cortical origin: a study of the projections from the barrel cortex in mice using Phaseolus vulgaris leuco-agglutinin (PHA-L). Exp. Brain Res. *87*:159-172.

Innocenti, G.M. (1981a) Transitory structures as substrates for developmental plasticity of the brain. In M.W. Van Hof and G. Mohn (eds): Functional Recovery from Brain Damage. Dev. Neurosci. *13*:305-333.

Innocenti, G.M. (1981b) Growth and reshaping of axons in the establishment of visual callosal connections. Science *212*:824-827.

Jhaveri, S., M.A. Edwards, and G.E. Schneider (1983) Two stages of growth during development of the hamster's optic tract. Anat. Rec. *205*:225.

Jhaveri, S., M.A. Edwards, R.S. Erzurumlu, and G.E. Schneider (1990) Elongation and arborization of CNS axons. In: (Mal)Nutrition and the Infant Brain. Wiley-Liss., pp. 111-125.

Jones, E.G. (1985) The thalamus. New York: Plenum.

Jones, E.G., and T.P.S. Powell (1969) Electron microscopy of synaptic glomeruli in the thalamic relay nuclei of the cat. Proc. Roy. Soc. B *172*:153-171.

Kalil, R.E. (1972) Formation of new retinogeniculate connections in kittens after removal of one eye. Anat. Rec. *172*:339-340.

Kalil, R.E., and T. Reh (1979) Regrowth of severed axons in the neonatal central nervous system: establishment of normal connections. Science *205*:1158-1161.

Land, P.W., and R.D. Lund (1979) Development of the rat's uncrossed retinotectal pathway and its relation to plasticity studies. Science *205*:698-700.

Langdon, R.B., and D.O. Frost (1991) Development of optic tract axons that project transiently to somatosensory thalamus in the neonatal hamster. J. Comp. Neurol. *310*:200-214.

Lund, R.D. (1972) Anatomic studies on the superior colliculus. Invest. Ophthal. *11*:434-441.

Lund, R.D., T.S. Cunningham, and J.S. Lund (1973) Modified optic pathways after unilateral eye removal in young rats. Brain Behav. Evol. *8*:51-72.

Majorossy, K., and M. Réthelyi (1968) Synaptic architecture in the medial geniculate body (ventral division). Exp. Brain Res. *6*:306-323.

Mesulam, M.M. (1978) Tetramethyl benzidine for horseradish peroxidase neurohistochemistry: a non-carcinogenic blue reaction product with superior sensitivity for visualizing neural afferents and efferents. J. Histochem. Cytochem. *26*:106-117.

Ojima, H. (1994) Terminal morphology and distribution of corticothalamic fibers originating from layers 5 and 6 of cat primary auditory cortex. Cerebral cortex *6*:646-663.

O'Leary, D.D.M. (1992) Development of connectional diversity and specificity in the mammalian brain by the pruning of collateral projections. Current Opinion in Neurobiol. *2*:70-77.

O'Leary, D.D.M., and T. Terashima (1988) Cortical axons branch to multiple subcortical targets by interstitial axon budding: implications for target recognition and "waiting periods". Neuron *1*:901-910.

O'Leary, D.D.M., A.R. Bicknese, J.A. De Carlos, C.D. Heffner, S.E. Koester, L.J. Kutka, and T. Terashima (1990) Target selection by cortical axons: alternative mechanisms to establish axonal connections in the developing brain. Cold Spring Harb. Symp. Quant. Biol. *55*:153-468.

Pallas, S.L., and M. Sur (1994) Morphology of retinal axons induced to arborize in a novel target, the medial geniculate nucleus. II. Comparison with arbors from the inferior colliculus. J. Comp. Neurol. *349*:363-376.

Pallas, S.L., J.-H. Hahm, and M. Sur (1994) Morphology of retinal axons induced to arborize in a novel target, the medial geniculate nucleus. I. Comparison with arbors in normal targets. J. Comp. Neurol. *349*:343-362.

Payne, B.R., H.E. Pearson, and P. Cornwell (1984) Transneuronal degeneration of beta retinal ganglion cells in the cat. Proc. R. Soc. Lond. B *222*:15-32.

Ramoa, A.S., G. Campbell, and C.J. Shatz (1989) Retinal ganglion ß cells project transiently to the superior colliculus during development. Proc. Natl. Acad. Sci. USA *86*:2061-2065.

Roe, A.W., P.E. Garraghty, and M. Sur (1989) Terminal arbors of single ON-center and OFF-center retinal ganglion cell axons within the ferret's lateral geniculate nucleus. J. Comp. Neurol. *228*:208-242.

Roe, A.W., P.E. Garraghty, M. Esguerra, and M. Sur (1993) Experimentally induced visual projections to the auditory thalamus: evidence for a W cell pathway. J. Comp. Neurol. *334*:263-280.

Rouiller, E.M., and E. Welker (1991) Morphology of corticothalamic terminals arising from the auditory cortex of the rat: A Phaseolus vulgaris-leucoagglutinin (PHA-L) tracing study. Hearing Res. *56*:179-190.

Rowe, M.H. (1990a) Evidence for degeneration of retinal W cells following early visual cortical removal in cats. Brain Behav. Evol. *35*:253-267.

Rowe, M.H. (1990b) Reduced conduction velocity of retinal Y-cell axons following partial removal of their central targets. Brain Res.

Schneider, G.E. (1973) Early lesions of superior colliculus: factors affecting the formation of abnormal retinal projections. Brain Behav. Evol. *8*:73-109.

Schneider, G.E., S. Jhaveri, M.A. Edwards, and K.-F. So (1985) Regeneration, re-routing, and redistribution of axons after early lesions: changes with age, and functional impact. In J.C. Eccles and M. Dimitrijevic (eds): Recent Achievements in Restorative Neurology 1: Upper Motor Neuron Functions and Dysfunctions. Karger, Basel, pp. 291-310.

Schneider, G.E., S. Jhaveri, and W. Davis (1987) On the development of neuronal arbors. In C. Chagas and R. Linden (eds): Developmental Neurobiology of Mammals. Vatican City: Pontifical Academy of Sciences, pp. 31-64.

Schreyer, D.J., and E.G. Jones (1982) Growth and target finding by axons of the corticospinal tract in prenatal and postnatal rats. Neuroscience *8*:1837-1853.

Schwartz, M.L., J.J. Dekker, and P.S. Goldman-Rakic (1991) Dual mode of corticothalamic synaptic termination in the mediodorsal nucleus of the rhesus monkey. J. Comp. Neurol. *309*:289-304.

So, K.-F., G.E. Schneider, and S. Ayres (1981) Lesions of the brachium of the superior colliculus in neonate hamsters: correlation of anatomy with behavior. Expl. Neurol. *72*: 379-400.

Stanfield, B.B., and D.D.M. O'Leary (1985) The transient corticospinal projection from the occipital cortex during postnatal development in the rat. J. Comp. Neurol. *238*:236-248.

Sur, M., P.E. Garraghty, and A.W. Roe (1988) Experimentally induced visual projections into auditory thalamus and cortex. Science *242*:1437-1441.

Terashima, T., and D.D.M. O'Leary (1989) Growth and branching of cortical axons: implications for target selection by developing axons. Soc. Neurosci. Abst. *15*:875.

Tong, L., P.D. Spear, R.E. Kalil, and E.C. Callahan (1982) Loss of retinal X-cells in cats with neonatal or adult visual cortex damage. Science *217*:72-75.

Weber, A.J., R.E. Kalil, and L.R. Stanford (1986) Morphology of single, physiologically identified retinogeniculate Y-cell axons in the cat following damage to visual cortex at birth. J. Comp. Neurol. *282*:446-455.

Winer, J.A. (1992) The functional architecture of the medial geniculate body and the primary auditory cortex. In D.D. Webster, A.N. Popper and R.R. Fay (eds): The Mammalian Auditory Pathway: Neuroanatomy. New York: Springer-Verlag, pp. 222-409.

Figure Legends

Figure 1. Hypothetical factors affecting the quantity of anomalous retinal projections to the medial geniculate nucleus (MGN). **A:** projections in normal animals. The retina projects mainly to the superior colliculus (SC) and lateral geniculate nucleus (LGN). By analogy with the cat MGN, we hypothesize that the MGN in ferrets receives projections from the ipsilateral inferior colliculus (IC) as well as from other auditory and non-auditory brainstem nuclei (other). **B:** experimental paradigm employed in previous studies to induce retinal projections to the MGN. If the SC is ablated, the LGN reduced in size, and alternative terminal space is created by removing the ipsilateral IC, or sectioning fibers ascending from it (namely the BIC), a small proportion of retinal axons project to MGN. **C:** If extent of MGN deafferentation affects the amount of anomalous retinal connections, then removing all the inputs to the MGN would induce a larger fraction of retinal axons to sprout into this nucleus. **D:** If both extent of MGN deafferentation and removal of normal retinal targets affect the quantity of retino-MGN projections, then complete removal of the SC, LGN, and MGN afferents would induce an even larger proportion of retinal cells to project to the auditory thalamus.

Figure 2. Ascending brainstem inputs to the medial geniculate nucleus (MGN) in a normal adult ferret. Camera lucida drawings of coronal sections of the ferret caudal thalamus and brainstem from rostral (top) to caudal (bottom) levels. The core of the horseradish peroxidase injection site in the MGN, and the surrounding halo are represented in black and gray, respectively. Dots represent retrogradely labeled cells, lines are retrogradely labeled fibers. In addition to inputs from the ipsilateral inferior colliculus (IC), many other brainstem nuclei in both hemispheres project to the ferret MGN. See Results for abbreviations.

Figure 3. Ascending brainstem inputs to the medial geniculate nucleus (MGN) following moderate MGN deafferentation. Camera lucida drawings of coronal sections of the caudal thalamus and brainstem of an adult ferret that received neonatal unilateral ablation of the BIC and IC. The core and halo of the HRP injection site in the MGN are indicated in black and gray, respectively. Dots represent retrogradely labeled cells, lines are retrogradely labeled fibers. After BIC and IC removal many inputs to the MGN are left intact (see Results). Many fibers follow novel pathways to reach the MGN (compare with Fig. 2). See Results for abbreviations.

Figure 4. Ascending brainstem inputs to the medial geniculate nucleus (MGN) following extensive MGN deafferentation. Camera lucida drawings of coronal sections of the caudal thalamus and brainstem of an adult ferret that received extensive bilateral lesions of the lateral mesencephalon, and bilateral ablation of the superior and inferior colliculus. The core and halo of the HRP injection site in the MGN are indicated in dark and light gray, respectively. Dots represent retrogradely labeled cells. Inputs to the MGN from auditory brainstem nuclei are markedly reduced compared to normal controls and cases with less extensive MGN deafferentation. See Results for abbreviations. A: anterior; D: dorsal.

Figure 5. Factors affecting the quantity of anomalous retinal projections to the medial geniculate nucleus (MGN). The extent of removal of MGN afferents and normal retinal targets is indicated in the two central columns. White, gray and black circles indicate the approximate percentage of a given structure that was lesioned at birth. The resulting amount of retino-MGN projections obtained in each lesioned case is indicated on the far right column. White, gray and black circles indicate the percentage of MGN area innervated by retinal fibers. Note that the amount of novel projections to the MGN correlates well with the extent of removal of MGN afferents, but not with the extent of removal of normal retinal targets (see Results).

BIC: brachium of the inferior colliculus; **BIN**: nucleus of the brachium of the inferior colliculus; **cIC**: contralateral inferior colliculus; **iIC**: ipsilateral inferior colliculus; **LGN**: lateral geniculate nucleus; **LLD**: dorsal nucleus of the lateral lemniscus; **LLV**: ventral nucleus of the lateral lemniscus; **PT**: pretectal nuclei; **SC**: superior colliculus; **SCC**: commissure of the superior colliculus; **STT**: spinothalamic tract.

Figure 6. Novel retinal projections to the medial geniculate nucleus (MGN) following moderate MGN deafferentation. **Left:** line drawings of coronal sections of a ferret standard thalamus and brainstem from rostral (top) to caudal (bottom) levels. Gray areas represent the extent of the lesion performed at birth in case F93-67 (see Fig. 5), estimated by comparison with the contralateral, unlesioned side. **Right:** Camera lucida drawings of coronal sections of the MGN in the same case, from rostral (top) to caudal (bottom) levels, showing the extent of the novel retinal projections obtained as a result of the neonatal lesions shown on the left. See Results for abbreviations.

Figure 7. Novel retinal projections to the medial geniculate nucleus (MGN) following extensive MGN deafferentation. **Left:** line drawings of coronal sections of a ferret standard thalamus and brainstem from rostral (top) to caudal (bottom) levels. Gray areas represent the extent of the lesion performed at birth in case F93-158 (see Fig. 5), estimated by comparison with the contralateral, unlesioned side. **Right:** Camera lucida drawings of coronal sections of the MGN in the same case, from rostral (top) to caudal (bottom) levels, showing the extent of the novel retinal projections obtained as a result of the neonatal lesions shown on the left. See Results for abbreviations.

Figure 8. Novel non-retinal inputs to the medial geniculate nucleus (MGN) following extensive removal of normal auditory MGN afferents. Camera lucida drawings of coronal sections of the medulla in case F96-8 (Fig. 5), showing cells (dots) retrogradely labeled by an

injection of WGA-HRP/HRP in the left MGN (the injection site of this case is shown in Fig. 4). See Results for abbreviations. A: anterior; D: dorsal.

Figure 9. Comparisons of retino-MGN axon diameters with different populations of retinal axons. **A:** comparison of retino-MGN axon diameters observed in this study (retino-MGN axons) with retino-MGN axon diameters following lesions of the visual cortex (retino-MGN axons after VC lesion). **B:** comparison of retino-MGN axon diameters observed in the present study with normal ferret retino-LGN X, Y and W axons. The retino-MGN population of this study is similar to the normal retino-LGN population.

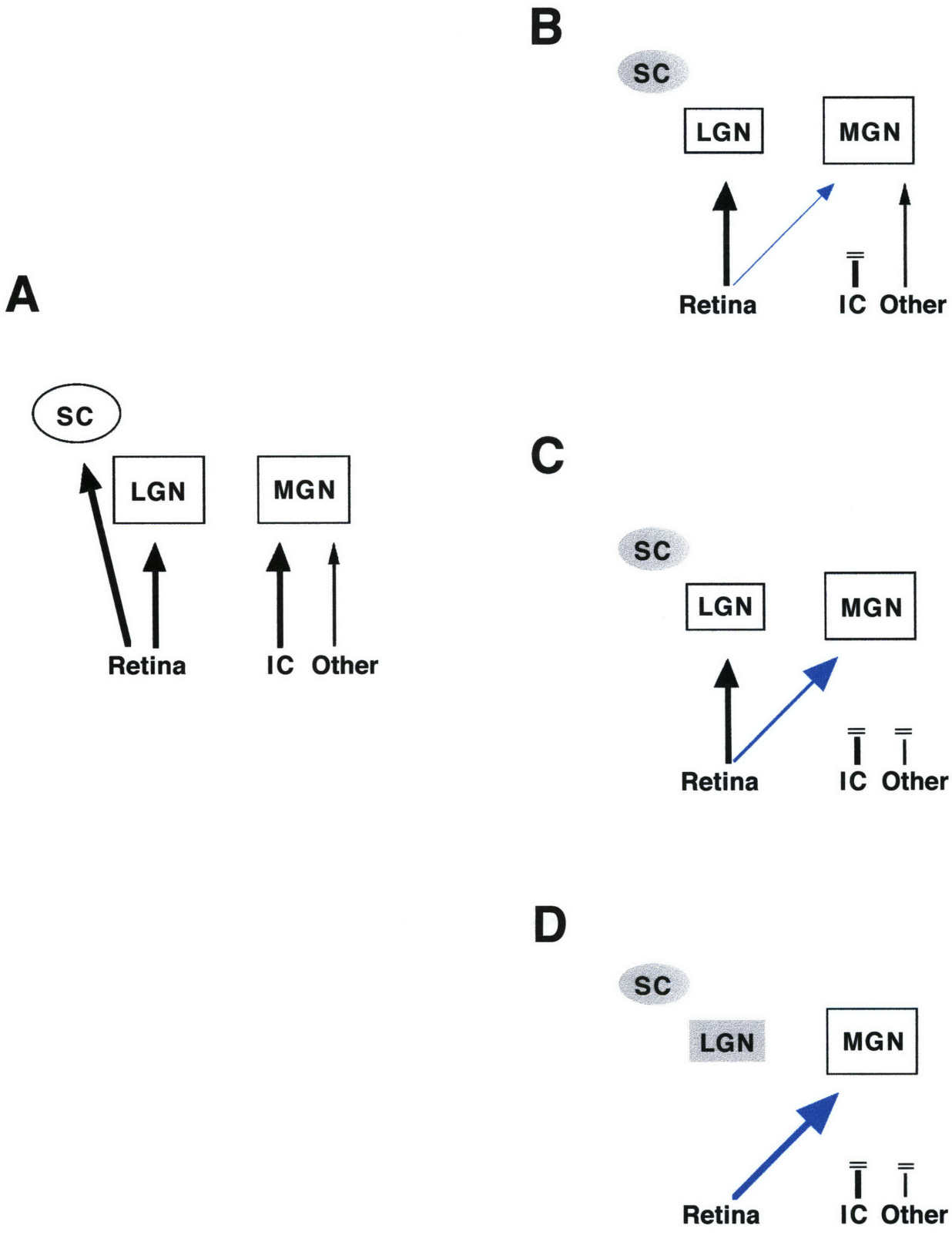
A
SC
LGN
MGN
Retina
IC
Other
B
SC
LGN
MGN
Retina
IC
Other
C
SC
LGN
MGN
Retina
IC
Other
D
SC
LGN
MGN
Retina
IC
Other

Fig. 1

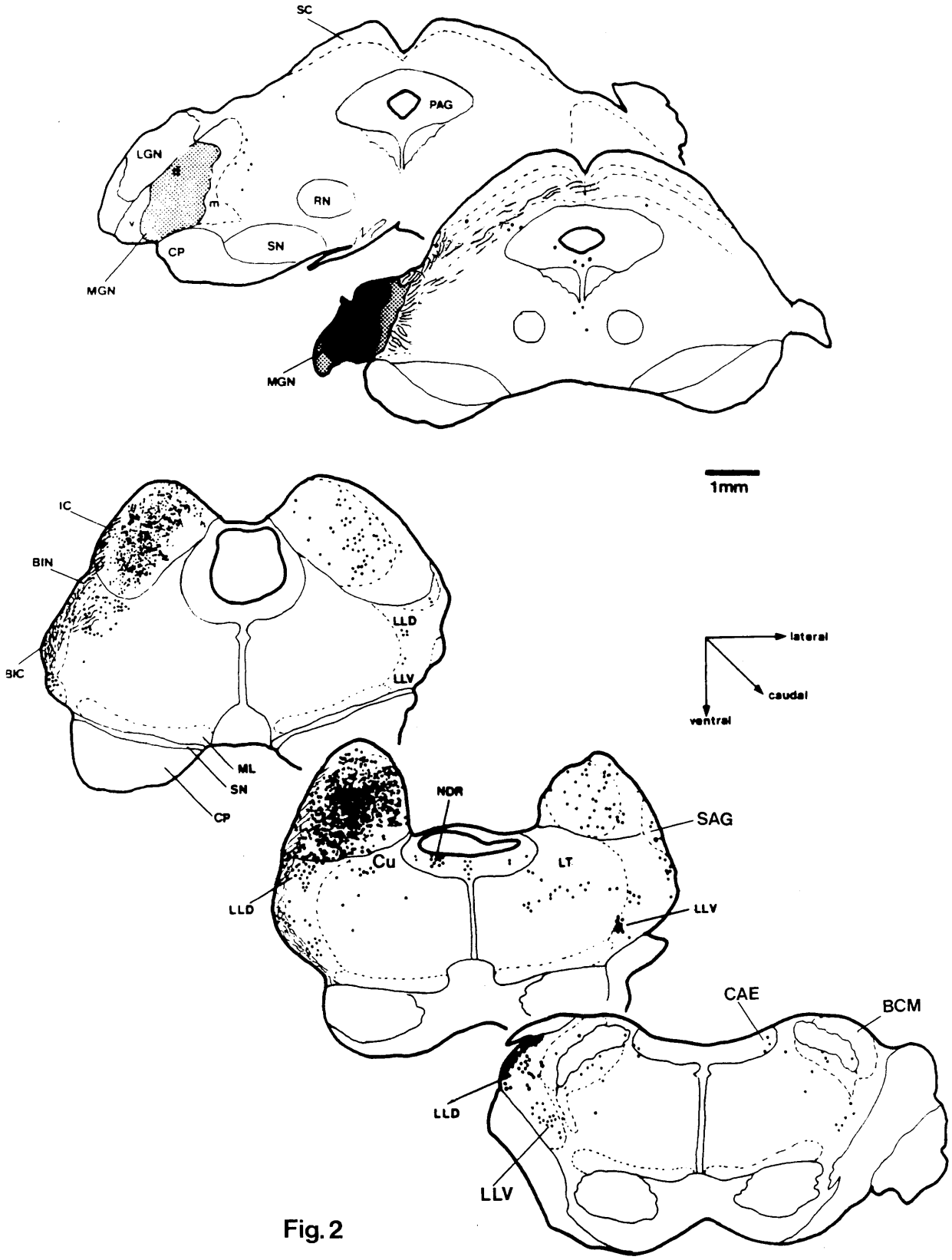
SC
PAG
LGN
RN
SN
CP
MGN
MGN
1mm
IC
BIN
BIC
LLD
LLV
ML
SN
CP
lateral
caudal
ventral
NDR
SAG
Cu
LT
LLD
LLV
CAE
BCM
LLD
LLV

Fig. 2

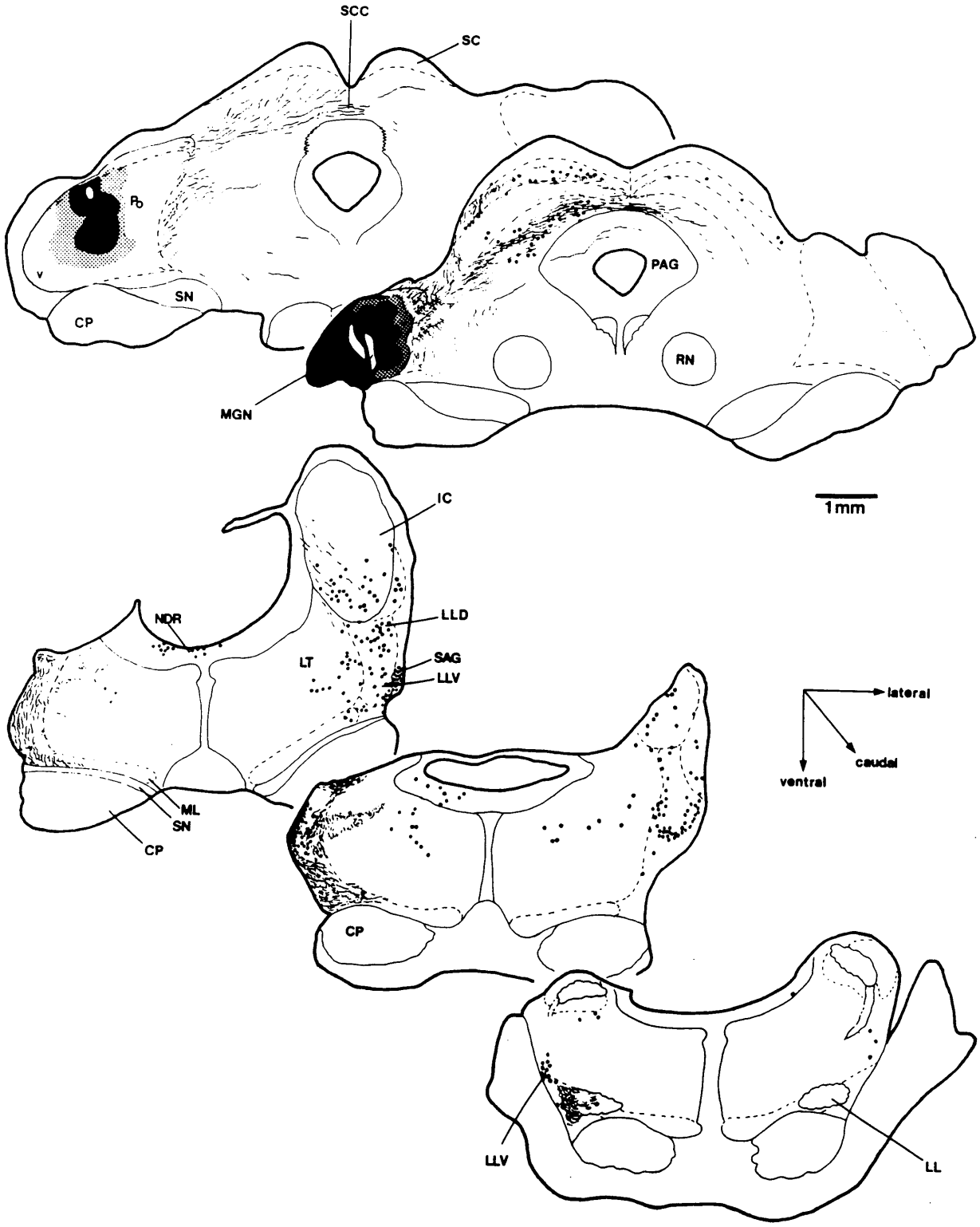
SCC
SC
Pb
v
SN
CP
MGN
PAG
RN
1mm
IC
NDR
LLD
LT
SAG
LLV
lateral
caudal
ventral
ML
SN
CP
CP
LLV
LL

Fig.3

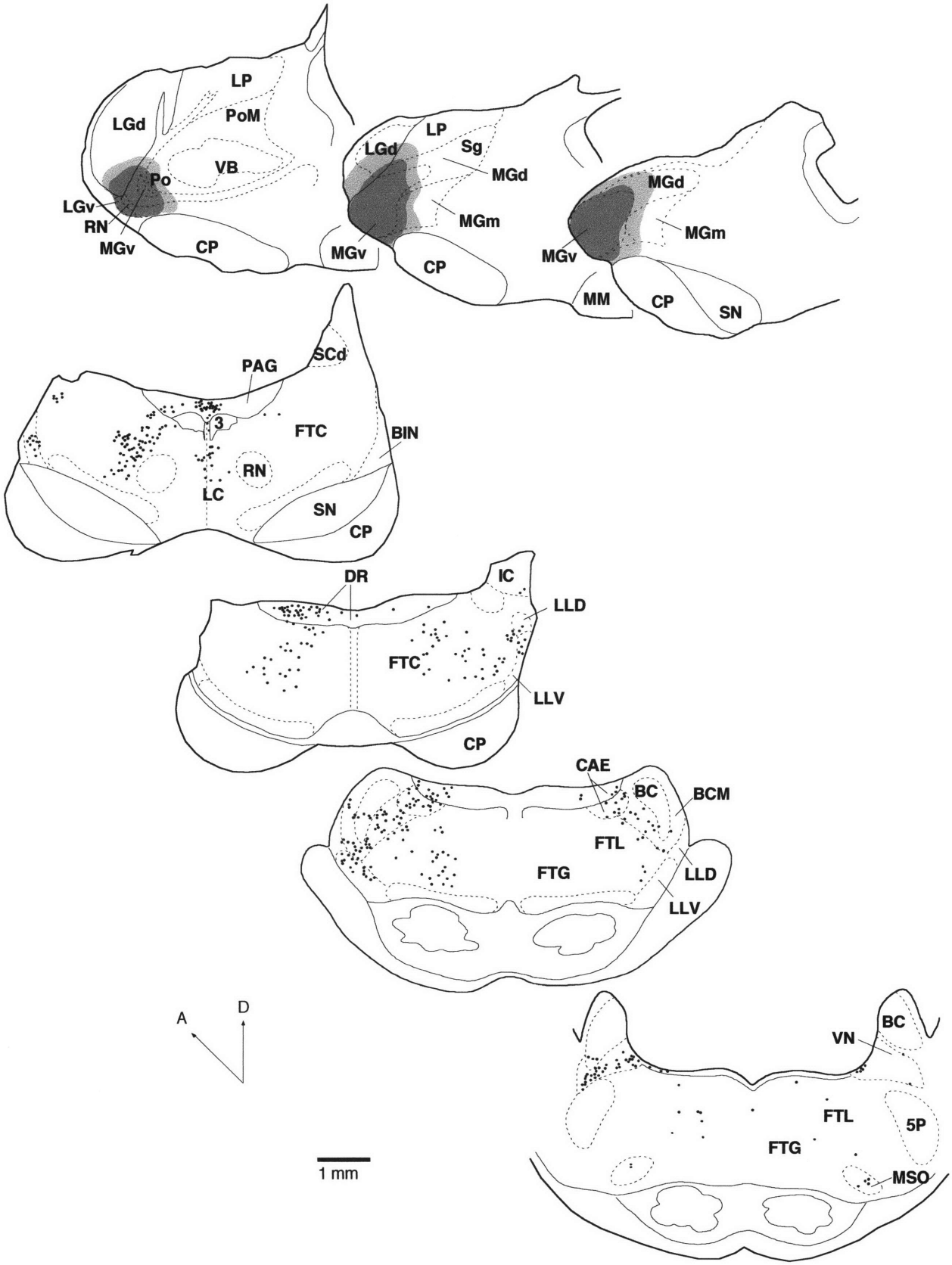
LP
PoM
LGd
VB
Po
LGv
RN
MGv
CP
LP
LGd
Sg
MGd
MGm
MGv
CP
MGd
MGm
MGv
MM
CP
SN
PAG
SCd
3
FTC
BIN
RN
LC
SN
CP
DR
IC
LLD
FTC
LLV
CP
CAE
BC
BCM
FTL
FTG
LLD
LLV
A
D
BC
VN
FTL
5P
FTG
MSO
1 mm

Fig. 4

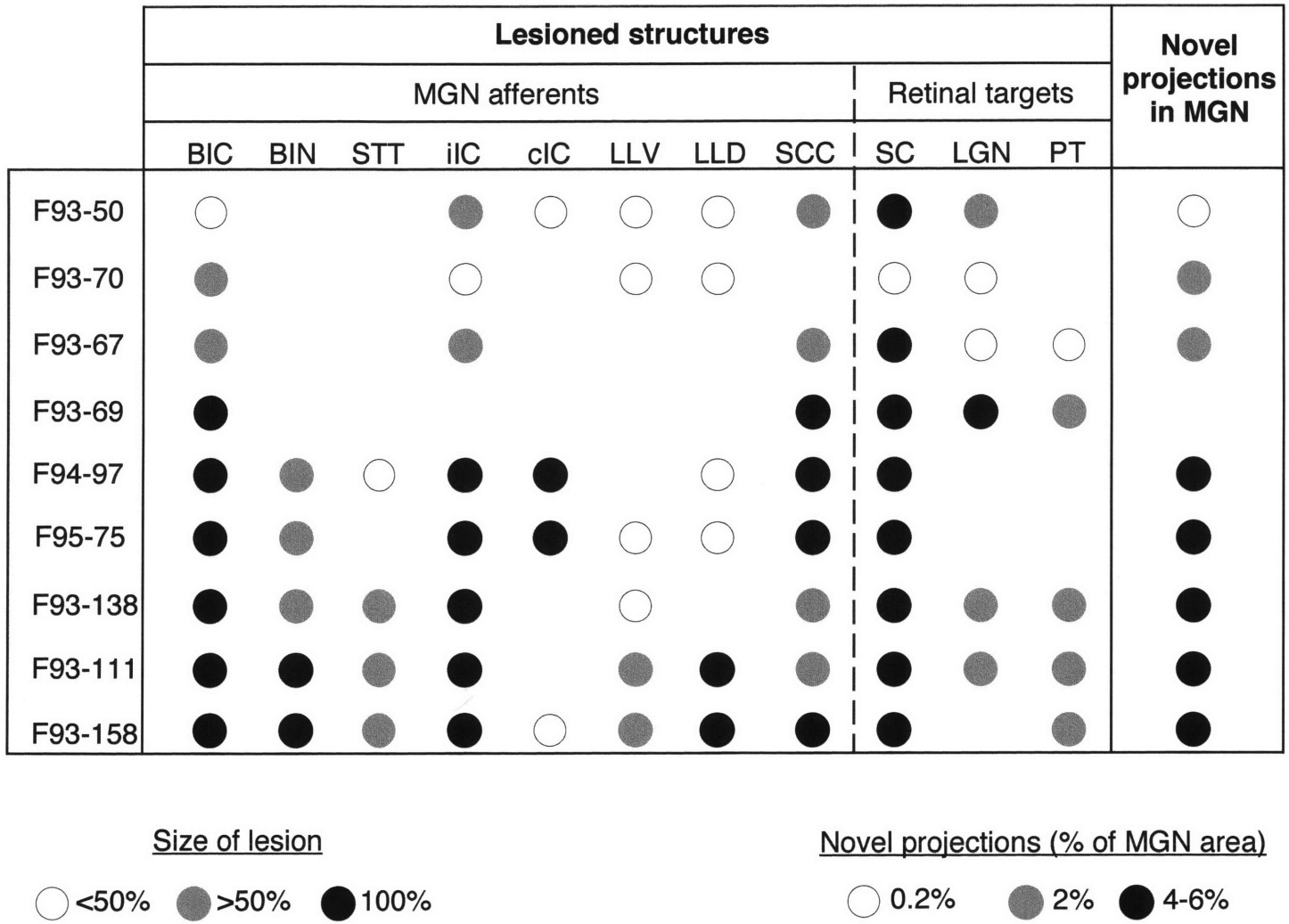
Lesioned structures
MGN afferents
Retinal targets
Novel projections in MGN
BIC
BIN
STT
iIC
cIC
LLV
LLD
SCC
SC
LGN
PT
F93-50
F93-70
F93-67
F93-69
F94-97
F95-75
F93-138
F93-111
F93-158
Size of lesion
<50%
>50%
100%
Novel projections (% of MGN area)
0.2%
2%
4-6%

Fig. 5

F93-67

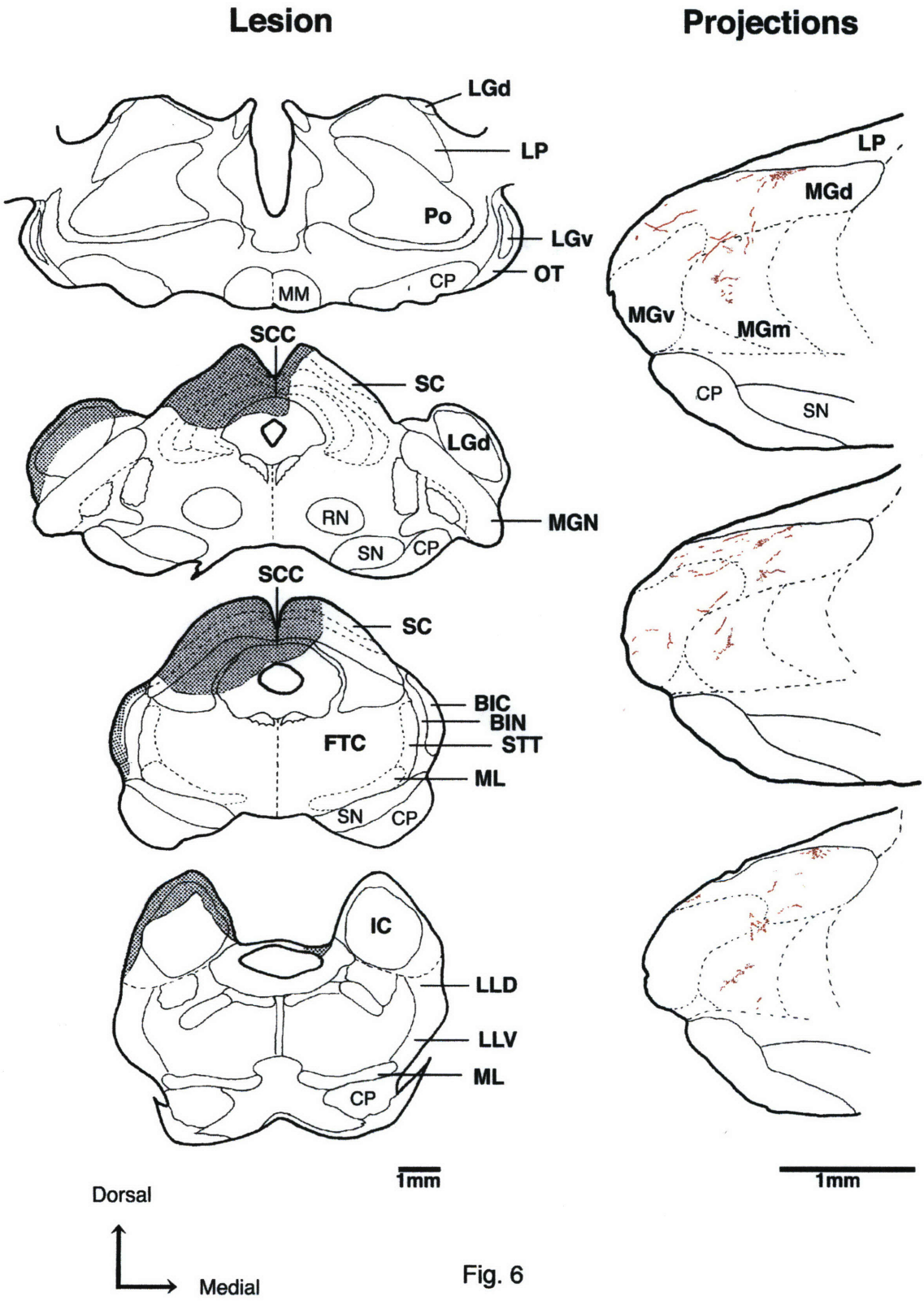
Lesion
Projections
LGd
LP
Po
LGv
OT
MM
CP
SCC
SC
LGd
RN
MGN
SN
CP
SCC
SC
BIC
BIN
FTC
STT
ML
SN
CP
IC
LLD
LLV
ML
CP
1mm
LP
MGd
MGv
MGm
CP
SN
1mm
Dorsal
Medial

Fig. 6

F93-158

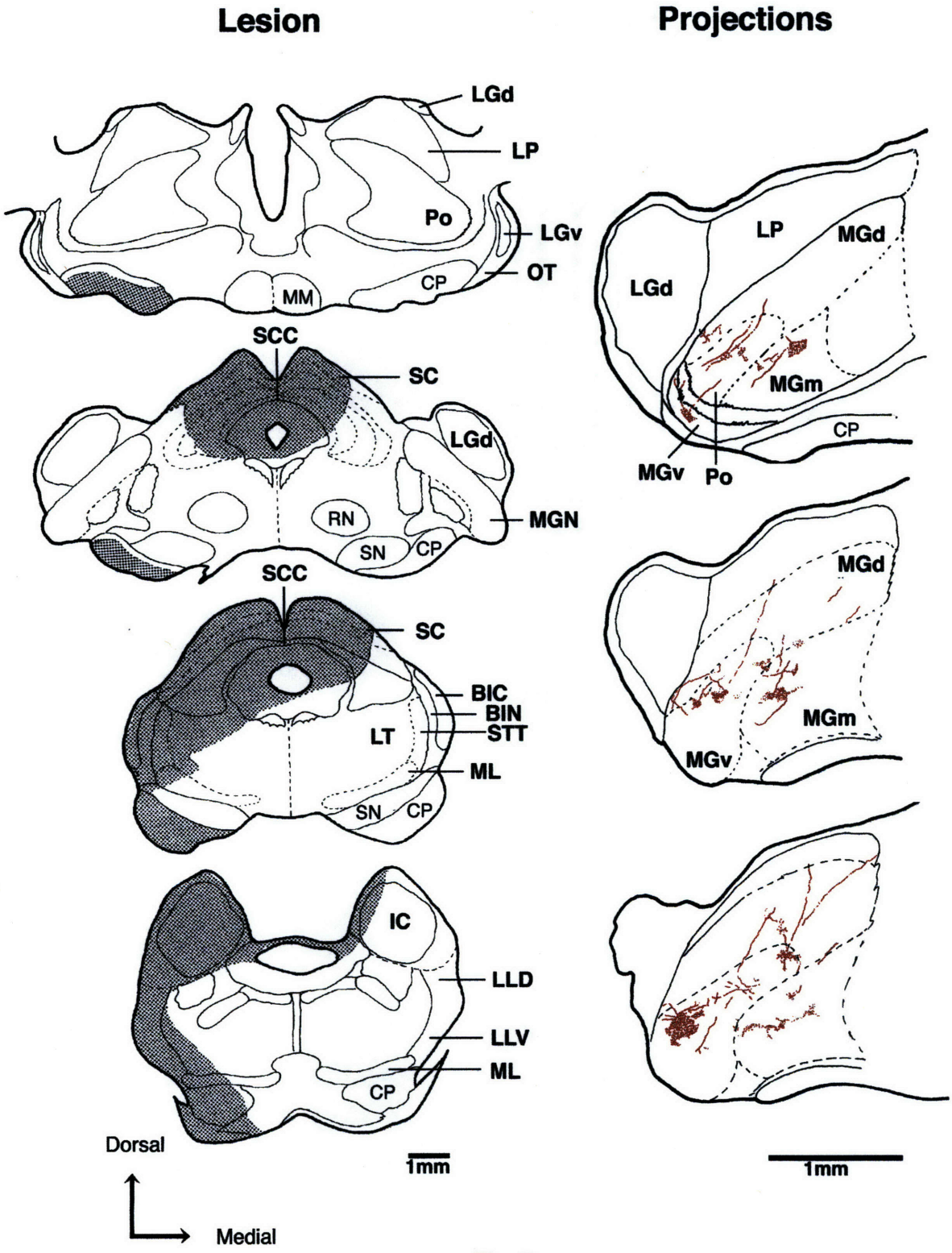
Lesion
Projections
LGd
LP
Po
LGv
OT
MM
CP
SCC
SC
LGd
RN
MGN
SN
CP
SCC
SC
BIC
BIN
STT
LT
ML
SN
CP
IC
LLD
LLV
ML
CP
Dorsal
Medial
1mm
LP
MGd
LGd
MGm
CP
MGv
Po
MGd
MGm
MGv
1mm

Fig. 7

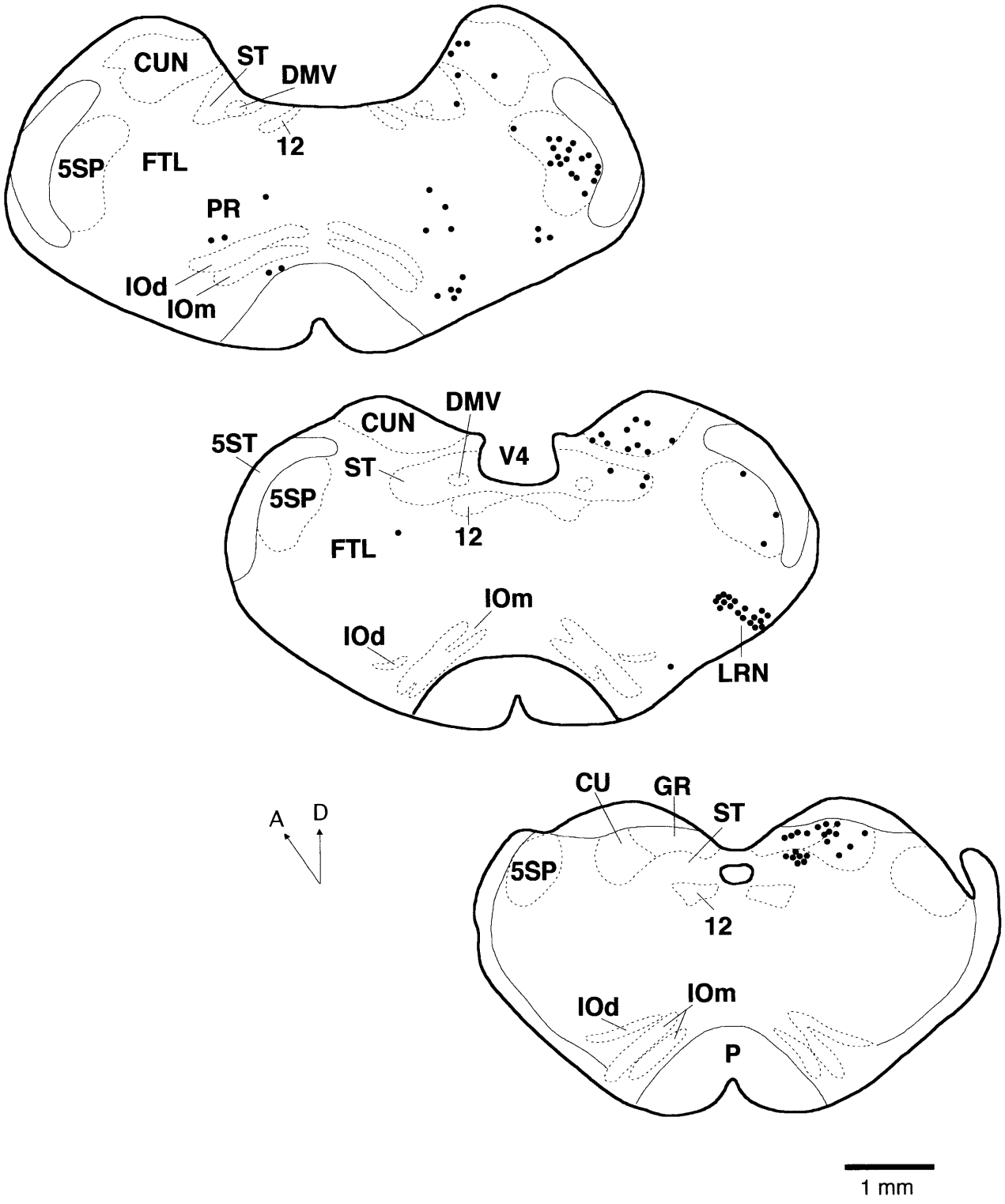
CUN
ST
DMV
12
5SP
FTL
PR
IOd
IOm
DMV
CUN
5ST
V4
ST
5SP
12
FTL
IOm
IOd
LRN
A
D
CU
GR
ST
5SP
12
IOd
IOm
P
1 mm

Fig. 8

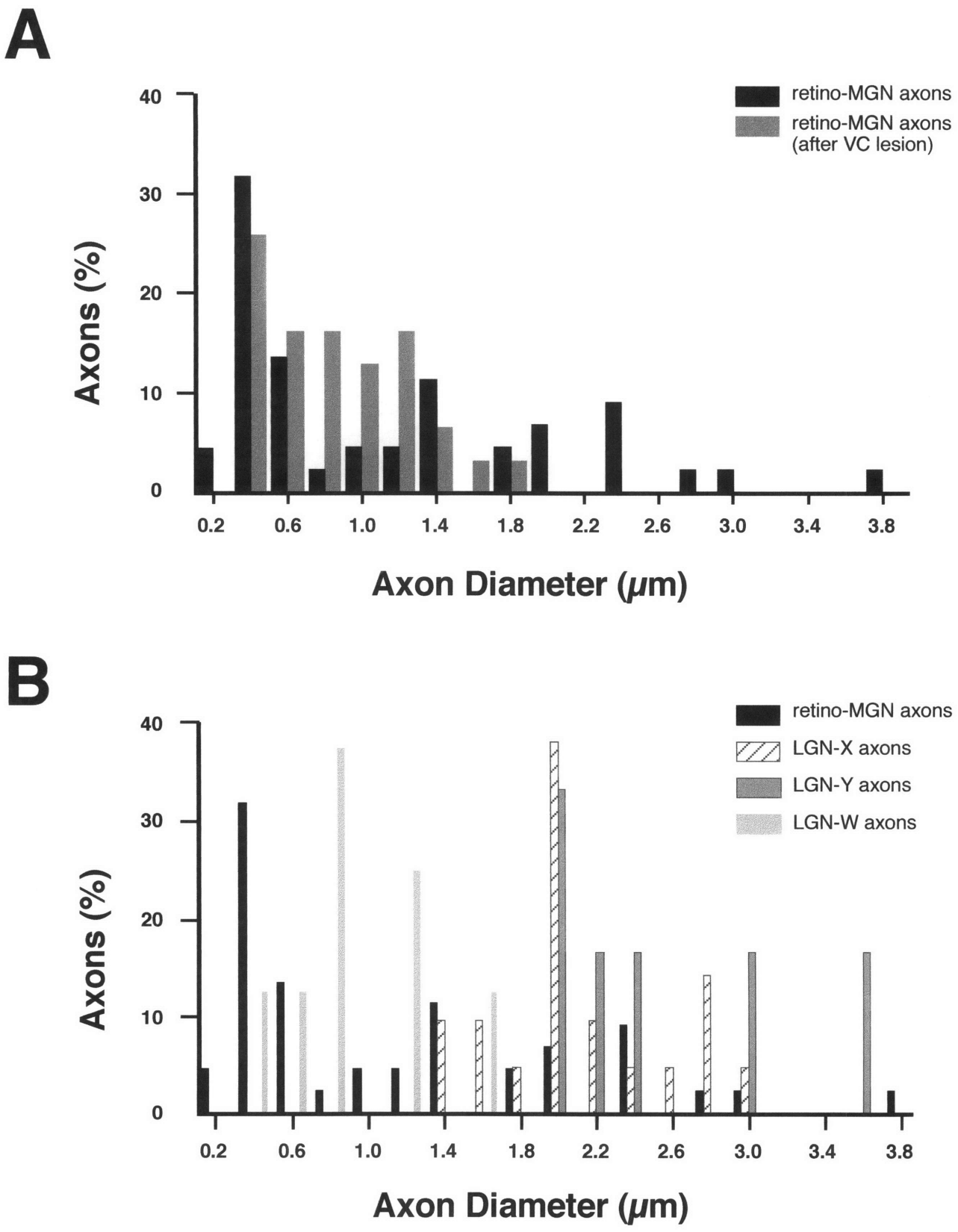
A
retino-MGN axons
retino-MGN axons
(after VC lesion)
Axons (%)
40
30
20
10
0
0.2
0.6
1.0
1.4
1.8
2.2
2.6
3.0
3.4
3.8
Axon Diameter (μm)
B
retino-MGN axons
LGN-X axons
LGN-Y axons
LGN-W axons
Axons (%)
40
30
20
10
0
0.2
0.6
1.0
1.4
1.8
2.2
2.6
3.0
3.4
3.8
Axon Diameter (μm)

Fig. 9

Chapter 2

Anterograde Axonal Tracing with the Subunit B of Cholera Toxin: A Highly Sensitive Immunohistochemical Protocol for Revealing Fine Axonal Morphology in Adult and Neonatal Brains.

Introduction

Few known anterograde axonal tracers reveal in detail the fine morphology of axons and their terminals. Among these are the plant lectin *Phaseolus Vulgaris* Leucoagglutinin (PHA-L; Gerfen and Sawchenko, 1984), Biocytin (King et al., 1989), Biotinylated Dextrans (Brandt and Apkarian, 1992) and Dextran-conjugated Rhodamine (Schmued et al., 1990). A limitation common to these tracers, however, is their relative lack of versatility. Factors such as the species or the age of the animal, or the particular neuronal pathway, may render the tracers unsuitable, due to reduced uptake, transport, or detectability, or a combination of these factors. Several of these problems occur, for example, when tracers are injected in the vitreal chamber of the eye to label the entire retinofugal projection. Similarly, most anterograde axonal tracers show a markedly reduced sensitivity when applied to label central connections in neonatal animals (Payne et al., 1988; Ramirez et al., 1990; Claps and Casagrande, 1991).

In the course of a series of studies on the retinofugal and thalamocortical pathways in adult and neonatal ferrets, we employed a variety of anterograde tracers. Among them, we tried the subunit B of Cholera Toxin (CTB). Although well known as a retrograde tracer (Luppi et al., 1987; Ericson and Blomqvist, 1988; Luppi et al., 1990) CTB had been only occasionally used for anterograde tracing, mainly due to the poor detail of the fiber labeling compared to other tracers (Ericson and Blomqvist, 1988; Bruce and Grofova, 1992). We have introduced modifications to the immunohistochemical method of Mikkelsen (1992) that significantly enhance the quality of the fiber staining. We report that, using this method, CTB yields complete and highly detailed anterograde axonal labeling, both after injections in the eye, and in the brain of young postnatal animals. In addition, we have developed a protocol that allows us to combine, in alternate sections, CTB immunostaining with tetramethylbenzidine (TMB) histochemical staining of wheat germ agglutinin conjugated to horseradish peroxidase (WGA-HRP; Mesulam, 1978).

Materials And Methods

Intraocular injections of tracers

To label anterogradely the entire retinofugal projection, we made unilateral or bilateral intraocular injections of one of the tracers indicated in Table I, in adult or in young postnatal (aged 4-54 days) pigmented ferrets (*Mustela putorius furo*). Animals were purchased from a commercial supplier or bred in our colony. Some of the CTB and WGA-HRP eye injections (18 in adults and 22 in postnatals) were made in animals that had been surgically manipulated at birth to reroute retinal axons to the auditory thalamus (Sur et al., 1988; Roe et al., 1993).

Animals older than 27 days were anaesthetized with ketamine (30 mg/kg) and xylazine (1.5 mg/kg). Between the age of 14 and 27 days only ketamine (40 mg/kg) was administered, while younger animals were anaesthetized by deep hypothermia. A 0.5% proparacaine hydrochloride solution was applied to the conjunctiva. Using a Hamilton microsyringe, we injected 10 µl (in adults) or 2-6 µl (in postnatals) of a solution of one of the tracers listed in Table I. After allowing a survival period for axonal transport (Table I), the animals were administered an overdose of sodium pentobarbital (80 mg/kg) and transcardially perfused with saline for 5 minutes, followed in most cases by 4% paraformaldehyde in 0.1 M phosphate buffer pH 7.4 (PB) for 30 minutes. The WGA-HRP-injected animals were perfused with 1% paraformaldehyde and 1.25% glutaraldehyde for 30 minutes, followed by a 5-10% sucrose solution in PB for 30 minutes. The brains were removed from the skull, post-fixed overnight in the same fixation solution at 4°C, and cryoprotected by soaking in 30% sucrose in PB for 24-48 hours at 4°C. The brains injected with WGA-HRP were soaked in 30% sucrose in PB without postfixation. The tissue was then freeze-sectioned at 40-50 µm.

Some of the animals (n=13) received injections of CTB into one eye and of WGA-HRP into the other eye. In animals older than 27 days we injected CTB into one eye as described above and, two days later, we injected 10 µl of a 4-5% solution of WGA-HRP into

the other eye. Two further days of survival were allowed prior to perfusion. In younger animals, 2-6 μl of each tracer were administered on the same day, and 1-2 days of survival allowed for transport. The animals were perfused with saline, followed by 2% paraformaldehyde in PB at 4°C for 30 minutes, and then the excess fixative was removed from the tissue by perfusing with 5-10% sucrose in PB for 30 minutes, before cryoprotecting and sectioning as above.

Intracerebral injections

We tested the performance of CTB as an anterograde tracer when injected directly into the brain tissue. For this purpose, a series of CTB injections was made in the cerebral cortex or thalamus of adult ferrets and postnatal animals aged 1 to 21 days. For comparison, we made similar injections of PHA-L, Biotinylated Dextran, Dextran Rhodamine and WGA-HRP in some further adult and postnatal cases (Table II).

In adult ferrets, anesthesia was induced with ketamine (30 mg/kg) and xylazine (1.5 mg/kg). Anesthesia was subsequently maintained with 1-2% isofluorane in 1:2 mixture of nitrous oxide and oxygen. Young animals were anaesthetized as described above. A small craniotomy and durotomy were performed over the area of interest, and the tracers (with the exception of Dextran Rhodamine) delivered iontophoretically through glass micropipettes (5-20 μm inside tip diameter) by applying positive current in 7 sec. on/off cycles. For CTB injections we used 2-3 μAmp current for 2-10 min., while 7-8 μAmp of current for 10-20 min. were used to deliver Biotinylated Dextran, PHA-L and WGA-HRP. Dextran Rhodamine (0.5-2μl) was pressure injected using a Picospritzer (General Valve) and glass micropipettes of 20-30 μm inside tip diameter. After appropriate post injection survival (Table II), the brains were fixed and sectioned as described above.

Staining procedures

To visualize anterogradely transported CTB, PHA-L, or WGA we used peroxidase-based immunohistochemistry. WGA-HRP was revealed by TMB histochemistry (Mesulam, 1978) and Biotinylated Dextran either using the high-affinity binding of an avidin-Alkaline Phosphatase conjugate (AP), or that of the avidin-biotin-HRP complex (ABC; Elite®, Vector). Dextran-Rhodamine was directly visualized under epifluorescence microscopy.

The CTB immunohistochemical protocol. The following steps were carried out on free-floating sections, under constant agitation at room temperature (RT) unless otherwise specified:

1) Rinsing 3 X 5 min. in 0.1M phosphate-buffered saline pH 7.4 (PBS).

2) Incubation in 0.3% H_2O_2 in PBS for 20 min.

3) Rinsing 3 X 5 min. in PBS, and then in 0.1M glycine (1 X 30 min.), followed again by rinsing in PBS (3 X 5 min.).

4) Incubation in 4-5% normal rabbit serum (NRS; Vector Labs), 2.5% bovine serum albumin (BSA; Boehringer Mannheim) and 0.3-0.5% Triton X-100 in PBS overnight at 4°C.

5) Rinsing 2 X 5 min. in PBS.

6) Incubation in goat anti-CTB (List Biological Labs, Campbell, CA) diluted 1:4000 in a PBS solution containing 2% NRS, 2.5% BSA, 2% Triton X-100, for either 2 days at RT or 4 days at 4°C.

7) Rinsing for 1 hour in 3-4 changes of PBS, followed by 1 X 10 min. in 2% NRS + 2.5% BSA.

8) Incubation in biotinylated rabbit anti-goat IgG (Vector Labs) diluted 1:200 in 2% NRS, 2.5% BSA and 1% Triton X-100 in PBS, for 1 hour.

9) Repeat step #7.

10) Incubation in ABC diluted 1:100 in PBS, for 1 hour.

11) Rinsing 4 X 15 min. in PBS and then 2 x 5 min. in 0.05M Tris buffer pH 7.4 (TB).

12) Incubation in 0.5% $CoCl_2$ in TB for 10 min.

13) 1 x 1 min. rinse in TB followed by 2 x 5 min. rinse in PBS.

14) Soaking in 3,3'-diaminobenzidine tetrahydrochloride (DAB; Sigma) 0.025% in PBS. After 5 min., 0.004% H_2O_2 was added to the solution, and 2-3 min were allowed for development.

15) Rinsing 5 X 1 min. in PBS, to stop the reaction.

As a non-carcinogenic alternative peroxidase substrate to DAB, Vector VIP® (Vector Labs) which produces an intense purple stain, can be used. Right after step #10, sections were washed for 1 hour in 3-4 changes of PBS and then incubated in VIP for 3-5 min. The reaction was then stopped by rinsing 2 X 5 min. in distilled water.

After the immunostaining was completed sections were immediately mounted onto gelatin-chromalum-coated slides, air dried, dehydrated in graded alcohols, defattened in Histoclear (National Diagnostic) for 20 min., and coverslipped with DePeX. We used bright and dark field optics at 32-800X for analyzing the labeling.

For brevity, the protocol described above is the one which yielded the best staining. In the course of this study, however, we systematically modified various parameters such as: a) time of incubation (1-5 days) in primary antibody (at RT vs. 4°C) and in Triton X-100; b) concentration of Triton X-100 (0 to 2%); c) thickness of the tissue sections (40 - 50 μm); and d) use of metal-enhanced vs. plain DAB staining, or Vector VIP® staining.

CTB immunohistochemistry and HRP histochemistry combined in adjacent tissue sections. For this procedure, we perfused the brains according to the light fixation protocol described above. We collected serial 40 μm-thick freeze-sectioned tissue slices in PB. WGA-HRP was revealed in one series of sections according to Mesulam's (1978) TMB method. The adjacent series of sections was postfixed in 2-4% paraformaldehyde for 2 to 24 hours. Peroxidase activity was bleached away by incubation for 20 minutes in a solution containing

90% methanol and 0.3% H_2O_2 in distilled water, and CTB immunohistochemistry was carried out as described above, starting from step #3.

PHA-L immunohistochemistry. PHA-L immunostaining was carried out using a slightly modified version of Gerfen and Sawchenko's (1984) protocol. Sections were first incubated overnight in a blocking solution containing 2% NRS, 2,5% BSA and 0.5-0.7% Triton X-100 in 0.02M potassium phosphate-buffered saline pH 7.4 (KPBS), and then transferred for 48 hours to a 1:3000 dilution of primary goat anti-PHA-L (Vector Labs) in KPBS containing 2% NRS and 2.5% BSA at 4°C. After a 3 X 10 min. rinse in KPBS, the tissue was incubated in a 1:200 dilution of biotinylated secondary antibody (rabbit anti-goat IgG; Vector Labs) in the same buffer with 0.5% Triton X-100, for 1 hour at RT. The final steps of the immunostaining were performed as for CTB (see above), starting from step #10.

Free WGA immunohistochemistry. We incubated the tissue sections at 4°C in one of the following dilutions of primary goat anti-WGA IgG (Vector Labs): 1:1000, 1:2000, 1:3000 and 1:5000 in PB containing 2% NRS, 2.5% BSA and 1% or 2% Triton X-100. After 1-4 days of incubation at 4°C, we rinsed the sections in PBS (5 X 5 min.), and incubated them in a 1:200 dilution of biotinylated rabbit anti-goat IgG (Vector Labs) for 1 hour at RT. We performed the remaining steps as for CTB (see above), starting from step #10.

Staining of Biotinylated Dextrans. For detection of Biotinylated Dextrans by means of alkaline phosphatase binding, we followed a modified version of Brandt and Apkarian's (1992) protocol. We pre-incubated the sections for 20 minutes in 90% methanol and 0.3% H_2O_2 in distilled water. After rinsing in Tris buffer pH 8.0 (5 X 5 min.), the tissue was incubated overnight at RT in a solution containing 0.1% ExtrAvidin®-Alkaline Phosphatase (Sigma), 0.1% Sodium Azide, and 1% Triton X-100 in Tris buffer pH 8.0. We then rinsed (6 X 5 min.) in Tris buffer pH 9.5, and developed the staining in a solution containing 0.08% of

5-Bromo-4-Chloro-3-indolyl Phosphate (BCIP; Sigma) 5% N,N-dimethyl-formamide (Sigma), 0.0125% Levamisole (Sigma), and 0.008% Nitro Blue Tetrazolium (NTB; Sigma) in Tris buffer pH 9.5. After 2-3 hours, we stopped the developing by rinsing in PB (5 X 5 min.). For dehydration, exposure to alcohols was short (20 sec. 70%, 90% and 100% alcohol solutions, respectively). Defattening and coverslipping were as for CTB.

For visualization of Biotinylated Dextrans by means of ABC binding, we first incubated the sections overnight in a blocking solution containing 2% NRS and 0.7% Triton X-100 in 0.02M PB overnight. After rinsing in PBS (5 X 5 min.), the tissue was transferred to a 1:100 solution of ABC Elite® for 2 hours at RT. Subsequently, we proceeded as for CTB (see above) from step #11 on.

Results

First, we describe our results after CTB injections in the vitreal chamber of the eye, either alone or combined with injections of WGA-HRP in the other eye for analysis of binocular relationships. Subsequently, we give an account of our observations after injections of other anterograde tracers in the vitreal chamber. Finally, we report our findings after injections of tracers into the brain tissue of adult and postnatal animals.

Labeling of retinofugal projections after CTB eye injections

Following injections of CTB in the eye, both in adult and neonatal ferrets, our immunohistochemical protocol revealed heavy anterograde axonal transport to all retinal targets (Fig. 1). High-contrast fiber staining was present in major targets, such as the eye specific layers of the lateral geniculate nucleus (LGN; Figs. 1A-C), the medial interlaminar nucleus (MIN; Fig. 1A) the superior colliculus, and the pretectal nuclei (PT; Fig. 1E). Sharp labeling was also present in the suprachiasmatic nucleus of the hypothalamus (SCN; Fig. 1D), and the nuclei of the accessory optic system. Likewise, in animals which had developed ectopic retinal projections as a result of surgical manipulations at birth (cf. Sur et al., 1988), such projections were also clearly labeled (Figs. 1F-G). Retinofugal axons were stained not only in the terminal fields, but also along their path through myelinated tracts such as the main (Figs. 1A-B) or accessory optic tracts. Labeled fibers, particularly the thinnest ones, were sharply refringent under dark field illumination, a feature that increased their detectability, even at relatively low magnification (Figs. 1E; see also Fig. 2D). In cases with high background or heavy staining, the fibers were less refringent in darkfield.

The most remarkable feature of the staining was the continuity of the fiber filling (Figs. 1C,F-G and 2D). Moreover, bouton-like enlargements appeared exclusively in terminal areas, suggesting that the technique reveals true terminal specializations, not artifactual

swellings; a feature that may allow one to distinguish with relative confidence between passing and terminating axons under the light microscope (Figs. 1C, F-G). We observed slight differences in the quality of staining between the various terminal regions. For example, in areas such as the contralateral LGN (Fig. 1A) where the density of retinal terminations is very high, the amount of reaction product was such that single fibers were impossible to follow, whereas in less densely innervated areas, the morphology of axon arbors and their terminal specializations was visible in striking detail (Figs. 1F-G).

Labeling was optimal at all survival times allowed after the injection (2-7 days), both in adults and young animals. The parameters that mostly influenced the quality of the staining were, in order, the concentration of Triton X-100 used, the time of incubation in primary antibody and Triton X-100, and the thickness of the tissue sections. Tissue series assayed with no Triton X-100 yielded very poor labeling of axons and high background staining, precluding further analysis. Using low to moderate concentrations of Triton X-100 (0.3-1%), staining was faint or absent at the center of the section thickness, making it difficult to follow individual fibers even allowing 4 days of incubation in primary antibody. Similar problems appeared when, using high Triton X-100 (2%), short incubation times (for example, 2 days at 4°C) in primary antibody were allowed, as well as when, the other parameters being optimal, tissue sections were thicker than 40μm. In addition, experiments using low Triton (<2%) characteristically failed to stain axons in myelinated tracts. A dramatic example of this effect is shown in Figure 1D. Using a low concentration (0.3%) of the detergent Triton X-100, terminal retinal arborizations are stained in the suprachiasmatic nucleus (SCN), while fibers in the optic chiasm (OC) remain unstained. For comparison note the intense labeling in the optic tract in Fig. 1A, which was stained using 2% Triton X-100. As indicated in the Methods, the best results were obtained using 40 μm sections, high (2%) Triton X-100 concentrations, and long incubation times (2 days at RT or 4 days at 4°C) in primary antibody. In addition the concentration of anti-CTB antibody (1:4,000) was higher than that recommended in previous protocols.

High contrast staining of the fibers was obtained either by using the Cobalt chloride enhanced DAB method or the Vector VIP® reaction, as opposed to the paler staining obtained with DAB alone. The Vector VIP method yielded a darker staining of densely innervated areas than the Cobalt chloride-DAB.

Retrograde labeling was consistently observed in motoneurons of the oculomotor nuclei, reflecting CTB spillage into extrinsic ocular muscles at the injection site in the eyeball.

Combined labeling of retinofugal projections with CTB and WGA-HRP

The quality of CTB labeling in animals perfused using our fixation protocol for combined WGA-HRP/CTB staining was similar to that in animals perfused for CTB immunostaining alone (compare Figs. 1B with 2B and 1C with 2D). Importantly, the TMB staining of WGA-HRP (Figs. 2A and C) was as intense as that observed routinely in ferrets (cf. Roe et al., 1993) using the standard fixation of Mesulam's (1978) method.

We found that while glutaraldehyde is not essential for good TMB histochemistry, limiting exposure to paraformaldehyde is crucial: failure to remove the excess fixative from the brain tissue led to faint or no WGA-HRP staining, even when low concentrations (1%) of paraformaldehyde had been used for the fixation.

Pretreatment with hydrogen peroxide in methanol completely bleached away the HRP activity from the sections used for CTB staining, thus allowing an unambiguous identification of the projections arising from each eye (Fig. 2B). In the sections used for revealing CTB, the contrast of the inmunostaining was markedly improved by postfixation in 4% paraformaldehyde after sectioning.

Anterograde labeling of retinofugal fibers using tracers other than CTB

Injections of Biotinylated Dextrans yielded a striking pattern of labeling: only a small group of retinal axons were heavily stained (Figs. 3A-B). These axons were relatively thick (1-2 μm diameter), and present only in the LGN. The remainder of the corresponding LGN

laminae showed a very faint tint, in which no organized structures were distinguishable. There was no labeling in other retinal targets.

Immunostaining of WGA labeling after injections in the vitreal chamber revealed only the terminal areas of retinofugal axons (Figs. 3C-D) in all retinal targets. However, the fiber staining had a grainy and discontinuous appearance (Fig. 3D), similar to that of WGA-HRP revealed by TMB histochemistry (Fig. 2C). This made it impossible to follow single fibers at branch or cross points, or to distinguish terminal specializations with confidence.

Finally, Dextran Rhodamine yielded dimly stained fibers in retinal targets such as the LGN and superior colliculus (not illustrated). We did not detect labeling in other retinal targets. An additional shortcoming of this technique was that the Rhodamine fluorescence became photobleached under the fluorescence epi-illumination at the high power magnification required for single axon arbor analysis.

Intracerebral injections

Both in adult and in young postnatal animals, CTB injections in the thalamus or cerebral cortex consistently produced anterograde labeling of the corresponding neural pathways (Fig. 4). The quality of axon staining was comparable to that seen after eye injections. In the adult cases, however, the labeling often showed a blurred appearance in those areas which contained a very high density of labeled terminals. This was particularly apparent after large injections, which labeled massive numbers of fibers.

In postnatal animals, the quality of anterograde labeling was remarkable even after only one day of survival post injection, although the best results were seen allowing 2-4 days of survival. For example, after one day of survival in newborn animals that received cortical injections, fibers were already labeled in structures situated as far away as the pyramidal tract. Moreover, CTB not only labeled established connections, but also developing, growth cone-tipped axons (Figs. 4D-E).

Because of retrograde axonal transport in the highly bi-directional pathways between the cerebral cortex and thalamus, CTB injections labeled, along with the anterogradely stained fibers, numerous neuronal bodies (Fig. 4B). However, this retrograde labeling, particularly in the cortex, was conspicuously different from the anterograde: only perikarya and main dendrites were stained, while axons or distal dendrites were always spared. Figures 4B and 4C show as an example, neocortical cells. It is unlikely that this reflected a failure of the staining technique, because such retrogradely labeled perikarya usually lay amidst well labeled axon arbors (Fig. 4B).

Using the parameters specified in the Methods, CTB injection sites remained small (200-400 μm diameter) even in the youngest postnatal animals (Fig. 4A). The core of the injection site, which presumably was the region from which the effective axonal transport originated, appeared as a small area covered by an amorphous grayish DAB-Cobalt precipitate. Around this core, there was a dense halo of heavily stained neuronal processes (Fig. 4A). The Vector VIP method yielded a much darker staining of the core of the injection than the Cobalt chloride-DAB (not shown). With the small tip diameters employed, leakage of the CTB along the micropipette track was negligible, even though retention currents were not applied during positioning of the micropipette.

As expected from previous reports, injections of Biotinylated Dextrans and PHA-L in the thalamus and cortex of adult ferrets were highly effective in labeling axon arbors and terminal specializations. However, in animals younger than 2 weeks, Biotinylated Dextrans and PHA-L performed worse than CTB. Biotinylated Dextrans labeled only a small numbers of fibers in a faint, discontinuous manner even after 4-5 days of survival. Anterograde labeling with PHA-L was capricious, being absent in many cases and faint in others. In general, well stained fibers were only seen in the vicinity of the injection site even after relatively long (4 days) survival times. On the other hand, it is to be noted that in newborns, both Biotinylated Dextrans and PHA-L performed efficiently as *retrograde* tracers.

As in the case of the eye injections, WGA-HRP deposits in the brain of adult ferrets produced heavy (although coarse) anterograde labeling of fibers and terminals. In young postnatal animals, however, WGA-HRP yielded only faint and grainy anterograde labeling as reported by previous authors (Payne et al., 1988; Ramirez et al., 1990). Moreover, in newborns, injection sites were relatively large even after small iontophoretic deposits.

Dextran Rhodamine produced detailed labeling of axon arbors after injections in the cortex of adult ferrets. However, we found this tracer completely unsuitable for use in neonatal animals. Apparently, the tracer diffused freely in the tissue, labeling glial and endothelial cells, but no neurons, extensively in the brain. Indeed, the fluorescence was ubiquitous and diluted to the point that even the injection site was barely recognizable.

Discussion

Using a modified immunohistochemical protocol, we have shown here that CTB stains with Golgi-like resolution axons along their entire length, including myelinated tracts and terminals. CTB performed better than the other tracers assayed (Biotinylated Dextrans, free WGA, WGA-HRP, Dextran Rhodamine and PHA-L) after injections into the vitreal chamber of the eye aimed at labeling the entire retinofugal projection, as well as after iontophoretic deposits in the brain tissue of neonatal ferrets aimed at labeling specific pathways between thalamus and cortex. When injected in the adult ferret brain, CTB was as sensitive an anterograde tracer as PHA-L or Biotinylated Dextrans, although was inadequate for analyzing dense terminal axonal arborizations.

CTB as an anterograde tracer

Since its introduction as an axonal tracer, the subunit B of *Vibrio cholerae* toxin has mostly been applied for retrograde labeling of neurons, in the peripheral (Flink and Westman, 1986; Horikawa and Powell, 1986; Hirakawa et al., 1992; Llewellyn-Smith et al., 1992) and in the central (Luppi et al., 1987; Berendse and Groenewegen, 1990; Berendse et al., 1992; Hay-Schmidt and Mikkelsen, 1992; Shinonaga et al., 1992; Gritti et al., 1994) nervous system. Although also reported to undergo anterograde axonal transport (Luppi et al., 1987; Ericson and Blomqvist, 1988; Luppi et al., 1990; Bruce and Grofova, 1992), anterograde labeling with CTB was judged inferior to PHA-L and Biotinylated Dextran (Ericson and Blomqvist, 1988; Bruce and Grofova, 1992). Indeed, our own initial experiments using previously published immunohistochemical protocols (Luppi et al., 1990; Mikkelsen, 1992) did not yield a complete staining of axons. Rather, we observed mainly terminal labeling consisting of swellings interconnected by thin fibers, and occasional, discontinuously labeled axons, similar to those shown in figure 4 of Mikkelsen (1992).

The present results demonstrate that, revealed properly, anterograde transport of CTB stains axons along their entire length up to the terminal specializations, including their path along myelinated tracts. The modifications that we have introduced may have improved the quality of staining chiefly by increasing the penetration of the primary antibody in the tissue, since we a) used higher concentrations of and longer exposure to the tensoactive agent Triton X-100; b) allowed longer incubation in primary antibody; c) used thin tissue sections, and d) used higher concentrations of primary antibody than previous studies (Ericson and Blomqvist, 1988; Berendse et al., 1990; Luppi et al., 1990; Bruce and Grofova, 1992; Mikkelsen 1992).

The increased penetration did not lead to a higher background staining. We attribute this to a) the pretreating of the tissue with H_2O_2 to inactivate endogenous peroxidases, b) the post-fixation of the tissue, and d) the blocking of unspecific binding with NRS and BSA. Cobalt chloride or Vector VIP® intensification added to the enhanced contrast of the staining.

Previous studies have shown that in the peripheral nervous system, CTB is selectively uptaken by a specific class of nerve fibers (Robertson and Arvidsson, 1985; Robertson and Grant, 1985). In the present study, following eye injections, we observed labeling in all known retinal targets of both thin (0.3-0.5 μm) and thick (2-3 μm) axons, suggesting that such a selectivity of staining does not occur in the CNS, at least not in the retinofugal pathways. Similarly, in newborn animals, CTB stained developing retinofugal connections in all known targets up to their growth cones.

Luppi et al. (1990), analyzing the connections of the amygdala, noted that when injected in the brain, retrogradely transported CTB is detected in cell bodies and proximal dendrites but not in axons or fiber bundles. The present results, using a more sensitive staining method, confirm that CTB is undetectable in retrogradely transporting axons. This remarkable difference between anterograde and retrograde staining may prove to be advantageous for analyzing highly reciprocal neural connections, such as those between the cerebral cortex and thalamus.

As a shortcoming, it is to be noted that when examined at high power magnification, CTB fiber labeling often showed a blurred appearance in the most densely labeled areas. For brain injections, this problem can be sidestepped by making smaller CTB injections, that label a more restricted number of fibers. In the retinofugal pathway, CTB is best suited for labeling the retinal projections as a whole, or for detailed analysis of small fiber contingents such as the accessory optic system, the retino-pretectal and retinohypothalamic projections, or the ectopic thalamic projections induced by experimental manipulations (Sur et al., 1988; Roe et al., 1993).

Combination of CTB and WGA-HRP staining

We have shown here that CTB immunohistochemistry can be combined in alternate sections with Mesulam's (1978) TMB histochemical staining of HRP. Such combination does not reduce the sensitivity achieved when using either technique alone. This double anterograde staining may be very useful for the analysis of converging axonal projections, such as the retinofugal projections arising from each eye.

The key steps for achieving a successful combination were a) the perfusion protocol, and b) the pretreatment of the sections to be used for CTB staining. Regarding the perfusion, first we removed glutaraldehyde from the perfusate because it can interfere with CTB immunostaining (Ericson and Blomqvist, 1988). Second, the long fixation and post fixation in 4% paraformaldehyde, which is usually employed for immunohistochemistry, but which sharply decreases the HRP activity, was replaced with a limited exposure to paraformaldehyde: 2% solution for 30 minutes, then removing the excess by perfusing with a sucrose solution. The light fixation did not affect CTB immunostaining, provided that the sections were post-fixed after cutting (see Methods).

The pretreatment of sections intended for CTB staining was aimed at inactivating any HRP activity from the tissue. This was necessary because we were using a HRP-based immunostain for revealing CTB. The sections were pretreated by a prolonged exposure to a

solution of hydrogen peroxide in methanol. Bleaching of peroxidase activity was so complete that even those regions most heavily stained by WGA-HRP were free of labeling in the adjacent sections processed for CTB.

Labeling of retinofugal projections by intravitreal injections

The pattern of labeling of the retinofugal projections after intraocular injections of the various tracers assayed in this study suggests that a critical limiting factor for anterograde axonal tracing with substances delivered into the vitreal chamber may have been the ability of the retinal ganglion cells to uptake the tracers.

Among the tracers assayed in this study, only CTB, free WGA and WGA-HRP were uptaken and transported by a majority of retinal ganglion cells. As discussed above, CTB proved to be the most sensitive, since it labeled all known retinal projections up to the thinnest terminal branches in complete detail, indicating that it had been uptaken in significant amounts by virtually all retinal ganglion cells. WGA and WGA-HRP showed fewer projections to some retinal targets such as those to the suprachiasmatic nucleus of the hypothalamus (Johnson et al., 1988; Mikkelsen and Serviére, 1992) or some of the ectopic projections induced by surgical manipulation at birth (Sur et al., 1988; Roe et al, 1993). Moreover, they consistently produced a grainy, discontinuous labeling, unsuited for detailed analysis of axonal arbors and terminals. It is interesting to note that fibers immunostained for WGA showed the same discontinuous appearance as fibers histochemically stained for WGA-HRP. This suggests that the incomplete fiber labeling is not an artifact of the TMB procedure, but rather reflects a real lack of continuity in the impregnation of the fibers by WGA.

Dextran Rhodamine labeling of the retinofugal projection was limited to targets which are massively innervated by the retina, such as the LGN and the superior colliculus. In addition, the lability of the dye under epi-illumination at high magnification rendered it unsuitable for detailed axon analysis.

When injected in the eye, Biotinylated Dextrans labeled in detail only a small subset of axons. Results were similar using the 10,000 and 3,000 MW compounds. Such axons were usually thick (2-3 μm), and present only in the LGN, suggesting that they were part of a specific subclass of retinal ganglion cells. The remainder retinal projections were not stained, or only faintly impregnated.

Anterograde axonal tracing in young postnatal animals.

It is known that most anterogradely transported tracers are less sensitive in newborn mammals than in adults (Payne et al., 1988; Ramirez et al., 1990; Claps and Casagrande, 1991). This limitation becomes particularly an issue in species such as ferrets, hamsters, or marsupials, which are born very immature. Because of this limitation, techniques based on physical diffusion of dyes (Godement et al., 1987), instead of on axonal transport, have become the standard method for fiber labeling in developing animals. Physical diffusion techniques, however, require very long times for labeling long pathways, become markedly less sensitive at progressively older postnatal ages (Ghosh and Shatz, 1992), and importantly, may lead to false positive staining because of intercellular diffusion (Godement et al., 1987; Clascá et al., 1995).

In very young brains, most water-soluble tracers, even when iontophoresed in minute amounts, tend to spread widely, creating big injection sites which are inadequate for selective analysis of pathways. This may relate to the fact that interstitial space in early brain tissue is wide (Rakic, 1972), as well as to the absence or immaturity (Bayer and Altman, 1991) of high-affinity binding glial cells (Steindler and Cooper, 1986). Among the tracers assayed in this study, Dextran Rhodamine epitomized this problem: following small iontophoretic deposits in the thalamus, the dye diffused so widely in the tissue that the injection site became unrecognizable, while labeling in endothelial and glial cells was present over most of both hemispheres of the brain. Similarly, although to a lesser degree, WGA-HRP showed a

tendency to create big injection sites even after minute deposits, as noted in previous studies (Payne et al., 1988; Ramirez et al., 1990).

A conceivable explanation for the poor performance of anterograde axonal tracers in early postnatal ages could be that the molecular systems for binding and/or uptake of the tracers (Rhoades et al., 1986; Steindler and Cooper, 1986) are not fully functional yet. However, the fact that all the injected tracers (except Dextran Rhodamine, see above) yielded good retrograde labeling even at the earliest ages examined argues against this possibility. On the other hand, given the heterogeneous nature of the various tracers, the fact that one of them (CTB) yielded good anterograde labeling from the earliest ages examined, while the rest performed poorly until older ages (cf. Claps and Casagrande, 1991), suggests that, more likely, the cellular systems used for the anterograde transport of some particular molecular species (Trojanowski and Schmidt, 1984) are less efficient in neonatal animals. Whatever the case, it is clear from our study that, among the known neuronal tracing methods based on anterograde axonal transport, CTB is decidely the tracer of choice for use in early postnatal brains.

References

Bayer, S.A, and Altman, J. (1991) Neocortical Development, Raven Press, New York.

Berendse, H.W. and Groenewegen, H.J. (1990) Organization of the thalamostriatal projections in the rat, with special emphasis on the ventral striatum, J. Comp. Neurol., 299: 187-228.

Berendse, H.W., Groenewegen, H.J. and Lohman, H.M. (1992) Compartmental distribution of ventral striatal neurons projecting to the mesencephalon in the rat, J. Neurosci., 12: 2079-2103.

Brandt, H.M. and Apkarian, A.V. (1992) Biotin-dextran: a sensitive anterograde tracer for neuroanatomic studies in rat and monkey, J. Neurosci. Methods, 45: 35-40.

Bruce, K. and Grofova, I. (1992) Notes on a light and electron microscopic double-labeling method combining anterograde tracing with Phaseolus vulgaris leucoagglutinin and retrograde tracing with cholera toxin subunit B, J. Neurosci. Methods, 45: 23-33.

Claps, A. and Casagrande, V. A. (1991) The distribution and morphology of corticogeniculate axons in ferrets, Brain Res., 530: 126-129.

Clascá, F., Angelucci, A. and Sur, M. (1995) Layer-specific programs of development in neocortical projection neurons, Proc. Natl. Acad. Sci. USA, in press.

Ericson, H. and Blomqvist, A. (1988) Tracing of neuronal connections with cholera toxin subunit B: light and electron microscopic immunohistochemistry using monoclonal antibodies, J. Neurosci. Methods, 24: 225-235.

Flink, R. and Westman, J. (1986) Different neuron populations in the feline lateral cervical nucleus: a light and electron microscopic study with the retrograde axonal transport technique, J. Comp. Neurol., 250: 265-281.

Gerfen, C.R. and Sawchenko, P.E. (1984) An anterograde neuroanatomical tracing method that shows the detailed morphology of neurons, their axons and terminals: immunohistochemical localization of an axonally transported plant lectin, Phaseolus vulgaris leucoagglutinin (PHA-L), Brain Res., 290: 219-238.

Ghosh, A. and Shatz, C.J. (1992) Pathfinding and target selection by developing geniculocortical axons, J. Neurosci., 12: 39-55.

Godement, P., Vanselow, J., Thanos, S., Bonhoeffer, F. (1987) A study in developing visual systems with a new system of staining neurons and their processes in fixed tissue, Development., 101: 697-713.

Gritti, I., Mainville, L. and Jones, B.E. (1994) Projections of GABAergic and cholinergic basal forebrain and GABAergic preoptic-anterior hypothalamic neurons to the posterior lateral hypothalamus of the rat, J. Comp. Neurol., 339: 251-268.

Hay-Schmidt, A. and Mikkelsen, J.D. (1992) Demonstration of a neuronal projection from the entopeduncular nucleus to the substantia nigra of the rat, Brain Res., 576: 343-347.

Hirakawa, M., McCabe, J.T. and Kawata, M. (1992) Time-related changes in the labeling pattern of motor and sensory neurons innervating the gastrocnemius muscle, as revealed by the retrograde transport of the cholera toxin B subunit, Cell Tissue Res., 267: 419-427.

Horikawa, K. and Powell, E.W. (1986) Comparison of techniques for retrograde labeling of the rat's facial nucleus, J. Neurosci. Methods, 17: 287-296.

Johnson, R.F., Morin, L.P. and Moore, R.Y. (1988) Retinohypothalamic projections in the hamster and rat demonstrated using cholera toxin, Brain Res., 462: 301-312.

King, M.A., Louis, P.M., Hunter, B.E. and Walker, D.W. (1989) Biocytin: a versatile anterograde neuroanatomical tract-tracing alternative, Brain Res., 497: 361-367.

Llewellyn-Smith, I.J., Phend, K.D., Minson, J.B., Pilowski, P.M. and Chalmers, J.P. (1992) Glutamate-immunoreactive synapses on retrogradely-labeled sympathetic preganglionic neurons in rat thoracic spinal cord, Brain Res., 581: 67-80.

Luppi, P.H., Sakai, K., Salvert, D., Fort, P. and Jouvet, M. (1987) Peptidergic hypothalamic afferents to the cat nucleus raphe pallidus as revealed by a double immunostaining technique using unconjugated cholera toxin as a retrograde tracer, Brain Res., 402: 339-345.

Luppi, P.H., Fort, P. and Jouvet, M. (1990) Iontophoretic application of unconjugated cholera toxin B subunit (CTb) combined with immunohistochemistry of neurochemical substances: a method for transmitter identification of retrogradely labeled neurons, Brain Res., 534: 209-224.

Mesulam, M.M. (1978) Tetramethyl benzidine for horseradish peroxidase neurohistochemistry: a non-carcinogenic blue reaction product with superior sensitivity for visualizing neural afferents and efferents, J. Histochem. Cytochem., 26: 106-117.

Mikkelsen, J.D. (1992) Visualization of efferent retinal projections by immunohistochemical identification of cholera toxin subunit B, Brain Res. Bull., 28: 619-623.

Mikkelsen, J.D. and Serviere, J. (1992) Demonstration of a direct projection from the retina to the hypothalamic supraoptic nucleus of the hamster, Neurosci. Lett., 139: 149-152.

Payne, B.R., Pearson, H.E. and Cornwell, P. (1988) Neocortical connections in fetal cats, Neursoci. Res., 5: 513-543.

Rakic, P. (1972) Mode of cell migration to the superficial layers of fetal monkey neocortex, J. Comp. Neurol., 145: 61-84.

Ramirez, J.J., Jhaveri, S., Hahm, J. H. and Schneider, G.E. (1990) Maturation of projections from occipital cortex to the ventrolateral geniculate and superior colliculus of postnatal hamsters, Devl. Brain Res., 55: 1-9.

Robertson, B. and Grant, G. (1985) A comparison between wheat germ agglutinin- and choleragenoid-horseradish peroxidase as anterogradely transported markers in the central branches of primary sensory neurons in the rat with some observations in the cat, Neuroscience, 14: 895-905.

Robertson, B. and Arvidsson, J. (1985) Transganglionic transport of wheat germ agglutinin-HRP and choleragenoid-HRP in rat trigeminal sensory neurons, Brain Res., 348: 44-51.

Roe, A.W., Garraghty, P.E., Esguerra, M. and Sur, M. (1993) Experimentally induced visual projections to the auditory thalamus in ferrets: evidence for a W cell pathway, J. Comp. Neurol., 334: 263-280.

Shinonaga, Y., Takada, M. and Mizuno, N. (1992) Direct projections from the central amygdaloid nucleus to the globus pallidus and substantia nigra in the cat, Neurosci., 51: 691-703.

Shmued, L., Kyriakidis, K. and Heimer, L. (1990) In vivo anterograde and retrograde axonal transport of the fluorescent rhodamine-dextran-amine, fluoro-ruby, within the CNS, Brain Res., 526: 127-134.

Stendler, D.A. and Cooper, G.F (1986) Wheat germ agglutinin binding sites in the adult mouse cerebellum: light and electron microscopy studies, J. Comp. Neurol., 249: 170-185.

Rhoades, C.H., Stieber, A. and Gonatas, N.K. (1986) A quantitative electron microscopic study of the intracellular localization of wheat germ agglutinin in retinal neurons, J. Comp. Neurol., 254: 287-296.

Sur, M., Garraghty, P.E. and Roe, A.W. (1988) Experimentally induced visual projections into the auditory thalamus and cortex, Science, 242: 1437-1441.

Trojanowski, J.Q and Schmidt, M.L. (1984) Studies with HRP and HRP conjugates of wheat germ agglutinin, choleratoxin and the subunit B of choleratoxin, Brain Res., 311: 366-369.

Figure Legends

Figure 1: Retinofugal projections labeled by intravitreal injections of CTB in ferrets. **A.** Coronal view of the lateral geniculate thalamic nucleus (LGN) contralateral to the injected eye in an adult ferret. Midline is to the right and dorsal is to the top of the image. Notice the heavy labeling in the eye-specific layers of LGN and the medial interlaminar nucleus (MIN), as well as in the myelinated fibers of the optic tract (OT). **B.** Labeling in the LGN ipsilateral to the injected eye. The labeling mirrors that of A. Fibers can be seen passing through layer A of the LGN on their way towards layer A1 (*arrowhead*). Medial is to the left, dorsal is up. **C.** High power detail of the passing fibers shown in B (*inset*). Note the continuous, smooth appearance of the axons. **D.** Terminal retinal arborizations stained in the suprachiasmatic nucleus (SCN) of the hypothalamus, above the optic chiasm (OC). **E.** Anterograde labeling in the pretectal nuclei (PT) of a 21 day old ferret pup viewed under darkfield illumination. (H): habenula. **F.** High power view of stained ectopic retinal axon arbors in the medial geniculate nucleus of an adult ferret. These projections are induced by means of surgical manipulations at birth (see text). Various terminal specializations (*arrows*), boutons *en passant,* and thick and fine collateral branches can be clearly discerned. **G.** A stained ectopic retinal axon arbor in another subdivision of the auditory thalamus. Scale bars = 500 μm (A), 300 μm (B), 200 μm (D, E), 50 μm (C, F, G).

Figure 2: Combined CTB immunohistochemistry and TMB histochemical staining of WGA-HRP in adjacent sections. **A.** Labeling in the LGN contralateral to the eye injected with WGA-HRP, viewed under darkfield illumination. Only lamina A of the LGN is stained. *Arrowhead* points to the unstained lamina A1. Dorsal is up and medial to the left. **B.** Brightfield micrograph of the section adjacent to A, showing the immunostaining in lamina A1 (*arrowhead*) of the LGN ipsilateral to the eye injected with CTB. Notice that, due to the

methanol and H_2O_2 treatment, the WGA-HRP staining in lamina A has completely been bleached away in this section. **C.** Detail of the WGA-HRP labeling in the contralateral LGN at high power. Note the discontinuity and grainy appearance of the TMB reaction product. **D.** High power view of the CTB labeling in lamina A of the ipsilateral LGN. Scale bars = 300 μm (A, B), 50 μm (C, D).

Figure 3: Staining of retinofugal pathways with Biotinylated Dextran and free WGA. **A.** Retinal projection to the LGN stained by an injection of Biotinylated Dextran 3,000 MW into the ipsilateral eye. Note the heavy staining of a small subset of fibers crossing lamina A and arborizing in lamina A1 (*arrow*). Dorsal is up, medial is to the left. *Arrowhead* points to the retinal axons shown at higher power in B. **B.** High power view of the same retino-geniculate axons shown in B (*arrowhead*) **C.** Terminal labeling in LGN obtained after injecting both eyes with free WGA. As a result, labeling is present in all laminae of the nucleus. Dorsal is up, medial is to the left. **D.** Detail of the WGA labeling in the pretectum at high magnification. Note the pale and blurred appearance of the reaction product. Scale bars = 300 μm (A, C), 50 μm (B, D).

Figure 4. CTB labeling of corticothalamic and thalamocortical connections in young postnatal animals. **A.** Example of an injection site in the pulvinar and the medial interlaminar nucleus (*arrowhead*) of a 9 day old ferret, obtained after iontophoresis of 1% CTB using 3 μAmp of current for 10 min., and a micropipette with tip diameter of 20 μm. (LP): lateral posterior thalamic nucleus. Dorsal is up, medial to the left. Brightfield illumination. **B.** Anterogradely labeled axon arbors (*arrowheads*) and retrogradely labeled cell bodies (*arrow*) in the occipital cortex, obtained after the thalamic injection shown in A. The labeling in the *inset* is shown at higher magnification in E. Darkfield illumination. Dorsal is up medial is to the right. **C.** Higher power detail of the retrogradely labeled cortical cells shown in B (*inset*). Note that only the perikaryon is stained (*arrows*), while the axon and distal dendrites are not

visible. Darkfield illumination. **D.** Bundle of developing corticofugal axons in the intermediate zone, labeled after an injection in the cortical plate of a one-day old animal. Note the growth cones at the tip of some axons (*arrow*). **E.** High power view of a growth cone. Note the delicate detail of the stained terminal specializations (*arrow*). Scale bars = 200 m (A, B); 50 m (C); 20 m (D) and 10 m (E).

Table 1

Intraocular injections

Tracer	Solution	# eyes adults	Survival adults	# eyes postnatals	Survival postnatals
Subunit B of Cholera Toxin (Low salt; List Biological Labs)	1%, H_2O	18	3-6 days	15	1-2 days
Free WGA (Vector Labs)	10%, saline	2	2 days		
WGA conjugated with horseradish peroxidase (WGA-HRP; Sigma)	5%, saline	6	2 days	12	1-2 days
Biotinylated Dextran (10,000 MW; Molecular Probes)	20% ,saline + 2% DMSO	2	7 days		
Biotinylated Dextran (3,000 MW; Molecular Probes)	20% ,saline + 2% DMSO	2	4-7 days		
Dextran Rhodamine (10,000 MW, Lysine fixable; Molecular Probes)	5% , H_20 + 2% DMSO	2	6 days		

Table 2

Injections in the cortex and thalamus

Tracer	Solution	# of adults	Survival adults	# of postnatals	Survival postnatals
CTB	1-2%, 0.1M PB (pH 6.0)	3	3-10 days	6	1-5 days
WGA-HRP	1-3%, 0.1MPB or saline	4	2 days	6	1-2 days
Biotinylated Dextran (3,000 MW)	10%, saline	2	10-12 days	6	1-5 days
Dextran Rhodamine	5%, H_20	5	10-14 days	4	1-4 days
PHA-L (Vector Labs)	2.5%,10 mM PBS (pH 8.0)	6	10-14 days	7	1-5 days

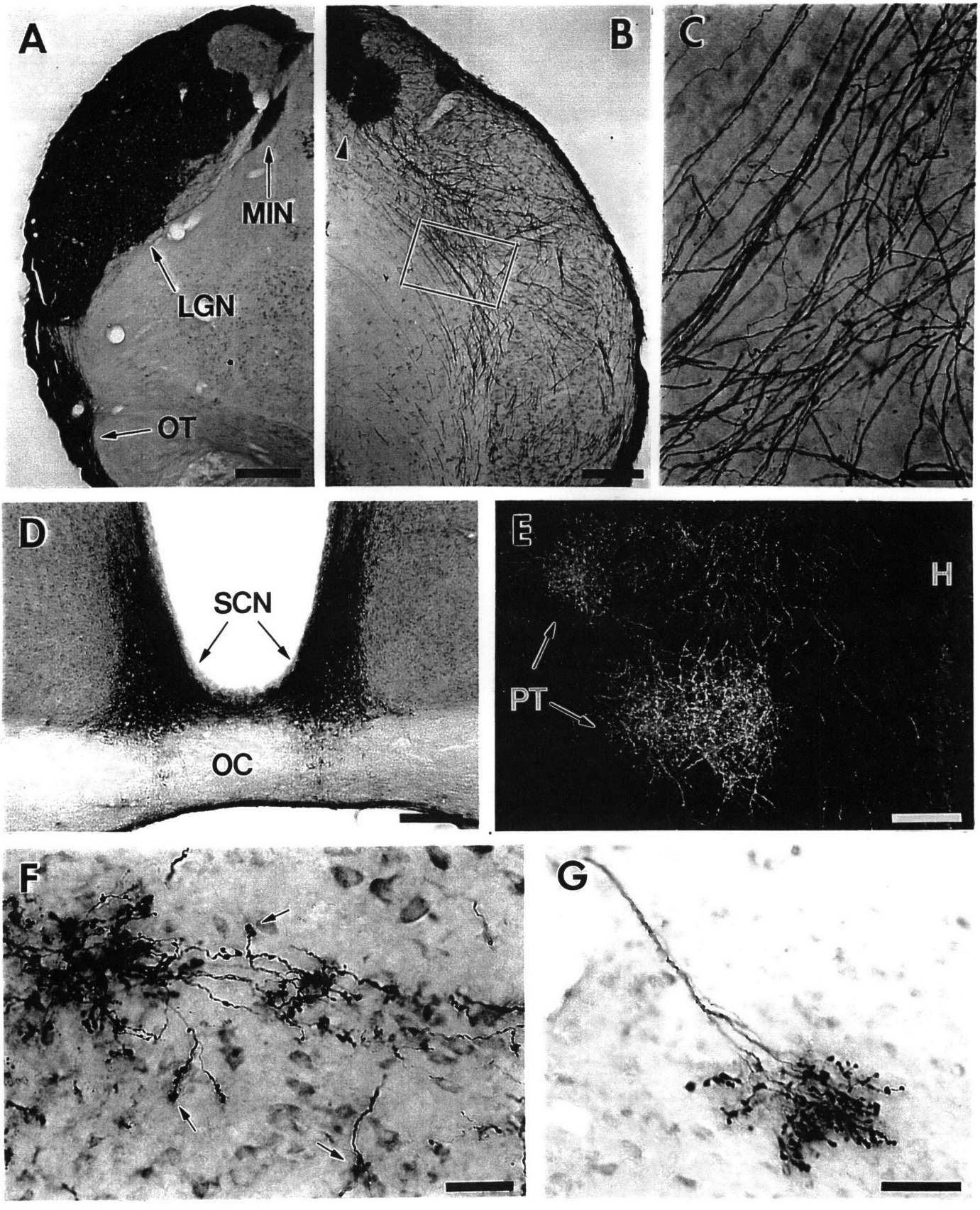

Fig.1

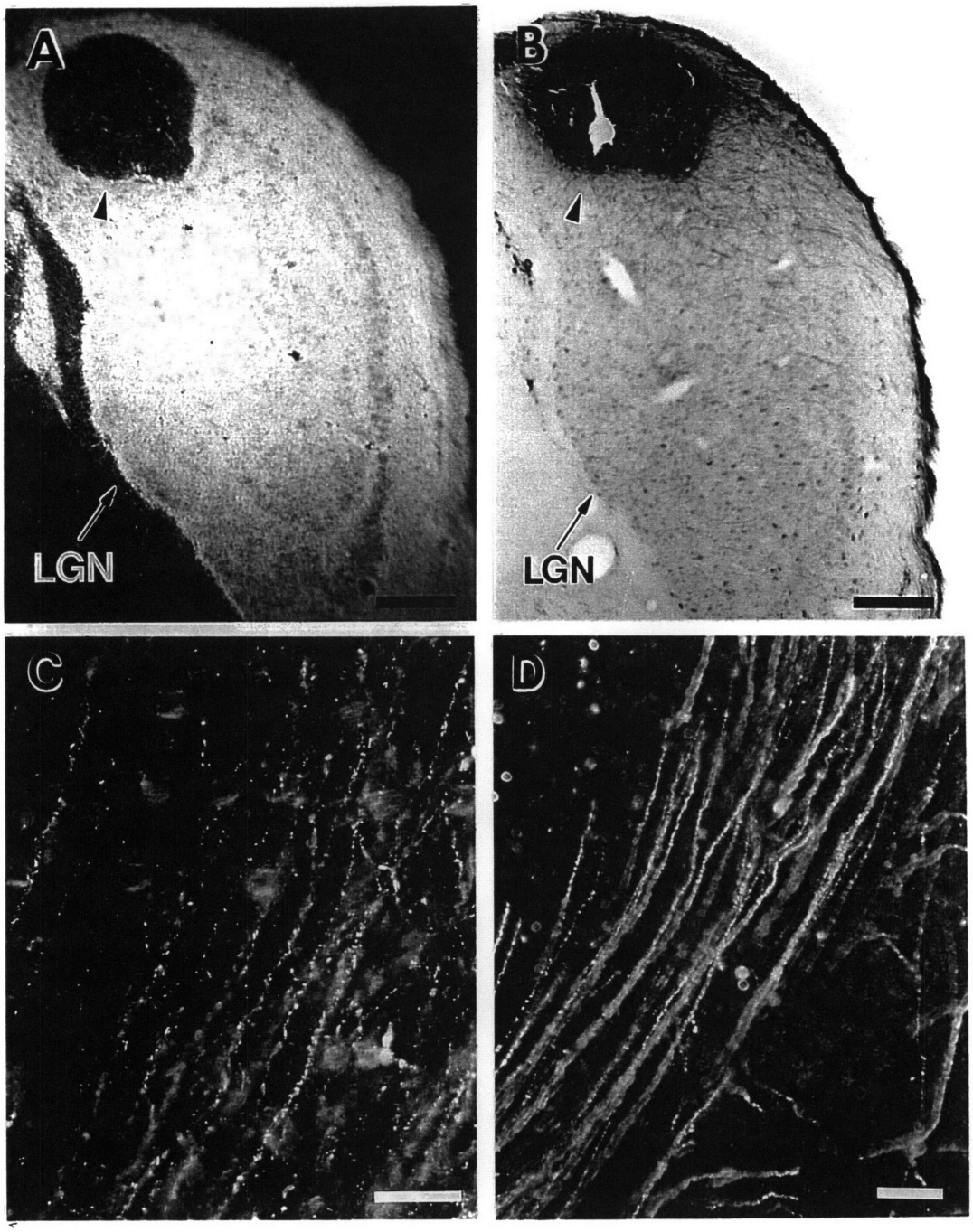

Fig. 2

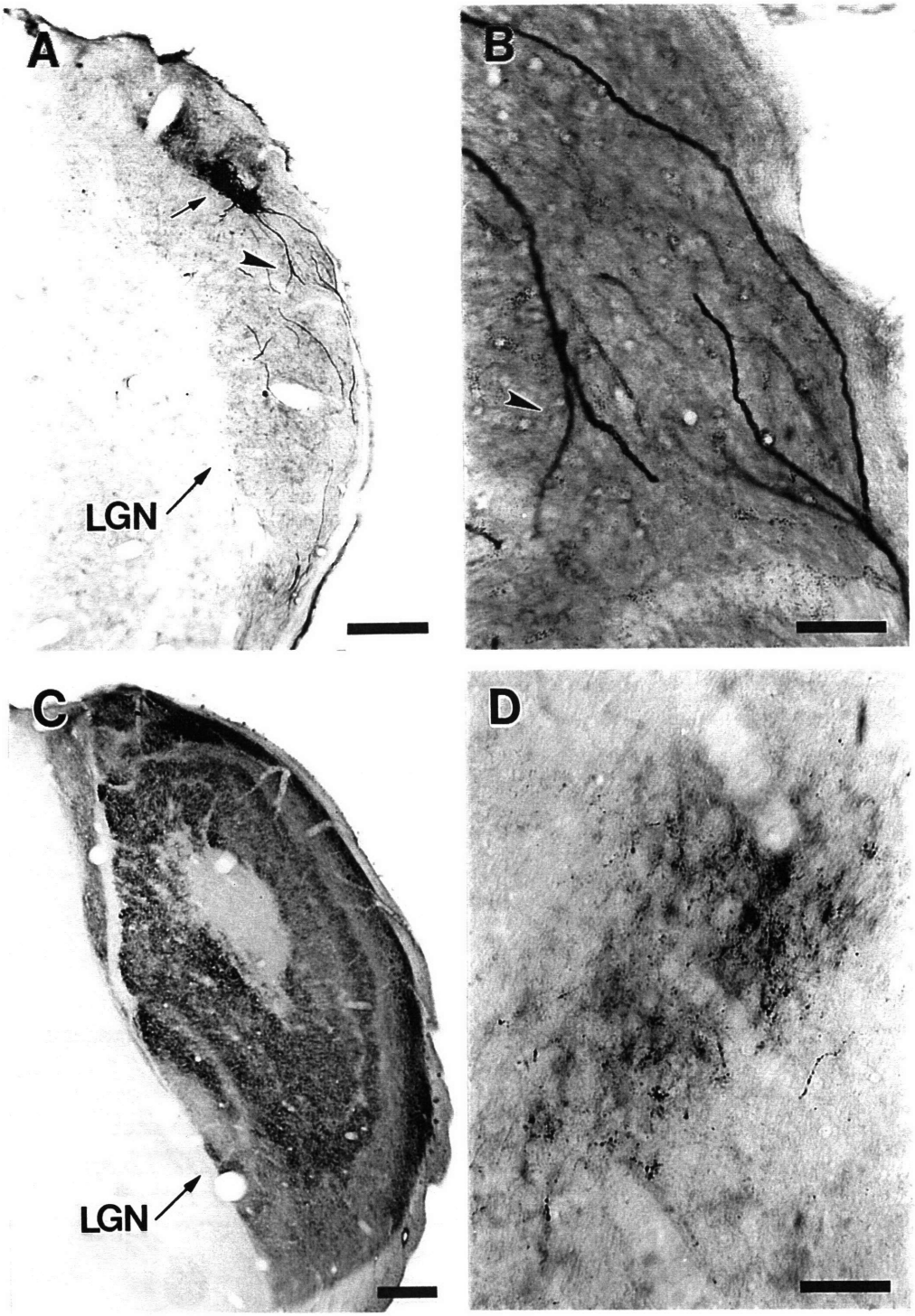

Fig. 3

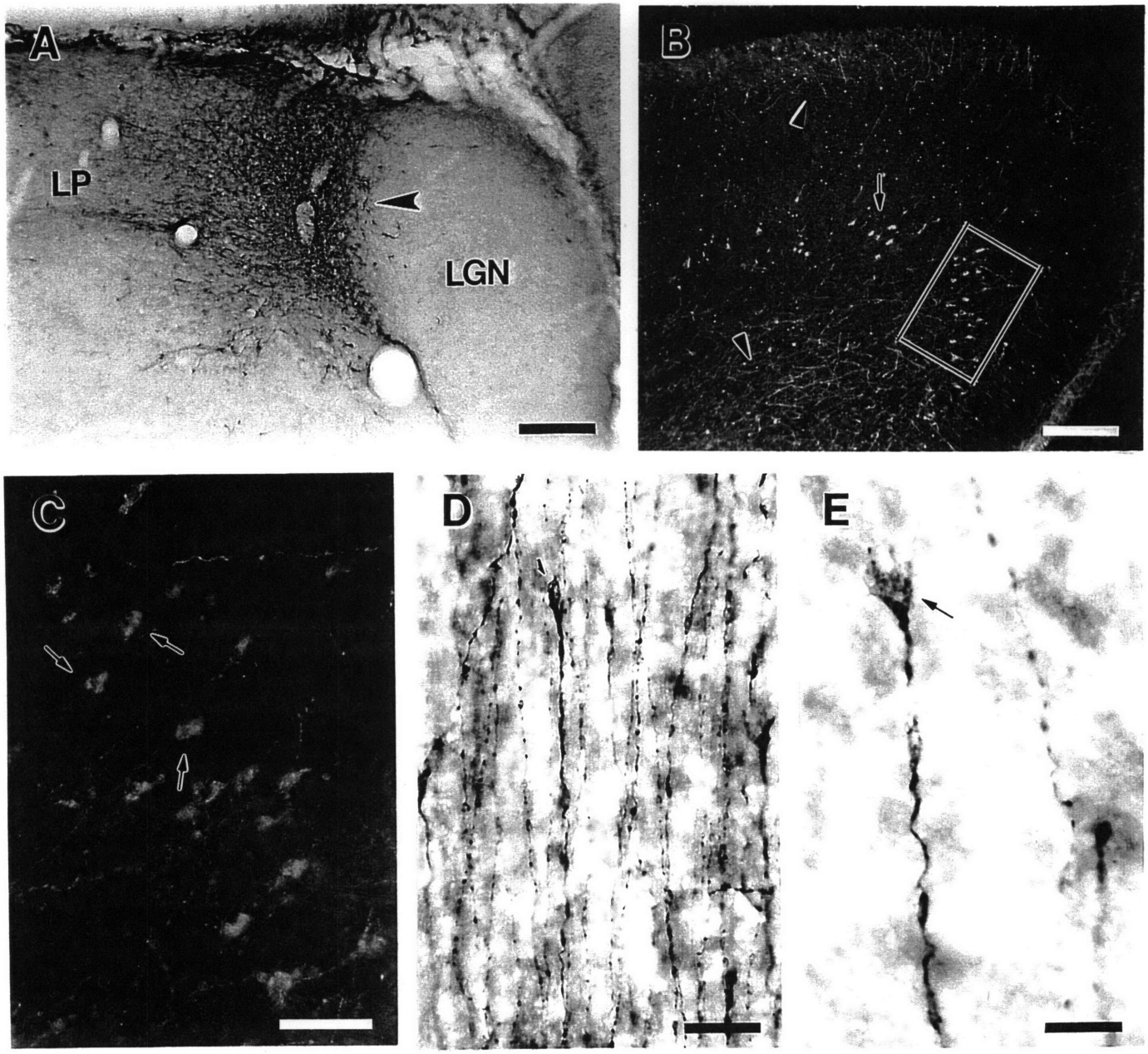

Fig. 4

Chapter 3

Experimentally Induced Retinal Projections to the Ferret Auditory Thalamus: Development of Clustered Eye-Specific Patterns in a Novel Target.

Introduction

Appropriate neonatal brain lesions in rodents (Schneider, 1973; Frost, 1981) and carnivores (Sur et al., 1988; Rocha et al., 1993) have been shown to induce some retinal axons to innervate non-visual thalamic targets such as the medial geniculate nucleus (MGN), lateral posterior nucleus (LP) and ventrobasal complex. In ferrets, the novel retino-MGN projection confers visual responsivity to many cells in the MGN (Roe et al., 1993) and in the primary auditory cortex (A1; Sur et al., 1988; Roe et al., 1990, 1992). Some receptive field properties of visually driven cells in A1 (Roe et al., 1992) are not observed in visually driven MGN cells, suggesting that they are generated within A1. However, other response properties of visual A1 cells are present in visually driven MGN cells (Roe et al., 1993), and thus arise from either MGN or retinal circuitry.

The precise anatomical organization of retino-MGN projections that underlies visual responses in MGN and A1 has not been described. Previous physiological studies have suggested that retinal projections may have substantial spread and a specific distribution pattern within the various subdivisions of the MGN. To investigate this issue we have used highly sensitive anatomical tracing methods to examine the extent, trajectories and distribution of retinal afferents to the MGN. We have also performed a similar analysis for the retinal projections to another ectopic target, LP.

Physiological studies have also shown that visually responsive cells in MGN can be driven exclusively by stimulation of one or the other eye (Roe et al., 1993), suggesting that both retinae project to MGN in a non-overlapping fashion. However, no information has so far been available on how inputs from the two eyes are spatially organized within MGN, and whether these inputs are anatomically segregated. In most mammals, retinal afferents segregate into eye-specific domains in the lateral geniculate nucleus (LGN; Guillery, 1970; Hickey and Guillery, 1974; Linden et al., 1981) and superior colliculus (SC; Graybiel, 1975; Chalupa and Rhoades, 1979; Lund et al., 1980; Hoffmann et al., 1984; Illing, 1989; Murphy et al., 1992).

During development of retinogeniculate (So et al., 1978; Linden et al., 1981; Shatz, 1983; Sretavan and Shatz, 1986) and retinocollicular (Frost et al., 1979; Land and Lund, 1979; Williams and Chalupa, 1982; Thompson, 1990) afferents, eye-specific segregation has been shown to occur as a refinement of initially diffuse and interspersed projections in a process dependent on afferent activity (for the LGN: Shatz and Stryker, 1988; for a review see Shatz, 1990; for the SC: Lund et al, 1973, 1980; Finlay et al., 1979; Insausti et al., 1984; Jen et al., 1984). However, the specific pattern of segregation, i.e. the shape and size as well as the mutual spatial relationship of eye-specific domains, differs between retinal targets and may be target-related. The "rewired" paradigm employed in the present study is particularly well-suited to directly address the issue of what aspects of connectivity are afferent or target dependent. In this preparation retinal afferents are induced to project to novel targets, such as MGN and LP, whose cytological organization differs dramatically from that of normal retinal targets. Similarities in the organization of retinothalamic projections between normal and "rewired" ferrets would argue for afferent control of connectivity. On the other hand, similarities between retinal projections to novel targets and the normal inputs to these targets, would indicate that the target plays an important role in specifying connectivity patterns. To address these issues we have examined the projection patterns and spatial relationship of eye-specific inputs to MGN and LP, and how such patterns emerge over development.

Parts of this work have been reported previously in abstract form (Angelucci et al., 1994, 1995, 1996a).

Materials and Methods

Animals

The animals used in the present study were pigmented ferrets (*Mustela putorius furo*; family Mustelidae, order Carnivora) bred in our colony or purchased from Marshall Farms. Gestation time was 41±1 days. The day of birth was designated postnatal day (P) 0. A total of 13 adult (Table 1) and 24 young postnatal (Table 2) ferrets were used. Most of these animals (n=33) received neonatal brain lesions to reroute retinal axons to the auditory thalamus. Some normal controls (n=4) were included in this study for comparison. Throughout this report we refer to the operated animals as "rewired" ferrets.

Neonatal surgery

The surgical protocol used in this study to reroute retinal fibers to the MGN is a modification of that reported previously from this laboratory (Sur et al., 1988; Pallas et al., 1994). One day after birth, ferret pups were anesthetized by hypothermia. Under sterile conditions and microscopic observation, the scalp was incised along the sagittal midline. A small craniotomy was made in the soft occipital bone overlying the posterior cerebral fossa, exposing the mesencephalon. To ablate the ascending ipsilateral auditory pathways to the MGN, the lateral third of the mesencephalon was coronally sectioned at the midcollicular level. This lateral cut transected the brachium of the inferior colliculus (BIC), but extended medial and ventral to it, to include extrabrachial inputs to the MGN. The latter consist of inputs from the ipsilateral nuclei of the lateral lemniscus and the nucleus of the BIC that course ventrally and medially to the BIC, respectively (see Chapter 1, this Thesis). The intercollicular commissure was cauterized to sever the contralateral auditory inputs to MGN, and both the superficial and deep layers of the superior colliculus were ablated on the side of the deafferented MGN. In some cases both inferior colliculi (IC) were also cauterized. A few animals were operated only on one side of the brain (n=5; Table 1). In the remaining animals the set of lesions described

above were performed bilaterally. On completion of surgery the wound was closed with reabsorbable 5-0 suture. The pups were revived under a heat lamp, returned to the jill and monitored until the time of intraocular injections.

Intraocular injections of tracers and staining procedures

Adult animals were anesthetized with ketamine (30 mg/kg, i.m.) and xylazine (1.5 mg/kg, i.m.). Between the ages of P12 and P27 only ketamine (40 mg/kg) was administered, while pups younger than P12 were anesthetized by deep hypothermia.

A first group of adult "rewired" ferrets received injections of cholera toxin subunit B (CTB) into the vitreal chamber of one or both eyes (n=11; Table 1). Procedures for CTB injections and immunohistochemical staining have been described in detail elsewhere (Angelucci et al., 1996b; Chapter 2, this Thesis). Briefly, under general and local anesthesia, 10 µl of a 1% solution of CTB (Low salt; List Biological Labs, Campbell, CA) in distilled water was injected into the vitreal chamber. The animals were allowed to survive for 3-6 days, euthanasized with sodium pentobarbital (80 mg/kg, i.p.) and transcardially perfused with saline, followed by 4% paraformaldehyde in 0.1 M phosphate buffer (PB), pH 7.4, for 30 minutes. The brains were then blocked stereotaxically, removed from the skull, post-fixed overnight in the same fixative and cryoprotected by soaking in 30% phosphate buffered sucrose for 1-2 days before sectioning with a freezing microtome. Serial 40 µm thick coronal sections were collected. Two brains (F95-92 and F95-93; Table 1) were sectioned in the parasagittal and horizontal planes, respectively. Alternate sections were pretreated in 0.3% H_2O_2 and then in glycine (0.1M) in 0.1M phosphate buffered saline pH 7.4. To block non-specific binding sites, sections were pre-incubated overnight at 4° C in 4-5% normal rabbit serum (NRS), 2.5% bovine serum albumin (BSA) and 0.3-0.5% Triton X-100 in PBS. Immunostaining was carried out by incubating the sections first in goat anti-CTB (List Biological Labs; 1:4000 with 2% Triton X-100, for 2 days at room temperature), then in biotinylated rabbit anti-goat IgG (Vector Labs, Burlingame, CA; 1:200 with 1% Triton X-100, for 1 hour), subsequently in avidin-biotin-peroxidase (ABC;

Vectastain Elite, Vector Labs; 1:100, for 1 hour) and finally developed with a $CoCl_2$-enhanced diaminobenzidine (DAB; Sigma, St. Louis, MO) reaction, or with Vector VIP substrate (Vector Labs). For cytoarchitectonic identification of the thalamic nuclei and MGN subdivisions, adjacent series of sections were stained for Nissl and cytochrome oxidase or acetylcholinesterase. Sections were mounted, air dried, dehydrated and coverslipped.

A separate group of adult "rewired" ferrets (n=2; Table 1) and all the young postnatal animals employed in the present study (n=24; Table 2) received injections of CTB into one eye and of wheat germ agglutinin conjugated to horseradish peroxidase (WGA-HRP) into the other eye. In animals older than P22, intraocular injections of CTB were made as described above, and two days later 10 µl of 4-5% WGA-HRP (Sigma) in saline was injected into the other eye. Two further days of survival were allowed prior to perfusion. In animals younger than P22, 2-6 µl of each tracer was administered on the same day and 1-2 days of survival were allowed for transport. The animals were perfused with 2% paraformaldehyde at 4°C for 30 minutes. The excess fixative was removed from the tissue by subsequent perfusion with 5% and 10% sucrose for 20-30 minutes (for details see Angelucci et al., 1996b). Age at perfusion was considered the age of the experiment (Table 2). After cryoprotection, brains older than P14 were sectioned at 40 µm in the coronal plane, while younger brains were cut at 50 µm. One series of sections was post-fixed in 2-4% paraformaldehyde for at least one day, soaked for 20 minutes in 90% methanol and 0.3% H_2O_2 in distilled water, to bleach endogenous and injected peroxidase activity, and then processed for CTB immunohistochemistry as described above. The adjacent series was processed using tetramethylbenzidine (TMB) to reveal HRP according to the protocol of Mesulam (1978), lightly counterstained with thionin, and coverslipped.

Data analysis

Microscopic analysis of CTB stained sections was carried out using bright- and darkfield illumination. The WGA-HRP-processed material was analyzed under darkfield and polarized light.

In one representative bilaterally "rewired" adult case (F94-97; Table 1), in which one eye had been injected with CTB, quantifications of retinal fibers to the contralateral and ipsilateral auditory thalami were performed by counting the number of axon trunks crossing the perimeter of the MGN. In order to avoid counting branches of the same axon in adjacent sections, axon trunks at the periphery of the nucleus that could not be traced back to their origin outside the MGN were excluded from counts. Axon counts were performed on one entire series (1:2) of coronal MGN sections, and the resulting number was multiplied by two. This analysis was performed under microscopic observation using a 40x objective.

The distribution and termination patterns of the ectopic projections were examined on coronal, parasagittal and horizontal CTB-stained sections, by reconstructing the terminal labeling with a camera lucida, using 10x and 25x objectives. Axon trajectories were reconstructed at higher magnification (40x) in coronal and horizontal MGN sections. Cytoarchitectonic boundaries and MGN subdivisions in "rewired" ferrets were identified by matching CTB stained sections to adjacent sections reacted for Nissl, cytochrome oxidase and acetylcholinesterase, and by comparison with coronal sections of normal ferret thalami stained with the same methods, as well as with myelin stain (see Chapter 4, this Thesis). Parcellation of the MGN was also based on the distinct pattern of thalamocortical projections examined in a previous study (Angelucci et al., 1993).

In adult animals the size of retino-MGN clusters was estimated on camera lucida reconstructions of CTB terminal labeling by drawing a perimeter around the outermost border of each cluster and measuring cluster diameter in two orthogonal planes. For this analysis a cluster was defined as an area of tightly packed terminal boutons formed by more than a single axon arbor. Individual, losely branched axonal arbors were not included in the analysis. Due to the high contrast of CTB staining (see Fig. 1), and to the complete filling of fibers and terminal specializations obtained with this tracer (Angelucci et al., 1996b; Chapter 2, this Thesis), it was easy to delineate high density terminal zones of clustered boutons. Clusters were then grouped according to the MGN subdivision in which they were located and for each group mean values

and s.e.m. were calculated separately for the long and the short diameters. No corrections were made for shrinkage, since all sections had been treated identically.

To examine how retino-MGN projections are assembled into terminal clusters during development, individual CTB-labeled axonal arbors were reconstructed at various developmental ages (first to fourth postnatal week; n=25) and at adulthood (n=9) using camera lucida and a 63x objective. Most axons were drawn within single MGN sections, because adjacent series were processed for WGA-HRP (to reveal projections from the opposite eye) or used for various histochemical reactions (to identify MGN subdivisions). Even though it is unlikely that an entire axonal arbor is confined to a 50 μm slice, the exclusion of parts of an arbor should occur randomly across cases, therefore allowing at least qualitative comparisons between populations of axonal arbors at different ages. However, it is likely that a smaller portion of an axon is contained within an MGN section at adulthood than at early postnatal ages, since the MGN grows dramatically from P8 to adulthood. For this reason, in some adult cases axons were entirely reconstructed in serial MGN sections.

The spatial relationship between inputs from the two eyes in MGN and LP was examined in bilaterally "rewired" animals that had received an injection of CTB into one eye and of WGA-HRP into the other eye. TMB and CTB stained sections were drawn by camera lucida, and adjacent sections superimposed. To compensate for differential shrinkage caused by the different histological procedures, the magnification of the drawings was adjusted and adjacent sections were aligned using the lateral edges of the nucleus and vascular landmarks as reference.

Development of retino-MGN projections and emergence of clusters: quantitative analysis. The following measurements were performed between P4 and adulthood (Table 2): 1) area of the MGN 2) area of retinal projections to MGN 3) percentage of the MGN area innervated by retinal projections 4) percentage of retinal projections forming clusters ("clustering index"). A total of 12 cases were used for this analysis (2 to 3 cases per postnatal

week and 2 adult cases). For each case we selected 2 representative coronal MGN sections contralateral to the eye injected with CTB, taken at comparable rostrocaudal levels. The caudalmost section was usually located at the border between regions of higher and lower density of projections, while the rostralmost section was often in the middle of the high density region. To allow for computerized calculations of optical densities, entire MGN sections were digitized, using a CCD camera attached to a microscope and connected to a computer. The density of CTB labeling in MGN was determined by a window smoothing method. For the pseudocolor images shown in figure 11A-B, the color of each pixel corresponds to the density of CTB labeling within a 29 μm x 29 μm square window centered at that pixel. For each case the images of MGN sections were normalized so that the brightest red corresponded to median CTB labeling in the LGN of the same case, and the darkest blue to the 85 percentile of the MGN section's background. Each pixel in the images corresponded to a square of side 4.2 μm.

The area of each MGN section was calculated as the sum of all the pixels in the section. The area of retinal projections to MGN was estimated as the sum of all the pixels in the section whose labeling density was more than 15.6% of the maximum labeling. Lower density values consisted essentially of the section's background. Clustered projections were estimated as the percentage of MGN pixels whose labeling density more than 46.8% of the maximum labeling. The choice of this threshold was based on the visual observation that lower density values consisted of sparse, non-clustered retino-MGN fibers. A smoothing and thresholding procedure was implemented in order to eliminate isolated pixels with high density values. The procedure effectively eliminated clusters composed of a small number of pixels. The "clustering index" was defined as the percentage of the retinal projection area occupied by clustered projections. It is important to point out that the values obtained (reported in figure 11C-F) are relative measures and do not reflect actual values, since for each case included in the quantification, measurements were performed on two representative sections. Moreover, the clustering index underestimates the percentage of retinal projections forming clusters, especially at later postnatal

ages, since a cluster in our analysis consists only of the densest core (represented in orange-red in figure 11A-B) of an actual retinal cluster in MGN.

Results

Methodological considerations

Redirection of retinal inputs to inappropriate thalamic nuclei has been previously shown to occur when some of the normal retinal targets (SC and/or LGN) are ablated, and alternative space is created by partially deafferenting an ectopic target (Schneider, 1973; Kalil and Schneider, 1975; Frost, 1981,1982,1986; Sur et al., 1988; Roe et al., 1993). In those studies, however, the MGN was only partially deafferented, as only the brachium of the inferior colliculus was sectioned. In the course of a series of studies on thalamic specification, we reassessed the lesion paradigm previously employed in this laboratory (see Chapter 1, this Thesis). We found that extensive deafferentation of the MGN, including both brachial and extra-brachial ascending pathways, combined to partial ablation of SC (see Materials and Methods) was sufficient to induce maximal retinal innervation of the auditory thalamus. Ablation of the LGN was neither sufficient nor necessary. Moreover, compared to the previously employed lesion paradigm, rerouting of retinal fibers to the MGN was obtained consistently with this new type of manipulation, likely due to a more comprehensive deafferentation of the nucleus (A. Angelucci, F. Clascá, and M. Sur, unpublished observations).

The observations described in the present paper were made in animals that were "rewired" one day after birth according to the new lesion paradigm. While the MGN was extensively deafferented, the visual cortex and the LGN were completely spared. However, the SC was extensively cauterized since deafferentation of the auditory thalamus requires removal of contralateral inputs that reach the MGN via the commissure of the SC, and of the deep layers of SC which project to the ipsilateral MGN (in the cat: Graham, 1977; Calford and Aitkin, 1983; Morest and Winer, 1986; in the ferret: A. Angelucci, unpublished observations). As a result of these lesions retinal afferents invariably invaded the MGN as well as another ectopic thalamic target, the LP. The SC is a major source of inputs to LP (in the cat: Graybiel, 1972;

McIlwain, 1978; Graybiel and Berson, 1980; Kawamura et al., 1980; Caldwell and Mize, 1981; Benedeck et al., 1983; in the ferret: A. Angelucci, unpublished observations), thus ablation of SC results in partial deafferentation of LP. Indeed, we observed that the extent of novel retinal projections to LP directly correlated with the extent of the superior collicular lesion, i.e. with the extent of LP deafferentation.

An additional advantage of the new surgical manipulation was that it produced virtually no distortion in the shape, size and relative position of the various thalamic nuclei. Thus, the cytoarchitectonic subdivisions of the thalamus and of the MGN could be easily identified in Nissl stained sections, allowing comparisons across experimental and normal cases. Our parcellation of the normal ferret MGN into various subdivisions was based on matching different staining methods such as Nissl, myelin stain, cytochrome oxidase and acetylcholinesterase, and on the distinct pattern of MGN projections to the auditory cortex (Angelucci et al., 1993). Following Morest (1964) and others (Imig and Morel, 1988; Winer, 1992) we could distinguish 4 main nuclei in the MGN of the ferret: the dorsal (MGd), the ventral (MGv) and the medial (MGm) divisions, and the lateral nucleus of the posterior thalamic complex (Po) (Fig. 1). We did not attempt to further subdivide MGv and MGd into subsidiary nuclei since our material did not allow for a clear demarcation of such regions. However, within the dorsal division we could distinguish the suprageniculate nucleus (Sg) from the rest of MGd because of the larger size and lower density of its cell bodies. Sg constitutes the medial part of the dorsal division, bordered ventrally by MGm and dorsally by the LP/Pulvinar nucleus.

Retinal projections to novel thalamic targets in adult animals

Following intraocular injections of CTB in adult "rewired" animals, retinal fibers were observed in all the normal targets as well as in the two ectopic targets, MGN and LP. A few retinal axon arbors, usually extending from axons in the LP or pretectum, could occasionally be detected also in the ventroposterior lateral thalamic nucleus (data not shown). Projections to normal retinal targets appeared indistinguishable from those described in normal animals, and

included the dorsal and ventral LGN, the lateral part of the pulvinar, remnants of the upper strata of the SC (when not completely ablated), the pretectal nuclei (PT), the accessory optic nuclei and the hypothalamus. Since the LGN was not lesioned in the animals used in the present study, retino-LGN projections in "rewired" ferrets appeared organized in eye-specific layers and ON- and OFF-sublayers, as previously described for normal retino-LGN afferents (Hahm et al., 1991). Myelinated fiber tracts such as the optic and the accessory optic tracts were also clearly labeled by CTB.

Projections to the Medial Geniculate Nucleus. In "rewired" ferrets, a significant number of retinal axons were found to arborize in the medial geniculate nucleus (Fig. 1). In one representative case (F94-94, Table 1; Fig. 1) retino-MGN fibers from the contralateral and ipsilateral eyes were quantified by counting axons entering the nucleus in coronal sections (see Materials and Methods). A total of 1,780 axons were counted, with the ipsilateral projection amounting to about 15% of the axons innervating the MGN. Observations of axon trajectories in horizontal sections revealed that many more retinal axons enter the MGN in this plane (see below). Since axon counts were performed on coronal MGN sections, these counts underestimate the actual number of retino-MGN axons. Based on the latter observation we estimated that at least 3,000 retinal axons innervate the MGN in "rewired" ferrets. The areal extent of contralateral retinal projections within MGN and the percentage of the MGN area innervated by retinal inputs were also quantified (see below).

We then examined the distribution and termination patterns of retinal inputs within the auditory thalamus. Axons from both retinae were found to innervate all the subdivisions of the MGN: MGv, MGd, MGm and Po (Fig. 1). However, terminal arbors were most abundant in the anterior half of the nucleus, while few axons terminated in the caudal third (Figs. 1-3). This rostral bias is apparent in figure 1 which shows a caudo-rostral sequence of coronal sections through the MGN contralateral to the CTB-injected eye, and in figure 3B illustrating contralateral retino-MGN projections in the horizontal plane.

Retinal projection patterns in MGN were fairly stereotyped across different animals. Typically, retinal projection zones were organized into clusters of terminals scattered throughout the nucleus (Figs. 1,3), but overall they innervated only a minor part of MGN (Fig. 1). Clusters in MGv and Po, and in the lateral parts of MGd appeared more dense and more restricted than those in MGm and in the medial aspect of MGd (Sg). In MGm, retinal projections had generally more diffuse terminal arborizations. In the coronal plane, clusters in MGv appeared elongated, with the longer axis oriented in the dorsoventral dimension (Figs. 1,3A), while in horizontal sections they were elongated rostrocaudally (Fig. 3B). Furthermore, in coronal sections of MGv, individual patches often seemed to align along a dorsoventral axis (Figs. 1C-E,3A; see also Fig. 6). By contrast, orientation and alignment of clusters were not typically observed in MGm or MGd (Figs. 1C-F,3A; see also Fig. 6). The above observations were quantified by measuring cluster size. In coronal MGv sections, the long (dorsoventral) axis of a patch had a mean length of 138 μm (s.e.m.=9.33, n=13), and the shorter axis (mediolateral) 80 μm (s.e.m.=7.4, n=13). In the horizontal plane, mean patch sizes in MGv were 61 μm (s.e.m.=5.18 , n=13) along the mediolateral axis, and 151 μm (s.e.m.=13.59, n=13) along the rostrocaudal axis. The dorsoventral and rostrocaudal axes were significantly longer than the mediolateral axis ($p < 0.001$ in both cases, Student's t-test), indicating that clusters in MGv are elongated both dorsoventrally and rostrocaudally. Cluster size was not significantly different in the horizontal and coronal planes ($p > 0.05$). In MGd, clusters had mean sizes of 57 x 158 μm in the coronal plane (s.e.m.=5.67, n=7 for the short axis; s.e.m.=11.78, n=7 for the long axis), indicating that clusters in MGd are also elongated. However, the longer axis of the patches in this division did not bear any consistent relation to any particular dimension, i.e. clusters were not oriented. Because clusters in MGm were less restricted than in other MGN subdivisions, it was more difficult to measure patch diameters in this division. Our measurements indicated that clusters vary considerably in size and shape in MGm (mean size in the coronal plane: 68 x 174 μm; s.e.m.= 5.5, n= 7 for the short axis; s.e.m.= 20.3, n= 7 for the long axis). Clusters in MGm, like those in MGd, were not oriented.

Axon trajectories were examined in coronal and horizontal MGN sections (Fig. 3). Retinal axons entered the MGN following several distinct pathways that generally correlated with their final destination within the nucleus. In the coronal plane, some axons entered laterally and dorsolaterally, arising directly from the optic tract in more caudal sections, and entering through the LGN at more rostral levels. These axons tended to arborize soon after entering the nucleus, and generally terminated within a cluster in MGv or in the lateral aspects of MGd (Fig. 3A). They appeared to have restricted terminal branched arbors with large clustered boutons. Another group of axons could be detected in coronal sections entering the MGN dorsomedially through the LP or pretectum, and terminating in MGd (including Sg), Mgm and Po (Fig. 3A). Some of these axons coursed for more than one mm within MGN without arbors, branches or boutons *en passant* before terminating. In the coronal plane, a third group of retinal axons entered the MGN ventrally, through the lateral terminal nucleus and ventral accessory optic tract, and usually terminated in MGm. The axons that innervated the medial division appeared to have sparser and less focal terminal arborizations with boutons often arranged in strings.

Observation of axonal trajectories in the horizontal plane indicated that retinal axons also entered the MGN rostrally, through the optic tract and LGN, as well as caudally from nuclei of the accessory optic system (Fig. 3B). Indeed, when compared to the observations made in coronal sections, it was clear that the majority of retinal axons originated from the optic tract and LGN, followed a rostro-caudal trajectory, and terminated predominantly in the anterior portion of MGN (compare Figs. 3A and 3B).

In order to understand the precise anatomical organization of retinal terminal clusters we reconstructed individual representative CTB-stained axonal arbors. Since our aim was to examine how individual axon arbors contribute to the formation of clusters, we preferentially selected for reconstruction axons that terminated within clusters. Moreover, since clusters were better defined in MGv and MGd, we only reconstructed axonal arbors in these subdivisions (Fig. 4). These arbors had simple terminations with a single, well-defined focus, had large clustered boutons, and closely resembled in morphology a group of retino-MGN axon arbors

described previously by Pallas et al. (1994; see their Figs. 6 and 7). Clusters were not formed by individual axon arbors but by the convergence and overlap of several of them. This is clearly indicated in figure 4B which shows an example of three different axons entering the MGN at three separate points along the optic tract, converging onto the same region and forming overlapped terminal arbors. Axon arbors were mostly restricted to a single cluster and did not send branches to several clusters. A previous study from this laboratory (Pallas et al., 1994), in which retino-MGN axons were reconstructed in their entirety in the parasagittal plane, similarly showed that the majority of these axons form only one focal terminal arbor in MGN.

Because of the large number of labeled axons in the optic tract, as well as in all the normal retinal targets which surround the MGN, it was impossible to follow axons for any distance outside the auditory thalamus. Thus, while we occasionally observed optic tract fibers sending a branch into the MGN, it is not clear whether retino-MGN axons are collaterals of fibers projecting to other targets.

Projections to the Lateral Posterior Nucleus. In "rewired" ferrets the LP received a substantial direct input from the retina (Fig. 5). Here, the retinal projection zones were consistently more extensive than in the MGN. As in "rewired" MGN and normal LGN, projections from the contralateral eye within LP were significantly more numerous than those from the ipsilateral eye (Fig. 5).

Retinal projections were most dense in the caudal half of LP. Posteriorly, they occupied the caudalmost part of the nucleus, which at this level forms a dorsomedial rim that caps the MGN (Figs. 5A,A'), while more anteriorly they were located in the medial portion of LP (Figs. 5B,B'). In contrast to the patchy pattern of termination observed in the auditory thalamus, retinal axons in LP tended to form terminal "slabs" that sloped from dorsomedial to ventrolateral in the coronal plane (Fig. 5). The location and shape of these retinal termination zones bear striking resemblance to the terminal zones of superior collicular inputs to the cat *pars medialis* of LP (LPm) previously described by Graybiel and Berson (1980). It is not surprising that in

"rewired" ferrets retinal projections would terminate predominantly in LPm, since, as a result of SC ablation, this should be the most extensively deafferented LP subdivision in our preparation (see above).

Retinal axons that innervate LP followed two main pathways. A first group of axons entered the nucleus laterally and dorsolaterally, arising directly from the optic tract. Optic tract fibers in normal adult ferrets cross the LP/Pulvinar on their way to the SC and PT, but do not normally terminate in LP. A second group of retinal fibers reached LP dorsomedially through the pretectum.

Binocular organization. Both eyes projected to the same regions within MGN and LP. In MGN, clusters of terminals related to one eye were adjacent to, but spatially segregated from, clusters related to the other eye (Fig. 6). However, because clusters from the contralateral retina were more numerous, it was not uncommon to detect contralateral clusters not apposed to ipsilateral ones. Isolated clusters of ipsilateral axons were less commonly observed. It is unlikely that the spatial proximity of terminals from the two eyes represents the outcome of a random phenomenon, given that retinal fibers innervate specific focal portions of the available terminal space in MGN.

Spatial segregation according to the eye of origin was observed also in the lateral posterior nucleus. In caudal LP, eye-specific segregation was more evident and occured in the form of parallel, largely non-overlapping "slabs" oriented from dorsomedial to ventrolateral, in coronal sections (Fig. 7). However, in more rostral sections it was not uncommon to observe areas of partial overlap between projections from the two eyes. This might have been related to the plane of sectioning. In fact, at more rostral levels, LP expands and its ventromedial border gradually slopes dorsally so that the overall orientation of the nucleus progressively changes moving rostralwards. Accordingly, the "slabs" of retinal terminals appeared more vertically oriented in rostral (Figs. 5B,B') than in caudal LP (Figs. 5A,A'). Thus, it is possible that at more rostral LP levels eye-segregation would be better observed in other planes of section.

Development of retinal projections to the Medial Geniculate Nucleus

The anatomical organization of the mature ectopic retinothalamic projections into terminal clusters and eye-specific domains, was reminiscent of clustering and eye-specific segregation of retinal afferents within some normal targets, such as the LGN and SC. By analogy with clustering in LGN and SC, the mature patterns of ectopic retinothalamic connections may result from the refinement of initially more diffuse and largely overlapped projections. Alternatively, such patterns may be established by the initial ingrowth and arborization of retinal axons into specific regions of the ectopic targets. To differentiate between these two possibilities, we have examined the development of retinal termination patterns in the MGN.

At birth in ferrets, the auditory thalamus was well differentiated and distinguishable from adjacent thalamic nuclei in Nissl stained sections. However, its cytoarchitectonic pattern appeared fairly homogeneous, and nuclear subdivisions were hard to assess based only on Nissl staining. Thus, in early postnatal animals we did not attempt to subdivide the MGN.

Qualitative observations. We first investigated whether the retino-MGN projection present in adult "rewired" ferrets is created *de novo*, or by the stabilization of transient retinal projections to this nucleus. To this end, normal ferret kits received intraocular injections of CTB (Table 2). In normal ferrets, retinal axons did not terminate in MGN at any age (data not shown). However, at all ages examined some optic tract axons directed towards more distal targets crossed the dorsolateral aspect of MGN at rostral levels, often forming fascicles. These axons were few in number at P4-P6 and, as the MGN increased in size, were displaced progressively more dorsolaterally so that by P27 only a few of them traversed the nucleus very superficially. However, none of these axons branched in the auditory thalamus. By contrast in "rewired" ferrets at P4 and P6, the MGN was invaded by a large number of simple, fairly

unbranched retinal axons that terminated in this nucleus. Thus, retinal projections to MGN are created *de novo* in "rewired" ferrets.

We then examined the development of retino-MGN projections both at the population (Fig.8) and at the single axon arbor (Fig. 9) level. At P4 both contralateral and ispilateral retinal projections had already invaded the MGN. During the first week of development, the retino-MGN projection appeared diffuse (Fig. 8A), and occupied most of the medio-lateral and antero-posterior extent of the nucleus. Retinal fibers entered the MGN from all around, as described above for the adult projection. Representative individual axons at P4 and P6 had at most a few short branches, traversed the nucleus for long distances in all directions, and had bouton-like enlargements along their course. Axons with these characteristics constituted the majority of the projection up to P8, and many were still present at the end of the second postnatal week (Fig. 9, axons 1 and 2).

During the second postnatal week, the projection was still very diffuse, although a tendency to cluster appeared around P8 in some areas (Fig. 8B, arrow), and by P14 clusters were even more apparent (Fig. 8C). Many axons were still very simple, resembling one-week old axons (see above), but by the end of the second postnatal week many had begun to form arbors (Fig. 9, axons 3-5). These arbors were very extensive, often sending branches to all the subdivisions of the MGN, which by this age had become discernible in Nissl stained sections. Figure 9 shows an example of such an axon (axon 3) forming an arbor in MGv which contributed to the formation of a cluster. From this arbor two long collaterals departed at an acute angle, with one collateral terminating in Sg and the other in MGm.

By the end of the third postnatal week most of the projection had become clustered, but axonal branches running between clusters were still evident in some animals (Fig. 8D). During the following week, clusters became denser and further restricted, and the overall pattern of retino-MGN projections appeared nearly adult-like (Fig. 8E). Moreover, the characteristic orientation and alignment of clusters along a dorsoventral axis in MGv was evident by P27 (Fig. 8E; see also Fig. 10D), but not yet at P22 (Fig. 8D; see also Fig. 10C). Figure 9 shows

some examples of reconstructed axon arbors from the fourth postnatal week. At P22, some axons had fairly simple arbors and still coursed for very long distances within the MGN gray matter emitting simple branches all along their length (Axons 6,7). Axons of this type were not observed at or after P25. Other axons had more complex arbors which, although confined to one MGN subdivision, were still fairly large and sent branches to more than one cluster (Axons 8,9). At P27, most arbors were more elaborate and much more focal than at previous ages (Axons 10-13) and were mostly confined to individual clusters. Comparisons of 4 week-old arbors (Fig. 9) with adult arbors (Fig. 4, this study, and Figs. 6,7, Pallas et al., 1994) indicate that, even though the overall pattern of retino-MGN projections appeared adult-like by P22-P27 (compare Figs. 8D-E and 10C-D with 1 and 6, respectively), minor refinements of individual axon arbors were still taking place after P27.

The emergence of eye-specific segregation was studied by superimposing CTB stained sections on adjacent sections processed for WGA-HRP (Fig. 10). During the first postnatal week of development, afferents from the two eyes were largely diffuse and terminated over the same MGN regions in an overlapped manner (Fig. 10A). At P14, even though clustering had already begun, overlap between inputs from the two retinae was still evident (Fig. 10B). Over the next two postnatal weeks, projections from the two eyes progressively segregated into eye-specific regions within the MGN, with clear eye-specific domains evident between P22 and P27 (Figs. 10C,D). Segregation of contra- and ipsilateral inputs in LP was also fully established by the end of the fourth postnatal week (Fig. 10D).

Quantitative Observations. All measurements were performed on digitized and normalized CTB-stained MGN sections (Fig. 11A,B; see Methods).

The MGN increased in mean area by 4.8 fold from P4 to P22 ($p < 0.001$, Student's t-test), and by 50% between P22 and adulthood ($p < 0.001$). Overall, there was a 7.7-fold increase in mean MGN area from P4 to adulthood ($p < 0.001$; Fig. 11C). The mean area of the retino-MGN termination zones peaked at P22, with a 4.3-fold increase in extent from the first to

the end of the third postnatal week ($p = 0.025$). The mean area of retinal projections at the end of the fourth week of development was not significantly different from the mean retinal projection area at the end of the third postnatal week ($p = 0.2$). Between P27 and adulthood no significant changes in the extent of retino-MGN projections were observed ($p = 0.2$). Overall the retinal projection area increased by about three and a half fold between P4 and adulthood ($p < 0.001$).

From the above results it follows that early in development retinal projections occupy a much larger proportion of MGN than at adulthood. Between the first and the third postnatal weeks, the percentage of MGN innervated by retinal fibers remained essentially unaltered ($p = 0.7$; Fig. 11E), since both the MGN and the ectopic projection grew at similar rates during this period (see above). However, between P22 and adulthood, the MGN continued to increase in size while the retino-MGN projection did not, so that the percentage of MGN invaded by retinal fibers decreased by about two-fold ($p < 0.05$; Fig. 11E).

Early in development most of the retino-MGN projection was diffuse and showed little or no clustering, until P8 (Fig. 11F). By the end of the third postnatal week the "clustering index" (defined as the percentage of the retino-MGN projection area that is clustered) increased by about seven fold ($p = 0.003$). No significant changes in the "clustering index" were observed between the end of the third and of the fourth postnatal weeks ($p > 0.05$).

Discussion

In the present study we have shown that retinal projections to the MGN in "rewired" ferrets are arranged in clusters that are scattered throughout the MGN subdivisions. Clusters arising from the ipsilateral eye are consistently apposed to, but spatially segregated from, clusters arising from the contralateral eye. Both clustering and eye-specific segregation in MGN arise as a refinement of initially diffuse and overlapped projections. Partial deafferentation of another ectopic thalamic target, LP, also results in eye-specific clustering and segregation.

In normal animals, MGN receives ascending projections from the IC and other brainstem auditory and non-auditory nuclei, and has reciprocal connections with the auditory cortex (for a review see Winer, 1992). LP receives projections from SC, PT and V1, and has reciprocal connections with extrastraiate visual cortical areas (for a review see Garey et al., 1991).

Distribution, trajectories and extent of the novel retinothalamic projections

The normal MGN is organized into several subnuclei (MGv, Po, MGd, MGm), each with a distinct cytoarchitectonic organization and a specific pattern of connections with the various auditory cortical fields (Winer et al., 1977; Imig and Morel, 1988; Winer, 1992). In the present study we have observed that the MGN in "rewired" ferrets retains a normal cytoarchitectonic pattern in Nissl stain, and that retinal projections innervate mainly the rostral half of the nucleus, terminating in all the MGN subdivisions. The rostral half of MGv sends a heavy projection to A1 and a sparser projection to the anterior field (A) in normal cats (Rose and Woolsey, 1949; Andersen et al., 1980; Imig and Morel, 1984; Morel and Imig, 1987) and ferrets (Pallas et al., 1990; Angelucci et al., 1993; A Angelucci, F Clascá, unpublished observations). A normal connectivity pattern between MGv and A1 is retained in "rewired" ferrets (Pallas et al., 1990). Thus, the anatomical substrate exists for visual A1 cells to be driven by the novel retino-MGN pathway.

In normal cats (Andersen et al., 1980; Morel and Imig, 1987) and ferrets (A Angelucci, F Clascá, unpublished observations), Po sends projections mainly to A, but also to A1. Projections from MGd predominantly reach the secondary auditory field (A2) and other non-primary auditory areas, while projections from MGm are quite widespread, extending to each cortical auditory field (Winer at al., 1977; Morel and Imig, 1987). These anatomical data suggest that visual input might reach other auditory cortical fields in addition to A1, including field A and other auditory areas. Optical recording in auditory cortex of "rewired" ferrets has recently confirmed the presence of visual activity in field A (Sharma et al., 1996).

Retinal axons were found to enter the MGN from all around the nucleus, arising from the optic tract and the retinal targets that surround MGN, including the LGN and LP. This observation suggests that a diffusible trophic factor might be released by the auditory thalamus in response to the neonatal deafferentation. A similar phenomenon was observed in LP which, however, is more abundantly reinnervated by retinal fibers than MGN. One possible explanation for the different extent of retinal innervation in LP and MGN is that proximity of growing axons to a potential terminal target determines whether and to what extent axons terminate in that target. In normal ferrets, the LP/Pulvinar is crossed by a large number of optic tract axons, directed to SC and PT. Partial LP deafferentation might induce reactive sprouting of these axons which, because they are already passing through LP, might have a competitive advantage over other more distantly placed inputs. Moreover, in "rewired" ferrets, the caudal part of LP is mainly surrounded by retinal targets, since the ventrally located auditory afferents to MGN have been extensively removed. Thus, other inputs to LP might also arise from the retinal targets surrounding this nucleus. By contrast, MGN in normal ferret kits is crossed by just a few optic tract axons, and is surrounded by retinal as well as non-retinal targets and fiber tracts. In Chapter 1 (this Thesis) we have shown that the MGN in "rewired" ferrets receives a variety of inputs which might compete with retinal axons for terminal synaptic space in MGN: somatosensory lemniscal and visceral sensory afferents, as well as remnants of normal auditory and non-auditory afferents spared by the neonatal lesion.

Clustering and eye-specific segregation of retino-MGN projections: specification by afferents and targets

Clustering of like inputs and their segregation from inputs of an opposite type are commonly observed in retinal projections to some normal targets, such as LGN and SC, and may depend on afferent activity. However, the specific pattern by which clustering and segregation occur varies in different retinal targets. Thus for example, the ferret retinogeniculate projection segregates into parallel eye-specific layers (Linden et al., 1981) and ON/OFF sublayers (Stryker and Zahs, 1983; Hahm and Sur, 1988; Hahm et al., 1991), while the retinocollicular projection segregates into a periodic pattern of eye-specific clusters (Zhang and Hoffmann, 1993). The generation of specific terminal patterns might depend on intrinsic features of the target. In the present study, we have addressed this issue by examining the resulting pattern of connections when inputs from the two eyes are redirected to novel targets whose cytological organization differs significantly from that of both SC and LGN. In the normal MGN, although the two ears are not represented separately, neurons in MGv tuned to the same sound frequency segregate into thin laminae oriented dorsoventrally (isofrequency axis), and a systematic progression of sound frequencies occurs across the lateromedial dimension (tonotopic axis). By contrast, no ordered tonotopic organization has been detected in MGd or MGm (for a review see Winer, 1992). The laminar pattern in MGv is physiologically and anatomically analogous to the retinotopic arrangement of retinal axons in LGN, and results from the ordered alignment of the typical MGv relay cells: the tufted neurons. These cells have characteristically elongated dendritic trees, oriented exclusively in the dorsoventral and rostrocaudal directions, with average diameters in the cat of 120 m (dorsoventral) and 22.5 m (mediolateral) (Morest, 1964, 1965; Majorossy and Kiss, 1976). Afferent fibers of the BIC contribute to the laminated pattern of MGv by terminating within a fibrodendritic lamina and by contacting dendrites of adjacent laminae (Morest, 1965). Thus, with respect to individual fiber spread, a fibrodendritic lamina consists of 2 dendritic layers and is about 50-100 m wide

(Winer, 1985). Clusters of retino-MGN projections in MGv of "rewired" animals seem to parallel the orientation of relay cell dendrites, being elongated exclusively dorsoventrally (mean diameter 138 m) and rostrocaudally, and to span approximately the width of a fibrodendritic lamina, being about 60-100 m wide. By contrast, clusters in MGd and MGm, although often elongated, do not show any systematic orientation, consistent with the normal lack of orientation of dendritic trees in these subdivisions (Winer, 1985).

Another striking feature of "rewired" MGN is the alignment of retinal clusters along the isofrequency axis in MGv, but not in MGd or MGm. Studies in the cat (Kudo and Niimi, 1980) and bat (Wenstrup et al., 1994) have demonstrated that following injections of anterograde tracers in IC, terminal labeling in MGv appears as dense clusters of terminals aligned dorsoventrally, often forming "bands". By contrast, in other subdivisions labeling consists of scattered "patches", consistent with the normal lack of a laminar pattern in these subdivisions. Thus, the pattern of retino-MGN projections resembles the normal pattern of IC-to-MGN afferents. Similarly, the terminal "slabs" formed by retino-LP afferents in "rewired" animals resemble the "slab-like" pattern of normal tectal projections to the cat LP (Graybiel, 1972; Graybiel and Berson, 1980). Together, the above observations suggest that the novel target restricts or defines the shape, size, and distribution of terminal retinal clusters. Consistent with our observations, previous studies of retinal projections to the hamster MGN and ventrobasal nucleus (Campbell and Frost, 1987,1988) have shown that at the ultrastructural level, synaptic morphology is controlled by intrinsic features of the target.

If the shape and size of clusters is constrained by the target, clustering *per se*, and eye-specific segregation of clusters in the novel targets, are more likely to be regulated by afferents or by interactions between afferents and their target cells. This hypothesis is suggested by previous evidence for activity-dependent sorting of retinal afferents to LGN (Shatz and Stryker, 1988; Sretavan et al., 1988; Hahm et al., 1991) and SC (for a review see White and Chalupa, 1991). Moreover, eye-specific segregation in a target that normally does not receive projections from both eyes has also been shown to occur in the optic tectum of embryonically created three-

eyed frogs (Constantine-Paton and Law, 1978; Law and Constantine-Paton, 1981), and to be dependent both on presynaptic (Reh and Constantine-Paton, 1985) and postsynaptic (Cline et al., 1987) activity. In the present study, we have shown that clustering and eye-specific segregation of retinal afferents occur also in non-retinal targets, and that their emergence involves a significant progressive remodeling of axon arbors, similar to that described for the emergence of retinal termination patterns within LGN. In addition, this remodeling in MGN occurs over the same time period as the formation of eye-specific layers and ON/OFF sublayers in the ferret LGN (Hahm et al., 1991), suggesting that these processes may share similar afferent-driven mechanisms.

Our hypothesis is that in the MGN of "rewired" ferrets at least two types of competition are taking place over development, one between retinal inputs and alternative inputs (see above), the other between eye-specific inputs. These competitions would result in segregation of retinal afferents from other types of inputs within MGN, as well as in eye-specific segregation within the retinal termination zones. Correlation-based models of development predict clustering of like inputs when these are better correlated in their activity than opposite-type inputs, and locally excitatory interactions (generated by intrinsic connections, diffusible factors or gap-junctions) exist among the target cells (for a review see Miller, 1990). Binocular competition in the "rewired" ferret MGN would occur in the absence of visual activity, since the two eyes segregate before eye opening (P30). Recent data on the activity patterns of spontaneous discharges in the two eyes early in development suggest that the activities of any pair of cells within the same eye are better correlated than the activities of any pair of opposite-eye cells. In fetal and early neonatal retinae *in vivo*, RGCs fire in bursts of a few seconds (Maffei and Galli-Resta, 1990), and in ferret and kitten retinae *in vitro*, this activity occurs as waves of correlated bursting which cross the entire retina in random directions (Meister et al., 1991). Since correlations between pairs of cells in these retinae decrease very slowly with retinotopic distance, and the activity waves have random trajectories, spontaneous discharges in the two eyes are very likely to be largely uncorrelated. Thus, eye-specific segregation in

"rewired" MGN and LP may occur as a result of activity-dependent competition between the two eyes.

References

Andersen RA, Knight PL, Merzenich MM (1980) The thalamocortical and corticothalamic connections of AI, AII, and the anterior auditory field (AAF) in the cat: evidence for two largely segregated systems of connections. J Comp Neurol 194:663-701.

Angelucci A, Clascá F, Sur M (1993) Multiple cortical auditory fields in the ferret defined by their architectonics and thalamocortical connections. Neurosci Abst 19:1427.

Angelucci A, Clascá F, Sur M (1994) Retinal projections induced into the auditory thalamus in ferrets: differential terminal distribution and eye-specific zones. Soc Neurosci Abst 20:1107.

Angelucci A, Cramer KS, Sur M (1995) Emergence of clustered eye-specific patterns in experimentally induced retinal projections to the ferret auditory thalamus. Soc Neurosci Abst 21:1307.

Angelucci A, Bricolo E, Sur M (1996a) Development of experimentally induced retinal projections to the ferret auditory thalamus: A quantitative study. Soc Neurosci Abst 22:1730.

Angelucci A, Clascá F, Sur M (1996b) Anterograde axonal tracing with the subunit B of cholera toxin: a highly sensitive immunohistochemical protocol for revealing fine axonal morphology in adult and neonatal brains. J Neurosci Methods 65:101-112.

Benedek G, Norita M, Creutzfeldt OD (1983) Electrophysiological and anatomical demonstration of an overlapping striate and tectal projection to the lateral posterior-pulvinar complex of the cat. Exp Brain Res 52:157-169.

Caldwell RB, Mize RR (1981) Superior colliculus neurons which project to the cat lateral posterior nucleus have varying morphologies. J Comp Neurol 203:53-66.

Calford MB, Aitkin LM (1983) Ascending projections to the medial geniculate body of the cat: evidence for multiple, parallel auditory pathways through the thalamus. J Neurosci 3:2365-2380.

Campbell G, Frost DO (1987) Target-controlled differentiation of axon terminals and synaptic organization. Proc Natl Acad Sci USA 84:6929-6933.

Campbell G, Frost DO (1988) Synaptic organization of anomalous retinal projections to the somatosensory and auditory thalamus: target-controlled morphogenesis of axon terminals and synaptic glomeruli. J Comp Neurol 272:383-408.

Chalupa LM, Rhoades RW (1979) An autoradiographic study of the retinotectal projection in the golden hamster. J Comp Neurol 186:561-570.

Cline HT, Debski EA, Constantine-Paton M (1987) N-Methyl-D-aspartate receptor antagonist desegregates eye-specific stripes. Proc Natl Acad Sci USA 84:4342-4345.

Constantine-Paton M, Law MI (1978) Eye-specific termination bands in tecta of three-eyed frogs. Science 202:639-641.

Finlay BL, Wilson KG, Schneider GE (1979) Anomalous ipsilateral retinotectal projections in Syrian hamsters with early lesions: Topography and functional capacity. J Comp Neurol 183:721-740.

Frost DO (1981) Orderly anomalous retinal projections to the medial geniculate, ventrobasal, and lateral posterior nuclei of the hamster. J Comp Neurol 203:227-256.

Frost DO (1982) Anomalous visual connections to somatosensory and auditory systems following brain lesions in early life. Dev Brain Res 3:627-635.

Frost DO (1986) Development of anomalous retinal projections to non-visual thalamic nuclei in syrian hamsters: a quantitative study. J Comp Neurol 252:95-105.

Frost DO, So K-F, Schneider GE (1979) Postnatal development of retinal projections in Syrian hamsters: a study using autoradiographic and anterograde degeneration techniques. Neuroscience 4:1649-1677.

Garey LJ, Dreher B, Robinson SR (1991) The organization of the visual thalamus. In: Neuroanatomy of the visual pathways and their development (Dreher B, Robinson SR, eds), pp 176-234. London: Macmillan Press.

Graham J (1977) An autoradiographic study of the efferent connections of the superior colliculus in the cat. J Comp Neurol 173:629-654.

Graybiel AM (1972a) Some extrageniculate visual pathways in the cat. Invest Ophthalmol 11:322-332.

Graybiel AM (1972b) Some fiber pathways related to the posterior thalamic region in the cat. Brain Behav Evol 6:363-393.

Graybiel AM (1975) Anatomical organization of the retinotectal afferents in the cat: an autoradiographic study. Brain Res 96:1-23.

Graybiel AM, Berson DM (1980) Histochemical identification and afferent connections of subdivisions in the lateralis posterior-pulvinar complex and related thalamic nuclei in the cat. Neurosci 5:1175-1238.

Guillery RW (1970) The laminar distribution of retinal fibers in the dorsal lateral geniculate nucleus of the cat: A new interpretation. J Comp Neurol 138:339-368.

Hahm J-O, Sur M (1988) The development of individual retinogeniculate axons during laminar and sublaminar segregation in the ferret LGN. Soc Neurosci Abst 14:460.

Hahm J-O, Langdon RB, Sur M (1991) Disruption of retinogeniculate afferent segregation by antagonists to NMDA receptors. Nature 351:568-570.

Hickey TL, Guillery RW (1974) An autoradiographic study of retinogeniculate pathways in the cat and fox. J Comp Neurol 156:239-254.

Hoffmann K-P, Ballas I, Wagner H-J (1984) Double labeling of retinofugal projections in the cat: a study using anterograde axonal transport of ^{3}H-proline and horseradish peroxidase. Exp Brain Res 53:420-430.

Illing R-B (1989) The mosaic of the uncrossed retinal projections in the superior colliculus of the cat. Exp Brain Res 74:641-644.

Imig TJ, Morel A (1984) Topographic and cytoarchitectonic organization of thalamic neurons related to their targets in low-, middle-, and high-frequency representations in cat auditory cortex. J Comp Neurol 227:511-539.

Imig TJ, Morel A (1988) Organization of the cat's auditory thalamus. In: Auditory Function. Neurobiological basis of hearing (Edelman GM, Gall WE, Cowan WM, eds), pp 457-484. New York: Wiley.

Insausti R, Blakemore C, Cowan WM (1984) Ganglion cell death during development of ipsilateral retinocollicular projection in golden hamster. Nature 308:362-365.

Jen LS, So K-F, Woo HH (1984) An anterograde HRP study of the retinocollicular projection in normal hamsters and hamsters with one eye enucleated at birth. Brain Res 294:169-173.

Kalil RE, Schneider ER (1975) Abnormal synaptic connections of the optic tract in the thalamus after midbrain lesions in newborn hamsters. Brain Res 100:690-698.

Kawamura S, Fukushima N, Hattori S, Kudo M (1980) Laminar segregation of cells of origin of ascending projections from the superficial layers of the superior colliculus in the cat. Brain Res 184:486-490.

Kudo M, Niimi K (1980) Ascending projections of the inferior colliculus in the cat: an autoradiographic study. J Comp Neurol 191:545-556.

Land PW, Lund RD (1979) Development of the rat's uncrossed retinotectal pathway and its relation to plasticity studies. Science 205:698-700.

Law MI, Constantine-Paton M (1981) Anatomy and physiology of experimentally produced striped tecta. J Neurosci 1:741-759.

Linden DC, Guillery RW, Cucchiaro J (1981) The dorsal lateral genicualate nucleus of the normal ferret and its postnatal development. J Comp Neurol 203:189-211.

Lund RD, Cunningham TS, Lund JS (1973) Modified optic pathways after unilateral eye removal in young rats. Brain Behav Evol 8:51-72.

Lund RD, Land PW, Boles J (1980) Normal and abnormal uncrossed retinotectal pathways in rats: an HRP study in adults. J Comp Neurol 189:711-720.

Maffei L, Galli-Resta L (1990) Correlation in the discharges of neighboring rat retinal ganglion cells during prenatal life. Proc Natl Acad Sci USA 87:2861-2864.

Majorossy K, Kiss A (1976) Specific patterns of neuron arrangement and of synaptic articulation in the medial geniculate body. Exp Brain Res 26:1-17.

McIlwain JT (1978) Properties of cells projectiong rostrally from the superficial layers of the cat's superior colliculus. Brain Res 143:445-457.

Meister M, Wong ROL, Baylor DA, Shatz CJ (1991) Synchronous bursts of action-potentials in ganglion cells of the developing mammalian retina. Science 252:939-943.

Mesulam MM (1978) Tetramethyl benzidine for horseradish peroxidase neurohistochemistry: a non-carcinogenic blue reaction product with superior sensitivity for visualizing neural afferents and efferents. J Histochem Cytochem 26:106-117.

Miller KD (1990) Correlation-based models of neural development. In: Neuroscience and connectionist theory (Gluck MA, Rumelhart DE, eds), pp 267-353. Hillsdale, NJ: Erlbaum.

Morel A, Imig TJ (1987) Thalamic projections to fields A, AI, P, and VP in the cat auditory cortex. J Comp Neurol 265:119-144.

Morest DK (1964) The neuronal architecture of the medial geniculate body of the cat. J Anat Lond 98:611-630.

Morest DK (1965) The laminar structure of the medial geniculate body of the cat. J Anat Lond 99:143-160.

Morest DK, Winer JA (1986) The comparative anatomy of neurons: homologous neurons in the medial geniculate body of the opossum and the cat. Adv Anat Embryol Cell Biol 97:1-96.

Murphy KM, Jones DJ, Van Sluyters RC (1992) Ocular dominance columns in cat superior colliculus. Invest Ophthal Vis Sci Abst 33:1214.

Pallas SL, Roe AW, Sur M (1990) Visual projections induced into the auditory pathway of ferrets. I. Novel inputs to primary auditory cortex (AI) from the LP/pulvinar complex and the topography of the MGN-AI projection. J Comp Neurol 298:50-68.

Pallas SL, Hahm J, Sur M (1994) Morphology of retinal axons induced to arborize in a novel target, the medial geniculate nucleus. I. Comparison with arbors in normal targets. J Com Neurol 349:343-362.

Reh TA, Constantine-Paton M (1985) Eye-specific segregation requires neural activity in the three-eyed *Rana pipiens*. J Neurosci 5:1132-1143.

Rocha M, Clascá F, Angelucci A, Sur M (1993) Experimentally induced retino-thalamic projections in ferrets: density and distribution of axon arbors. Soc Neurosci Abst 19:45.

Roe AW, Pallas SL, Hahm J-O, Sur M (1990) A map of visual space induced into primary auditory cortex. Science 250:818-820.

Roe AW, Pallas SL, Kwon YH, Sur M (1992) Visual projections routed to the auditory pathway in ferrets: receptive fields of visual neurons in primary auditory cortex. J Neurosci 12:3651-3664.

Roe AW, Garraghty PE, Esguerra M, Sur M (1993) Experimentally induced visual projections to the auditory thalamus: evidence for a W cell pathway. J Comp Neurol 334:263-280.

Rose JE, Woolsey CN (1949) The relations of thalamic connections, cellular structure, and evocable electrical activity in the auditory region of the cat. J Comp Neurol 91:441-466.

Schneider GE (1973) Early lesions of superior colliculus: factors affecting the formation of abnormal retinal projections. Brain Behav Evol 8:73-109.

Sharma J, Angelucci A, Rao SC, Sheth BR, Sur M (1996) Auditory cortex with induced visual projections: horizontal connectivity and optical imaging of functional responses. Soc Neurosci Abst 22:1730.

Shatz CJ (1983) The prenatal development of the cat's retinogeniculate pathway. J Neurosci 3:482-499.

Shatz CJ (1990) Impulse activity and the patterning of connections during CNS development. Neuron 5:745-756.

Shatz CJ, Stryker MP (1988) Prenatal tetrodotoxin infusion blocks segregation of retinogeniculate afferents. Science 242:87-89.

So K-F, Schneider GE, Frost DO (1978) Postnatal development of retinal projections to the lateral geniculate body in Syrian hamsters. Brain Res 142:343-352.

Sretavan DW, Shatz CJ (1986) Prenatal development of retinal ganglion cell axons: segregation into eye-specific layers within the cat's lateral geniculate nucleus. J. Neurosci 6:234-251.

Sretavan DW, Shatz CJ, Stryker MP (1988) Modification of retinal ganglion cell axon morphology by prenatal infusion of tetrodotoxin. Nature 336:468-471.

Stryker MP, Zahs K (1983) ON and OFF sublaminae in the lateral geniculate nucleus of the ferret. J Neurosci 3:1943-1951.

Sur M, Garraghty PE, Roe AW (1988) Experimentally induced visual projections into auditory thalamus and cortex. Science 242:1437-1441.

Thompson ID (1990) Retinal pathways and the developmental basis of binocular vision. In: Vision: coding and efficiency (Blakemore C, ed), pp 209-223. Cambridge UP.

Wenstrup JJ, Larue DT, Winer JA (1994) Projections of physiologically defined subdivisions of the inferior colliculus in the mustached bat: targets in the medial genicualte body and extrathalamic nuclei. J Comp Neurol 346:207-236.

White CA, Chalupa LM (1991) Development of mammalian retinofugal pathways. In: Neuroanatomy of the visual pathways and their development (Dreher B, Robinson SR, eds), pp 129-149. London: Macmillan Press.

Williams RW, Chalupa LM (1982) Prenatal development of retinocollicular projections in the cat: An anterograde tracer transport study. J Neurosci 2:604-622.

Winer JA (1985) The medial geniculate body of the cat. Adv Anat Embryol Cell Biol 86:1-98.

Winer JA (1992) The functional architecture of the medial geniculate body and the primary auditory cortex. In: The Mammalian Auditory Pathway: Neuroanatomy (Webster DD, Popper AN, Fay RR, eds), pp 222-409. New York: Springer-Verlag.

Winer JA, Diamond IT, Raczkowski D (1977) Subdivisions of the auditory cortex of the cat: the retrograde transport of horseradish peroxidase to the medial geniculate body and posterior thalamic nuclei. J Comp Neurol 176:387-418.

Zhang HY, Hoffmann K-P (1993) Retinal projections to the pretectum, accessory optic system and superior colliculus in pigmented and albino ferrets. European J Neurosci 5:486-500.

Figure Legends

Figure 1. Distribution and pattern of termination of retinal projections to the medial geniculate nucleus (MGN) in an adult "rewired" ferret. Retino-MGN projections were labeled by injecting CTB into the contralateral eye (case F94-97; Table 1). **A-F:** Caudal-to-rostral sequence of coronal sections through the MGN. The spacing between sections is indicated in Fig. 2. Note that retinal fibers form terminal clusters scattered throughout the MGN subdivisions (MGv, MGd, MGm), predominantly in the rostral half of the nucleus (see Results). Patches in MGv are oriented and aligned along an oblique dorsoventral axis (see Results). MGN subdivisions for D are indicated in Fig. 3A. MGd, MGm, MGv: dorsal, medial and ventral divisions of MGN, respectively. Sg: suprageniculate nucleus. Dorsal is up, medial to the right. Scale bar: 500 m.

Figure 2. Lateral view of the dorsal thalamus. The vertical lines (**A-F**) indicate the approximate anteroposterior level of each MGN section shown in Fig. 1. The horizontal dashed line marks the rostrocaudal extent of the MGN. MGN: medial geniculate nucleus; LGN: lateral geniculate nucleus; D: dorsal. A: anterior. Scale bar: 1 mm.

Figure 3. Trajectories of retinal axons that innervate the medial geniculate nucleus (MGN) in adult "rewired" animals. **A**: Camera lucida drawing of the coronal MGN section illustrated in Fig. 1D, shown at higher magnification to demonstrate axon trajectories. Note that retinal axons enter the MGN from all around the nucleus. Terminal clusters of retinal projections are more evident in MGv and MGd. One cluster (*arrowhead*) is partly reconstructed at higher magnification in Fig. 4 (arrowhead). **B:** Camera lucida drawing of a horizontal MGN section showing axon trajectories in the anteroposterior dimension. Clusters of retinal projections are elongated anteroposteriorly. LGN: lateral geniculate nucleus; LP: lateral posterior nucleus; LTN: lateral terminal nucleus; MGd, MGm, MGv: as in Fig. 1; OT: optic tract; Sg: suprageniculate

nucleus; vl: ventrolateral nucleus of MGv; A: anterior; D: dorsal; M: medial. Scale bars: 200 m.

Figure 4. Camera lucida reconstructions of six retino-MGN axonal arbors in adult "rewired" ferrets. These axons have focal terminal arbors with large clustered boutons (see Results). The *insets* on the left show a coronal view of the location of each reconstructed axon within MGN. The diameters of these axons are indicated (m). **A:** Axons 2 and 3 are shown in gray and black, respectively, to demonstrate the overlap between their terminal arbors. **B:** partial reconstruction of one cluster (*arrowhead*:) shown in figure 3A (arrowhead). This cluster was formed by the terminal arbors of several axons (see Fig. 3A). Here we reconstructed only three of them. MGd, MGm, Mgv : as in Fig. 1; LGN, OT: as in Fig. 3; D: dorsal; M: medial. Scale bar: 100 m.

Figure 5. Retinal inputs to the lateral posterior thalamic nucleus (LP) in an adult "rewired" ferret. **A, B:** Darkfield micrographs of retino-LP projections labeled by an injection of WGA-HRP in the contralateral eye. **A', B':** Brightfield micrographs of ipsilateral retino-LP projections labeled with CTB. Sections in A and B are immediately adjacent to sections in A' and B', respectively. *Arrowheads* point to corresponding blood vessels in adjacent sections. A composite drawing of A and A' is shown in Fig. 7. Note the terminal "slab-like" pattern of retinal projections to LP. Sg: suprageniculate nucleus. Dorsal is up, medial to the right. Scale bars: 200 m.

Figure 6. Spatial relationship between eye-specific inputs in the medial geniculate nucleus (MGN) of adult "rewired" ferrets. **A, B**: **(Right)**: Composite reconstructions of the retinal label from each eye, obtained by superimposing camera lucida drawings of two adjacent MGN sections (see Materials and Methods). Projections from the contralateral eye, stained with WGA-HRP, are represented in *red*, while CTB-stained ipsilateral projections are represented in

blue. Only terminal zones are plotted (fibers are not shown). Note that retinal inputs from the two eyes terminate mainly in the same regions of MGN in a non-overlapping fashion (see Results). Right scale bar: 200 m (valid for both A and B). **A, B (Left)**: Camera lucida drawings of coronal thalamic hemisections, showing the location (*insets*) of the retinal label drawn at higher magnification on the right. Left scale bar: 500 m (valid for both A and B). Abbreviations as in previous figures. Dorsal is up, medial to the right.

Figure 7. Eye-specific segregation in the lateral posterior nucleus. **Right**: Composite camera lucida drawing of retino-LP projections arising from each eye, obtained by superimposing section A and A' of Fig. 5 (see Materials and Methods). Contralateral retinal projections are represented in *red*. Projections from the ipsilateral eye are represented in *blue*. Only terminal zones are illustrated. Projections from the two eyes form parallel, largely segregated "slabs" in LP (see Results). Right scale bar: 200 m. **Left**: same as Fig. 4 (Left). Left scale bar: 500 m. Abbreviations as in previous figures. Dorsal is up, medial to the right.

Figure 8. Emergence of clustered retinal projections to the medial geniculate nucleus (MGN) in young postnatal "rewired" ferrets. **A-E:** Developmental sequence of coronal MGN sections. Retino-MGN projections were labeled by injecting CTB in the contralateral eye at various developmental ages. Postnatal (P) ages are indicated at the side of each figure. White dotted lines outline the contour of the MGN. Note that clustering of retino-MGN projections occurs progressively over development. *Arrow* in B: a tendency to cluster first appears at P8. Dorsal is up, medial to the right. Scale bars: 200 m.

Figure 9. Camera lucida reconstructions of thirteen retino-MGN axonal arbors during the second and fourth postnatal weeks of development. Postnatal ages (P) are indicated on the left of each panel. Axons **1** and **2** have few (1) or no (2) branches, and run for long distances in MGN, resembling one- and two-week old axons (see Results). Axons **3-7** have begun to form

arbors and send long branches to distant regions in MGN. Axons **8** and **9** are restricted to one MGN subdivision and send branches to several clusters. These axons are shown in black (8) and gray (9) to demonstrate the overlap of one of their terminal arbors. Axons **10-13** have more elaborate arbors restricted to a single cluster. D: dorsal; M: medial. Scale bar: 100 m.

Figure 10. Emergence of eye-specific segregation in the medial geniculate nucleus (MGN). **A-D:** Composite camera lucida drawings of the retinal label from each eye at four different ages. Postnatal (P) ages are indicated in each panel. Projections from the contralateral eye are shown in *red*, and were labeled with WGA-HRP; CTB-labeled ipsilateral projections are shown in *blue*. Projections from the two eyes are initially overlapped (A), but progressively segregate into eye-specific domains (B-D). Abbreviations as in previous figures. Dorsal is up, medial to the right. Scale bars: 200 m.

Figure 11. Summary of the developmental changes occuring in the MGN and the retino-MGN projections in "rewired" ferrets. **A, B:** Pseudo-colored representations of normalised optical densities of CTB-labeled retinal projections to the MGN at P8 (A) and adulthood (B). The brightest red represents the densest staining, and corresponds to median CTB labeling in the LGN (see Materials and Methods). A and B are computer generated images of the same MGN coronal sections shown in Figs. 8B and 1D, respectively. *Arrow* in A, points to the same cluster marked by an arrow in Fig. 8B. Dorsal is up, medial to the right. Scale bars: 200 m. **C:** Histogram indicating the area of MGN as a function of age. **D:** Histogram of the area of retinal projections to the MGN as a function of age. **E:** Histogram indicating the percentage of the MGN area innervated by retinal fibers as a function of age. **F:** Histogram of the percentage of retinal projections forming clusters (clustering index; see Materials and Methods) as a function of age. For number of animals analyzed in each developmental group see Materials and Methods. Error bars: s.e.m.

Table 1

Intraocular injections in adult "rewired" ferrets

Case #	Lesioned hemisphere/s	Eye/s injected with CTB	Eye injected with WGA-HRP
F94-82	left	right	
F94-85	left	both	
F94-89	both	both	
F94-97	both	right	left
F94-146	left	left	
F94-178	right	right	
F94-212	left	both	
F94-251	both	left	
F94-252	both	left	
F95-5	both	left	
F95-75	both	right	left
F95-92	both	right	
F95-93	both	right	

CTB: cholera toxin subunit B; WGA-HRP: wheat germ agglutinin conjugated to horseradish peroxidase.

Table 2

Intraocular injections in young postnatal animals

	No. of animals								
	P4	**P6**	**P7**	**P8**	**P14**	**P22**	**P25**	**P26**	**P27**
Rewired	2	2	2	2	2	4	1	1	4
Normal	1	1				1			1

Ages of postnatal animals, and number of animals analyzed at each age. All "rewired" ferrets were operated on both sides of the brain, with surgery on P1. All animals in the table received an injection of CTB in one eye and WGA-HRP in the opposite eye.

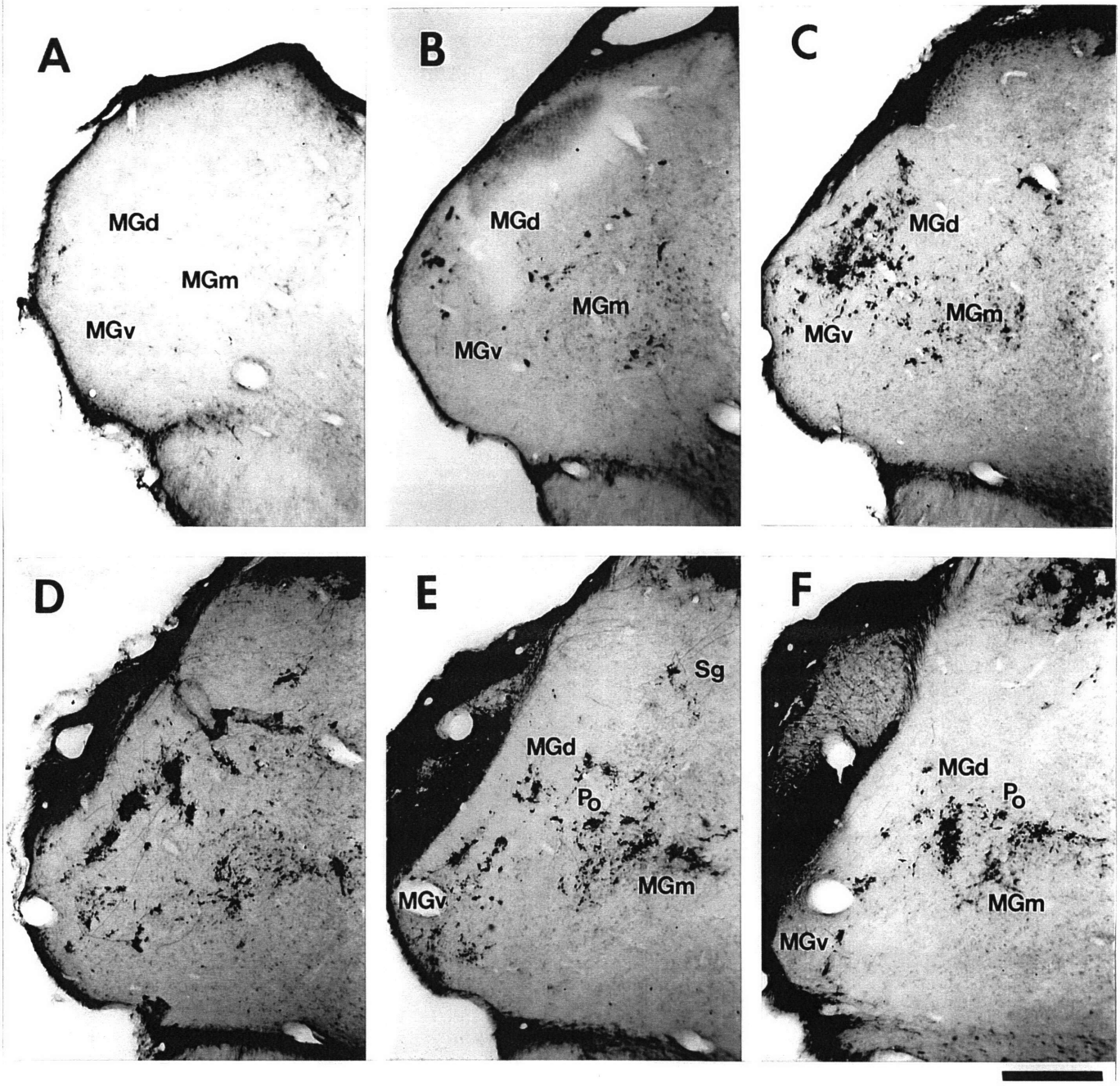
A
MGd
MGm
MGv
B
MGd
MGm
MGv
C
MGd
MGm
MGv
D
E
Sg
MGd
Po
MGm
MGv
F
MGd
Po
MGm
MGv

Fig.1

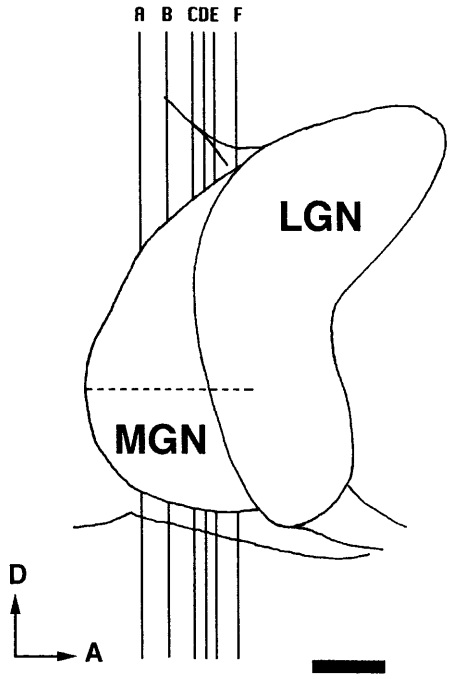

Fig. 2

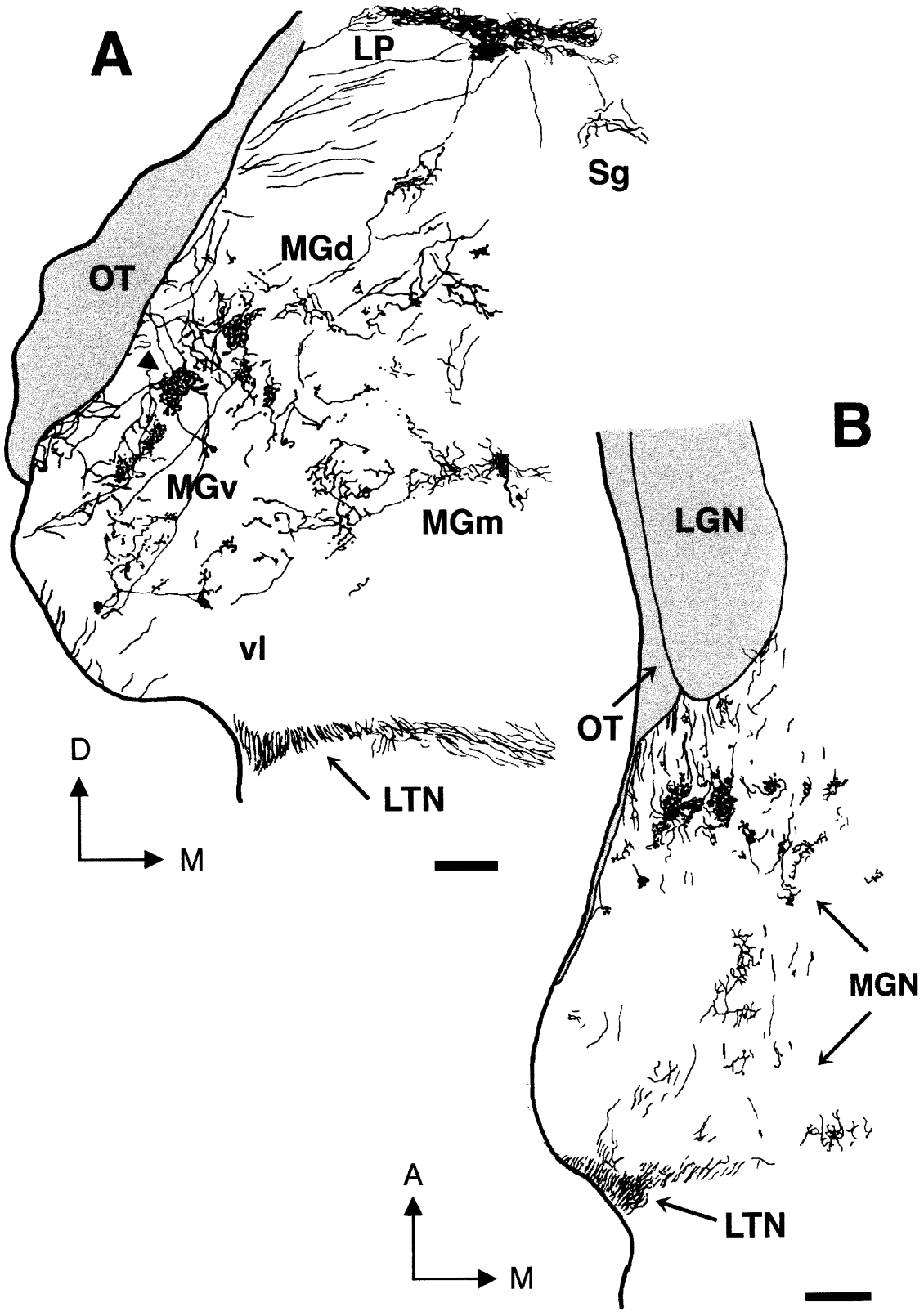

Fig. 3

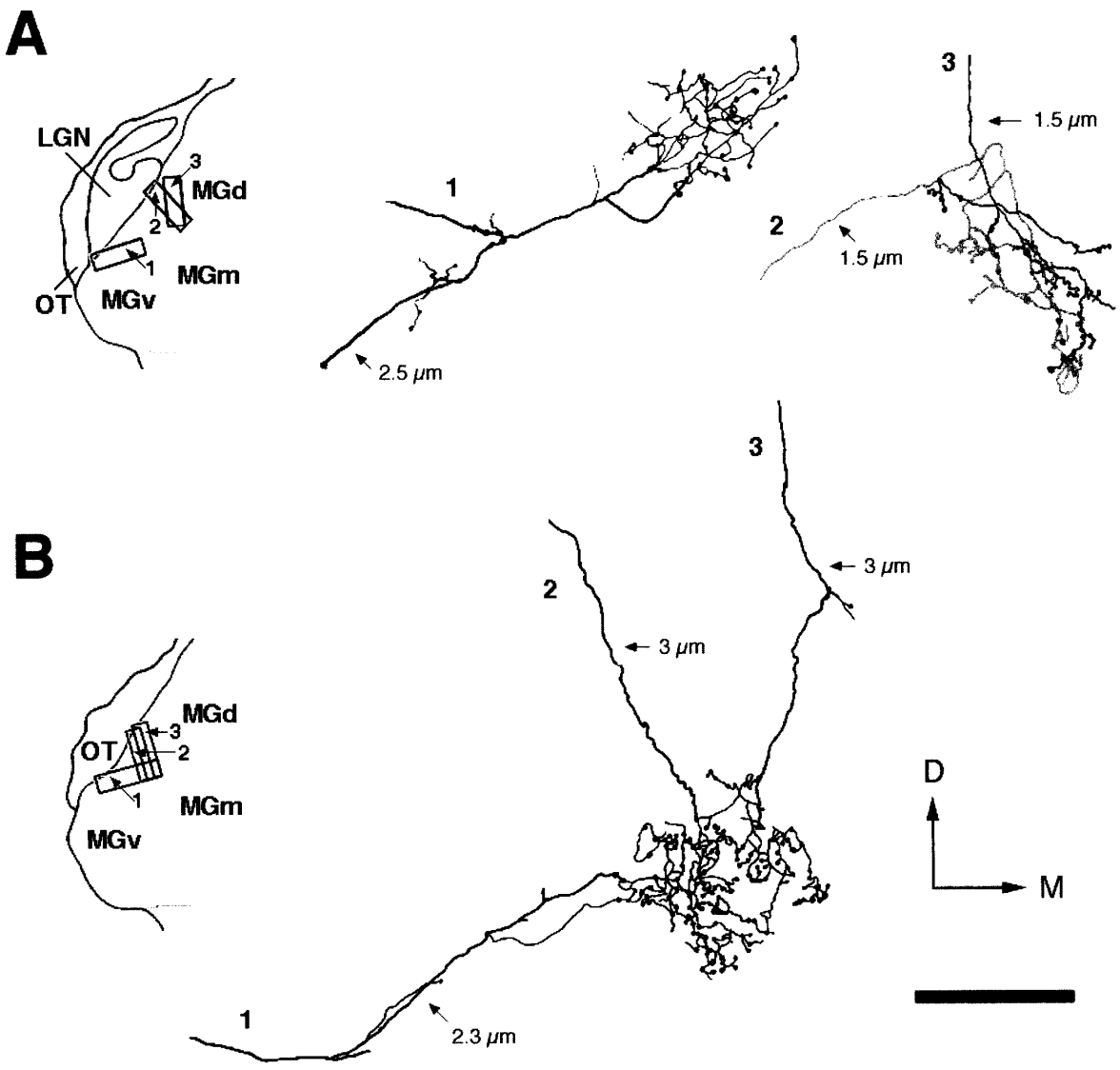
A
LGN
3
MGd
2
1
MGm
OT
MGv
1
2.5 μm
3
1.5 μm
2
1.5 μm
B
MGd
3
OT
2
1
MGm
MGv
3
3 μm
2
3 μm
1
2.3 μm
D
M

Fig. 4

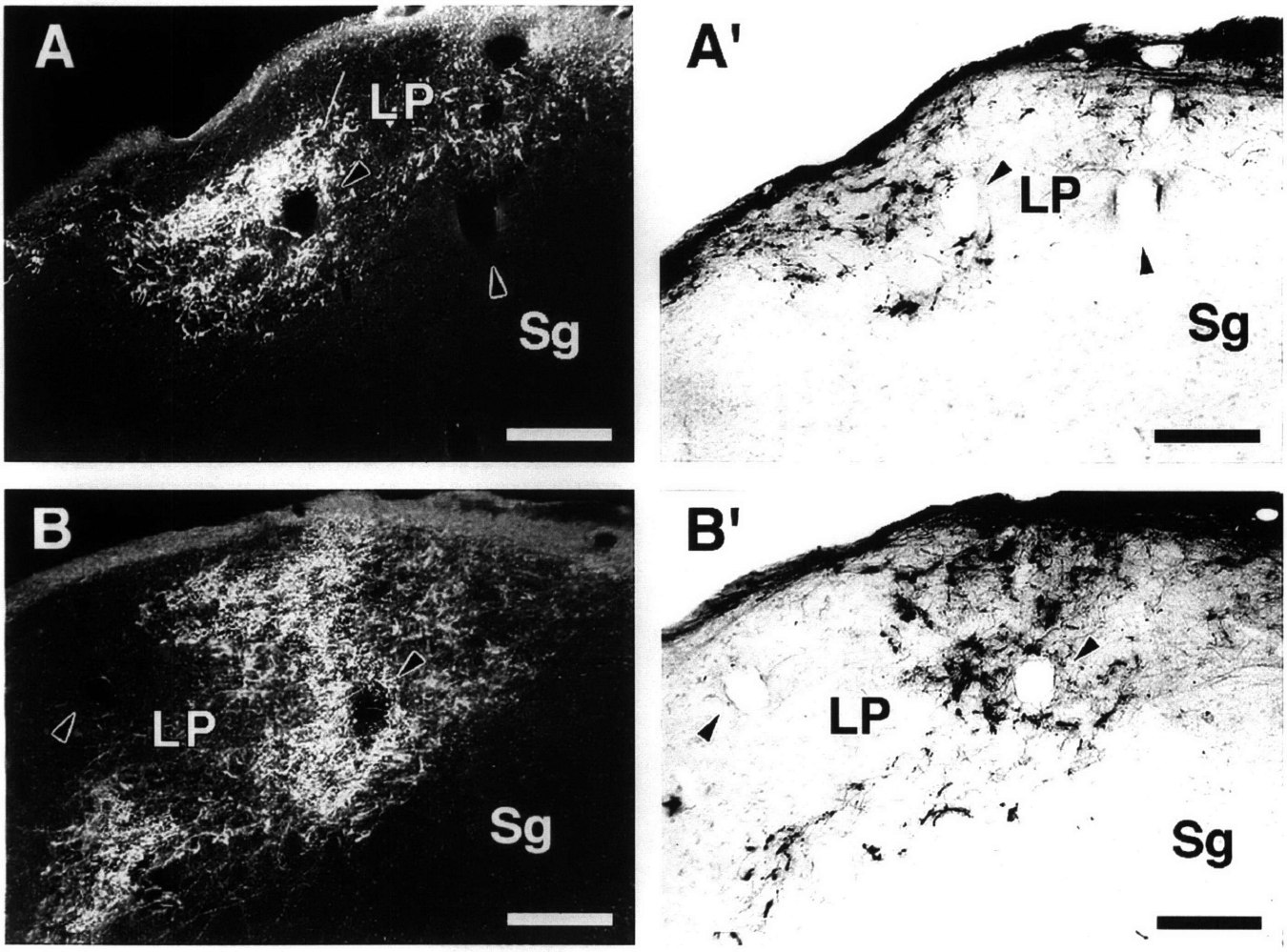

Fig. 5

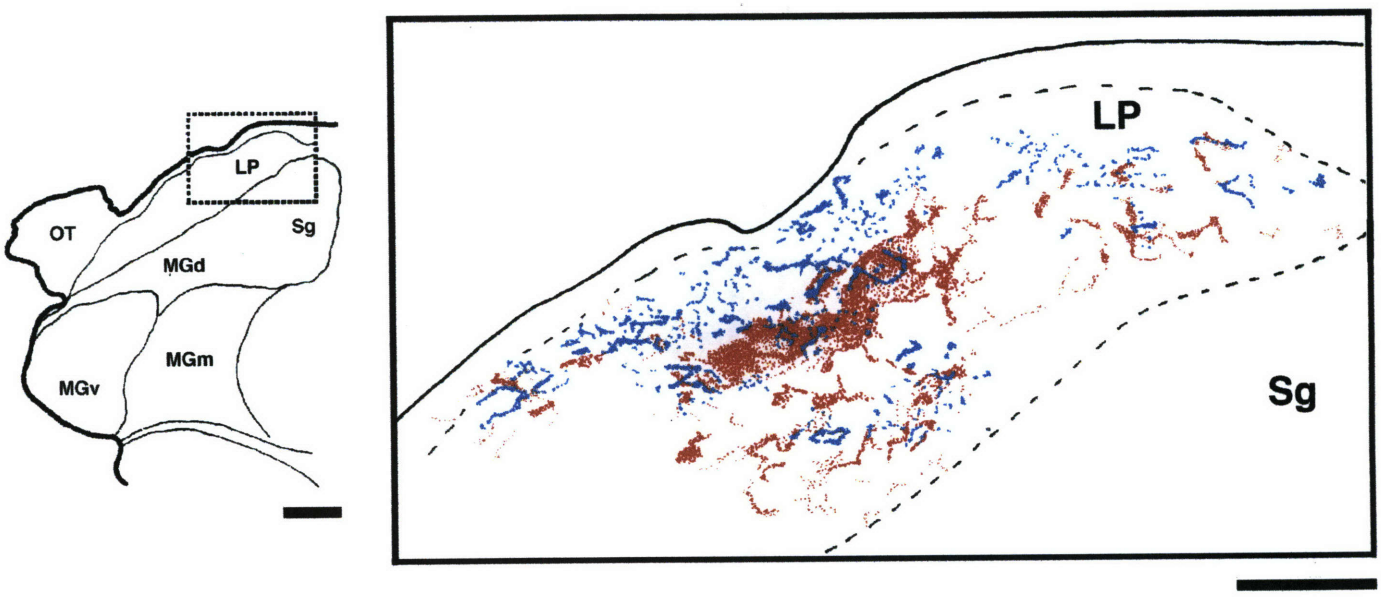

Fig. 7

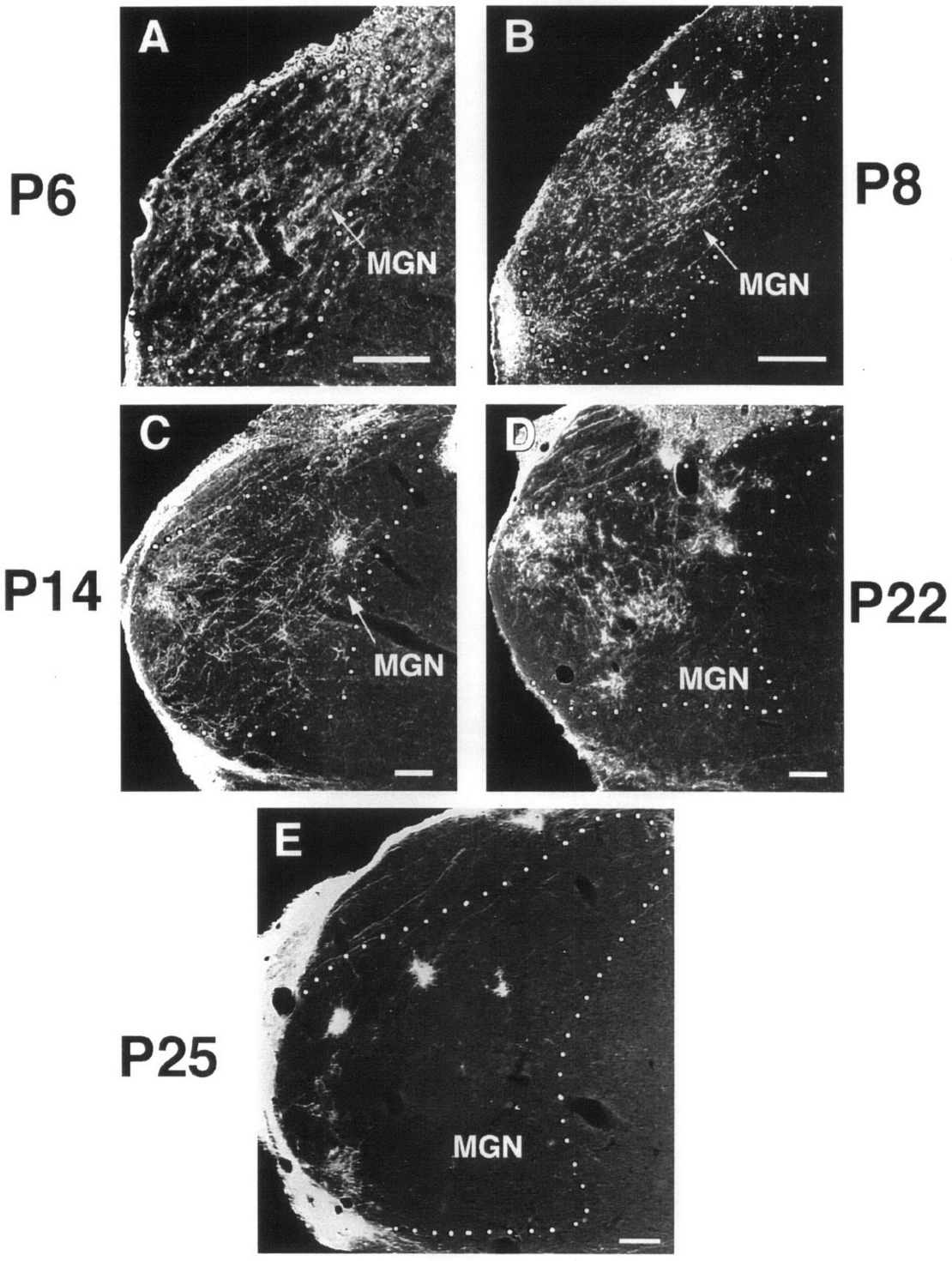

Fig. 8

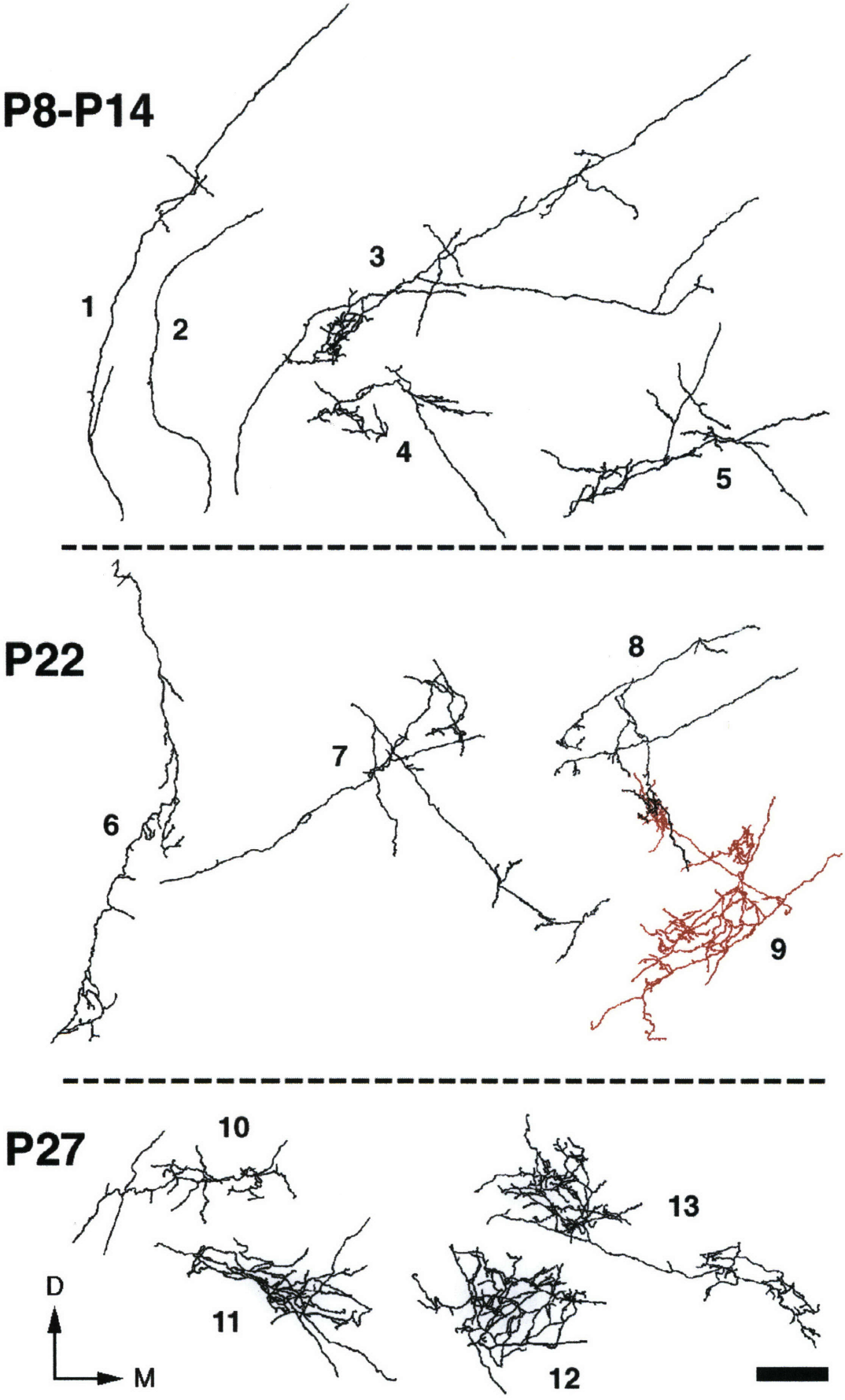

Fig. 9

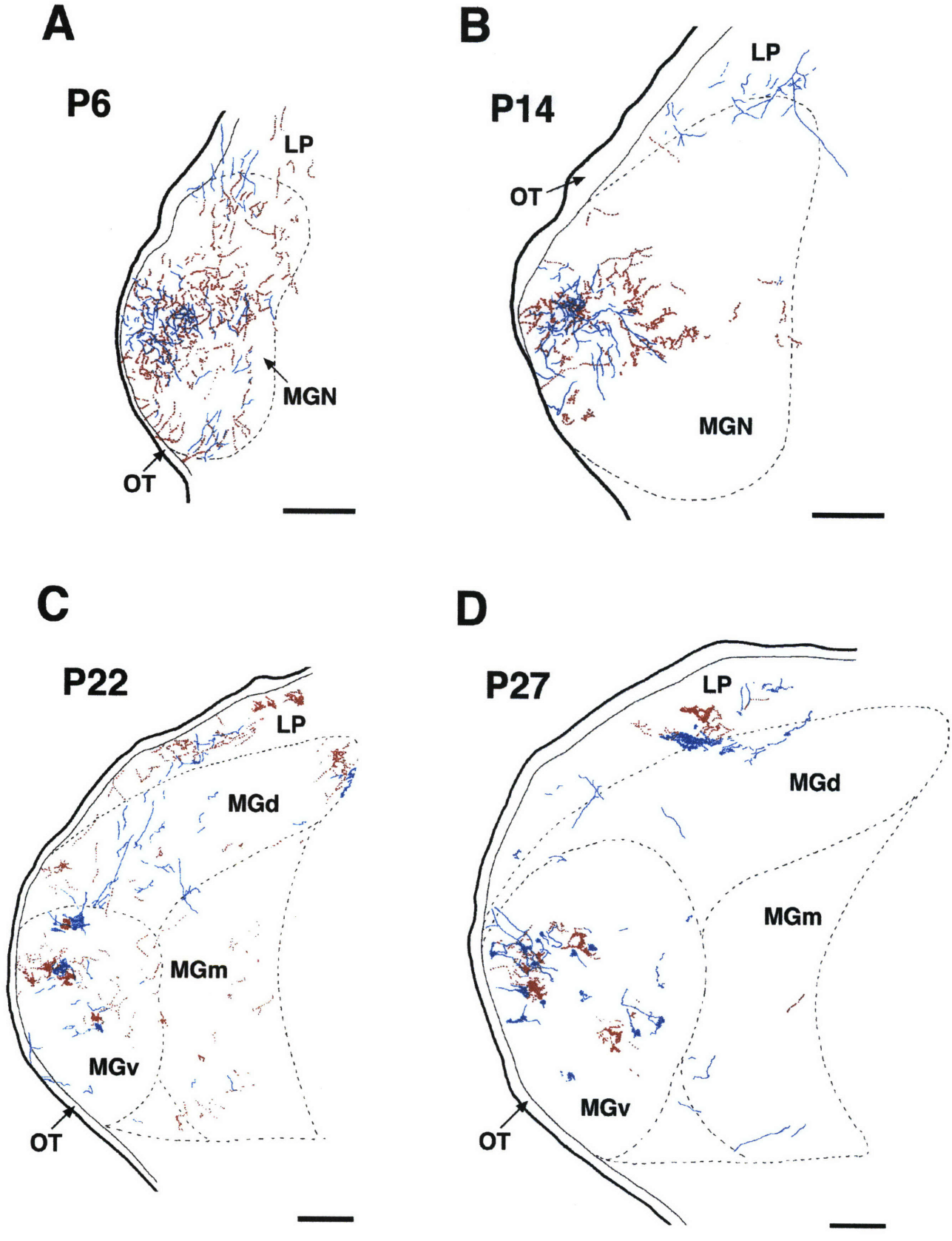
A
P6
LP
MGN
OT
B
P14
LP
OT
MGN
C
P22
LP
MGd
MGm
MGv
OT
D
P27
LP
MGd
MGm
MGv
OT

Fig. 10

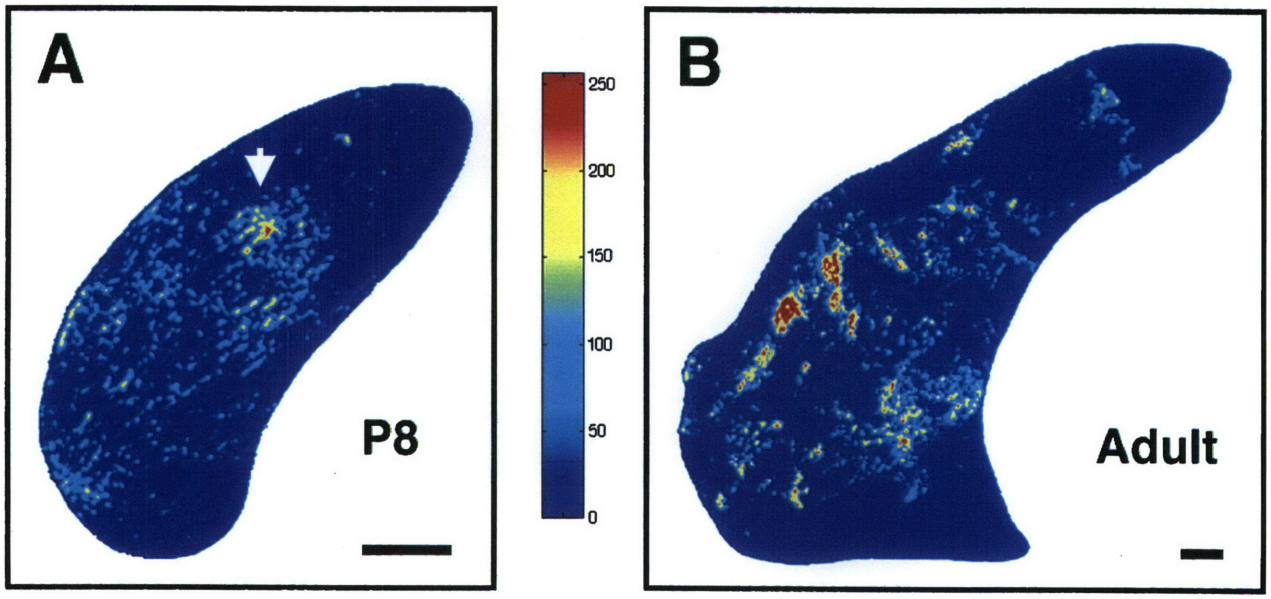
A
P8
250
200
150
100
50
0
B
Adult

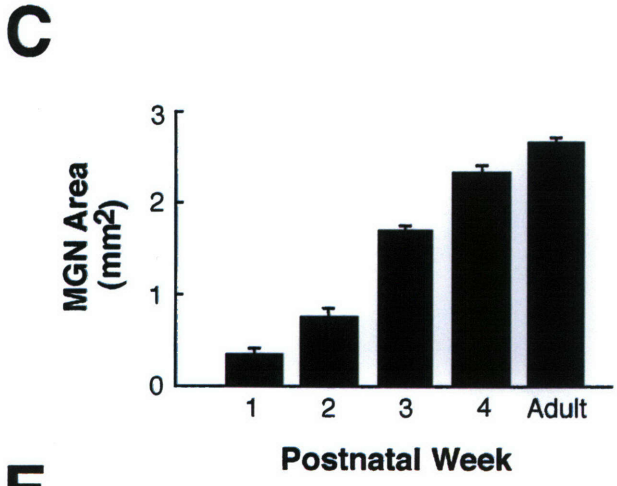
C
MGN Area (mm2)
3
2
1
0
1
2
3
4
Adult
Postnatal Week

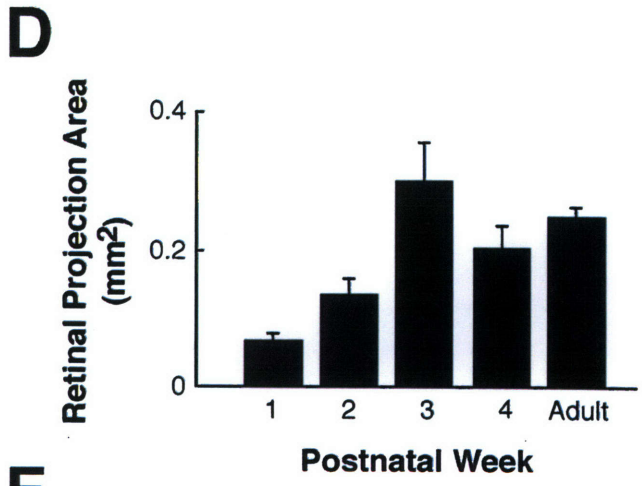
D
Retinal Projection Area (mm2)
0.4
0.2
0
1
2
3
4
Adult
Postnatal Week

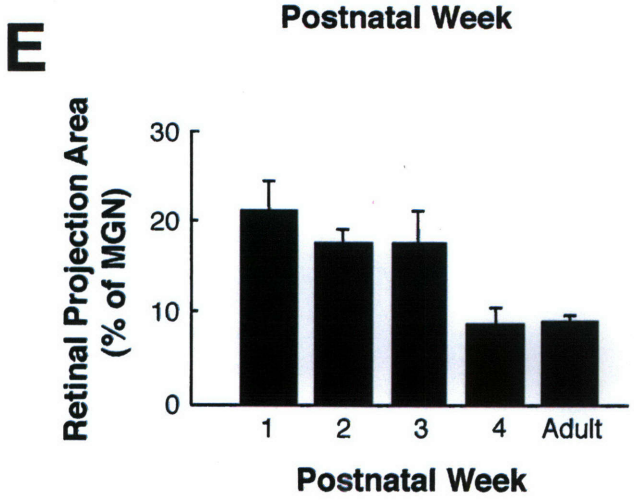
E
Retinal Projection Area (% of MGN)
30
20
10
0
1
2
3
4
Adult
Postnatal Week

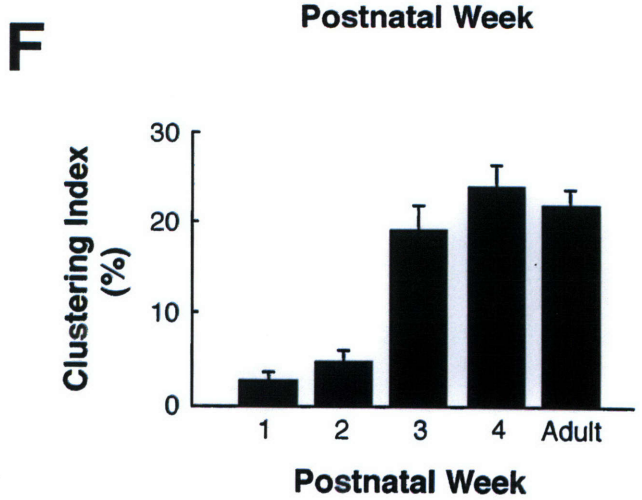
F
Clustering Index (%)
30
20
10
0
1
2
3
4
Adult
Postnatal Week

Fig.11

Chapter 4

Thalamocortical Projection Patterns from Cyto- and Chemo-Architectonically Identified Subdivisions of the Ferret Medial Geniculate Body

Introduction

The auditory cortex of mammals contains multiple fields that are distinguished from one another anatomically and physiologically (for reviews see Brugge and Reale, 1985; Aitkin, 1990; Clarey et al., 1992; Winer, 1992). On the base of physiological mapping studies, we now recognize the existence of several "core" auditory cortical fields (four in the cat) characterized by the "cochleotopic" (or tonotopic) organization and frequency selectivity of their neurons. These "core" areas are surrounded by a belt of auditory cortical fields in which broad tuning of single cells to sound frequencies and blurred tonotopy have been observed. Consistent with the physiological parcellation of auditory cortex, connectional studies have revealed that the "core" areas receive thalamic inputs from tonotopically organized subdivisions of the medial geniculate nucleus (MGN) (Rose and Woolsey, 1949; Andersen et al., 1980; Imig and Morel, 1984; Morel and Imig, 1987; Pallas et al., 1990; Angelucci et al., 1993), whereas non-primary, non-tonotopic cortical fields receive inputs from non-tonotopically organized MGN subnuclei (Winer et al., 1977; Imig and Morel, 1988; Winer, 1992). All of the identified tonotopically organized cortical fields contain maps of sound frequency and binaural interactions (Phillips et al., 1991; Clarey et al., 1992). The term tonotopy refers to the peculiar representation of the cochlear sensory epithelium within a cortical field. Cells representing the same characteristic frequency are arrayed along columns that have been referred to as "isofrequency lines", and a systematic representation of sound frequencies occurs across one cortical dimension (Merzenich et al., 1975, 1977; Knight, 1977). For example, in the cat the isofrequency lines run in a dorsoventral direction, with lines representing high frequencies located rostrally in AI, and those representing lower frequencies located progressively more caudally. By contrast, in the ferret AI the isofrequency contours have a rostrocaudal orientation, with high-frequency lines located medially, and lower-frequency lines progressively more laterally (Kelly et al., 1986; Phillips et al., 1988). Several recent studies have provided evidence of the existence of a second functional map

within AI. This map consists of binaural interaction bands in which neurons with predominantly excitatory-excitatory (EE) response properties (responses to simultaneous stimulation of both ears are greater than those to stimulation of either ear alone) alternate with bands of neurons with excitatory-inhibitory (EI) response properties (responses to stimulation of one ear are inhibited by simultaneous stimulation of the other ear) (Imig and Adrian, 1977; Middlebrooks et al., 1980; Kelly and Sally, 1988). In the cat AI, EE/EI bands are oriented orthogonal to the isofrequency lines and recent data have shown that this is the case also for the ferret AI (Kelly and Judge, 1994).

A functional organization into tonotopic and binaural maps has also been described in the ventral nucleus of the MGN (MGv) in the cat (Middlebrooks and Zook, 1983; Imig and Morel, 1985). Studies on the cat thalamocortical system have suggested that the geniculocortical projections are topographically organized into a highly divergent and convergent manner (Merzenich et al., 1982, 1984). Thus, injections of retrograde tracers into physiologically defined frequency loci in the cat AI have shown that arrays of neurons in MGN project to restricted AI loci of similar frequency and binaural properties (Merzenich et al., 1982; Middlebrooks and Zook, 1983). At the same time, a restricted locus in MGv projects to divergent cortical sites along an isofrequency line. More recently, other studies have challenged the divergent/convergent theory of auditory thalamocortical organization, providing evidence in support of a more "point-to-point" topographic organization (Brandner and Redies, 1990) similar to that previously described for other sensory systems, such as the visual and somatosensory thalamocortical pathways.

Previous studies from this laboratory have examined the functional effects of redirecting visual inputs to the auditory thalamus and cortex early in development (Sur et al., 1988). It was found, that even though retinal inputs to the MGN occupy only a small fraction of the entire MGN volume (Sur et al., 1988; Angelucci, chapter 1, this volume), a much larger portion of AI receives visual input (Roe et al., 1992). This finding would be consistent with a divergent/convergent pattern of projections from MGN to AI. At the same time, it was

reported that in AI of "rewired" ferrets there is a topographic representation of visual space (Roe et al., 1990), and that visually responsive cells have spatially localized receptive fields (Roe et al., 1992). The latter two findings would not be predicted solely on the base of an anatomical divergent pattern of projections from MGN to AI, whereas they could be accounted for by a topographic order of these projections along the isofrequency dimension. A previous retrograde study on the normal pattern of projections from MGN to AI in the ferret has provided some evidence in support of a divergent/convergent scheme of auditory thalamocortical organization, and has shown that such pattern is unaltered in "rewired" ferrets (Pallas et al., 1990). However, that study as well as most of the anatomical studies on the auditory thalamocortical projections have so far relied on retrograde tracing methods, while only a few recent studies in the rabbit (McMullen and de Venecia, 1993) and monkey (Hashikawa et al., 1995) have employed sensitive anterograde tracing techniques.

In the present study we have examined the pattern of auditory thalamocortical projections and the extent of their intracortical arborization following small injections of highly sensitive anterograde tracers (PHA-L and Biotinylated Dextran) in the ferret MGN. In addition, as a necessary prerequisite to identify location of injections sites, we have identified the main subdivisions of the ferret auditory thalamus.

Regional parcellations of the MGN in the ferret have so far relied exclusively on Nissl-staining and on comparisons with location and cytoarchitecture of MGN subdivisions in the cat (Pallas et al., 1990). However, species differences in the configuration of the diencephalon can be remarkable. Thus for example, the ferret MGN is rotated dorsomedially relative to its position in the cat. Furthermore, the degree of cytoarchitectonic differentiation of the dorsal thalamus in Nissl-stained sections varies considerably among species. For these reasons a more accurate parcellation of the ferret MGN requires the use of different staining methods as well as connectional data. Recently, chemoarchitectonic criteria have been used in conjunction with cytoarchitectonic criteria and various immunohistochemical staining methods to characterize the subdivisions of the MGN in several species (Jones and Hendry,

1989; Caballero-Bleda et al., 1991; Hashikawa et al., 1991; Campbell and Pandya, 1994; de Venecia et al., 1995). In the present study we have used a combination of cyto- and chemoarchitectonic criteria as well as calcium-binding protein and Cat-301 immunohistochemistry to identify the location and boundaries of subnuclei within the ferret MGN.

Materials and Methods

A total of 12 adult pigmented ferrets (*Mustela putorious furo*) were bred in our colony or obtained from a commercial supplier (Marshall Farms). To identify MGN subdivisions 7 animals were euthanized with sodium pentobarbital (80 mg/kg, i.p.) and transcardially perfused with saline, followed by 4% paraformaldehyde in 0.1M phosphate buffer pH 7.4. Brains were blocked stereotaxically, removed from the skull and post-fixed overnight in the same fixative. After cryoprotection by soaking in 30% phosphate-buffered sucrose, brains were sectioned in the coronal plane at 40 μm on a freezing microtome. Three brains were cut into three adjacent series of sections that were stained for Nissl, cytochrome oxidase (CO) and acetylcholinesterase (AChE), respectively. Three series of adjacent sections in two additional brains were reacted for Nissl, CO and Cat-301, respectively, while the two remaining brains were cut into five series that were processed for Nissl, CO, AChE, parvalbumine (PV) and calbindin, respectively. Sections to be reacted for AChE and CO histochemistry as well as for immunohistochemistry were incubated free floating, while sections to be stained for Nissl substance were mounted onto gelatin-subbed slides and reacted on the slides. CO histochemistry was performed according to the method described by Wong-Riley (1979). For AChE histochemistry sections were incubated according to the method of Geneser-Jensen and Blackstad (1971), with the silver intensification procedure of Hardy et al. (1976). Staining for Nissl substance was obtained with cresyl violet. Procedures for Cat-301 immunohistochemistry have been previously described (McKay and Hockfield, 1982). Briefly, sections were incubated overnight in monoclonal antibody Cat-301 (kindly donated by Dr. S. Hockfield), diluted 1:2 in tissue culture medium (Dulbecco's modified Eagle's medium; Sigma) with 2% Triton X-100 and 5% fetal calf serum (FCS). After rinsing, sections were incubated in a solution containing an HRP-conjugated secondary antibody (HRP-conjugated goat anti-mouse IgG,A,M; Cappel) diluted 1:250 in tissue culture medium with 5% FCS and 2% Triton X-100 for 2 hr. Sections were then reacted for ~ 20 min. with 3,3'-

diaminobenzidine (DAB; Sigma) for visualization of HRP. For calcium-binding protein immunohistochemistry, sections were pre-incubated for 1 hr. in 3% normal horse serum (NHS) with 1% Triton-X-100, then incubated in anti-PV (Swiss Antibodies #235) or anti-CB (Swiss Antibodies #300) mouse monoclonal antibodies (1:10,000, with 3% NHS) for 72 hr at 4°C, followed by biotinylated horse anti-mouse IgG (1:200 with 3% NHS) for 2 hr, and avidin-biotin-peroxidase complex (ABC, 1:100; Vector Labs) for 90 min. HRP was finally visualized by incubating the sections in a cobalt-enhanced DAB solution. Sections were mounted, dehydrated in ascending alcohols, and coverslipped with DPX mounting medium.

The pattern of thalamocortical projections was studied by delivering injections of PHA-L or Biotinylated Dextran (BD) into the MGN of 5 adult ferrets. Tracer injections were performed under direct visual guidance. The surgical protocol is described in detail in the Materials and Methods of Chapter 1 (this thesis). Briefly, animals were pre-anesthetized with ketamine (30 mg/kg) and xylazine (1.5 mg/kg), intubated with an endotracheal tube and placed in a stereotaxic apparatus. Anesthesia was subsequently maintained with 1-2% isoflurane in a 1/1 mixture of nitrous oxide and oxygen. A large craniotomy and durotomy were performed and the occipital cortex was gently pulled forward using smooth brain retractors. After cauterization of the posterior veins, and gentle suction of part of the white matter and hippocampus overlying the dorsal thalamus, PHA-L (Vector Labs; 2.5%, 10 mM in phosphate buffer saline, pH 8.0) or BD (3000 MW; Molecular Probes; 10% in saline) were injected into the left MGN under direct visual control. The tracers were delivered iontophoretically through glass micropipettes (15-20 μm inside tip diameter) by applying 7-8 μA of positive current in 7s on/off cycles for 7-12 min. After survival periods of 10-20 days animals were sacrificed with an overdose of sodium pentobarbital and transcardially perfused with saline followed by either 4% paraformaldehyde (for BD) or 4% paraformaldehyde and 0.1% glutaraldehyde (for PHA-L). The brains were blocked stereotaxically, removed from the skull and post-fixed in the same fixatives. After cryoprotection, some brains were cut in the coronal plane at 50-60 μm on a freezing microtome. For other brains, the cortex was dissected

away from the diencephalon, and while the thalamus was sectioned in the coronal plane, blocks containing the auditory cortex were cut in the tangential plane. All the cortical sections and one series of thalamic sections were immunoreacted for PHA-L or BD. For identification of MGN subdivisions one in three thalamic sections were counterstained with cresyl violet, and the remaining series of MGN sections was reacted for CO or AChE.

The immunohistochemical reaction to visualize PHA-L was performed using a slightly modified version of the protocol developed by Gerfen and Sawchenko (1984). Sections were first incubated overnight in a blocking solution of 2% normal rabbit serum (NRS), 2,5% bovine serum albumin (BSA) and 0.5-0.7% Triton X-100 in 0.02M potassium phosphate-buffered saline (KPBS), pH 7.4, and then transferred for 48 hr. at 4°C in primary goat anti-PHA-L antibody (Vector Labs; diluted 1:3000 in KPBS with 2% NRS, 2,5% BSA and 0.5% Triton X-100). Tissue sections were then incubated in a 1:200 dilution of biotinylated secondary antibody (rabbit anti-goat IgG; Vector Labs) with 0.5% Triton X-100, 2% NRS and 2.5% BSA, for 1 hr at room temperature. After a 1 hr incubation in avidin-biotin-peroxidase (1:100), HRP was visualized via a cobalt-enhanced DAB reaction.

BD was revealed by using the high-affinity binding of an avidin-alkaline phosphatase conjugate (AP) according to the protocol of Brandt and Apkarian (1992). Sections were incubated for 20 min. in 90% methanol and 0.3% H_2O_2 in distilled water. After rinsing in Tris buffer (TB) pH 8.0, the tissue was incubated overnight in a solution of 0.1% ExtrAvidin-AP (Sigma), 0.1% sodium azide and 1% Triton X-100 in TB pH 8.0. After rinses in TB pH 9.5, the staining was developed for 2-3 hr in a solution containing 0.08% 5-bromo-4-chloro-3-indolyl phosphate (Sigma), 5% N,N-dimethyl-formamide (Sigma), 0.0125% Levamisole (Sigma), and 0.008% Nitro Blue Tetrazolium (Sigma) in TB pH 9.5. All sections were mounted, dehydrated and coverslipped as described above.

Results

Parcellation of the ferret medial geniculate nucleus

The medial geniculate nucleus (MGN) in the ferret is located in the most caudal part of the dorsal thalamus. Its caudal pole protrudes laterally as a bulge clearly discernible on the ventrolateral aspect of the diencephalon. Its anterior half, instead, is bounded dorsolaterally by the lateral geniculate nucleus (LGN), dorsally by the lateral posterior thalamic nucleus (LP), and medially by the pretectal nuclei and the fibers of the medial lemniscus. The fibers of the auditory radiation separate the rostral pole of MGN from the ventrobasal complex (Figs. 1E,2E,3E,4E).

To identify the different subdivisions of the MGN we employed a combination of Nissl staining, acetylcholinesterase (AChE) and cytochrome oxidase (CO) histochemistry, as well as parvalbumin (PV), calbindin (CB) and Cat-301 immunohistochemistry, in adjacent MGN sections.

Whereas no single staining method by itself allowed us to clearly distinguish all the different MGN nuclei, each method identified at least one particular subdivision, with the exception of parvalbumin immunohistochemistry. Indeed, in contrast to what has been previously described in other species, such as the rabbit (de Venecia et al., 1995) and monkey (Jones and Hendry, 1989; Hashikawa et al., 1991; Campbell and Pandya, 1994), we observed heavily labeled PV+ neurons widely distributed in all the MGN subdivisions. The homogenous staining of MGN by PV immunohistochemistry did not allow us to discern any particular subdivision. For this reason, PV staining will not be described further.

By contrast, the combination of all the other staining methods delineated four main subdivisions in the ferret MGN: the ventral (MGv) the dorsal (MGd) and the medial (MGm) nuclei, as well as the lateral part of the posterior group of thalamic nuclei (Po).

Parcellation of the caudal half of the medial geniculate nucleus (Figs. 1-2). The caudal pole of the ferret MGN was entirely occupied by cells of the dorsal division (MGd). Immediately rostral to this level, both the ventral (MGv) and medial (MGm) nuclei became also apparent (Fig. 1).

The ventral division was located in the ventrolateral aspect of the MGN, and in the coronal plane appeared as an ovoid-shaped nucleus with its long axis oriented obliquely from ventrolateral to dorsomedial (Figs. 1,2). In the caudal half of MGN, MGv was best discernible in Nissl and CO stained sections (Figs. 1,2). In Nissl-stained sections MGv was distinguished by the high packing density of its constituent neurons, which contrasted with the lower density of cells in MGd and MGm. A lamellar organization of MGv could be discerned in Nissl staining, with the cellular laminae oriented approximately from ventrolateral to dorsomedial (Figs. 1B,2B). In sections stained for CO histochemistry, MGv stood out as a region of high CO activity (Figs. 1D,2D,5B). By contrast, CB, AChE and Cat-301 staining did not allow for a clear demarcation of MGv. CB immunohistochemistry yielded a fairly homogeneous staining of cell bodies and neuropil in both MGv and MGd (Figs. 1A,2A). AChE and Cat-301, although unevenly distributed in the three main subdivisions, did not reveal clear nuclear boundaries. (Figs. 1C,2C, and 5A, respectively).

Previous studies describing the Golgi cytoarchitecture of the ventral division of the MGN in the cat recognized lateral and ovoidal divisions within MGv (Morest, 1965). In our material a clear distinction between these two MGv components was not apparent. A further subdivision of MGv was described in Golgi stained sections as located along the ventral border of MGv, and was designated pars ventrolateralis (Vl) of the ventral MGN division (Morest, 1964; Winer, 1985, 1992). Subsequently, physiological and connectional data prompted the reclassification of Vl as part of the dorsal division (Imig and Morel, 1988; Winer, 1992). Consistent with the latter studies, we could recognize Vl as a separate nucleus located ventral to MGv, which in CO stained sections appeared as a region less intensely

stained than the rest of MGv, and whose staining intensity resembled that of the dorsal division (Figs. 1D,2D).

The caudal half of the dorsal nucleus of MGN, similar to MGv, was distinguished best in Nissl and CO stained sections (Figs. 1,2). It appeared as an elongated ovoid with a concave ventral contour that capped the ventral division, and that occupied approximately the same MGN area as MGv. In Nissl-stained sections MGd was clearly distinguishable from MGv because of the larger size and lower packing density of its neurons. Furthermore, the lower cell density in MGm (compared to MGd) allowed one to easily distinguish between these two nuclei. In sections reacted for CO, MGd appeared as a region of less intense staining than MGv, but more than MGm. These differences in density of staining allowed one to clearly delineate the MGv borders(Figs. 1D,2D). Within the dorsal nucleus, CO histochemistry revealed a separate subnucleus, the superficial dorsal nucleus (DS), as a small strip located along the lateral contour of the dorsal division, which was more intensely stained than the rest of MGd, but less intensely stained than MGv (Figs. 1D, 2D). When matched to adjacent sections stained with Nissl, DS appeared formed by closely spaced cells that had a similar orientation within MGd (Figs. 1B,2B). CB immunohistochemistry yielded a homogeneous intense labeling of MGv and MGd which did not allow one to distinguish between these two subdivisions. However, the paler CB staining of MGm, allowed one to demarcate the medial border of both MGv and MGd (Fig. 2A). AChE histochemistry yielded a non-uniform, patchy labeling of the neuropil throughout the caudal MGN, with no clear demarcation of the nuclear subdivisions (Figs. 1C,2C). However, the dorsal nucleus appeared generally more intensely stained than the other subdivisions, and at some levels the DS could be distinguished from the adjacent MGv (Fig. 1C). No Cat-301 immunoreactivity was found in the dorsal nucleus(Fig. 5A).

The medial division of the ferret MGN lay medial and ventromedial to the ventral and dorsal divisions, respectively. In the caudal half of the MGN, MGm was clearly discernible in Nissl-, CO-, CB- and Cat-301-stained sections (Figs. 1A,B,D, 2A,B,D, 5A). In Nissl-stained

sections MGm appeared as a region of much lower cell density than the other subdivisions, with a heterogeneous cellular composition which included small- and medium sized-cell bodies as well as the largest neurons of the MGN (Figs. 1B,2B). In MGm, both CO histochemistry and CB immunohistochemistry revealed few thin fibers as well as a sparse distribution of cells. While CB stained only a few small and medium sized cells (Figs. 1A,2A), CO also stained some large neurons (Figs. 1D,2D). In Cat-301-immunoreacted sections, MGm could be further subdivided into a magnocellular and a parvocellular component. The magnocellular component stood out as an area of intense Cat-301 immunoreactivity, as opposed to the parvocellular component that was completely devoid of Cat-301 staining (fig. 5A).

Parcellation of the rostral half of the medial geniculate nucleus (Figs. 3-4). The ventral division extended through most of the anterior half of the MGN, being absent in the rostral pole of the nucleus (Figs. 3E,4E). At rostral MGN levels, MGv was better identified in CB- and CO-stained sections (Figs. 3A,D), since in Nissl staining nuclear boundaries became indistinguishable (Fig. 3B). While CB staining appeared homogeneous throughout the caudal aspect of MGv and MGd (see above), at more rostral levels the intensity of neuropil staining in the ventral nucleus was intermediate between the darker staining of MGd and the paler staining of MGm, thus allowing to clearly demarcate the major nuclear boundaries (Fig. 3A). As observed in caudal MGN, Vl was best identified in CO-stained sections as a ventral region of paler CO activity than the rest of MGv (Fig. 3D).

The borders of the dorsal division were also clearly delineated by CB immunohistochemistry (Figs. 3A,4A), but less clearly by CO histochemistry (Figs. 3D,4D). However, subsidiary nuclei within MGd were best seen in AChE-stained sections (Figs. 3C,4C). AChE activity was highest in the suprageniculate nucleus (Sg), intermediate in MGd, while pale staining of a few thin fibers delineated DS along the lateral edge of the ventral division.

In the rostral pole of the MGN, the medial division was better identified in Cat-301-stained sections, where the intense staining of the magnocellular portion of MGm contrasted with the lack of Cat-301 immunoreactivity in the surrounding MGN regions (Fig 5C).

The lateral part of the posterior group of thalamic nuclei (Po) appeared in the rostral third of the MGN. Po was crossed by fibers of the auditory radiation and was contiguous with the ventral and medial divisions of the MGN (Fig. 4E). It appeared in Nissl as a region of small- and medium-sized cells located along the ventrolateral border of a magnocellular region (MGm) (Fig. 4B). While the Po/MGd border was clearly evident in AChE-stained sections (Fig. 4C), the Po/Mgm border could be demarcated by matching adjacent sections stained for Nissl and Car-301, respectively (Figs. 4B,5C).

Thalamocortical projections in normal ferrets

Auditory cortical fields, and the topography of thalamocortical connections in the ferret. The pattern of auditory thalamocortical projections is better understood when related to the topographic organization of the ferret auditory cortex as well as to its parcellation into several fields. The latter two will be described first.

Previous physiological studies have revealed the presence of two tonotopically organized cortical areas, one located in the middle ectosylvian gyrus (Kelly et al., 1986; Phillips et al., 1988) and identified as AI on the basis of its connections with the ventral division of MGN (Kavanagh and Kelly, 1987), and the other located in the most anterior part of the middle ectosylvian gyrus extending into the depth of the suprasylvian sulcus (Kowalski et al., 1995). Anatomical studies in our laboratory have recently identified additional fields within the ferret auditory cortex as well as the general topographic organization of the thalamocortical connections (Clascá, Angelucci and Sur, manuscript in preparation). Anatomical mapping of the ferret auditory cortex was obtained in those studies by injecting multiple retrograde tracers into several cortical regions and subsequently examining the resulting pattern of retrogradely labeled cells into the various MGN subdivisions.

Figure 6 shows a diagram of the ferret auditory cortex based on the physiological and connectional data presently available. While only two tonotopic fields have been mapped physiologically in the ferret, connectional studies in our laboratory have identified at least one additional tonotopic field located in the posterior ectosylvian gyrus ventral to AI, indicated in figure 6 as V.

AI was shown to contain a tonotopic map of sound frequencies with the high frequencies represented dorsally and lower frequencies progressively more ventrally. Isofrequency lines run in an approximate anteroposterior direction, while binaural bands have an approximate dorsoventral orientation. Our connectional data indicated that this tonotopic field receives projections mainly from the ventral division of MGN (MGv). A caudal-to-rostral gradient was observed in these projections: while the rostral half of MGv projected to the rostral part of AI, more caudal MGv regions sent projections to the caudal part of AI. The caudal one third of MGv did not project to AI, but to the region designated as V in figure 6. The MGv-to-AI projections were organized in a topographic manner. Focal injections of retrograde tracers in the low frequency region of AI labeled a sheet of cells roughly parallel to the lateral border of the ventral nucleus of MGN. Higher frequency regions of AI received projections from sheets of cells located progressively more medially in MGv (see also Pallas et al., 1990).

A clear reversal in topography was observed in the posterior ectosylvian gyrus ventral to AI (Fig. 6), where tracer injections located progressively more ventrally labeled sheets of neurons located progressively more medially in the caudal half of MGv. More accurate physiological mapping studies are necessary to identify the exact orientation of the isofrequency contours, as well as potential additional fields within this ventral (V) region.

The connectivity of the tonotopic field physiologically identified in the rostral part of the middle ectosylvian gyrus, and in the posterior bank of the adjacent suprasylvian sulcus (Kowalski et al., 1995) suggested that this cortical area might correspond to the anterior auditory field (AF; Fig. 6) previously described in the cat (Andersen et al., 1980; Morel and

Imig, 1987). AF received projections mainly from Po, but also from the rostromedial part of MGv. AF has been shown to share a high frequency border with AI, and isofrequency lines in AF run in a plane approximately orthogonal to that of the isofrequency contours in AI (Fig. 6).

An additional field that received a massive projection from the dorsal nucleus of the MGN was identified in the anterior ectosylvian gyrus ventral to AF, and designated in figure 6 as AII. Other auditory fields connected to non-tonotopic MGN subdivisions are indicated in figure 6. All the cortical areas indicated in figure 6 received sparse projections from the medial division of MGN (MGm).

Pattern of auditory thalamocortical projections as revealed by sensitive anterograde tracers. Small PHA-L and Biotinylated Dextran (BD) injections were made into the MGN of adult ferrets and the resulting pattern of thalamocortical projections was examined in the tangential or coronal planes. The projection patterns observed in serial reconstructions of tangential sections of auditory cortex will be described first, followed by the observations in the coronal plane.

Figure 7 shows two examples of focal PHA-L injections made in the ventral division of the MGN (MGv). Within MGv, both injections were located approximately midway through the anteroposterior extent of MGN, and involved a region of putative middle/low frequency representation. Both injections were elongated dorsoventrally in the coronal plane, and the size of their dense core was comparable, measuring about 200-250 ⌊m mediolaterally and 500 ⌊m dorsoventrally. The injection in case F92-149 (Fig. 7) had a larger anteroposterior extent (about 250 ⌊m) than that in case F92-150 (about 200 ⌊m), and at its most rostral level involved a small part of the medial division (MGm).

Dense terminal ramifications of fibers in both cases were found in low frequency regions of AI, as well as in the posterior ectosylvian gyrus ventral to AI, in the region designated as V in figure 6 (Figs. 8-10). When all the sections were superimposed onto a flat

plane parallel to the lateral surface of auditory cortex, the overall pattern of labeling appeared "slab-like" (Figs. 8,10A). The "slabs" in AI were oriented in an oblique anteroposterior plane, and extended for about 2 mm along this plane. In case F92-150 two parallel "slabs" were observed (Fig. 8), while one "slab" was found in the other case (Fig. 10A). By contrast, in V the "slabs were oriented approximately dorsoventrally, and while a single main "slab" was observed in case F92-150 (Fig. 8), three parallel slabs were found in case F92-149 (Fig. 10A). Separate reconstructions of the labeling in the deep layers of AI and V, respectively, revealed a discrete organization within the "slabs" of terminal labeling. An example is shown for case F92-150 in figure 9. In the posterior ectosylvian gyrus ventral to AI a single injection of PHA-L in MGv labeled six terminal "patches" of thalamocortical axons in the ipsilateral hemisphere (Fig. 9A). The main terminal projection zone, where the density of labeling was highest, consisted of three contiguous "patches" about 500 μm wide, aligned along a dorsoventral axis. The "patches" of the main plexus, tended to expand to join three neighboring satellite "patches" of slightly smaller size and less dense labeling. Two of the satellite "patches" were contiguous with one another and aligned with the "patches" of the main plexus, but separated from the latter by a gap in which only a few fibers were labeled. The third satellite "patch" was located posteriorly to the main plexus. A similar organization was observed in field V in case F92-149 (Fig. 10A) in which, however, the main terminal plexus was flanked by two parallel "slabs". In figure 10A, a "patchy-like" organization is not clearly visible within the main labeled plexus, since the figure shows a composite reconstruction of the overall label. However, an organization into alternating "patches" is apparent in the "slabs" adjacent to the main terminal plexus, due to the lower density of labeling in these regions. A satellite "patch" was present in this case ventral to the region of densest labeling.

A "patch-like" organization within the terminal slabs of thalamocortical labeling was observed also in A1, as demonstrated in figure 9B. Here two parallel slabs oriented roughly anteroposteriorly were found. One of them was more densely stained and organized into two

contiguous "patches" of about 500 μm in width. The second slab, located ventral to the first one, consisted of three less densely stained "patches" of similar size as the ones in the main plexus, separated by gaps where only a few fibers were present. The size of these gaps was approximately the same as that of the "patches" in the same slab. Two satellite "patches" of smaller size were present ventral to the main terminal plexus.

In addition to the axonal "patches" within the deep cortical layers, much fewer axons terminated in the upper cortical layers. Reconstruction of the overall labeling in the upper layers, by superimposing cortical sections cut in the tangential plane, revealed a very different pattern of thalamocortical projections than that observed in the deep cortical layers. An example of MGN projections to the upper layers of auditory cortex is shown in figure 10B. These axons coursed tangentially for very long distances, were very poorly branched, and covered the same cortical regions of the axons in the deeper layers. Thus, they were located in both A1 and in V in figure 6. Some of these axons sent branches to both cortical fields. In case F92-150 (Fig. 8), projections to the upper layers appeared similar to those in case F92-149 (Fig. 10), but were fewer in number (not shown).

Following focal injections of PHA-L or BD (250-400 μm wide) in MGv, Po or MGm, a "patchy-like" organization of thalamocortical projections was observed also in the coronal plane. Injections in Po resulted in sparse labeling of axons in the rostral high-frequency region of A1, and in dense "patchy-like" terminations in the rostral part of the middle ectosylvian gyrus or in the posterior bank of the adjacent suprasylvian sulcus, i.e. in the cortical area identified as AF by previous physiological and connectional studies (Fig. 6). Injections of PHA-L (~ 400 μm wide) in rostral MGv labeled 2 to 3 densely stained "patches" in the rostral part of AI, and sparse axons in AF. In coronal sections of both AI and AF, the "patches" were contiguous and aligned dorsoventrally (not shown). Following small injections of PHA-L into the medial division terminal labeling extended to a very wide portion of the auditory cortex. One example is shown in figure 11. In the coronal plane, the core of the injection site extended for about 200 μm mediolaterally and 150 μm anteroposteriorly (Fig. 11C).

Thalamocortical projections were observed in the low frequency regions of AI, in AF, in a region posterior to AF and just anterior to the pseudosylvian sulcus, and in V. While sparse labeling of axons was found throughout most of these areas, terminal "patches" were also observed. In individual coronal sections 3-4 "patches" (about 500 μm in dorsoventral diameter) were labeled, separated by much wider gaps in which few or no axons were stained (Fig. 11A). When the labeling was reconstructed through serial coronal sections and projected onto a lateral view of the same animal's auditory cortex, it was evident that the "patches" observed in coronal sections extended in the tangential plane, and that they were located in different cortical fields (Fig. 11B). Although a "patchy-like" organization in the tangential plane was not revealed by this type of reconstruction, it was evident that the most densely labeled regions tended to form terminal "slabs". Four dorsoventrally-oriented "slabs" are apparent in figure 11B. One was located in AF adjacent to the suprasylvian sulcus. A second "slab" with a similar dorsoventral orientation was located posterior to the first one, in the proximity of the pseudosylvian sulcus. Two additional parallel "slabs", were observed in the ventral part of the posterior ectosylvian gyrus.

Following injections of anterograde tracers in Mgv, MGm and Po, dense terminal labeling was observed in cortical layer IV and in the deep part of layer III. In all the injected cases occasional axons could be seen reaching layer I and coursing tangentially (Fig. 11A). Terminal labeling of a much lower staining intensity than that observed in layer IIIB/IV was also found in the upper part of layer VI following tracer injections in MGv and Po. A projection to layer VI was not observed after injections in MGm.

Discussion

In the present study we have shown that similar to the cat and other mammalian species, four main subdivisions can be distinguished in the ferret MGN on the basis of their distinct cyto- and chemoarchitecture as well as of the differential distribution of calbindin and Cat-301 immunoreactivity.

In addition we have found that fibers from the two main tonotopic MGN subdivisions, MGv and Po, as well as fibers from the magnocellular division (MGm) tend to form "slab-like" terminations in several tonotopically organized auditory cortical fields, and that the terminal "slabs" are further organized into discrete "patches".

Parcellation of the ferret MGN

The MGN of several species is composed of several anatomically and physiologically distinct nuclei, each one receiving a specific set of ascending fibers from the brainstem, and projecting to specific auditory cortical fields. These nuclei are believed to represent relay stations of anatomically and functionally distinct parallel ascending systems to the auditory cortex (for a review see Winer, 1992). In the present study we have matched different staining methods such as Nissl, CO and AChE histochemistry, CB and Cat-301 immunohistochemistry, to delineate the major subdivisions of the ferret MGN. AChE is the hydrolytic enzyme of the cholinergic mechanism, whose activity in the brain shows marked regional variations (Olivier et al., 1970; Graybiel and Berson, 1980; Mesulam et al., 1984; Robertson et al., 1986; Wallace et al., 1991). However, the presence of AChE does not provide evidence for cholinergic transmission (Shute and Lewis, 1966). CB is a calcium-biding protein whose precise physiological function is unknown, but which may contribute to Ca^{++} homeostasis by buffering transient increases in intracellular calcium, thus affecting calcium-dependent neuronal properties such as excitability and neurotransmitter release

(Andressen et al., 1993). Recently, calcium-binding proteins have been used as specific neuronal markers (Andressen et al., 1993).

Cat-301 is a monoclonal antibody (McKay and Hockfield, 1982) which recognizes a cell-surface proteoglycan (Zaremba et al., 1990) on subpopulations of neurons in many parts of the mammalian central nervous system (Hockfield et al., 1983). Regardless of their physiological functions, the differential expression of CO, AChE, CB and Cat-301, often reflects dissimilar functional and structural characteristics of neurons, and serves to distinguish subpopulation of neurons processing different types of information (Hashikawa et al., 1991; Rausell and Jones, 1991a,b; Rausell et al., 1992; Molinari et al., 1995).

Following Morest (1964) and others (Winer, 1985; Imig and Morel, 1988) we could distinguish four main nuclei in the auditory thalamus of the ferret: the ventral (MGv) , the dorsal (MGd) and the medial (MGm) divisions, and the lateral nucleus of the posterior thalamic complex (Po). Furthermore, the differential staining intensities obtained with CO and AChE allowed us to further subdivide the dorsal division into three subsidiary nuclei: the dorsal and superficial dorsal nucleus, as well as the suprageniculate nucleus. A deep dorsal nucleus, as described in Golgi staining by Morest (1964) in the cat MGd, could not be discerned within the ferret MGd in our material. We have not attempted to subdivide MGv into a lateral and an ovoidal component (Morest, 1964), since these nuclei were not clearly delineated by the staining methods employed in this study. However, in CO-stained sections a pars ventrolateralis (Morest, 1964) could clearly be distinguished from the rest of MGv. Within Mgm, a magnocellular division was clearly delineated by Cat-301 immunostaining.

Termination patterns of auditory thalamocortical projections within tonotopically-organized cortical areas

Studies on the auditory thalamocortical system in the cat using injections of retrograde tracers in the cortex have led to a "divergence/convergence" model of auditory geniculocortical organization (Merzenich et al., 1982, 1984). Such a model predicts that a

focal injection of an anterograde tracer in MGv would label a terminal "band" within AI whose longer axis is oriented parallel to the isofrequency contours. Recently, this model has been challenged in favor of a more point-to-point topographic organization of MGv-to-AI projections (Redies et al., 1989; Brandner and Redies, 1990).

Results obtained in the present study using focal injections of sensitive anterograde tracers are consistent with a highly divergent pattern of connectivity between several MGN subdivisions and the auditory cortex. Three main observations made in the present study support a divergent model of auditory thalamocortical organization:

1) Fibers from restricted MGN loci projected to more than one cortical field. Injections in MGv and Po labeled terminal axons in two tonotopic fields. The latter consisted of fields AI and V for injections located in the caudal part of MGv, and of fields AI and AF for injections located in rostral MGv or Po. Injections in MGm gave off less densely labeled, but even more widespread projections to several auditory fields, with little label in AI.

2) Within one tonotopic cortical field, a small injection in MGv produced labeling of 1-3 parallel "slabs" of axon terminals measuring approximately 2 mm in length. Labeling of terminal "slabs" of similar size was also observed in several auditory tonotopic areas following injections in MGm.

The "slabs" in AI were elongated anteroposteriorly, while in V and AF they had a dorsoventral orientation. The orientation of the "slabs" in AI and AF observed in the present study correlates well with the orientation of the isofrequency contours reported in previous physiological mapping studies for these areas of the ferret auditory cortex (Kelly et al., 1986; Phillips et al., 1988; Kowalski et al., 1995). The precise orientation of isofrequency lines in area V is not presently known. Whereas our findings suggest a dorsoventral orientation of isofrequency contours in this area, physiological studies are required to further characterize the tonotopic organization of this cortical field.

3) Within each cortical field, terminal labeling following small injections in MGv consisted of a main plexus of densely stained axons surrounded by several smaller satellite patches of less

dense terminations, separated from the main plexus by intervening empty spaces. These satellite patches were located outside the axis of orientation of the main plexus. While the functional significance of the satellite patches cannot be inferred from the present study, their presence indicates that although most of the neurons of a given MGv cluster project to a corresponding cortical domain in AI, V or AF, some cells within the same MGv cluster project to surrounding non-tonotopically related loci in the same cortical field. This finding suggests that coincident cell groups within MGv give rise to divergent projections within a tonotopic cortical field. Such divergence of thalamocortical axons in the auditory system may form one basis for representational plasticity under activity-dependent conditions (Robertson and Irvine, 1989; Irvine et al., 1991; Recanzone et al., 1993). Recent studies on the thalamocortical projections in the visual and somatosensory systems suggest that in these other sensory pathways as well, classically viewed as organized in a point-to-point fashion (Jones et al., 1979; Nelson and Kaas, 1981), thalamocortical projections are more divergent than previously thought on the basis of less sensitive anatomical tracing methods (Darian-Smith et al., 1990; Garraghty and Sur, 1990; Rausell and Jones, 1995).

Another striking finding of the present study is the "patch-like" organization of geniculocortical axons within the "slabs" of terminal labeling. "Patch-like" terminations have been demonstrated for other thalamocortical pathways (Jones, 1985) in a variety of species, suggesting that they represent a fundamental organizational feature of the thalamocortical system. In our study, terminal patches of thalamocortical axons were observed in both the coronal and tangential planes. Following focal tracer injections in MGv, multiple patches, about 500 μm wide, were labeled in layer IIIB/IV of two adjacent tonotopic cortical areas. Serial reconstruction of the labeling in a plane parallel to the lateral surface of the auditory cortex revealed that the majority of the patches were aligned along one main axis, thus forming "slabs" of terminal labeling (see above). Although patchy terminations of thalamocortical axons in AI have been described previously in rabbits (McMullen and de Venecia, 1993) and monkeys (Hashikawa et al., 1995), this is the first clear demonstration

that the patches align along an axis oriented parallel to that of the physiologically-defined isofrequency contours. Following injections of anterograde tracers in the rabbit MGv, McMullen and de Venecia (1993) found "patches" of terminal labeling in coronal sections of AI. However, since in the rabbit, as in the ferret, isofrequency contours run in an anteroposterior direction (McMullen and Glaser, 1982), it was difficult to extrapolate the pattern observed in the coronal plane to the tangential plane, i. e. to a plane parallel to the rabbit isofrequency lines. Thus, it was unclear in that study whether the "patches" of thalamocortical projections bore any relationship to the orientation of isofrequency domains in AI. In the monkey, "patchy" terminations of thalamocortical axons were observed both in coronal and tangential sections of auditory cortex (Hashikawa et al., 1995). However, the labeled "patches" showed no particular orientation along the axis of the isofrequency contours in this species. The latter observation can be attributed to the relatively large size of the injections made in that study. Furthermore, no attempt was made in the same study to reconstruct the overall pattern of labeling through serial tangential sections.

What is the functional correlate of the "patches" observed in the present study as well as in previous studies? One physiological function for a "patchy" organization along the isofrequency dimension is that of binaural interaction bands. In ferret AI these bands run dorsoventrally (Kelly and Judge, 1994) in the form of alternating EE/EI bands. Middlebrooks and Zook (1983) demonstrated in the cat that neurons projecting to the cortical EE/EI bands are spatially segregated in MGv. "Patchy" connections between MGv and AI have been predicted on the basis of the latter study, as well as of other retrograde tracer experiments in the cat (Andersen et al., 1980; Merzenich et al., 1982). It was hypothesized that either single MGv axons diverge to multiple binaural patches within a cortical isofrequency line, or that coincident cell groups within an MGv binaural cluster project to multiple patches of similar binaural properties along an isofrequency contour in AI. The "patches" in our study were either adjacent, or separated by intervening empty spaces of similar size. In the cases examined in the tangential plane, the injection sites were elongated from dorsolateral to

ventromedial. It is possible that contiguous thalamocortical "patches" resulted from injections involving two adjacent binaural MGv bands, while alternating "patches" might have resulted from injections confined to a single binaural domain. Similarly, the finding of multiple parallel "slabs" within the same cortical field might relate to the size of the injection involving several adjacent isofrequency MGv lamellae. Studies combining electrophysiological mapping of binaural classes and frequency selectivity with anterograde labeling will be necessary to determine if the thalamocortical "patches" represent binaural response-specific pathways to AI and other tonotopically organized fields. However, our study is consistent with the latter hypothesis.

Another finding of the present study suggests the existence of two different populations of thalamocortical projections, one projecting mainly to layer IIIB/IV, the other projecting to layer I. Both types of laminar projections arose from all the MGN subdivisions that received a tracer injection in the present study, including Mgv, MGm and Po. Different from the projections to layer IIIB/IV, fibers directed to layer I were much fewer in number, were poorly branched, and showed a very long tangential course, often crossing different fields and branching in multiple areas. The different pattern of terminations of these two subsets of thalamocortical axons might underlie dissimilar functional properties.

Thalamocortical projections in "rewired" ferrets

While the data described in this chapter pertain to normal animals, preliminary data on thalamocortical projections in "rewired" ferrets indicate that these projections are also highly divergent, resembling the projections in normal animals. Briefly, focal injections of PHA-L in MGv label fibers whose terminations are "patchy" and widespread in AI. Injections of WGA-HRP into the vitreal chamber of one eye in young "rewired" animals (postnatal day 4) label not only retinal projections to the MGN (as described in Chapter 2B), but also, after transneuronal transport, the projections of thalamic cells to the cortex. Such projections demonstrate retinal input at these ages to layer I as well as to the deeper layers of the cortical plate in most of auditory cortex. Finally, focal injections of retrograde tracers in AI label sheets of cells oriented roughly dorsomedially in MGv (Pallas et al., 1990).

The spread of thalamocortical terminations in AI of "rewired" animals is consistent with the size of domains of activity that can be imaged optically in AI following visual stimulation (see Chapter 4). While such divergent terminations can relay visual input to a relatively large part of AI through focal retinal termination patches in the MGv, additional mechanisms must be required for the restriction of visual receptive fields of AI neurons (Roe et al., 1992) and for the creation of a map of visual space in AI (Roe et al., 1990; see Introduction). One mechanism that has been hypothesized is the activity-dependent selection of subsets of synapses along the isofrequency axis (Roe et al., 1990), possibly coupled with a rearrangement of inhibition within the cortex to restrict the divergence of thalamocortical excitation (Sur et al., 1990).

References

Aitkin, L. (1990) The Audirory Cortex. Structural and Functional Basis of Auditory Perception. London: Chapman and Hall.

Andersen, R.A., P.L. Knight, and M.M. Merzenich (1980) The thalamocortical and corticothalamic connections of AI, AII, and the anterior auditory field (AAF) in the cat: evidence for two largely segregated systems of connections. J. Comp. Neurol. *194*:663-701.

Andressen, C., I. Blumcke, and M.R. Celio (1993) Calcium binding proteins: selective markers of nerve cells. Cell Tissue Res. *271*:181-208.

Angelucci, A., F. Clascá, and M. Sur (1993) Multiple cortical auditory fields in the ferret defined by their architectonics and thalamocortical connections. Soc. Neurosci. Abst. *19*:1427.

Brandner, S., and H. Redies (1990) The projection from medial geniculate to field AI in the cat: organization in the isofrequency dimension. J. Neurosci. *10*:50-61.

Brandt, H.M., and A.V. Apkarian (1992) Biotin-dextran: a sensitive anterograde tracer for neuroanatomic studies in rat and monkey. J. Neurosci. Methods *45*:35-40.

Brugge, J.F., and R.A. Reale (1985) Auditory Cortex. In A. Peters and E.G. Jones (eds.): Cerebral Cortex, Vol. 4. New York: Plenum, pp. 229-271.

Caballero-Bleda, M., B. Fernandez, and L. Puelles (1991) Acetylcholinesterase and NADH-diaphorase chemoarchitectonic subdivisions in the rabbit medial geniculate body. J. Chem. Neuroanat. *4*:271-280.

Campbell, M.J., and D.N. Pandya (1994) Medial geniculate body chemoarchitectonic subdivisions. Soc. Neurosci. Abstr. *20*:977.

Clarey, J.C., P. Barone, and T.J. Imig (1992) Physiology of thalamus and cortex. In A.N. Popper and R.R. Fay (eds.): The Mammalian Auditory Pathway: Neurophysiology. New York: Springer-Verlag, pp. 232-334.

Darian-Smith, C., I. Darian-Smith, and S.S. Cheema (1990) Thalamic projections to sensorymotor cortex in the macaque monkey: use of multiple retrograde fluorescent tracers. J. Comp. Neurol. *299*:17-46.

de Venecia, R.K., C.B. Smelser, S.D. Lossman, and N.T. McMullen (1995) Complementary expression of parvalbumin and calbindin D-28k delineates subdivisions of the rabbit medial geniculate body. J. Comp. Neurol. *359*:595-612.

Garraghty, P.E., and M. Sur (1990) Morphology of single intracellularly stained axons terminating in area 3b of macaque monkeys. J. Comp. Neurol. *294*:583-593.

Geneser-Jensen, F.A., and T.W. Blackstad (1971) Distribution of achetylcholinesterase in the hippocampal region of the guinea pig-I. Entorhinal area, parasubiculum, and presubiculum. Z. Zellforsch. *114*:460-481.

Gerfen, C.R., and P.E. Sawchenko (1984) An anterograde neuroanatomical tracing method that shows the detailed morphology of neurons, their axons and terminals: immunohistochemical localization of an axonally transported plant lectin, *Phaseolus vulgaris* leucoagglutinin (PHA-L). Brain Res. *290*:219-238.

Graybiel, A.M., and D.M. Berson (1980) Histochemical identification and afferent connectiosn of subdivisions in the lateralis posterior-pulvinar complex and related thalamic nuclei in the cat. Neurosci. *5*:1175-1238.

Hashikawa, T., E. Rausell, M. Molinari, and E.G. Jones (1991) Parvalbumin and calbindin-containing neurons in the monkey medial geniculate complex: Differential distribution and cortical layer specific projections. Brain Res. *544*:335-341.

Hashikawa, T., M. Molinari, E. Rausell, and E.G. Jones (1995) Patchy and laminar terminations of medial geniculate axons in monkey auditory cortex. J. Comp. Neurol. *362*:195-208.

Hockfield, S., R.D.G. McKay, S.J.C. Hendry, and E.G. Jones (1983) A surface antigen that identifies ocular dominance columns in the visual cortex and laminar features of the lateral geniculate nucleus. Cold Spring Harbor Symp. Quant. Biol. *48*:877-889.

Imig, T.J., and H.O. Adrian (1977) Binaural colums in the primary field (AI) of cat auditory cortex. Brain Res. *138*:241-257.

Imig, T.J., and A. Morel (1984) Topographic and cytoarchitectonic organization of thalamic neurons related to their targets in low-, middle-, and high-frequency representations in cat auditory cortex. J. Comp. Neurol. *227*:511-539.

Imig, T.J., and A. Morel (1985) Tonotopic organization in ventral nucleus of medial geniculate body in the cat. J. Neurophysiol. *53*:309-340.

Imig, T.J., and A. Morel (1988) Organization of the cat's auditory thalamus. In G.M. Edelman, W.E. Gall and W.M. Cowan (eds): Auditory Function. Neurobiological Basis of Hearing. New York: Wiley, pp. 457-484.

Irvine, D.R.F., R. Rajan, L.Z. Wize, and P. Heil (1991) Reorganization in auditory cortex of adult cats with unilateral restricted cochlear lesions. Soc Neurosci. Abstr. *17*:1485.

Jones, E.G. (1985) The Thalamus. New York: Plenum Press.

Jones, E.G., and S.H.C. Hendry (1989) Differential calcium binding protein immunoreactivity distinguishes classes of relay neurons in monkey thalamic nuclei. Eur. J. Neurosci. *1*:222-246.

Jones, E.G., S.P. Wise, and J.D. Coulter (1979) Differential thalamic relationships of sensory motor and parietal cortical fields in monkeys. J. Comp. Neurol. *183*:833-882.

Kavanagh, G.L., and J.B. Kelly (1987) Contribution of auditory cortex to sound localization by the ferret (*Mustela putorius*). J. Neurophysiol. *57*:1746-1766.

Kelly, J.B., and P.W. Judge (1994) Binaural organization of primary auditory cortex in the ferret (*Mustela putorius*). J. Neurophysiol. *71*:904-913.

Kelly, J.B., and S.L. Sally (1988) Organization of auditory cortex in the albino rat: binaural response properties. J. Neurophysiol. *59*:1756-1769.

Kelly, J.B., P.W. Judge, and D.P. Phillips (1986) Representation of the cochlea in primary auditory cortex of the ferret (*Mustela putorius*). Hearing Res. *24*:111-115.

Knight, P.L. (1977) Representation of the cochlea within the anterior auditory field (AAF) of the cat. Brain Res. *130*:447-467.

Kowalski, N., H. Versnel, and S.A. Shamma (1995) Comparison of responses in the anterior and primary auditory fields of the ferret cortex. J. Neurophysiol. *73*:1513.

McKay, R.D.G., and S. Hockfield (1982) Monoclonal antibodies distinguish antigenically discrete neuronal types in the vertebrate central nervous system. Proc. Natl. Acad. Sci. USA *79*:6747-6751.

McMullen, N.T., and E.M. Glaser (1982) Tonotopic organization of the rabbit auditory cortex. Exp. Neurol. *75*:208-220.

McMullen, N.T., and R.K. de Venecia (1993) Thalamocortical patches in auditory neocortex. Brain Res. *620*:317-322.

Merzenich, M.M., P.L. Knight, and G.L. Roth (1975) Representation of cochlea within primary auditory cortex in the cat. J. Neurophysiol. *38*:231-249.

Merzenich, M.M., G.L. Roth, P.L. Knight, and S.A. Colwell (1977) Some basic features of organization of the central auditory system. In E.F. Evans and J.P. Wilson (eds.): Psychophysics and Physiology of Hearing. London: Academic Press, pp. 485-495.

Merzenich, M.M., S.A. Colwell, and R.A. Andersen (1982) Auditory forebrain organization. Thalamocortical and corticothalamic connections in the cat. In C.N. Woolsey (ed.): Multiple Sensory Areas, Vol. 3. Clifton: Humane, pp.43-57.

Merzenich, M.M., W.M. Jenkins, and J.C. Middlebrooks (1984) Observations and hypotheses on special organizational features of the central auditory nervous system. In G.W. Edelman et al. (eds.): Dynamic Aspects of Neocortical Function. New York: Wiley, pp.397-424.

Mesulam, M.M., A.D. Rosen, and E.J. Mufson (1984) Regional variations in cortical cholinergic innervation: chemoarchitectonics of acetylcholinesterase-containing fibers in the macaque brain. Brain Res. *311*:245-258.

Middlebrooks, J.C., and J.M. Zook (1983) Intrinsic organization of the cat's medial geniculate body identified by projections to binaural response-specific bands in the primary auditory cortex. J. Neurosci. *3*:203-224.

Middlebrooks, J.C., R.W. Dykes, and M.M. Merzenich (1980) Binaural response-specific bands in primary auditory cortex (AI) of the cat: topographical organization orthogonal to isofrequency contours. Brain Res. *181*:31-48.

Molinari, M., M.E. Dell'Anna, E. Rausell, M.G. Leggio, T. Hashikawa, and E.G. Jones (1995) Auditory thalamocortical pathways defined in monkeys by calcium-binding protein immunoreactivity. J. Comp. Neurol. *362*:171-194.

Morel, A., and T.J. Imig (1987) Thalamic projections to fields A, AI, P, and VP in the cat auditory cortex. J. Comp. Neurol. *265*:119-144.

Morest, D.K. (1964) The neuronal architecture of the medial geniculate body of the cat. J. Anat. *98*:611-630.

Morest, D.K. (1965) The laminar structure of the medial geniculate body of the cat. J. Anat. *99*:143-160.

Nelson, R.J., and J.H. Kaas (1981) Connections of the ventroposterior nucleus of the thalamus with the body surface representations in cortical areas 3b and 1 of the cynomolgus macaque (*Macaca fascicularis*). J. Comp. Neurol. *199*:29-64.

Olivier, A., A. Parent. and L.J. Poirier (1970) Identification of the thalamic nuclei on the basis of their cholinesterase content in the monkey. J. Anat. *106*:37-50.

Pallas, S.L., A.W. Roe, and M. Sur (1990) Visual projections induced into the auditory pathway of ferrets. I. Novel inputs to primary auditory cortex (AI) from the LP/pulvinar complex and the topography of the MGN-AI projection. J. Comp. Neurol. *298*:50-68.

Phillips, D.P., P.W. Judge, and J.B. Kelly (1988) Primary auditory cortex in the ferret (*Mustela putorius*): Neural response properites and topographic organization. Brain Res. *443*:281-294.

Phillips, D.P., R.A. Reale, and J.F. Brugge (1991) Stimulus processing in the auditory cortex. In R.A. Altschuler et al. (eds.): Neurobiology of Hearing: The Central Auditory System. New York: Raven, pp. 335-365.

Rausell, E., and E.G. Jones (1991a) Chemically distinct compartments of the thalamic VPM nucleus in monkeys relay principal and spinal trigeminal pathways to different layers of the somatosensory cortex. J. Neurosci. *11*:226-237.

Rausell, E., and E.G. Jones (1991b) Histochemical and immunocytochemical compartments of the thalamic VPM nucleus in monkeys and their relationship to the representational map. J Neurosci. *11*:210-225.

Rausell, E., and E.G. Jones (1995) Extent of intracortical arborization of thalamocortical axons as a determinant of representational plasticity in monkey somatic sensory cortex. J. Neurosci. *15*:4270-4288.

Rausell, E., C.S. Bae, A. Vinuela, G.W. Huntley, and E.G. Jones (1992) Calbindin and parvalbumin cells in monkey VPL thalamic nucleus: Distribution, laminar cortical projections and relations to spinothalamic terminations. J Neurosci. *12*:4088-4111.

Recanzone, G.H., C.E. Schreiner, and M.M. Merzenich (1993) Plasticity in the frequency representation of primary auditory cortex following discrimination training in adult owl monkeys. J. Neurosci. *13*:87-103.

Redies, H., S. Brandner, and O.D. Creutzfeldt (1989) Anatomy of the auditory thalamocortical system of the guinea pig. J. Comp. Neurol. *282*:489-511.

Robertson, D., and D.R.F. Irvine (1989) Plasticity of frequency organization in auditory cortex of guinea pigs with partial unilateral deafness. J. Comp. Neurol. *282*:456-471.

Robertson, R.I., G.H. Kageyama, I Mostamand, K.A. Gallaido, and J. Yu (1986) Transient patterns of acetylcholinesterase activity in geniculocortical projections to primary auditory cortex in developing rats. Anat. REc. *226*:86A.

Roe, A.W., S.L. Pallas, J.-O. Hahm, and M. Sur (1990) A map of visual space induced into primary auditory cortex. Science *250*:818-820.

Roe, A.W., S.L. Pallas, Y.H. Kwon, and M. Sur (1992) Visual projections routed to the auditory pathway in ferrets: receptive fields of visual neurons in primary auditory cortex. J. Neurosci. *12*:3651-3664.

Rose, J.E., and C.N. Woolsey (1949) The relations of thalamic connections, cellular structure, and evocable electrical activity in the auditory region of the cat. J. Comp. Neurol. *91*:441-466.

Shute, C.C.D., and P.R. Lewis (1966) Electron microscopy of cholinergic terminals and acetylcholinesterase-containing neurones in the hippocampal formation of the rat. Z.Zellforsch. mikrosk. Anat. *69*:334-343.

Sur, M., P.E. Garraghty, and A.W. Roe (1988) Experimentally induced visual projections into auditory thalamus and cortex. Science *242*:1437-1441.

Sur, M., S.L. Pallas, and A.W. Roe (1990) Cross-modal palsticity in cortical development: differentiation and specification of sensory neocortex. TINS *13*:227-233.

Wallace, M.N., L.M. Kitzes, and E.G. Jones (1991) Chemoarchitectonic organization of the cat primary auditory cortex. Exp. Brain Res. *86*:518-526.

Winer, J.A. (1985) The medial geniculate body of the cat. Adv. Anat. Embryol. Cell Biol. *86*:1-98.

Winer, J.A. (1992) The functional architecture of the medial geniculate body and the primary auditory cortex. In D.D. webster, A.N. Popper and R.R. Fay (eds.): The Mammalian Auditory Pathway: Neuroanatomy. New York: Springer-Verlag, pp. 222-409.

Winer, J.A., I.T. Diamond, and D. Raczkowski (1977) Subdivisions of the auditory cortex of the cat: the retrograde transport of horseradish peroxidase to the medial geniculate body and posterior thalamic nuclei. J. Comp. Neurol. *176*:387-418.

Zaremba, S., J.R. Naegele, C.J. Barnstable, and S. Hockfield (1990) Neuronal subsets express multiple high-molecular-weight cell-surface glycoconjugates defined by monoclonal antibodies Cat-301 and VC1.1. J. Neurosci. *10*:2985-

FIGURE LEGENDS

Figure 1. Serial coronal sections through the caudal one third of the anteroposterior extent of the MGN. **A:** calbindin (CB) immunohistochemical stain. **B:** Nissl stain. **C:** acetylcholinesterase (AChE) histochemical stain. **D:** cytochrome oxidase (CO) histochemical stain. **E:** outline diagram drawn from the serial coronal sections shown in A-D, showing the location and boundaries of the MGN subdivisions. For details see Results. Dorsal is up, medial to the right.

BIC: brachium of the inferior colliculus; CP: cerebral peduncle; D: dorsal division of the MGN; Ds: superficial dorsal nucleus of the dorsal division of the MGN; M: medial division of the MGN; ML: medial lemniscus; SpfL: subparafascicular lateral field; V: ventral division of the MGN; Vl: pars lateralis of the ventral division of the MGN.

Figure 2. Serial coronal sections through the mid third of the anteroposterior extent of the MGN. **A-E:** as in figure 1. For details see Results. Dorsal is up, medial to the right.

D, Ds, M, ML, SpfL, V, Vl: see figure 1; LGd: dorsal lateral geniculate nucleus; Sg: suprageniculate nucleus.

Figure 3. Serial coronal sections through the rostral third of the anteroposterior extent of the MGN. **A-E:** as in figure 1. For details see Results. Dorsal is up, medial to the right.

CP, D, Ds, M, ML, SpfL, V: see figure 1; LGd, Sg: see figure 2; LP: lateral posterior thalamic nucleus.

Figure 4. Serial coronal sections through the anterior pole of MGN. **A-E:** as in figure 1. For details see Results. Dorsal is up, medial to the right.

CP, D, M, ML, SpfL: see figure 1; LGd, Sg: see figure 2; LGv: ventral lateral geniculate nucleus; LP-Pu: lateral posterior-pulvinar complex; Po: lateral part of the posterior group of thalamic nuclei; SLF: supralemniscal field; ZI: zona incerta.

Figure 5. A-B: two adjacent coronal sections through the caudal third of the anteroposterior extent of the MGN, stained for Cat-301 and CO, respectively. **C-D:** two adjacent coronal sections through the rostral pole of the MGN, stained for Cat-301 and CO, respectively. For details see Result. Dorsal is up, medial to the right.

Figure 6. Diagram of the auditory cortical areas in the ferret summarizing physiological and connectional data presently available. The figurine at the top left is a schematic drawing of the lateral view of a ferret brain, showing the location of auditory cortex. A magnified lateral view of the ferret auditory cortex is shown in the middle. Gray areas represent two tonotopically organized fields that have been physiologically characterized (AI and AF). The tonotopic axes in these fields are indicated by gradients of gray, with the darkest and lightest gray representing regions of highest- and lowest-frequency representations, respectively. Dashed lines within AI and AF indicate the orientation of the isofrequency contours. The bottom panel shows three coronal sections of auditory cortex taken at the anteroposterior levels indicated by the vertical gray lines. The location of the main tonotopic fields on coronal sections is indicated.
AI: primary auditory field; AII: secondary auditory field; AF: anterior auditory field; Pr: perirhinal cortex; SA: anterior sylvian area; V: ventral field; *PSS*: pseudosylvian sulcus; *SSS*: suprasylvian sulcus; A: anterior; D: dorsal; M: medial.

Figure 7. Injections of PHA-L in the medial geniculate nucleus. Camera lucida drawings of two coronal MGN sections from anterior (left) to posterior (right) levels, showing the location

and extent of the PHA-L injection sites in two different animals (F92-149 and F92-150, respectively).
D, M, V: dorsal, medial and ventral division of the MGN, respectively; CP: cerebral peduncle; LGd: dorsal lateral geniculate nucleus; LP: lateral posterior thalamic nucleus; Sg: suprageniculate nucleus; Vl: pars ventrolateralis of the ventral division of MGN; A: anterior; D: dorsal; L: lateral.

Figure 8. Overall pattern of thalamocortical projections following small injections of PHA-L in MGv in case F92-150 (see Fig. 7). Terminal labeling (shown in black) was reconstructed in tangential sections of the auditory cortex using camera lucida, and individual sections (dotted lines) were superimposed using blood vessels and the sections' contour as reference. Labeled terminal axons are located in the low frequency region of AI and in V. The overall pattern of labeling appears "slab-like" (see Results). AI: primary auditory field; V: ventral field; PSS: pseudosylvian sulcus; SSS: suprasylvian sulcus; A: anterior; D: dorsal.

Figure 9. "Patches" of auditory thalamocortical projections to the deep layers of AI and V. **A-B:** Tangential reconstructions of terminal PHA-L labeling in the deep layers of cortical auditory field V and AI, respectively, in case F92-150 (see Fig. 7). PHA-L labeling is represented in black. Dotted lines represent the outlines of individual tissue sections. Note the "patch-like" organization of the terminal labeling in both cortical fields (see Results). Abbreviations as in previous figure.

Figure 10. Thalamocortical projection patterns following small injections of PHA-L in the MGv in case F92-149 (see Fig. 7). **A:** Reconstruction of the overall terminal labeling of thalamocortical projections obtained by superimposing adjacent tangential cortical sections. PHA-L labeling is shown in black. Dotted lines represent the sections' outline. Three parallel "slabs" of terminal labeling are present in V, one "slab" is located in AI (see Results). **B:**

Reconstruction of terminal labeling in the most superficial layers of AI and V. Note the long tangential course of axons in the upper cortical layers (see Results). **C:** Schematic drawing of the lateral view of the brain in case F92-149. Shaded area indicates the location in auditory cortex of the reconstructions shown in A and B.
Abbreviations as in figure 8. In A-C dorsal is up, anterior to the left.

Figure 11. Pattern of thalamocortical projections following a small injection of PHA-L in the medial division of MGN. **A:** Camera lucida drawings of two coronal sections through the auditory cortex of a ferret. The anteroposterior level of each section is indicated by the dotted arrows in B. Dotted lines represent the layer VI/white matter border, while thick continuous lines delineate the cortical surface. A "patch-like" pattern of thalamocortical projections is apparent also in the coronal plane (see Results). AF: anterior field; PSS: pseudosylvian sulcus; SSS: suprasylvian sulcus; V: ventral field; D: dorsal; L: lateral. **B:** Lateral view of the overall labeling obtained in the same case as in A. Terminal labeling was reconstructed in single coronal sections and projected onto a line parallel to the section's surface. The location of the labeling in each section was then transferred onto a photograph of the lateral view of the same animal's auditory cortex, using the sulci and the anteroposterior level of the section as reference. Intensity of staining is indicated by shades of gray, with black and the lightest gray representing the most and least dense labeling, respectively. The most densely-stained regions form terminal "slabs in AF and V (see Results). D: dorsal; P: posterior. **C:** Camera lucida drawing of a coronal MGN section showing the location and size of the PHA-L injection site in the medial division of MGN (MGm). LGN: lateral geniculate nucleus; MGd, MGv: dorsal and ventral division of the MGN, respectively; D: dorsal; M: medial.

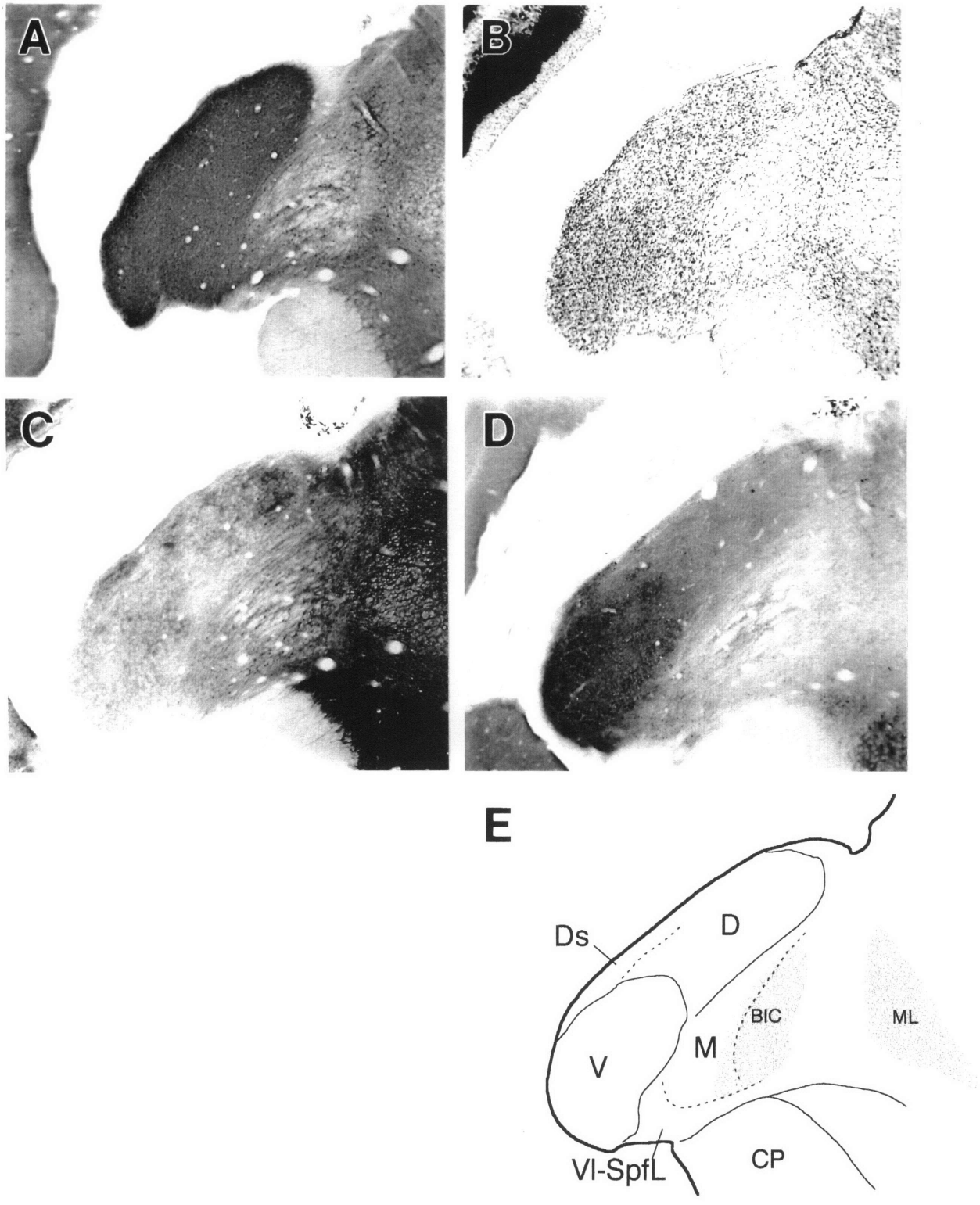

Fig.1

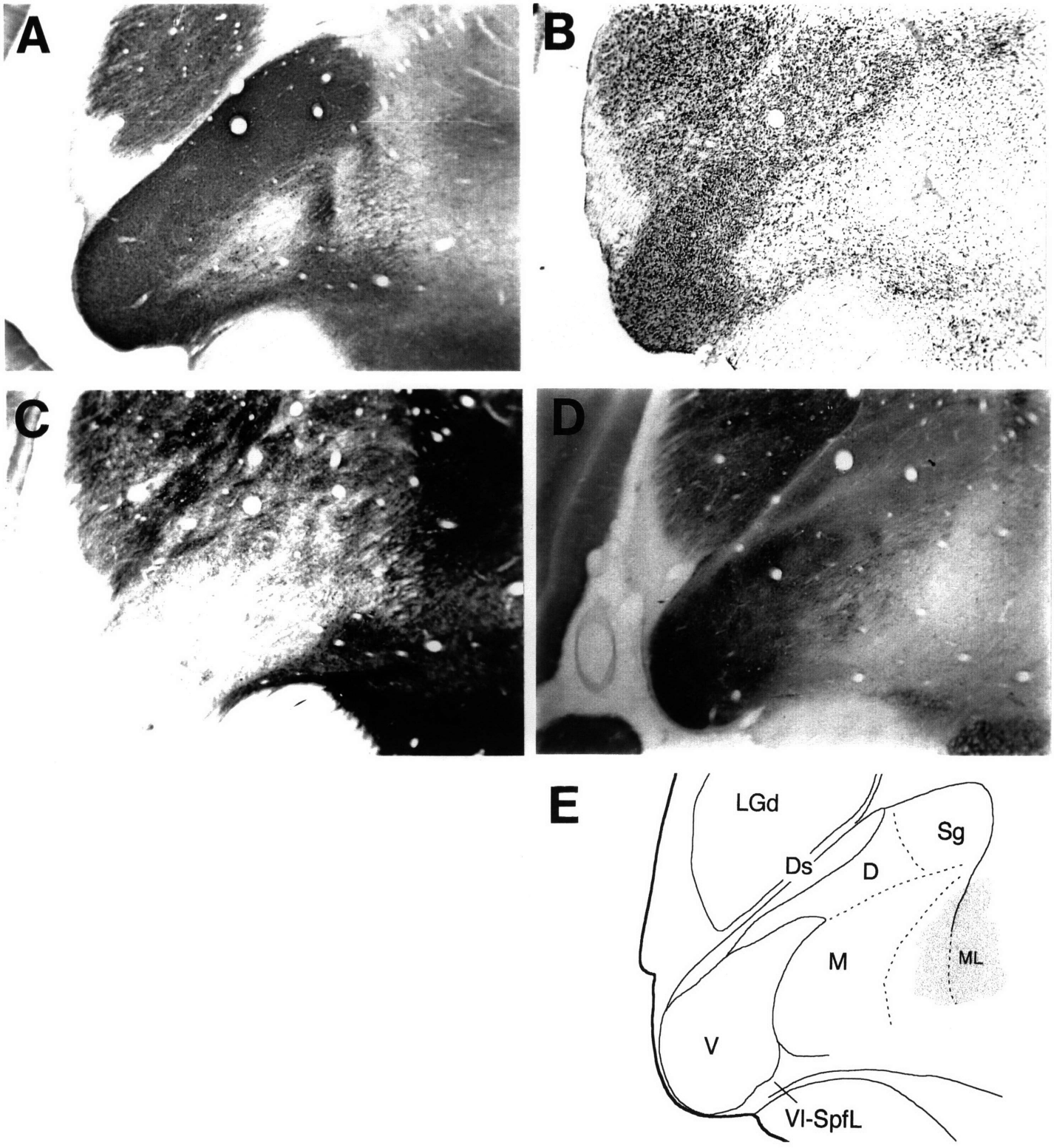

Fig. 2

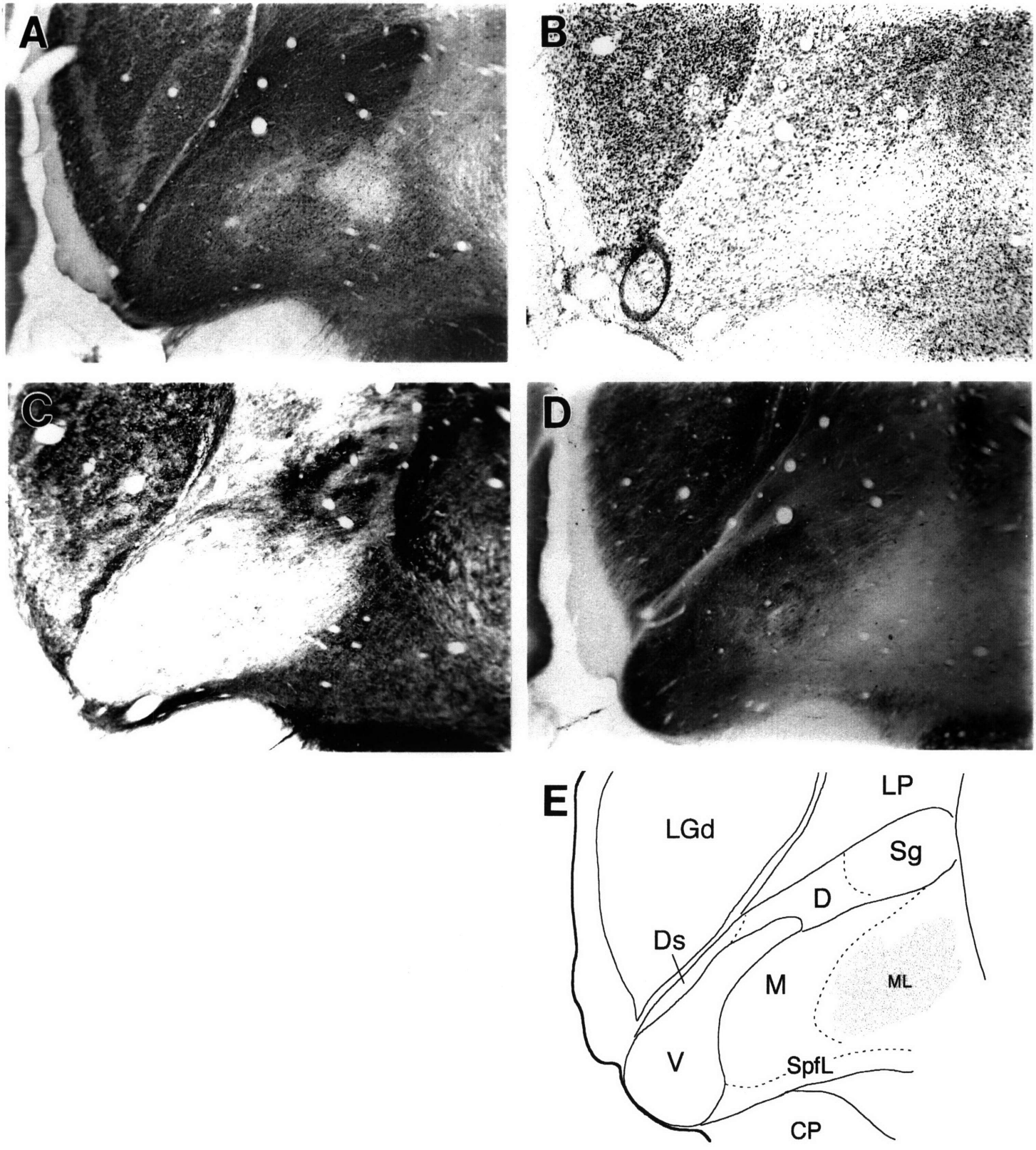

Fig. 3

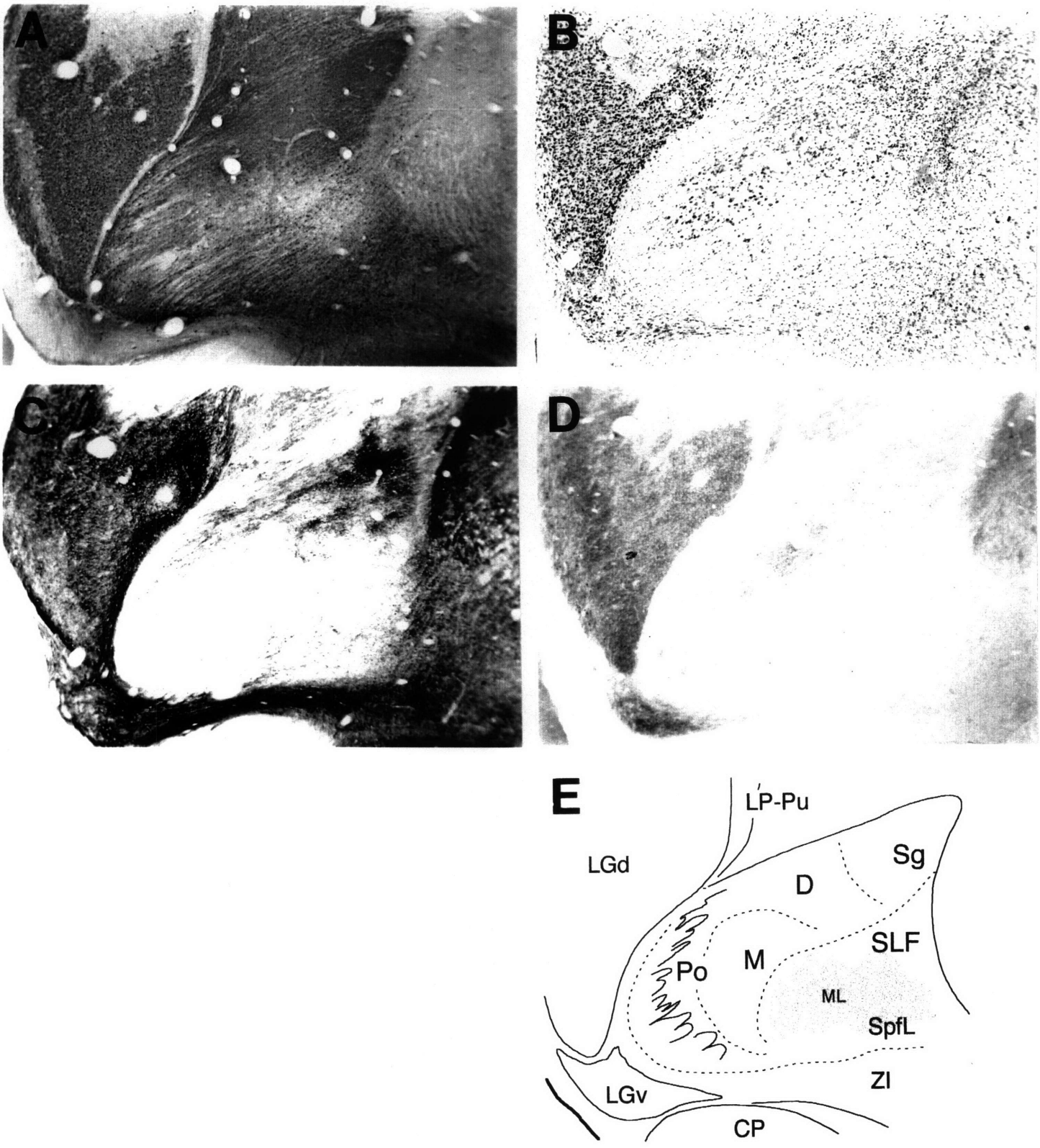

Fig. 4

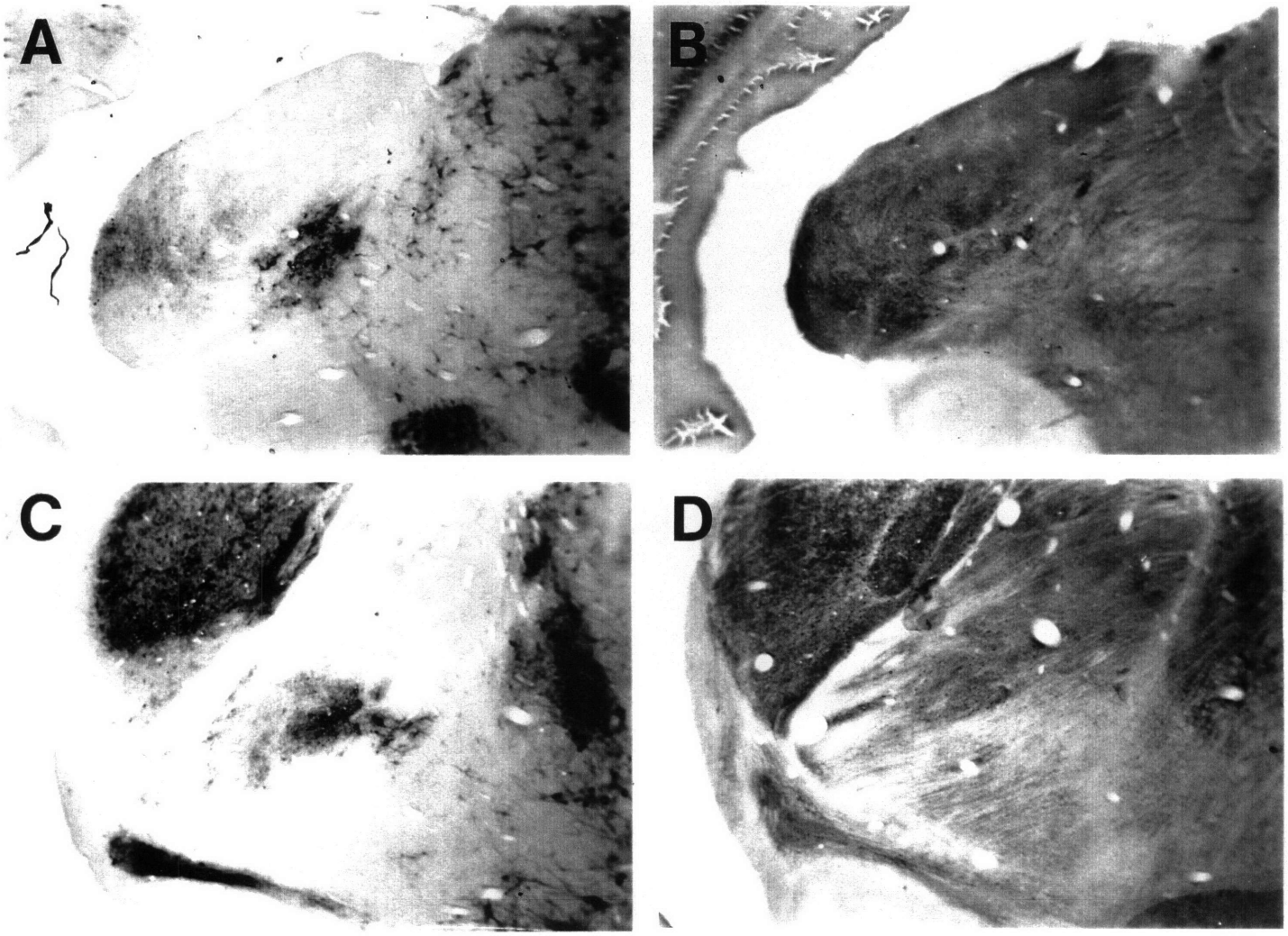

Fig. 5

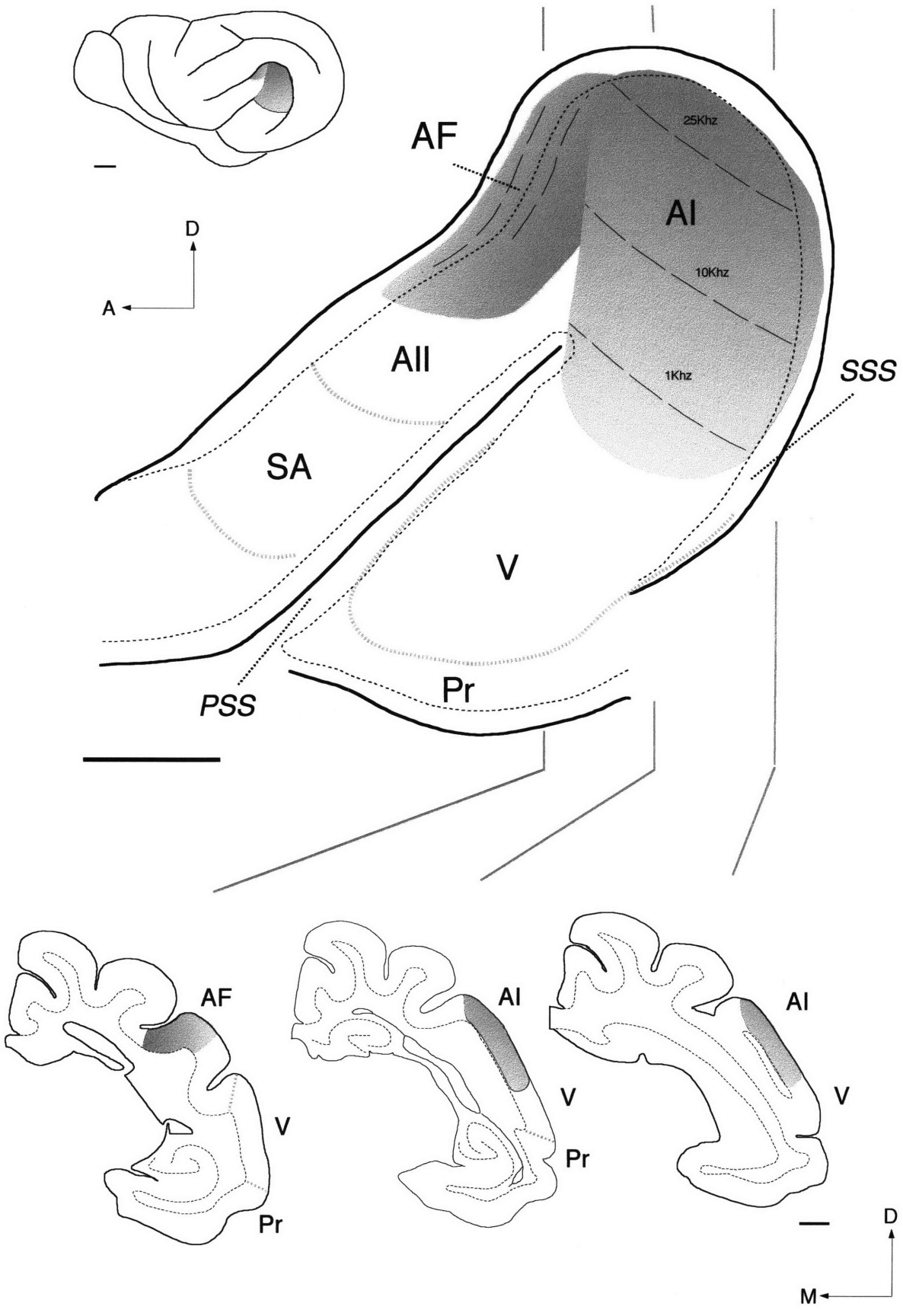

Fig. 6

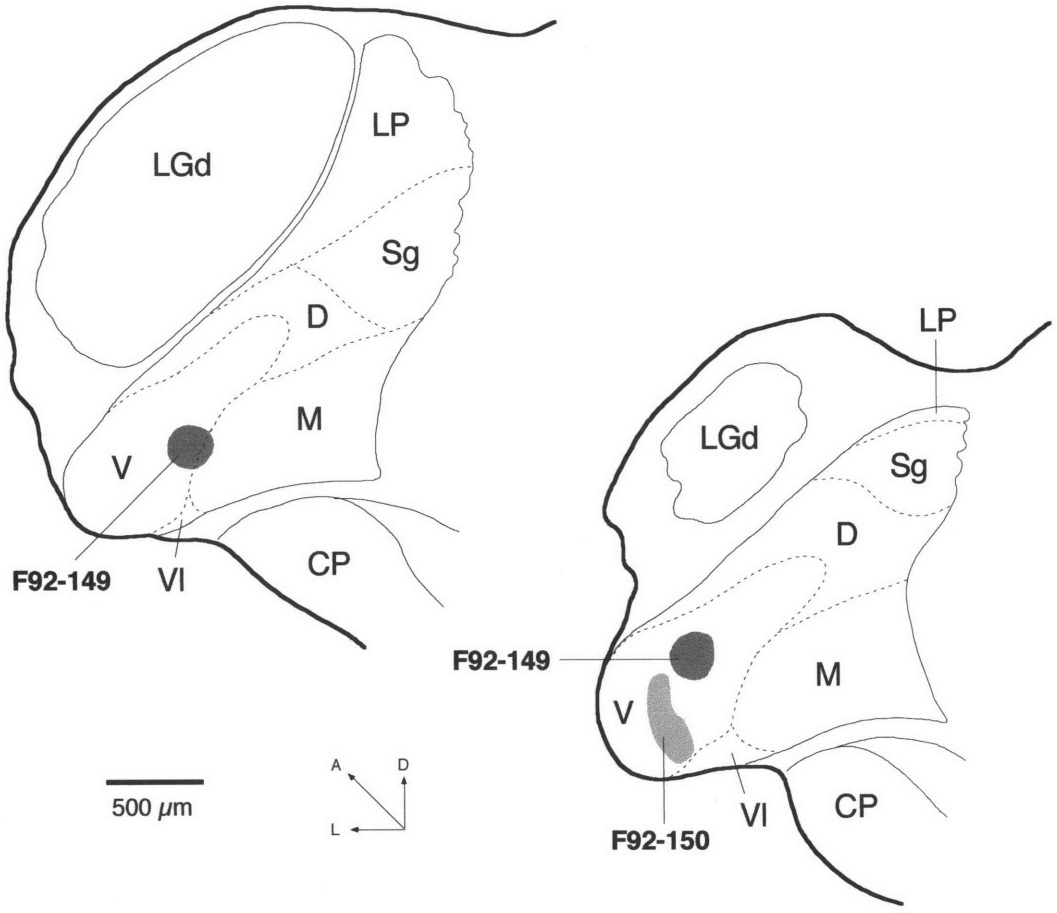
LGd
LP
Sg
D
M
V
F92-149
Vl
CP
500 μm
A
D
L
LP
LGd
Sg
D
F92-149
M
V
Vl
CP
F92-150

Fig. 7

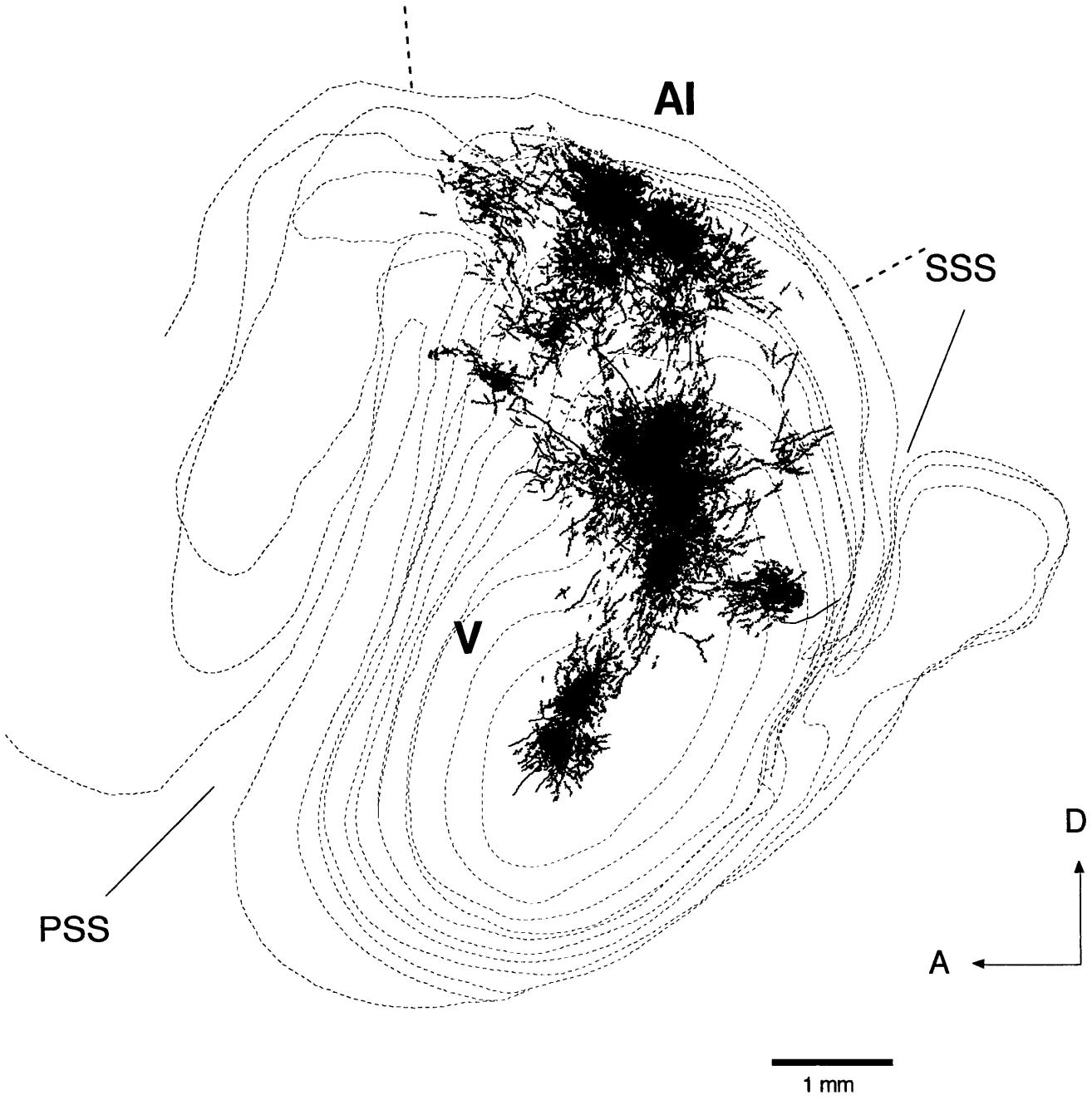

Fig.8

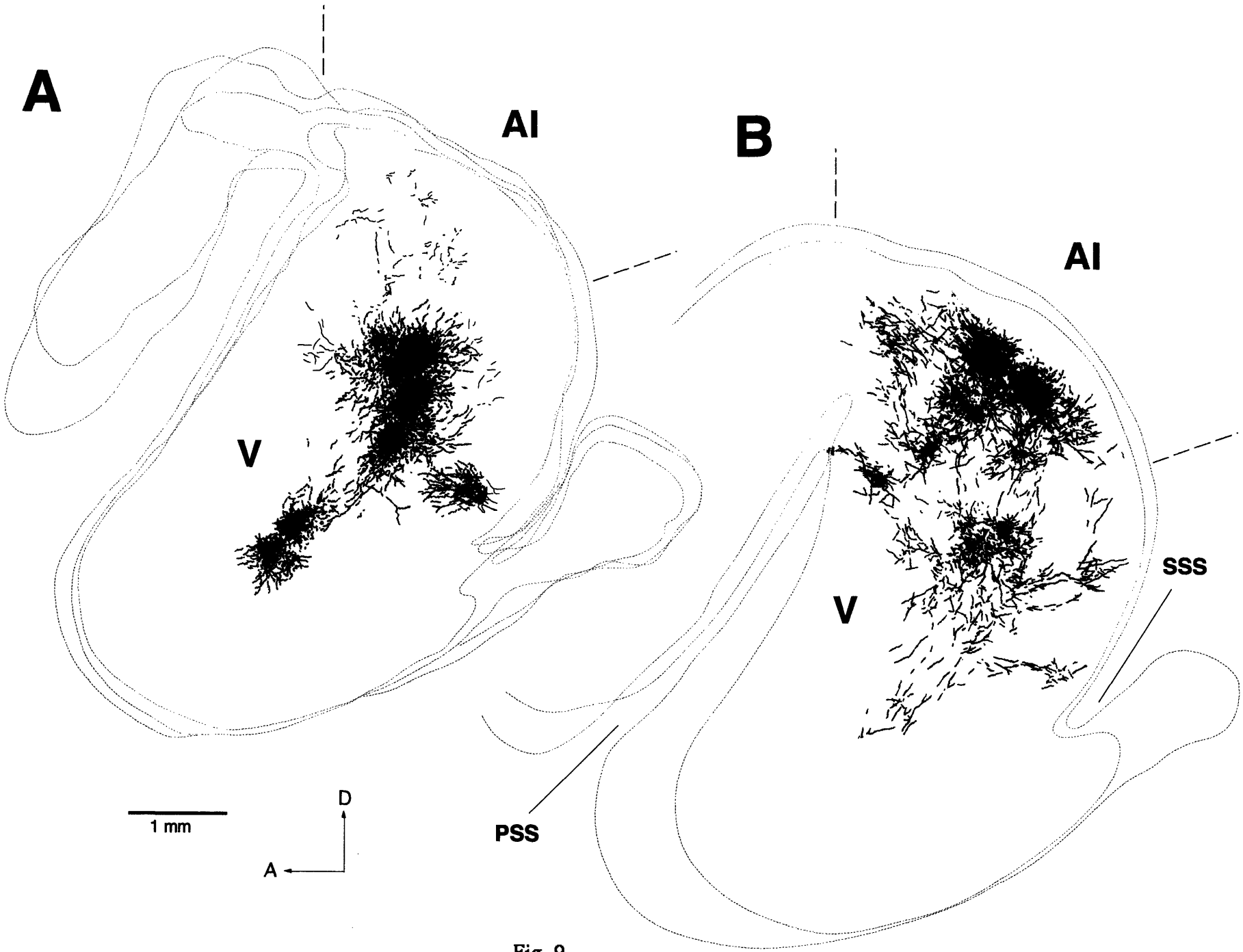

Fig. 9

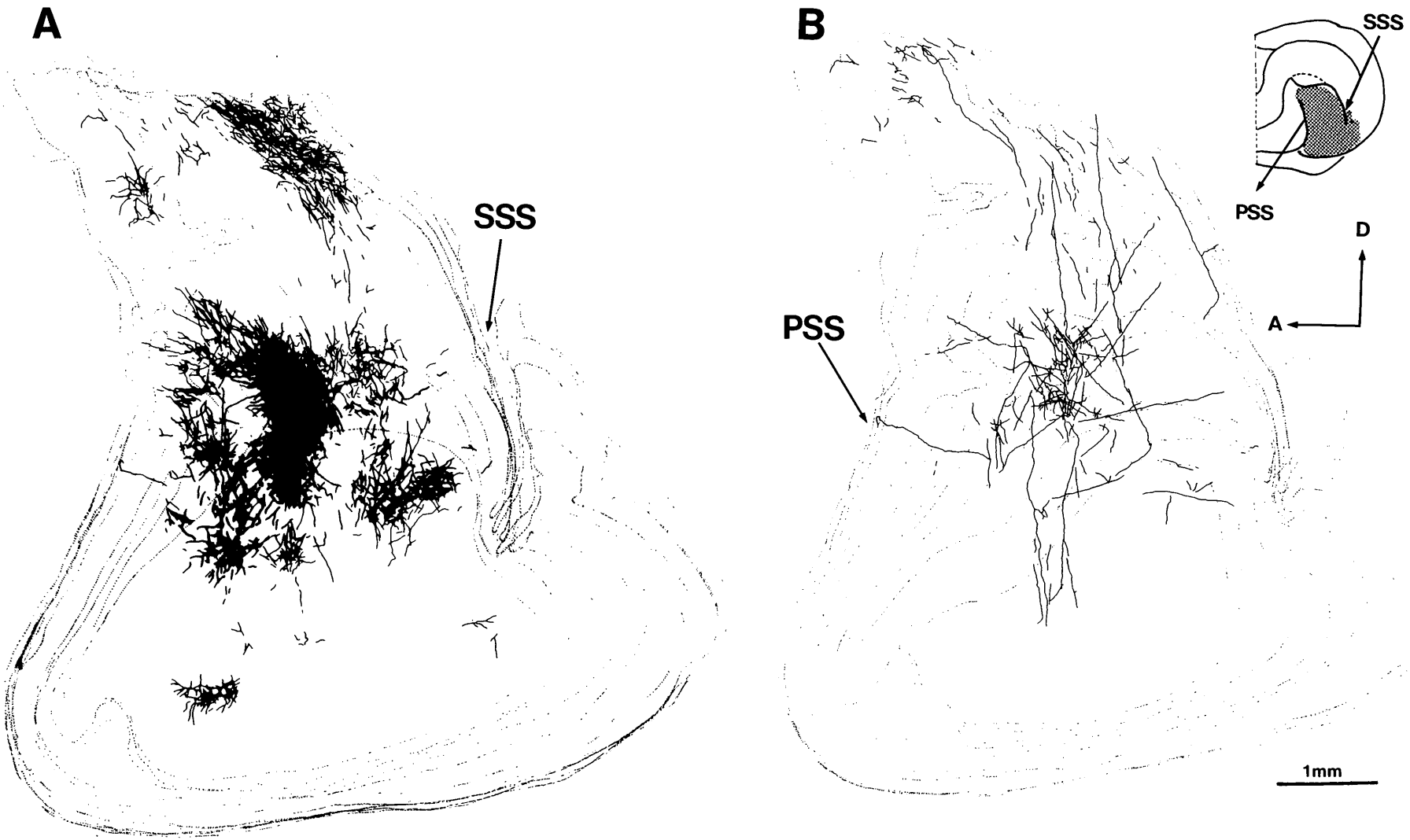

Fig.10

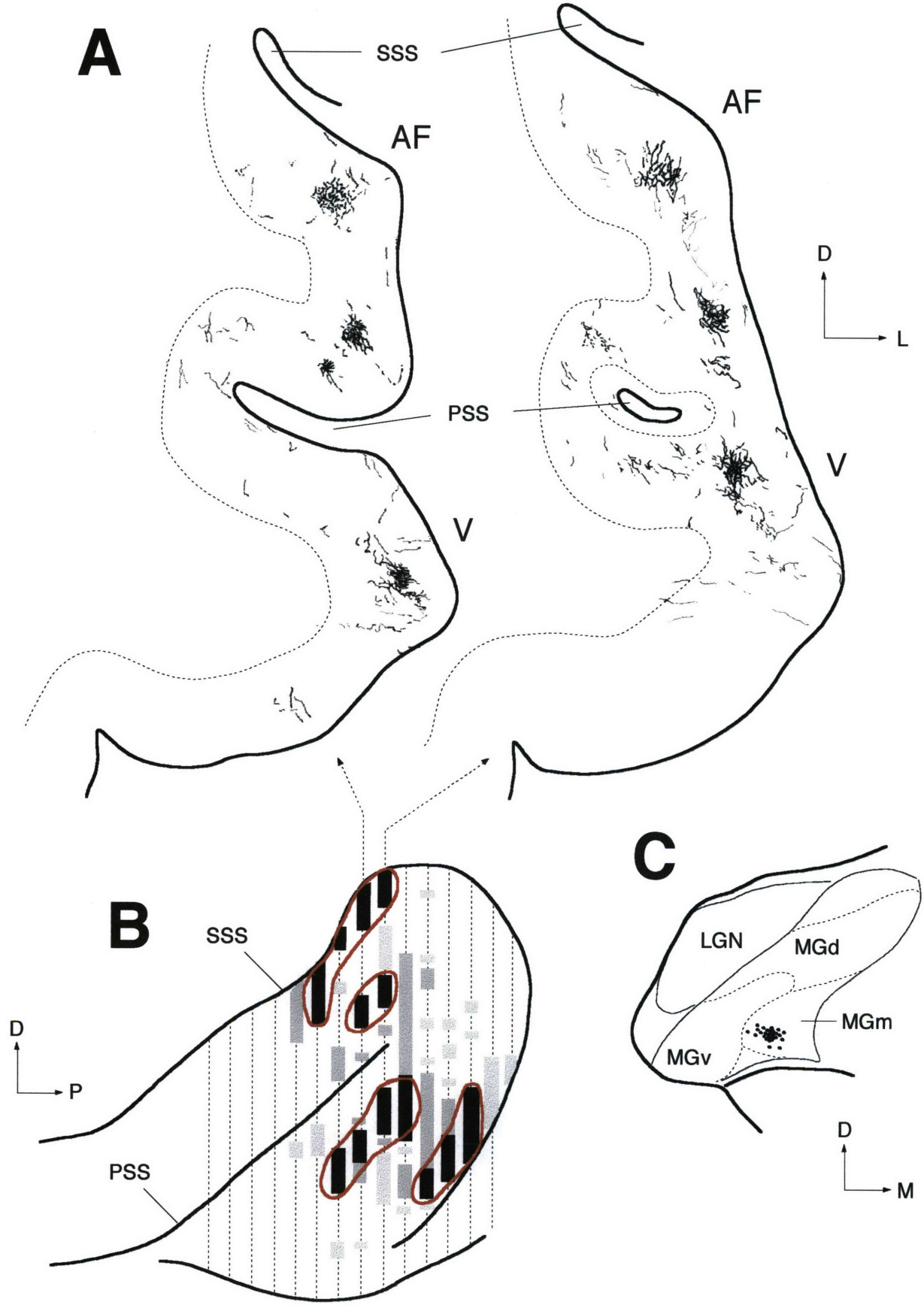

Fig. 11

Chapter 5

Auditory Cortex with Induced Visual Projections: Horizontal Connectivity and Optical Imaging of Functional Responses

Introduction

A basic feature of sensory cortex is the organization of cells into modules in which neurons that prefer a particular value of a stimulus feature are grouped together and represented adjacent to neurons that prefer an adjacent value. A fundamental functional module in primary visual cortex (V1) relates to stimulus orientation: orientation selective cells in V1 appear early in cortical development (Chapman and Stryker, 1993), and modules of these cells form systematic and compact maps in V1 (Bonhoeffer and Grinvald, 1993). Orientation maps are the first modular representation to arise in V1, and their appearance precedes that of other kinds of modules, such as those related to ocular dominance (Albus, 1975). There is evidence that the development of orientation selective cells and orientation maps in V1 is regulated by afferent activity (Chapman and Stryker, 1993), as is the system of long-range orientation-specific horizontal connections that link iso-orientation modules (Callaway and Katz, 1990). At the same time, orientation selective cells exist in cortex even at eye opening (Chapman and Stryker, 1993), indicating that spontaneous activity rather than visual activity is sufficient for their formation. Furthermore, orientation maps from the two eyes are exquisitely aligned in cortex even without conjoint visual experience (Godecke and Bonhoeffer, 1996), and monocular lid suture followed by reverse suture causes precise restoration of the maps from either eye (Kim and Bonhoeffer, 1994). These data argue for intrinsic determinants of the location of orientation maps in cortex. More generally, the extent to which afferent activity on the one hand and intrinsic cortical substrates on the other regulate modular organization in cortex remains an open question. The issue has broad experimental and theoretical significance for understanding cortical development.

We have addressed the question using a novel preparation, in which retinal inputs are directed into the auditory pathway in ferrets (Sur et al., 1988). Specifically, extensive deafferentation of the auditory thalamus in neonatal ferrets (Angelucci, Chapter 1, this Thesis) induces retinal axons to innervate the medial geniculate nucleus (MGN). The MGN projects to

primary auditory cortex (A1) in relatively normal fashion (Pallas et al., 1990; see also Angelucci, Discussion of Chapter 3, this Thesis). Thus, visual inputs activate A1, which presumably develops with a very different pattern of input activity compared to normal A1. Previous data from this laboratory have reported that A1 in rewired ferrets develops a map of visual space (Roe et al., 1990), and contains orientation selective cells (Roe et al., 1992). We have now asked whether these cells are organized further into an orientation map, and if so, whether the horizontal connections in rewired A1 are shaped by the map (i.e. organized into iso-orientation clusters) as they are in V1 of normal animals.

Materials and Methods

Animals

The animals used in the present study were pigmented ferrets (*Mustela putorius furo*; family Mustelidae, order Carnivora) bred in our colony or purchased from a commercial supplier (Marshall Farm). A total of 15 adult ferrets were used. Some of these animals (n= 8) received neonatal brain lesions to reroute retinal axons to the auditory thalamus (see below). Throughout this study we refer to the neonatally operated animals as "rewired" ferrets.

Neonatal surgery to induce retinal projections to the auditory thalamus

The surgical protocol used in this study to reroute retinal fibers to the medial geniculate nucleus (MGN) is similar to that described previously (Angelucci, Chapters 1 and 2, this Thesis). Briefly, one day after birth, ferret kits were anesthetized by hypothermia. Under sterile conditions and microscopic observation, the scalp was incised and a small craniotomy was made in the occipital bone overlying the midbrain. To extensively deafferent the MGN the lateral third of the mesencephalon was coronally sectioned at midcollicular level, and the superior colliculus (SC), as well as the commissure of the SC and both inferior colliculi were ablated by heat cauterization. All lesions were performed bilaterally. On completion of surgery the skin was sutured and the kits revived under a heat lamp. The kits were then returned to the jill for rearing to adulthood. These procedures have been previously shown to significantly reduce the number of normal auditory afferents to the MGN, and to induce some retinal axons to innervate the auditory thalamus (Angelucci, Chapter 1, this Thesis).

Optical imaging of intrinsic signals

Responses to oriented full field square wave gratings were imaged optically in primary visual cortex (V1) of normal adult female ferrets (n= 6), and in primary auditory cortex (A1) of 1 normal and 8 "rewired" adult ferrets.

Surgical Preparation. Animals (weighing between 750-900 gm) were initially anesthetized with ketamine (20-25 mg/kg i.m.) and xylazine (1.5 mg/kg i.m.). Atropine (0.04 mg/kg) and dexamethasone (0.7 mg/kg) were administered i.m. to prevent respiratory congestion and cerebral edema, respectively. A tracheostomy was performed to facilitate artificial ventilation. Anesthesia was subsequently maintained either by inhalation of isofluorane (0.5-1.2%) in a 70/30 mixture of N_20 and O_2, or by continuous infusion of sodium pentobarbital (1.5 - 2.0 mg/kg/hr). ECG, EEG and heart rate were monitored continuously to ensure adequacy of anesthesia. End tidal CO_2 was maintained at 4% throughout by adjusting ventilator volume and rate. Rectal temperature was maintained at 38°C and a solution of 5% dextrose and lactated Ringers were continuously infused intravenously to maintain fluid balance. A large craniotomy and durotomy were performed to expose V1 or A1. To focus the eyes on the screen and to prevent corneal drying, the eyes were equipped with contact lenses.

Optical Chamber Placement and Recording. A stainless steel chamber (20 mm in diameter) was placed around the cranial opening and cemented with dental acrylic. To further ensure proper sealing, the inner margins were sealed with wax. The chamber was then filled with silicon oil (50 cs viscosity) and covered with a quartz window. This helped to minimize cortical pulsations due to respiratory and cardiac activities. Intrinsic signal imaging was performed following the method developed by Grinvald et al. (1986). Briefly, the exposed cortical surface was illuminated by a bifurcated fiber-optic light guide attached to an 100 W tungsten-halogen lamp with a regulated power supply. After passing through an IR cut-off filter and then through a 610 nm (orange) filter, light was made to evenly illuminate the cortex at an intensity within linear range of the camera sensitivity. A slow scan video camera (Bischke CCD-5024N, RS 170, 30 Hz, 60 dB s/n) fitted with a microscope consisting of back to back camera lenses (50 and 55 mm, f 1.2) was used. This arrangement allows high numerical aperture and shallow depth of field (Ratzlaff and Grinvald, 1991). To image surface

vasculature, light of 540 nm was used before commencing imaging of activity dependent intrinsic signals at a focal depth of 300-350 μm below the surface. Animals were stimulated binocularly using full field square wave gratings presented in 4 or 8 different orientations in a randomly interleaved fashion. Two different spatial frequencies of 0.375 and 0.175 Hz were presented to the animal. Data was collected using Imager 2001 (Optical Imaging Inc.) which subtracted the gray reference image from the stimulus image collected during binocular presentation of a full field oriented bar stimulus (4 or 8 orientations randomly presented). Digitized images were stored in real time for analysis.

Intracortical injections of cholera toxin B

At the end of the optical imaging session, one injection of cholera toxin subunit B (CTB; low salt; List Biological Labs, CA) was made in V1 of 6 normal animals and in A1 of 1 normal and 2 "rewired" ferrets on the optically imaged hemisphere. In some of the normal animals (n= 4) CTB injections were also made in A1 on the contralateral, non-imaged hemisphere. The sites of the injection were chosen on the basis of the recorded optical activity maps, using the corresponding surface vasculature maps as guides. CTB was delivered iontophoretically 250-300 μm below the cortical surface, through a glass micropipette (7-15 μm inside tip diameter), by applying positive current of 2 μA at 7 sec duty cycle for 7-15 min. Fiducial marks were made at 4 surrounding locations on the same cortex and served as alignment landmarks. Lesion electrodes were smeared with india ink, lowered into the cortex perpendicular to the cortical surface, and their location was recorded manually onto the surface vasculature map. Finally the craniotomy was closed and the muscle and skin sutured. After a survival period of 16-35 hr, the animals were euthanized with sodium pentobarbital (80 mg/kg) and transcardially perfused with saline for 3-5 min, followed by 2 % paraformaldehyde in 0.1M phosphate buffer pH 7.4 for 15-20 min. To allow for sectioning of the cortex in the tangential plane, the cortical area of interest was slightly flattened by removing most of the white matter and post-fixing for 1-2 days in 4 % paraformaldehyde between two glass slides. After

cryoprotection in 30% sucrose, the cortex was sectioned with a freezing microtome at 50 μm in the tangential plane. Brain sections were processed for CTB immunohistochemistry according to the protocol of Angelucci et al. (1996). Briefly, immunostaining was carried out by incubating the sections first in goat anti-CTB (List Biological Labs, CA; 1:4000), then in biotinylated rabbit anti-goat IgG (Vector Labs, CA; 1:200), subsequently in avidin-biotin-peroxidase (ABC; 1:100) and finally developed with a cobalt-enhanced diaminobenzidine (DAB; Sigma, MO) reaction, or with Vector VIP substrate (Vector Labs). Sections were mounted, air dried, dehydrated and coverslipped.

Alignment of optical maps with camera lucida reconstructions of retrograde labeling

Retrogradely labeled neurons, injection sites and fiducial marks were reconstructed using camera lucida and a 10x objective. Camera lucida reconstructions were scanned on a laser scanner at resolutions similar to those of the optical images. The scanned anatomical images were then warped onto each other with the help of fiducial marks. The composite warped image was then overlaid onto the orientation angle map of the imaged cortex using the fiducial marks as alignment reference points, and the location of the injection site as well as of the retrogradely labeled cells was thus transferred onto the functional images.

Results

Optical maps in rewired A1

The orientation map in rewired A1 is understood best when compared to the map in normal V1; the latter will be described first, followed by the results from rewired A1.

Fig. 1 shows the organization of orientation selective cells in V1 of a normal ferret. A full-field grating of a particular orientation elicits activity from iso-orientation domains that have a stereotypical size and spacing within V1 (Figs. 1a,b). Gratings of adjacent orientations elicit activity from partially overlapped iso-orientation domains, while a grating of an orthogonal orientation leads to an essentially complementary system of domains. To understand how the modular representation of individual orientations is organized into an orientation map, we compute for each pixel a vector average of signals obtained in response to individual stimulus orientations (Bonhoeffer and Grinvald, 1993). The resulting orientation map (vector angle map), color coded to depict the angle of the orientation vector at each pixel, demonstrates the spatially compact organization of orientation domains in V1 (Fig. 1d). A basic feature of the map is the pinwheel-like organization of orientation selective cells around singularities, termed pinwheel centers (Fig. 1c). An analysis of the magnitude of orientation preference at each pixel indicates that orientation magnitude is highest within iso-orientation regions and lowest at pinwheel centers and associated "fractures" where the angle of orientation preference changes rapidly (Rao et al., 1996). It has been demonstrated that orientation-specific single cell responses underlie the imaged maps (Blasdel and Salama, 1986). These data confirm previous descriptions of the organization of ferret V1 from this laboratory (Rao et al., 1994; Toth, 1995), and agree with reports of the organization of orientation selectivity in V1 of ferrets described briefly by others (Weliky et al., 1995, 1996).

The organization of orientation selective cells in A1 of rewired ferrets has important similarities and differences with the organization in V1 of normal animals. In a rewired animal, imaging A1 (Fig. 2a,3a) in response to a grating of a particular orientation yields essentially one

large activity domain (Fig. 2b) located in the rostral part of A1; for some orientations, a second, smaller domain appears as well. Such optical activity strongly correlates with the stimulus parameters. While randomly interleaved full field gratings of spatial frequency 0.375 Hz elicit strong activity, the same area, when stimulated by 0.175 Hz fails to elicit any such response. Presentation of stimuli of similar parameters to normal control animals yields no activity in A1.

The size of the main activity domain (mean length= 980 μm, mean width= 950 μm, n=4) is significantly larger than that of the multiple domains in normal V1 (mean diameter, 370 μm; Rao et al., 1996). Although a domain of similar, but not identical, size and location appears following presentation of stimuli at any orientation, the magnitude of the signal within this large visual domain is not homogeneous, and varies with stimulus orientation. A quantitative analysis of signal magnitude performed for each stimulus orientation, where signals are normalized to 3% and 10% of the maximum signal value, shows that for each orientation there are regions of higher signal magnitude within the large visual domain, immersed within regions of lower magnitude (Fig. 3b). In the higher-activity regions different orientations overlap only in part. Orientation magnitude in rewired A1 is about half that in normal V1. A vector angle representation of orientation reveals a bias towards spatial segregation of cells into domains of orientation preference (Fig. 3d). This is evident from the vector angle map (Fig. 3d) which shows at least a crude, but systematic organization of orientations into pinwheels (Fig. 3c). When orientation magnitude is overlaid on the vector angle map, such as in a polar map, orientation magnitude seems to be low towards the center of the map, near a pinwheel center, and to increase away from the pinwheel center. The latter observation is similar to what is normally observed in polar maps of V1 at pinwheel centers. Thus, the polar map in rewired A1 is consistent with there being only one pinwheel center in the visual A1 domain. By contrast, normal V1 has a pinwheel density of about 5.5/sq mm (Rao et al., 1996). Similar data was obtained from another rewired animal. A similar analysis of signal magnitude and of vector angle representation of orientation in normal A1 shows no bias towards spatial segregation of

cells into orientation-selective domains, nor pinwheel centers. The latter observation suggests that orientation structure in rewired A1 is not artifactual.

Horizontal connections in rewired A1

We next examined the distribution of horizontal connections in rewired A1. In normal V1, long-range intracortical horizontal connections link cells with similar orientation preference, as demonstrated by combining tracer injections in cortex with 2-DG labeling in cats (Gilbert and Wiesel, 1989; Lowel and Singer, 1992). We first demonstrated that tracer injections can be combined with optical imaging in normal ferret V1 to examine the orientation specificity of horizontal connections. Fig. 4a shows a cholera toxin B injection site in V1 and retrogradely labeled cells superimposed on iso-orientation domains imaged optically in the same animal. The injection site measures about 300 μm in diameter and is confined to an iso-orientation domain. An analysis of the location of retrogradely labeled cells from the center of the nearest physiological domain indicates that the vast majority of cells lie in or very near these domains (Fig. 4b; note that the figure depicts distance of cells from the centers of patches, and patches are 0.2-0.8 mm in size along their short and long dimensions). Thus, horizontal connections in normal V1 are generally specific for cells with similar orientation preference.

A similar analysis in rewired A1 is shown in figure 5. The injection site and retrogradely labeled cells are superimposed on physiologically imaged iso-orientation domains in figure 5a. The injection site in this case is about 200 μm in diameter and is located within the main large activity domain. The distribution of cells as a function of distance from the nearest domain center (Fig. 5b) shows quantitatively what is apparent qualitatively in figure 5a: labeled cells are essentially restricted to the one large domain of visual activity. When the injection site and labeled cells were superimposed to the vector angle map, we found that the injection site was located in a region of overlap of different orientations. Consequently, retrogradely-labeled cells were found in domains of all orientations. Thus, it is not clear yet whether in rewired A1 horizontal connections link preferentially neurons with the same orientation preference.

Finally, we asked whether the distribution of horizontal connections in rewired A1 has been shaped by visual activity so that it differs from that in normal A1. Fig. 6b shows a CTB injection site (200 μm in diameter) and retrogradely labeled cells in rostral A1 of a normal animal. In agreement with previous descriptions of horizontal connections in A1 of cats (Reale et al., 1983; Matsubara and Phillips, 1988; Wallace et al., 1991) and with the horizontal axonal spread of pyramidal neurons in A1 (Ojima et al., 1991), these connections in ferrets are highly anisotropic, spreading much more in the anteroposterior dimension (the presumed iso-frequency axis) compared to the dorsoventral dimension (the presumed variable frequency axis). Figure 7 shows this anisotropy in 3 normal animals, by plotting the ratio of the long and short axes of label. In contrast, the spread of horizontal connections in rewired A1 in 2 animals is seen to be much more symmetric, with the long and short axes of label being similar in extent (Figs. 6a and 7) and not related to the orientation of the presumed isofrequency axis. Thus, a direct effect of visual activity on cortical connectivity is to shape horizontal connections into symmetric and unoriented domains.

Discussion

These data emphasize both the role of the pattern of input activity in the formation of functional and anatomical modules during cortical development.

Specific features of optical maps in rewired A1

Before discussing the implications of orientation maps in rewired A1, it is useful to consider some of their details. The maps represent optically imaged measures of population activity (local conversion of oxy- to deoxyhemoglobin) in rewired A1. Considerable signal averaging, over prolonged recording times, was required for the signals to be reliably measured; thus, single unit recordings to correlate neuronal responses at specific locations in the optically imaged maps were not viable. Nonetheless, the data are consistent with previous single unit recordings of visually responsive neurons in rewired A1 (Sur et al., 1988; Roe et al., 1992). A reasonable proportion of cells in rewired A1 (about 35%) was found to be visually driven, and the well-driven cells were tuned as sharply for orientation as cells in V1 (Roe et al., 1992). However, the responsiveness of visual neurons was much poorer in rewired A1, probably reflecting a combination of putative W cell dominated input from the retina (but see Angelucci, Chapter 1, this thesis) and weak synaptic drive from MGN cells to widely dispersed cortical locations. The weak responses found at the single neuron level in previous studies (Roe et al., 1992) are reflected in the weak signals recorded optically in the present study.

Even though only restricted portions of the MGN receive retinal input, the projections from the MGN spread extensively in A1 of normal ferrets (Angelucci, Chapter 3, this Thesis), and retrograde (Pallas et al., 1990) as well as preliminary anterograde data (see Angelucci, Chapter 3, this Thesis) suggest that this is the case also in "rewired" ferrets. Thus, optical signals, as also visual responses (Roe et al., 1990), can be recorded from a reasonable portion of A1.

Following visual stimulation with variously oriented moving gratings, a large visual domain is activated in "rewired" A1. Three main observations indicate that such domain reflects activation of visually-responsive neurons in A1: 1) the strength of activity elicited correlates strongly with the stimulus parameters; 2) no activity is observed in normal control animals following presentation of the same stimuli, regardless of the stimulus' spatial frequency and orientation; 3) the location of the activated region in rostral A1 is consistent with the topography of auditory thalamocortical projections relaying visual inputs to the cortex. Specifically, retino-MGN projections terminate in the rostral half of MGN (Angelucci, Chapter 2B, this thesis), which in turn is connected to rostral A1 in both normal and "rewired" ferrets (Angelucci, Chapter 3, this Thesis; Pallas et al., 1990). Within the domain of visual activity there is a bias towards spatial segregation of cells into domains of orientation preference, with a systematic organization of preferred orientations. By contrast, no bias towards spatial segregation of orientation preference, and no pinwheel-like organization is observed in normal A1.

The finding in rewired A1 can be interpreted on the basis of previous physiological findings (Roe et al., 1992). While the tuning of individual orientation-selective cells in rewired A1 was sharp, they represented a minority of cells in A1, since the majority of neurons showed poor responsiveness to visual stimulation (see above). Thus, while a majority of cells within the optically active domain might be generally and poorly responding to stimuli of any orientation, a minority of cells might show a sharp orientation preference and be organized into a crude orientation map.

An interesting finding of the present study is that the size of the visual domain imaged optically in "rewired" A1 is comparable to the size of the overall intracortical spread of single thalamocortical axons, or of thalamocortical axons arising from a small group of MGN neurons labeled by PHA-L, both in normal as well as in "rewired" A1 (Angelucci, Chapter 3; this Thesis).

The role of input activity in development of orientation-specific responses and connections

Activity is known to play a major role in the development of orientation selectivity in normal V1, along with organizing the orientation map and horizontal connections in V1. A brief review of the key experiments is as follows.

Orientation selectivity in visual cortex appears to arise by a combination of inputs from the LGN and local intracortical connections: LGN inputs provide an initial bias along the orientation axis while profuse excitatory local cortical connections amplify this bias and sharpen tuning (Somers et al., 1995; see, for an alternative view, Ferster et al., 1996). The development of orientation selectivity in V1 of ferrets occurs progressively, maturing to adult-like proportions and tuning by 7 postnatal weeks (Chapman and Stryker, 1993). At least some orientation specificity can develop prior to visual experience, for about 25% of neurons at postnatal weeks 4-5, i.e. at and around eye-opening (which occurs at postnatal day 30), have adult-like tuning for orientation. Both afferent and intracortical activity are required for the subsequent maturation of orientation selectivity; binocular lid suture, which reduces afferent activity, and intracortical infusion of TTX, which blocks cortical activity, prevent or delay the maturation of orientation tuning (Chapman and Stryker, 1993).

The organization of orientation selective cells into an orientation map occurs over roughly the same time course as the development of orientation tuning in individual cells (Chapman and Bonhoeffer, 1994). Normally, the orientation map elicited by stimulating one eye is precisely aligned with the map from the other eye (Bonhoeffer and Grinvald, 1993). Monocular lid suture during map development disrupts the orientation map from that eye (Kim and Bonhoeffer, 1994). However, reverse suture restores the map precisely, suggesting that a scaffold for the orientation map might be intrinsic to the cortex. In the same vein, the two eyes can develop identical orientation maps even without any common visual experience (Godecke and Bonhoeffer, 1996).

Finally, the clustered organization of long-range horizontal connections in visual cortex (Callaway and Katz, 1990) develops from a more uniform distribution over a time course that parallels the development of orientation selectivity and orientation maps in ferret V1 (Durack and Katz, 1996). In adult cat and ferret V1, long-range horizontal connections link cells with similar orientation preference (Gilbert and Wiesel, 1989; Sharma et al., 1995). Binocular lid suture in cats prevents the clustering of horizontal connections in V1 (Callaway and Katz, 1991), and artificially induced strabismus causes long-range horizontal connections in V1 to link cells driven by the same eye (Lowel and Singer, 1992), arguing for an important role for correlated input activity in selecting these connections.

The organization of orientation selective cells in rewired A1 into modules, although crude, suggests an instructive role for visual activity in creating modular organization in cortex. Although our anatomical data do not clarify whether horizontal connections in "rewired" A1 link preferentially neurons with similar orientation preference, they clearly demonstrate that horizontal connections are restricted to visual domains, linking preferentially neurons activated by visual inputs. Furthermore, while horizontal connections in normal A1 have a propensity to be elongated along the isofrequency axis (Reale et al., 1983; Matsubara and Phillips, 1988; Ojima et al., 1991), these connections are much more symmetric in rewired A1. The latter findings suggest that visual activity, which has a spatial and temporal correlation structure that is very different from that of auditory activity, shapes the horizontal connections so that they are much more symmetric and unoriented, and link visual neurons in rewired A1.

References

Albus K (1975) A quantitative study of the projection of the central and paracentral visual field in area 17 of the cat : the spatial organization of orientation domains. Exp. Brain Res. 24:181-202.

Angelucci A, Clascá F, Sur M (1996) Anterograde axonal tracing with the subunit B of cholera toxin: a highly sensitive immunohistochemical protocol for revealing fine axonal morphology in adult and neonatal brains. J. Neurosci. Methods 65:101-112.

Blasdel GG, Salama G (1986) Voltage sensitive dyes reveal a modular organization in monkey striate cortex. Nature 321:579-585.

Bonhoeffer T, Grinvald A (1993) The layout of iso-orientation domains in area 18 of cat visual cortex. Optical imaging reveals pin-wheel like organisation. J. Neurosci. 13:4157-4180.

Callaway EM, Katz LC (1990) Emergence and refinement of clustered horizontal connections in cat striate cortex. J. Neurosci. 10:1134-1153.

Callaway EM, Katz LC (1991) Effects of binocular deprivation on the development of clustered horizontal connections in cat striate cortex. Proc. Natl. Acad. Sci. USA 88:745-749.

Chapman B, Stryker MP (1993) Development of orientation selectivity in ferret visual cortex and effects of deprivation. J. Neurosci. 13:5251-5262.

Chapman B, Bonhoeffer T (1994) Chronic optical imaging of the development of orientation domains in ferret area 17. Soc. Neurosci. Abst. 20:214.

Durack JC, Katz LC (1996) Development of horizontal projections in layer 2/3 of ferret visual cortex. Cerebral Cortex 6:178-183.

Ferster D, Chung S, Wheat H (1996) Orientation selectivity of thalamic input to simple cells of cat visual cortex. Nature 380:249.

Gilbert CD, Wiesel TN (1989) Columnar specificity of intrinsic horizontal connections in cat visual cortex. J. Neurosci. 9:2432-2442.

Godecke I, Bonhoeffer T (1996) Development of identical orientation maps for two eyes without common visual experience. Nature 379:251- 254.

Grinvald A, Lieke EE, Frostig RD, Gilbert CD, Wiesel TN (1986) Functional architecture of cortex revealed by optical imaging of intrinsic signals. Nature 324:361-364.

Kim DS, Bonhoeffer T (1994) Reverse occlusion leads to a precise restoration of orientation preference maps in visual cortex. Nature 370: 370-372.

Löwell S, Singer W (1992) Selection of intrinsic horizontal connections in the visual cortex by correlated neuronal activity. Science 255:209-211.

Matsubara, JA and Phillips, DP (1988) Intracortical connections and their physiological correlates in primary auditory cortex (A1) of cats. J. Comp. Neurol. 268:38-48.

Ojima H, Honda CN, Jones EG (1991) Patterns of axon collateralization of identified supragranular pyramidal neurons in cat auditory cortex. Cerebral Cortex 1:80-94.

Pallas SL, Roe AW, Sur M (1990) Visual projections induced into auditory pathway of ferrets. I. Novel inputs to primary auditory cortex (A1) from LP/pulvinar complex and topography of MGN-A1 projections. J Comp. Neurol. 298:50-68.

Rao SC, Toth LJ, Sur M (1994) Invariance of orientation domains in area 17 of cat revealed by intrinsic signal imaging. Soc. Neurosci. Abstr. 20:836.

Rao SC, Toth LJ, Sur M (1996) Optical maps of orientation preference in primary visual cortex of cats and ferrets: organization principles and rules of representation (submitted).

Ratzlaff EH, Grinvald A (1991) A tandem-lens epifluorescence microscope: hundred fold brightness advantage for wide field imaging. J. Neurosci. Meth. 36:127-137.

Reale RA, Brugge JF, Zhen Feng J (1983) Geometry and orientation of neuronal processes in cat primary auditory cortex (AI) related to characteristic-frequency maps. Proc. Natl. Acad. Sci. USA 80:5449-5453.

Roe AW, Pallas SL, Hahm J-O, Sur M (1990) A map of visual space induced into primary auditory cortex. Science 250:818-820.

Roe AW, Pallas SL, Kwon YH, Sur M (1992) Visual projections routed to the auditory pathway in ferrets: receptive fields of visual neurons in primary auditory cortex. J Neurosci. 12:3651-3664.

Sharma J, Angelucci A, Rao SC, Sur M (1995) Relationship of intrinsic connections to orientation maps in ferret primary visual cortex: iso-orientation domains and singularities. Soc. Neurosci. Abstr. 21:392.

Somers DC, Nelson SB, Sur M (1995) An emergent model of orientation selectivity in cat visual cortex simple cells. J. Neurosci. 15:5448-5465.

Sur M, Garraghty PE, Roe AW (1988) Experimentally induced visual projections into auditory thalamus and cortex. Science 242:1437-1441.

Toth LJ (1995) Layout and connectivity of orientation domains in mammalian visual cortex: a physiological description. Ph.D. Thesis, MIT Cambridge MA.

Wallace MN, Kitzes LM, Jones EG (1991) Intrinsic inter- and intralaminar connections and their relationship to the tonotopic map in cat primary auditory cortex. Exp. Brain Res. 86:527-544.

Weliky M, Kandler K, Fitzpatrik D and Katz LC (1995) Patterns of excitation and inhibition evoked by horizontal connections in visual cortex share a common relationship to orientation columns. Neuron 15:541-552.

Weliky M, Bosking WH, Fitzpatrik D (1996) A systematic map of direction preference in primary visual cortex. Nature 379:725-728.

Figure Legends

Figure 1. Organization of orientation selective cells in V1 of a normal ferret. **a:** Schematic diagram of a lateral view of the ferret brain, showing the location of the area imaged optically (*black bar*). **b:** Single condition map obtained in response to presentation of a full-field grating of one particular orientation. Such a map was obtained by mathematically subtracting the images obtained before and after presentation of the visual stimulus. Active areas appear as dark "spots", while unresponsive areas appear as white "spots". **c:** A basic feature of the vector angle map, shown in d, is the systematic organization of orientations in a "pinwheel-like" fashion around singularities, termed pinwheel centers. **d:** Vector angle map obtained by computing for each pixel a vector average of the signals obtained in response to eight individual stimulus orientations, and color coded to depict the angle of the orientation vector at each pixel. A clear spatial segregation of cells into domains of orientation preference is present in V1 (see Results).

Figure 2. Presentation of oriented gratings in rewired A1 yields mainly one large activity domain. **a:** Schematic diagram of a lateral view of the ferret brain, showing the location of the area in A1 imaged optically (*gray*). **b:** Single condition map obtained in response to presentation of a full-field grating of one particular orientation. Presentation of gratings of different orientations yield domains of similar size and location to the one shown in b

Figure 3. Organization of orientation selective cells in A1 of a rewired ferret. **a:** Same as figure 2a. **b:** Map of signal magnitude obtained by normalizing signals to 3% and 10% of the maximum signal value for each stimulus orientation. Different colors represent different orientation preferences. Regions of higher signal magnitude for each of four individual orientations are shown by continuous lines, while regions of lower signal magnitude are indicated by dashed lines. The higher-magnitude regions show only partial overlap for different

orientations (see Results). **c:** A pinwheel center located approximately at the center of the vector angle map shown in d. A systematic representation of orientations is observed around this pinwheel center. **d:** Color coded vector angle map obtained by summing four single condition maps obtained in response to gratings of four different orientations. A crude organization into domains of orientation preference is present in rewired A1 (see Results and Discussion).

Figure 4. Horizontal long-range intrinsic connections in V1 of a normal ferret. **a:** CTB injection site (*black*) and retrogradely-labeled cells (*dots*) superimposed to a single condition map imaged optically in the same animal. **b:** Histogram plotting the distance of retrogradely-labeled cells from the center of the nearest physiological domain. Note that the majority of cells lie in or very near domains of the same orientation preference as the domain injected with CTB.

Figure 5. Horizontal long-range intrinsic connections in A1 of a rewired ferret. **a:** CTB injection site (*black*) and retrogradely-labeled cells (*dots*) superimposed on the visual activity domain imaged optically in the same animal. **b:** Histogram of the distribution of cells as a function of distance from the nearest domain center. Labeled cells appear restricted to the visually-responsive domain (see Results).

Figure 6. Comparison of connectivity patterns of horizontal connections in A1 of rewired and normal ferrets. **a:** CTB injection site (*black*) and retrogradely labeled cells (*dots*) in rostral A1 of a rewired ferret. Note that the tangential spread of horizontal connections in rewired A1 is fairly symmetric and slightly elongated along the mediolateral axis (presumed tonotopic axis). **b:** CTB injection site (*black*) and retrogradely labeled cells (*dots*) in rostral A1 of a normal ferret. Note that in normal ferrets horizontal connections are highly anisotropic, spreading much more in the anteroposterior dimension (presumed isofrequency axis) (see Results).

Figure 7. Histogram plotting the ratio of the long and short axis of the overall retrograde label for three normal (N1-3) and two rewired (R1-2) ferrets. Note that horizontal connections in A1 of normal animals are much more anisotropic than horizontal connections in A1 of rewired animals (see Results).

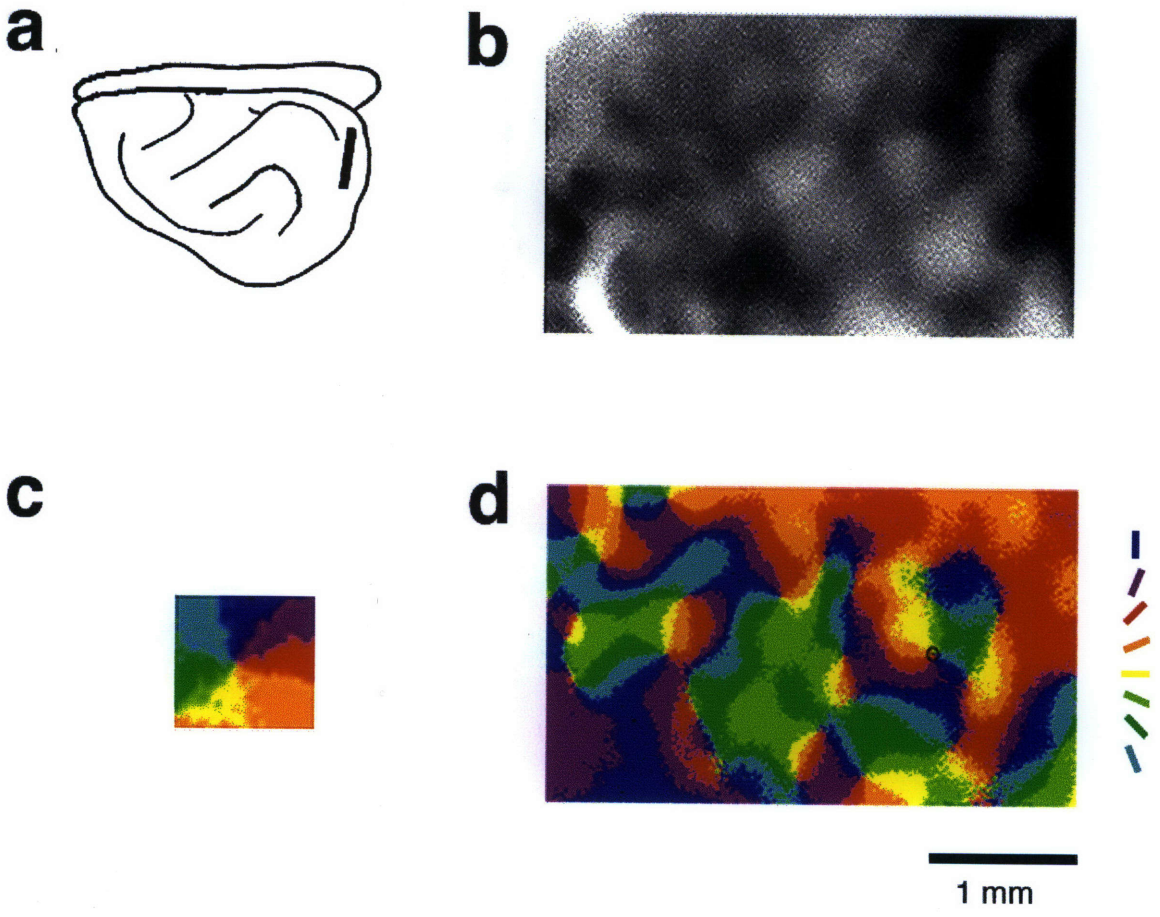

Fig. 1

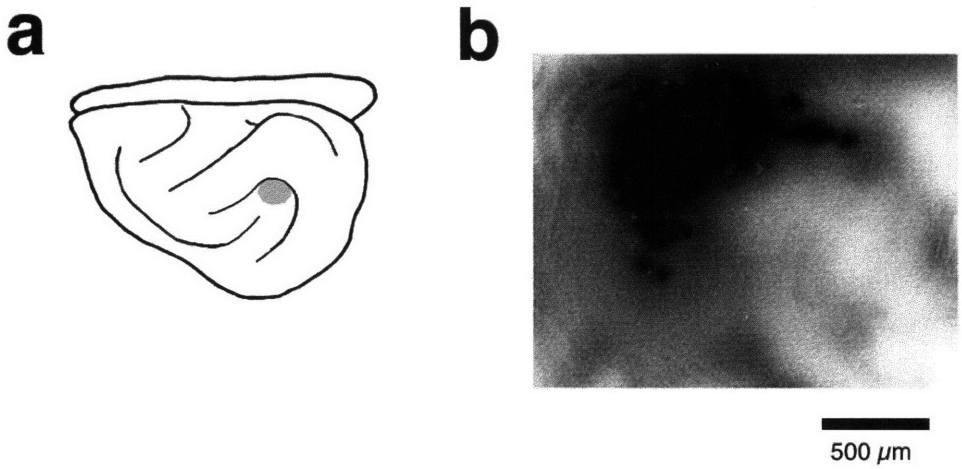

Fig. 2

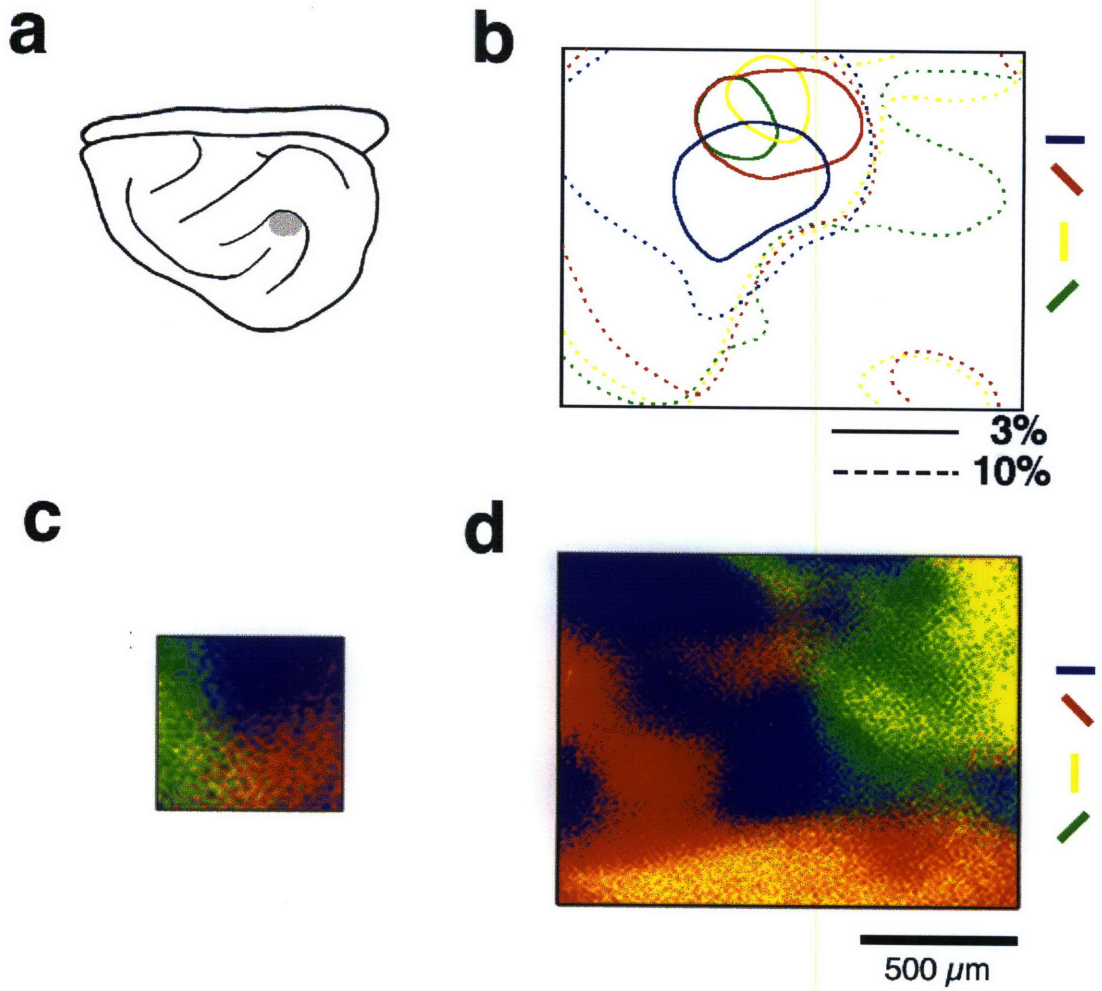

Fig. 3

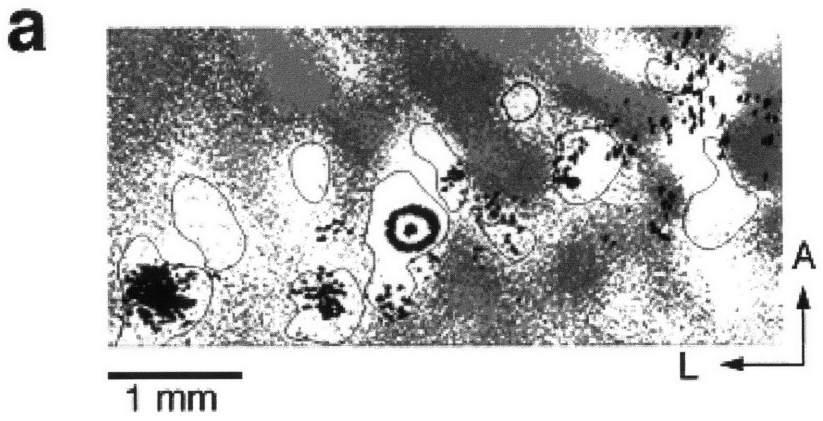
a
A
L
1 mm

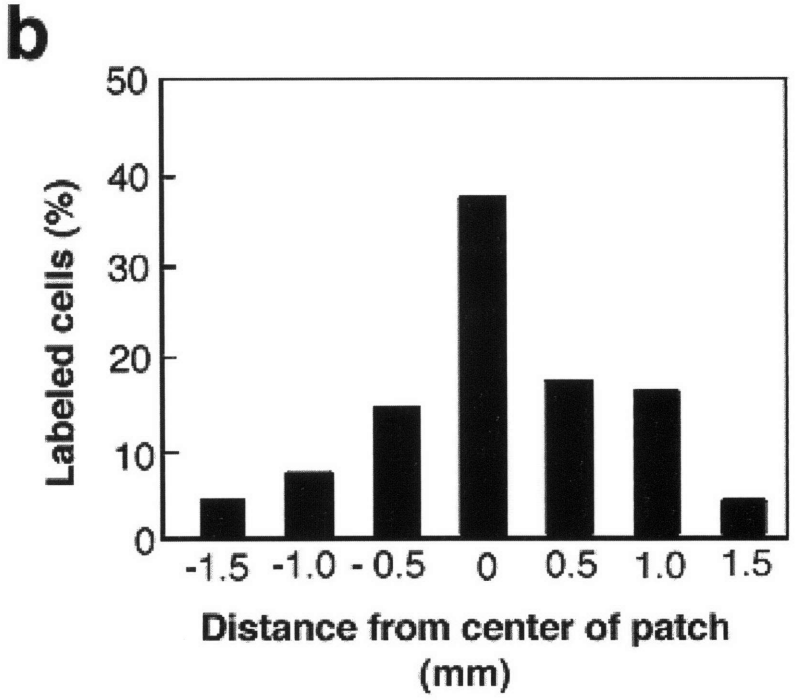
b
Labeled cells (%)
50
40
30
20
10
0
-1.5
-1.0
-0.5
0
0.5
1.0
1.5
Distance from center of patch
(mm)

Fig. 4

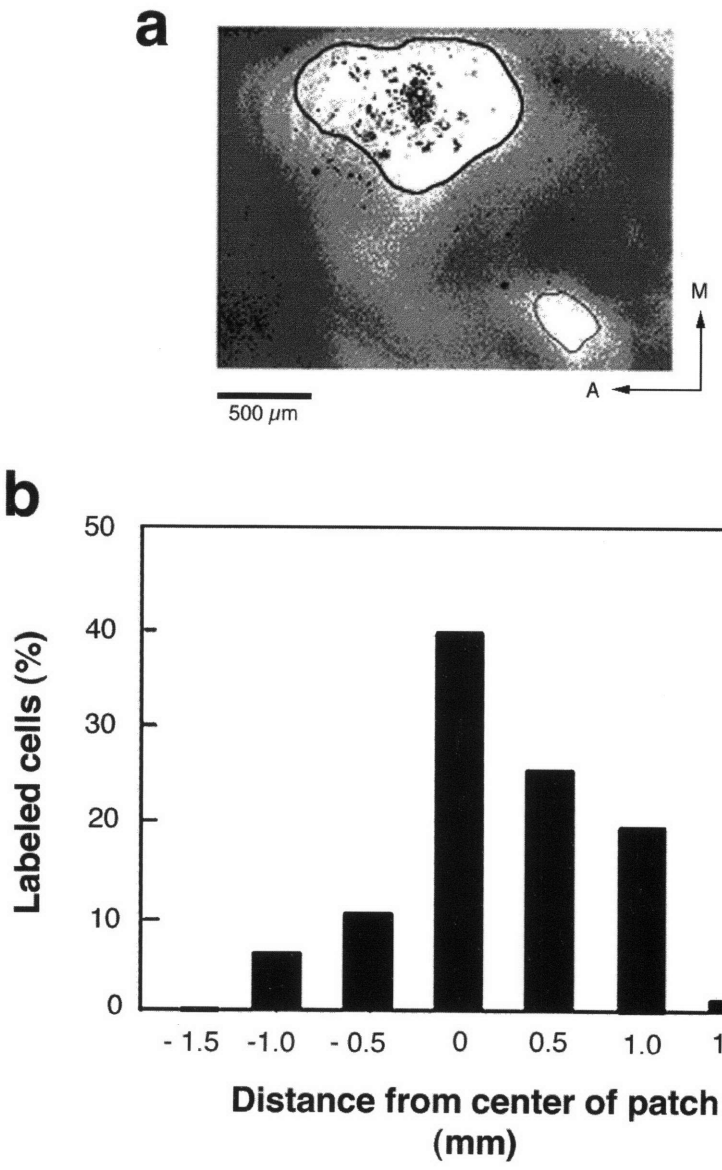
a
M
A
500 μm
b
Labeled cells (%)
50
40
30
20
10
0
- 1.5
-1.0
- 0.5
0
0.5
1.0
1.5
Distance from center of patch
(mm)

Fig. 5

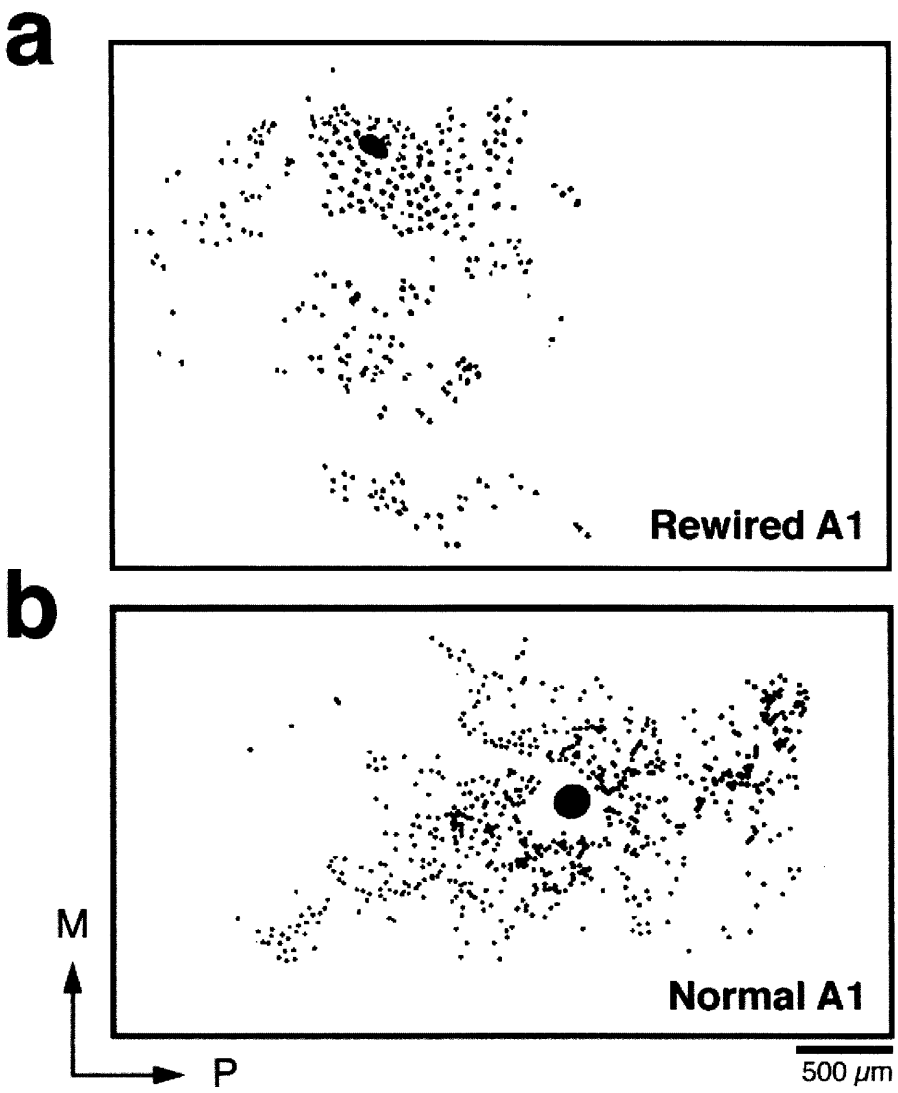

Fig. 6

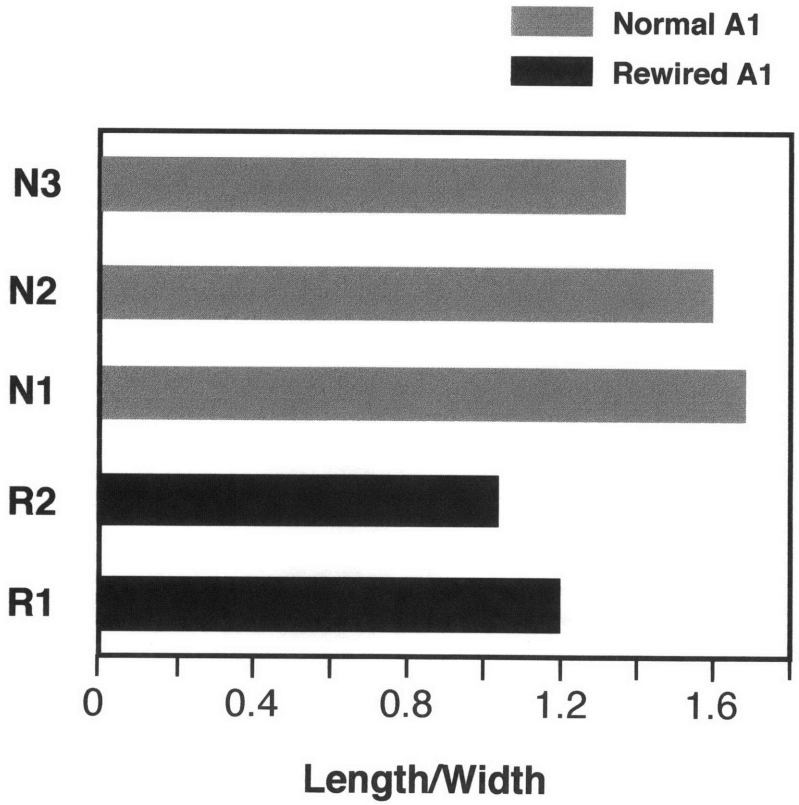

Fig. 7

Conclusions

A fundamental feature of the development of the mammalian brain is the generation of specific sets of connections between different brain regions and the formation of patterned terminations in a target structure by afferents from a source structure.

A good example of specific and patterned connections is offered by the visual pathway of higher mammals. Thus, for example, in higher mammals the retina projects to the visual thalamus (lateral geniculate nucleus, LGN), but not to other thalamic nuclei. The LGN, in turns, projects specifically to the primary visual cortex (V1). Furthermore, in ferrets and other mammalian species, retinal axons from the two eyes terminate in eye-specific layers in the LGN (Linden et al., 1981), and, in turn, axons from eye-specific layers of the LGN terminate in ocular dominance columns in V1 (Law et al., 1988). The retino-LGN-V1 pathway is further characterized by a "point-to-point" pattern of connectivity, such that adjacent points in the retina project to adjacent points in the LGN, and adjacent LGN points project to adjacent loci in V1 (see Sur et al., 1990). A further example of patterned connections in the visual system is offered by the horizontal long-range intracortical connections within V1. Such connections, established by cells of the supragranular cortical layers, display a clustered pattern (Gilbert and Wiesel, 1979, 1983) and link neurons with similar orientation preference (Ts'o et al., 1986; Gilbert and Wiesel, 1989; Sharma et al., 1995; see also Chapter 5, this Thesis).

A central question in developmental neuroscience is what determines the generation of such specific patterns of connections. Several studies have indicated that neural activity plays an important developmental role in the generation of patterned retinogeniculate (Shatz and Stryker, 1988; Cramer and Sur, 1996) and geniculocortical (Stryker and Harris, 1986) connections, as well as of intracortical horizontal connections in V1 (Callaway and Katz, 1991). While those studies support a role for activity in the generation of patterned connections, they do not distinguish between the relative roles of afferents and targets, since the manipulations employed

to block afferent activity (i.e. eyelid suture, intraocular injections of tetrodotoxin, TTX) inevitably affect target activity as well.

An issue that remain unresolved is the relative role of afferent and target structures in different aspects of pattern formation. We have examined this issue in a novel preparation, in which retinal axons are induced to innervate the auditory thalamus (medial geniculate nucleus, MGN), thus creating a functional mismatch between afferents and targets. Our choice of redirecting visual inputs to central structures that normally process auditory information was motivated by the marked differences in connectivity patterns that exist between the visual and the auditory pathways.

The auditory pathway differs from the visual pathway in many respects. The normal auditory pathway is schematically illustrated in Fig.1 (left diagram).

1) Auditory inputs from the cochlea reach the inferior colliculus (IC) via several relay stations in the brainstem. Afferents from the IC, the main source of inputs to the MGN, form terminal clusters in MGN. Within one of the cytoarchitectonic subdivisions of the MGN, the ventral division (MGv), terminal clusters are aligned along the dorsoventral axis (the isofrequency axis), forming "bands" (Kudo and Niimi, 1980; Wenstrup et al., 1994). While inputs from the two ears are not segregated in MGN, cells and afferents tuned to the same sound frequency segregate in parallel "lamellae" or "bands".

2) Projections from the MGN to the primary auditory cortex (A1) are highly divergent (Merzenich et al., 1982, 1984; Pallas et al., 1990; see also Chapter 4, this Thesis), as opposed to the point-to-point projection patterns of the visual geniculocortical system. A focal point in MGN projects to a "slab" of cells in A1. Terminal "slabs" are elongated along the anteroposterior axis of A1 (the isofrequency axis).

3) Intracortical projections within A1 are highly anisotropic, being elongated along the anteroposterior dimension (the isofrequency axis) (Reale et al., 1983; Matsubara and Phillips, 1988; Wallace et al., 1991; see also Chapter 5, this Thesis).

The functional mismatch created by redirecting visual inputs to central auditory structures, and the marked differences in connectivity patterns between the normal visual and auditory systems allowed us to investigate the relative roles of afferents and targets, as well as the role of afferent activity in shaping patterned connections. Specifically we asked:

1) under which conditions can retinal axons innervate the auditory thalamus?

2) do afferents from the two eyes segregate within the novel target (the MGN) as they do in their normal target, the LGN? And if they do, do they form eye-specific layers, and does the MGN differentiate into layers with interlaminar spaces? Such a finding would demonstrate afferent regulation of target differentiation. Conversely, do eye-specific terminations align themselves with the cellular organization of the MGN? Such a finding would demonstrate target regulation of afferent arbor location.

3) is the pattern of projections from the MGN to A1 altered by visual activity in "rewired" ferrets? Specifically, are these projections divergent and "slab-like" as they are in the normal auditory pathway, or are they point-to-point as the projections from the LGN to V1?

4) is the distribution of horizontal intrinsic connections in rewired A1 shaped by visual activity so that it differs from that in normal A1?

Our findings are schematically illustrated in Fig.1 (right diagram), and summarized below.

1) Retinal axons can be induced to innervate ectopic targets, such as the MGN. The factor that seems to be most important in regulating the formation and the amount of novel retino-MGN projections is the creation of vacated terminal space in the novel target. Thus, if a preference of axons for their targets exists, this preference is relative.

2) The pattern of retino-MGN projections shares features of the normal retino-LGN projections, in that the two eyes segregate in the MGN as they do in the LGN. However, it also shares features of the normal IC-to-MGN projections, in that retino-MGN projections are arranged in terminal clusters whose size, shape and orientation closely match those of relay cell dendrites in the normal MGN. In addition, the retinal terminal clusters are aligned along the dorsoventrally-oriented MGN lamellae, like the afferents from the IC to the normal MGN. Both clustering and eye-specific segregation of retinal afferents to the MGN arise over development as a refinement of initially diffuse and overlapped projections, as also demonstrated for the development of eye-specific layers in the LGN (Shatz, 1983; Sretavan and Shatz, 1986). In addition, remodeling of retinal axons in MGN occurs over the same time period as the development of patterned connections in the normal retinogeniculate system (Linden et al., 1981; Hahm et al., 1991). We conclude that afferent-driven mechanisms are implicated in the development of clustering and eye-specific segregation, whereas target-driven mechanisms specify shape, size and distribution of terminal clusters.

3) Projections from the MGN to A1 in "rewired" ferrets are highly divergent and form terminal "slabs" oriented along the isofrequency axis, resembling the projections in normal animals. We conclude that visual activity, and thus the pattern of afferent activity does not alter auditory thalamocortical projection patterns. By contrast, the visual thalamocortical system has been shown to be very susceptible to manipulations of afferent activity, such as lid suture or intraocular injections of TTX (Hubel et al., 1977; Shatz and Stryker, 1978; Stryker and Harris, 1986; Antonini and Stryker, 1993). While it is possible that the development of thalamocortical projections in the auditory system differs from that in the visual system in the susceptibility to alteration of afferent activity, two alternative hypotheses could explain our findings. One possible explanation for the unaltered pattern of thalamocortical projections in "rewired" ferrets is that our manipulations are performed at a late stage in the development of such projections,

past their critical period. Another possibility is that our manipulations of activity are much more subtle than manipulations such as monocular deprivation or intraocular injections of TTX which completely abolish afferent activity, and as such may not induce dramatic changes of thalamocortical connectivity patterns.

4) The intrinsic long-range horizontal connections in A1 are altered by visual activity. These projections in "rewired" ferrets are much more symmetric than those in normal animals, and their longer axis does not parallel the isofrequency axis, as seen for horizontal connections in normal A1. Moreover, in "rewired" A1 these connections link predominantly visually-responsive cells.

We propose that the development of specific and patterned connections is an interplay between afferent and target features.

References

Antonini A, Stryker MP (1993) Development of individual geniculocortical arbors in cat striate cortex and effects of binocular impulse blockade. J Neurosci 13:3549-3573.

Callaway EM, Katz LC (1991) Effects of binocular deprivation on the development of clustered horizontal connections in cat striate cortex. Proc Natl Acad Sci USA 88:745-749.

Cramer KS, Sur M (1996) Blockade of afferent impulse activity disrupts ON/OFF sublamination in the ferret lateral geniculate nucleus. Dev Brain Res, in press.

Gilbert CD, Wiesel TN (1979) Morphology and intracortical projections of functionally identified neurons in cat visual cortex. Nature 280:120-125.

Gilbert CD, Wiesel TN (1983) Clustered intrinsic connections in cat visual cortex. J Neurosci 3:1116-1133.

Gilbert CD, Wiesel TN (1989) Columnar specificity of intrinsic horizontal connections in cat visual cortex. J Neurosci 9:2432-2442.

Hahm J-O, Langdon RB, Sur M (1991) Disruption of retinogeniculate afferent segregation by antagonists to NMDA receptors. Nature 351:568-570.

Hubel DH, Wiesel TN, LeVay S (1977) Plasticity of ocular dominance columns in the monkey striate cortex. Phil Trans R Soc (Lond.) B 278:377-409.

Kudo M, Niimi K (1980) Ascending projections of the inferior colliculus in the cat: an autoradiographic study. J Comp Neurol 191:545-556.

Law MI, Zahs KR, Stryker MP (1988) Organization of primary visual cortex (area 17) in the ferret. J Comp Neurol 278:157-180.

Linden DC, Guillery RW, Cucchiaro J (1981) The dorsal lateral genicualate nucleus of the normal ferret and its postnatal development. J Comp Neurol 203:189-211.

Matsubara JA, Phillips DP (1988) Intracortical connections and their physiological correlates in primary auditory cortex (A1) of cats. J Comp Neurol 268:38-48.

Merzenich MM, Colwell SA, Andersen RA (1982) Auditory forebrain organization. Thalamocortical and corticothalamic connections in the cat. In C.N. Woolsey (ed.): Multiple Sensory Areas, Vol. 3. Clifton: Humane, pp.43-57.

Merzenich MM, Jenkins WM, Middlebrooks JC (1984) Observations and hypotheses on special organizational features of the central auditory nervous system. In G.W. Edelman et al. (eds.): Dynamic Aspects of Neocortical Function. New York: Wiley, pp.397-424.

Pallas SL, Roe AW, Sur M (1990) Visual projections induced into the auditory pathway of ferrets. I. Novel inputs to primary auditory cortex (AI) from the LP/pulvinar complex and the topography of the MGN-AI projection. J Comp Neurol 298:50-68.

Reale RA, Brugge JF, Zhen Feng J (1983) Geometry and orientation of neuronal processes in cat primary auditory cortex (AI) related to characteristic-frequency maps. Proc Natl Acad Sci. USA 80:5449-5453.

Sharma J, Angelucci A, Rao SC, Sur M (1995) Relationship of intrinsic connections to orientation maps in ferret primary visual cortex: iso-orientation domains and singularities. Soc Neurosci Abstr 21:392.

Shatz CJ (1983) The prenatal development of the cat's retinogeniculate pathway. J Neurosci 3:482-499.

Shatz CJ, Stryker MP (1978) Ocular dominance in layer IV of the cat's visual cortex and the effects of monocular deprivation. J Physiol 281:267-283.

Shatz CJ, Stryker MP (1988) Prenatal tetrodotoxin infusion blocks segregation of retinogeniculate afferents. Science 242:87-89.

Sretavan DW, Shatz CJ (1986) Prenatal development of retinal ganglion cell axons: segregation into eye-specific layers within the cat's lateral geniculate nucleus. J. Neurosci 6:234-251.

Stryker MP, Harris W (1986) Binocular impulse blockade prevents the formation of ocular dominance columns in cat visual cortex. J Neurosci 6:2117-2133.

Sur M, Pallas SL, Roe AW (1990) Cross-modal palsticity in cortical development: differentiation and specification of sensory neocortex. TINS 13:227-233.

Ts'o D, Gilbert CD, Wiesel TN (1986) Relationships between horizontal connections and functional architecture in cat striate cortex as revealed by cross-correlation analysis. J Neurosci 6:1160-1170.

Wallace MN, Kitzes LM, Jones EG (1991) Intrinsic inter- and intralaminar connections and their relationship to the tonotopic map in cat primary auditory cortex. Exp Brain Res 86:527-544.

Wenstrup JJ, Larue DT, Winer JA (1994) Projections of physiologically defined subdivisions of the inferior colliculus in the mustached bat: targets in the medial genicualte body and extrathalamic nuclei. J Comp Neurol 346:207-236.

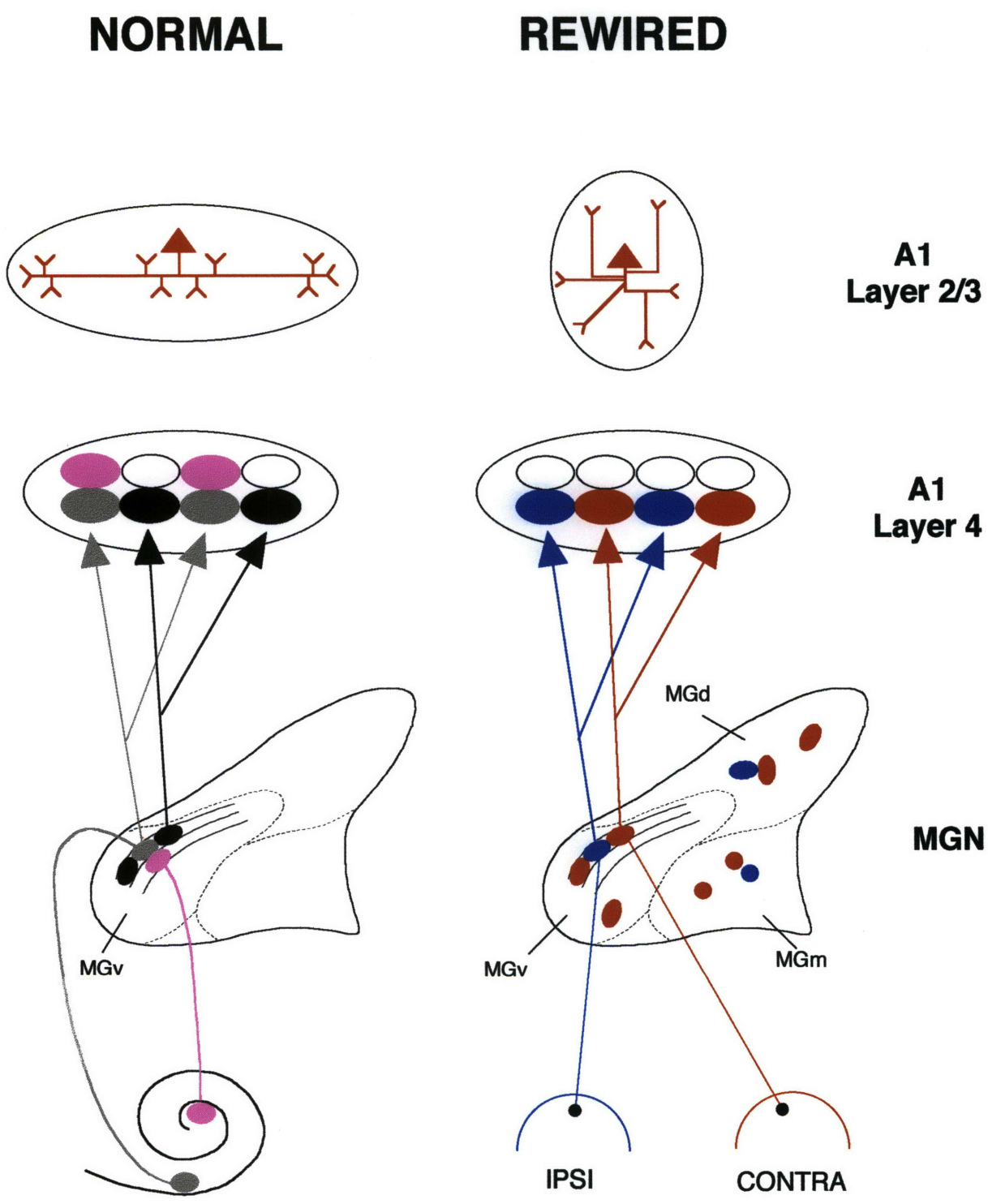
NORMAL
REWIRED
A1
Layer 2/3
A1
Layer 4
MGd
MGN
MGv
MGv
MGm
IPSI
CONTRA

Fig. 1